PREPARATION AND STABILITY OF ORGANIC NANOCRYSTALS

UNIVERSITY OF BRADFORD

2012

PREPARATION AND STABILITY OF ORGANIC NANOCRYSTALS

Experimental and Molecular Simulation Studies

Shahzeb Khan

Submitted for the degree of Doctor of Philosophy

School of Life Sciences

University of Bradford

2012

Shahzeb Khan

Preparation and Stability of Organic Nanocrystals

Key words: Nanocrystals, Crystallisation, Precipitation, Molecular simulation, Molecular dynamics, Ibuprofen, Glibenclamide, Artemisinin, Glycine, Polymer stabilisers.

A major challenge affecting the likelihood of a new drug reaching the market is poor oral bioavailability derived from low aqueous solubility. Nanocrystals are rapidly becoming a platform technology to address poor solubility issues, although several challenges including stabilisation and control of particle size distribution for nanosuspensions still need to be addressed. The aim of this study was to revisit the simplest approach of re-precipitation and to identify the critical parameters, including the effect of different stabilisers as well as process conditions. We utilised a combined approach of both experiments and molecular modelling and simulation, not only to determine the optimum parameters but also to gain mechanistic insight. The experimental studies utilised three rather distinct, relatively insoluble drugs, the hypoglycaemic glibenclamide, the anti-inflammatory ibuprofen, and the anti-malarial artemisinin. The choice of crystal growth inhibitors/stabilizers was found to be critical and specific for each drug. The effect of the process variables, temperature, stirring rate, and the solute solution infusion rate into the anti-solvent, was rationalized in terms of how these factors influence the local supersaturation attained at the earliest stages of precipitation. Coarse grained simulation of antisolvent crystallisation confirmed the accepted two step mechanism of nucleation at high supersaturation which involves aggregation of solute particles followed by nucleation.

Recovery of nanocrystals from nanosuspensions is also a technical challenge. A novel approach involving the use of carrier particles to recovery the nanocrystals was developed and shown to be able to recover more than 90% of the drug nanocrystals. The phase stability of nanocrystals along with bulk crystals for the model compound glycine was explored using molecular dynamics simulation. The simulations were consistent with experimental data, a highlight being the β phase transforming to the δ phase at temperature >400K and 20kbar respectively, as expected. Nanocrystals of α, β and γ glycine, however did not show any phase transformation at high temperature.

In summary the study demonstrates that standard crystallization technology is effective in producing nanocrystals with the primary challenge being physico-chemical (rather than mechanical), involving the identification of molecule-specific crystal growth inhibitors and/or stabilizers. The developed nanocrystal recovery method should enable the production of nanocrystals-based solid dosage forms. The molecular simulation studies reveal that crystal-crystal phase transformations can be predicted for hydrogen-bonded systems.

Acknowledgements

First of all I am very grateful to Almighty Allah who bestowed me with his blessings to complete this project. This thesis is dedicated to my parents, Gul bad Shah Khan and Karil Zubana whose guidance, support and encouragement provided me a substantial piece of grooming and a range of successes in my life.

I must express my special thanks to my supervisors Prof. Jamshed Anwar and Dr Marcel de Matas for their motivations, enthusiasm, worthy piece of advice and guidance during the entire period of this project.

I would like to express my warm thanks to my elder brother Jehanzeb Khan and my wife Aneela Khan whose indispensable support certainly led me towards completion of my PhD studies.

At IPI, I must acknowledge the technical support of people including, Dr John Kendrick, Smitha Plakkot, Stuart Fox, Andrew Healey and Dennis Farweil. I am very thankful to Shah Hassan who helped me in formatting this thesis.

Finally I would like to thank HEC Pakistan and University of Malakand KP (Khyber Pakhtunkhwa) for the award of FDP scholarship to pursue my PhD studies.

Contents

List of Figures

List of Tables

Chapter 1

Introduction

1.1 Statement of the Problem

A major problem affecting the likelihood of a new drug reaching the market is poor oral bioavailability derived from low aqueous solubility. Recent publications suggest that many drugs identified by high throughput screening are poorly water soluble and belong to the BCS class II family of drugs (Lipinski, 2002). These drugs although having greater tendency to pass through the lipophilic intestinal membrane often demonstrate low rate and extent of absorption from the gastrointestinal tract (GIT) which is typically limited by slow dissolution rate (Amidon et al., 1995). Amongst the technologies developed to address low aqueous solubility, nanocrystals have received notable attention and are rapidly becoming a platform solution due to the immense surface area that they present. In principle, methods for nanocrystal production can be categorized as top down and bottom-up (Horn and Rieger, 2001, Rabinow, 2004) and include milling, high pressure homogenisation (Liversidge and Cundy, 1995, Muller and Akkar, 2004) and precipitation by compressed antisolvent (PCA) (Bodmeier and McGinity, 1998). Rapid expansion from supercritical to aqueous solution (RESAS),

rapid expansion of supercritical solution (RESS) and spray freezing into liquid have been developed over the past decade (Rabinow, 2004, de Waard et al., 2010). Each of these methods has notable issues which include high energy input, long processing times and uncontrolled particle growth. This study aimed to investigate the preparation of stable nanocrystals with a uniform size distribution using bottom up controlled precipitation coupled with a physico-chemical approach where the focus is on crystal growth inhibitors/stabilizers. The experimental study is complemented by molecular simulation to provide a molecular rationale for the formation and stabilization of these systems, and also to explore the phase stability of nanocrystals using the glycine as a model compound.

This chapter presents the broader background to the study including the significance of crystal engineering in pharmaceutical development, principles of crystallization and crystal growth, and polymorphism and phase stability. This is followed by a critical review of our current understanding of the fundamental science and associated technology for preparing stable nanocrystals as well as their applications in drug delivery. As the study combined both experiment and molecular simulation, we also review and present the relevant background to molecular modelling and simulation. Finally the aims and objectives of the proposed study are given.

1.2 Crystal Engineering

The term crystal engineering was probably first used by Schmidt (1971) with respect to photodimerisation reactions in crystalline cinnamic acids. A modern and more comprehensive definition has been given by Desiraju (Desiraju, 2001), who defined crystal engineering as “the understanding of

intermolecular interactions in the context of crystal packing and in the utilization of such understanding in the design of new solids with desired physical and chemical properties".

Crystal engineering has enabled researchers to design suitable solid state structures by optimising the non-covalent interactions which exist between the ionic or molecular components of the structures with desired electrical, magnetic, and optical attributes. Hippel (1962) had described the detailed background of crystal engineering (von Hippel, 1962). It has also become evident that the directionality of intermolecular hydrogen bonds can effectively be utilized to assemble supramolecular structures with a controlled resultant dimensionality (Subramanian and Zaworotko, 1995). Supramolecular chemistry has been described by Lehn as the chemistry of intermolecular bonds between molecules and the atoms within the molecules are connected by covalent bonds (Lehn, 1988).

The discipline of crystalline engineering is maturing and there are many successes where crystalline materials with novel properties have been prepared by design across a range of industries including the pharmaceutical and health care sector (Steed et al., 2000).

The increasing cost of therapeutic molecules including products recall from the market owing to side effects and quality issues have provided notable challenges for pharmaceutical companies in their attempts to improve quality. As>85% of dosage forms contain the drug in solid state, pharmaceutical engineering represents an important approach to ensure quality and performance of these drugs and circumvent barriers to commercial success. Low aqueous solubility has adversely impacted the performance of multitude

of candidate therapies. More than 40% of the drugs in development pipeline and 70% coming from synthesis or high-throughput screening are poorly water soluble (Shegokar and Müller, 2010). It is known that poorly-water soluble drugs are mostly hydrophobic in nature, having greater tendency to pass through the lipophilic intestinal membrane more swiftly. In spite of this, absorption of these drugs from GI tract has been found to be erratic. However, the oral route of administration for these drugs can still be affective, if faster dissolution rate from the GI tract can be achieved (Amidon et al., 1995).

On the basis of solubility and permeability through biological membranes, drugs can be characterised into four classes as defined by the Biopharmaceutical Classification System (BCS) (Figure 1.1).

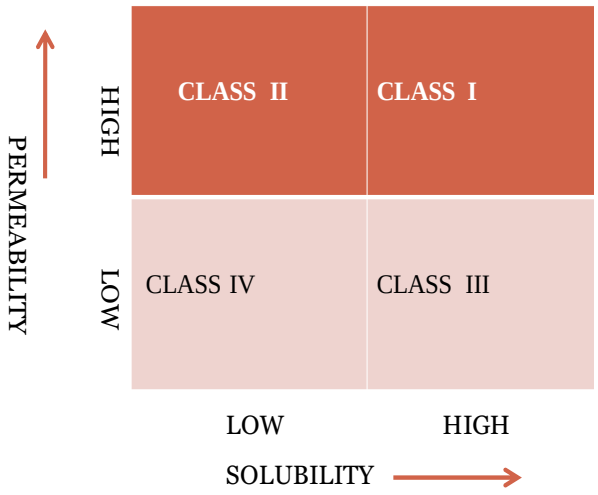

Figure 1.1 Biopharmaceutical classification of drugs

Owing to high permeability but poor solubility, class II compounds pose significant challenges during drug development. These compounds can have poor dissolution profiles which can delay the drug's onset of action and result in low bioavailability. It might be possible to address the issue of poor

solubility by increasing the drug dose to enhance exposure of the drug to the membrane without serious side effects, but in many cases solubility is so limited that negligible increases in exposure are experienced through increasing dose. This low aqueous solubility also limits the ability to formulate these drugs in an injectable form. It is clear therefore, that this crucial problem has been a major hurdle in pharmaceutical development. In this regard formulation scientists have been struggling to address poor water solubility problems by utilising a variety of approaches including solid dispersions (Serajuddin, 1999), solubilisation (Aungst, 1993), emulsions (Floyd, 1999), microemulsions (Lawrence and Rees, 2000), micronisation (Charoenchaitrakool et al., 2000), micelles, salts, liposomes (Schwarz et al., 1994), and inclusion complexes using cyclodextrin (Loftsson and Brewster, 1996). These approaches have only been modestly successful. Examples of crystal engineering approaches employed to address the poorly soluble issue include the use of metastable polymorphs, ultra fine particles, crystal habit modification and co-crystal design (Blagden et al., 2007). A particularly notable development is the use of nanocrystals with the specific physical and chemical attributes.

1.2.1 Crystallisation

Crystallisation is the process by which atoms, ions or molecules assemble to pack into a regular three dimensional structure under specific conditions. The process is controlled by the driving force, which in solution equates to the supersaturation. Supersaturation is defined as the concentration of a substance in solution relative to its saturation solubility. More precisely, it given by

Supersaturation ratio $(S) = \frac{C}{C^*}$ **Equation 1.2**

Where, C is the solution concentration and C^* is the equilibrium saturation solubility. In chemical engineering, high yields of crystalline materials are desired and the following relationship for supersaturation is employed.

Supersaturation$(\Delta C) = C_{ss} - C_{eq}$ **Equation 1.3**

Where C_{ss} is the supersaturation concentration, Ceq is the equilibrium concentration. Clearly, the greater the difference between equilibrium and supersaturation state, the greater the driving forces for crystallisation to occur. Crystallisation occurs under conditions of supersaturation, where solute concentration exceeds the equilibrium solubility of the molecule. Figure 1.2 shows the different regions that exist for a substance in solution in terms of its concentration as a function of temperature. Three distinct zones can be observed, the first zone being defined as undersaturation where the concentration too low for spontaneous crystallisation to occur. In the metastable region the solution is above saturation but is still insufficient to induce spontaneous nucleation, whilst in the supersaturated region the concentration is well in excess of equilibrium solubility and crystal nucleation occurs spontaneously.

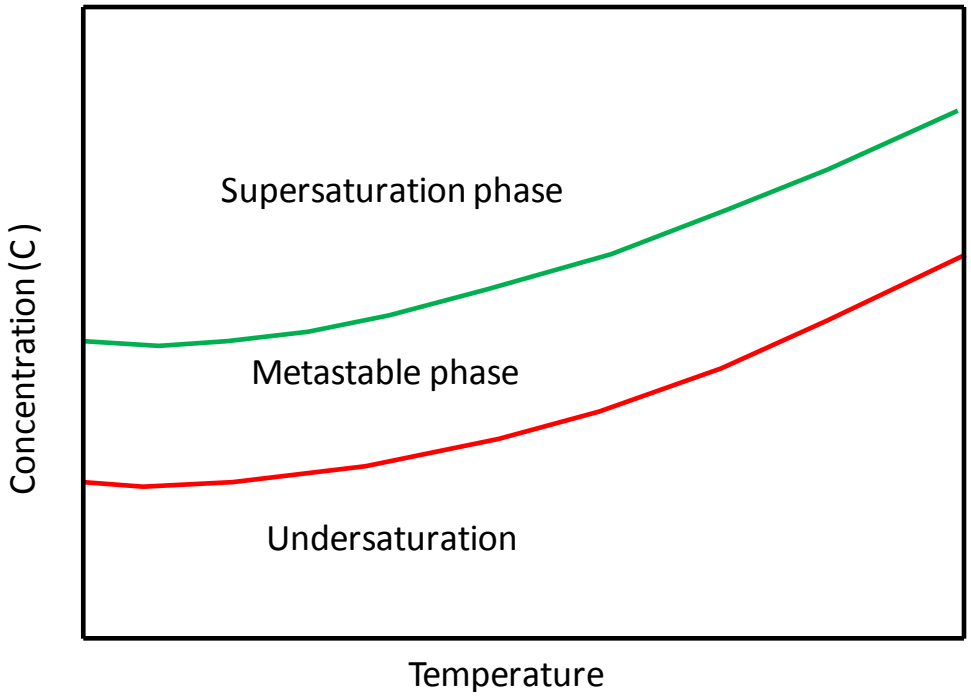

Figure 1.2 The solubility/supersolubility diagram (Garside and Davey, 2000)

Nucleation represents the first step towards crystallisation and refers to the formation of a small stable cluster which has the characteristics of the emerging crystalline phase upon which further deposition of solute particles occurs. Nucleation can be classified into homogeneous, heterogeneous, and secondary nucleation. Homogeneous nucleation begins spontaneously without foreign particles/surface. Clusters of molecules comprising 10-1000 molecules (the actual number depends on the supersaturation) are formed which continue to grow once a critical size (stable form) has been achieved. Gibbs (1928) and Volmer (1939) investigated the change in free energy required for the origination of a cluster which is the sum of change in free energy related with the phase transformation (ΔG_{vol}) and formation of nucleus surface (ΔG_{surf}) respectively.

$$\Delta G = \Delta G_{vol} + \Delta G_{surf} \qquad \textbf{Equation1.4}$$

In crystallisation process supersaturated is followed by spontaneous deposition of solute molecules to form a solid. Owing to high stability attributes of the solid state compared to liquid, ΔG_{vol} becomes negative which favours crystal growth. Whilst the newly born solid state creates solid/liquid interface which increases the free energy of a system. The competition between ΔG_{vol} and ΔG_{surf} decides growth of nuclei. High value of ΔG_{surf} causes dissolution of the nuclei. Whereas decrease in ΔG_{surf} results in crystal growth. It is shown in the Figure 1.3 at a critical size (r*) of nuclei ΔG becomes maximum and the solution is likely to be nucleated. The nuclei with a size below the critical size would dissolve back into the solution because of the high free energy.

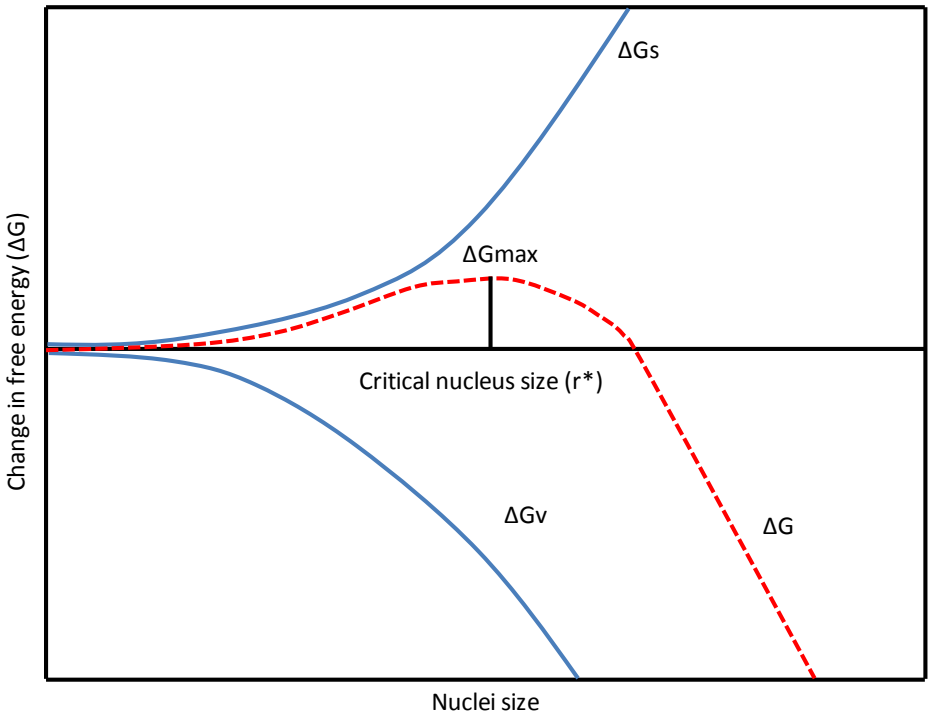

Figure 1.3 Gibbs free energy change as a function of nuclei size

Heterogeneous nucleation occurs when nucleation occurs on or is induced by foreign surfaces. A lower level of supersaturation and free energy change

is required for heterogeneous and secondary nucleation compared to homogenous nucleation (Marashall, 1987). A decrease in the energy required for nucleation occurs if the foreign particles and crystals have more similar structures.

In secondary nucleation, nuclei form on the solid surface composed of the same solute molecules and generally characterises the process of seeding to induce nucleation. There have been reported several theories including dust breeding, collision breeding, dendritic growth and needle breeding to understand the mechanism of generation of secondary nuclei and its growth. Tig and McCab (1934) has investigated that a seed crystal has a larger size compared to the size of nuclei which acts as a nucleation site and induce the nucleation process at lower supersaturation level. In addition, at high supersaturation levels the formation of needle and dendiritic crystals has also been reported which fragment in the solution and these fragments provide new nucleation sites (Myerson, 2002a). Some authors propose that macroabrasion of crystals because of high stirring speed results in fragments with subsequent new nucleation sites (Myerson, 2002b). Cooke (1966) proposed that dendritic growth occurs at a seed crystal surface which could be broken down due to fluid shear or due to high coarsening of the dendrites, resulting fragments in solution which provide new sites for nucleation. The rate of nucleation in a supersaturated solution is represented by the equation given as follows

$$\frac{dN}{dt} = K_n\,(C_i - C^*)^a \qquad \textbf{Equation 1.5}$$

Where K_n shows the solute nucleation rate, and C_i and C* represent the solute concentration on particle surface and saturation concentration

respectively. The value of parameter *a* has been reported to be between 5 and 18 (J.A. Dirksen, 1991). The diffusion of the solute particles to the surface of the particles is represented by the following equation

$$\frac{dm}{dt} = K_d(C - C_i)^b \qquad \textbf{Equation 1.6}$$

Where K_d is the diffusion rate constant of the solute molecules and C shows bulk solution concentration. Nucleation is followed by growth of the particles. The growth rate is given as follow

$$\frac{dl}{dt} = K_g(C_i - C^*)^b \qquad \textbf{Equation 1.7}$$

Where K_g denotes the particle growth constant. Usually the value of parameter b is placed between 1 and 3. However there has been reported a higher value of parameter *b* at higher temperature (Chan and Kwok, 2011). Equations 1-3 show that supersaturation can affect both nucleation and particle growth. Higher supersaturations result in a higher nucleation rate and consequently smaller particle size is achieved (Matteucci et al., 2006).

1.2.1.1 Crystal Growth

In supersaturated environments, crystal growth is likely to occur through diffusion of solute molecules from the bulk solution towards the crystal surfaces, followed by de-sorption and diffusion of the solvent away from both the crystal surface and from the solvation shell around the solute particles leading to consequent incorporation of solute molecules into the crystal lattice (Figure 1.4) (Dirksen 1991). Hartman and Perodck have classified faces of crystals as Kinked (K), Stepped (S) and Flat (F) depending on the bonds/interaction potentially been involved at the crystal surface (Hartman, 1973). The K, S and F faces involve three, two and single bonds or

interactions respectively (Figure 1.5). The kink sites having the most potential interactions are the preferred site for incorporation of the solute molecules onto the crystal surface. Numerous mechanisms have been reported for crystal growth and some of the common ones are described below.

Convection and Diffusion

The convection and diffusion mechanism dominates crystal growth when either or both these steps of transport of solute molecules to crystal surfaces are limiting. The solvation shell diffuses away from crystal surface before integration of the solute molecule in the crystal lattice.

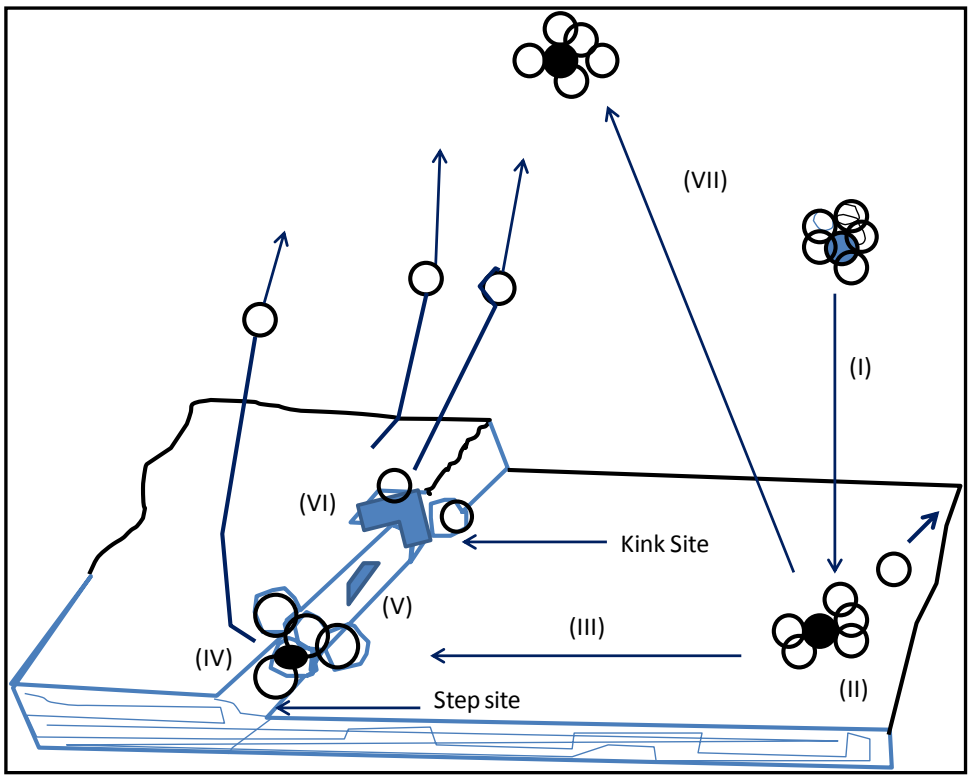

Figure 1.4 Mechanism of crystal growth from solution, adopted from (Elwell and Scheel, 1975, Dirksen and Ring, 1991). (I) transport of solute molecules to the surface of crystal; (II) adsorption onto the surface; (III) diffusion; (IV) coupling at step site; (V) diffusion through step site (VI) Diffusing into the crystal lattice. (VII) Solvent molecules diffuse away from crystal surface.

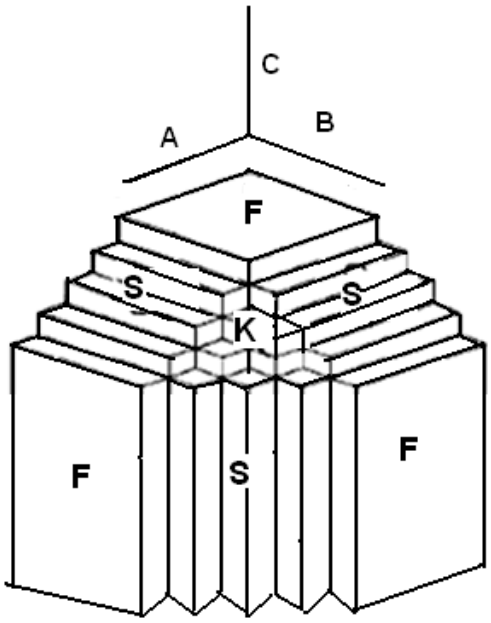

Figure 1.5 Hypothetical crystal with three main faces: flat (F), step (S) and kink (K) faces (Dirksen and Ring, 1991)

(b) Surface Nucleation

Crystal imperfections, surface roughness or the ledges of growth layers can provide growth sites for incoming molecules. As the roughness of the crystal surface decreases or as the layers become complete, there are few if any incorporation sites and the solute molecules return back into solution. For further growth to occur a new layer has to be created which requires 2-d surface nucleation. Figure 1.6 shows surface nuclei which present new kinked sites enabling adsorption of additional units. These nuclei spread laterally across the surface with subsequent growth occurring normal to the plane of the face.

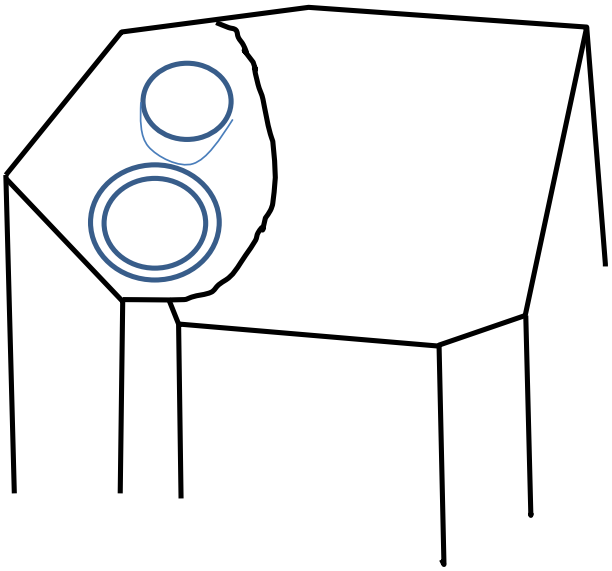

Figure 1.6 Development of crystal nuclei on the surface of growing crystal (Garside and Davey, 2000)

(c) Dislocation or Spiral Growth

Crystal dislocations generate step and kinked sites on crystal surface which provide opportunity for new molecules to be adsorbed on the surface. The newly emerging lines of dislocation result in growth patterns while removing the need for surface nucleation. In this respect screw dislocations are considered paramount as they provide a never ending steps for molecule incorporation, producing spiral growth on the crystal surface (see Figure 1.7). This mechanism of crystal growth was proposed by (Frank, 1949) and the presence of screw dislocations was confirmed only much later by means of electron microscopy. Burton,Caberera and Frank also envisaged a theory to promote crystal growth using the screw dislocation mechanism where the shape of spirals affect the rate of crystal growth (Burton et al., 1951)

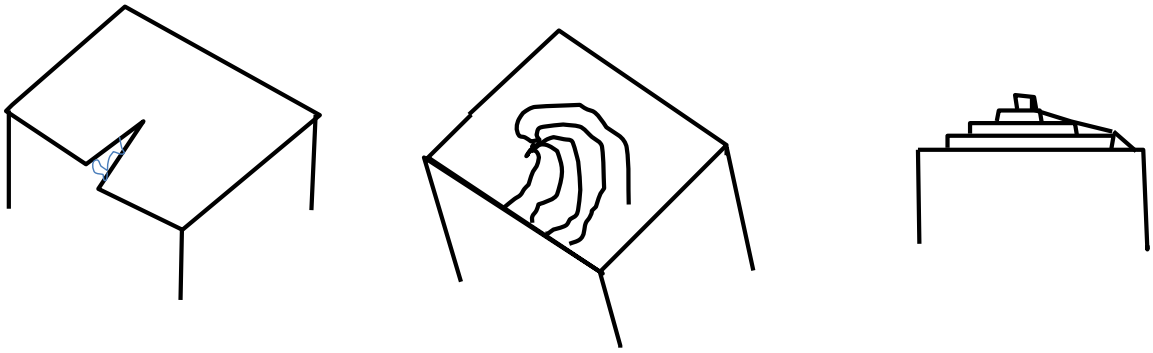

Figure 1.7 Development of growth spirals originating from a screw dislocation (Mullin, 2001)

1.3 Crystal Polymorphism

Compounds which can exist in more than one crystalline form are considered to polymorphic and the differing phases are termed polymorphs. In pharmaceutical products, the existence of polymorphs is critical to product development owing to their unique characteristics (Byrn et al., 1994). In crystallisation, the most stable form may not be directly produced but is often isolated after subsequent transformation in accordance with Ostwald's rule of successive (Ostwald, 1897). One of the techniques which is used to obtain the required polymorph of a drug is through the choice of specific solvents, variation in crystallisation conditions, and by inclusion of specific impurities. The inclusion of appropriate impurities may inhibit the transformation of the required metastable crystal form to the most stable phase. An example of the use of impurities for controlling polymorphism is that involving glutamic acid. Trismisic acid has been used as an impurity, which is conformationally similar to the stable form of glutamic acid. Rapid growth of the stable form is therefore inhibited in the presence of this substance resulting in the production of the metastable phases (P.T. Cardew, 1985)

Polymorphs can have different physicochemical and mechanical properties (Singhal and Curatolo, 2004). In pharmaceutical industries >85% of the products contain active pharmaceutical ingredients (APIs) and excipients in crystalline forms (Erdemir et al., 2009), therefore it is paramount to understand the physicochemical properties of API and excipients before there are formulated into a solid dosage form. From drug development prospective, selection of an appropriate crystalline form of a drug compound and its respective polymorphs is considered very important to ensure the original crystal form of API is stable in the final product. Polymorphism can have significant effect on dissolution and bioavailability of drug compounds (Zhang et al., 2004). Aguiar (1967) investigated that different polymorphs of chloramphenicol palmitate have different dissolution rate and bioavailability. For good economic purposes, pharmaceutical companies are showing extensive interest in formulation of solid dosage forms with a polymorph of APIs that has enhanced dissolution rate and bioavailability but is stable. How polymorphs behave when subjected to certain unit operation processes including milling, granulation, compaction, drying and heating is also important as these processes can cause phase transitions in the crystalline forms of API and excipients (Zhang et al., 2004). Phase transition between polymorphs can induced by high pressure, temperature or exposure to high humidities (Kitamura, 2002, Moggach et al., 2008)

Two types of phase transition in polymorphs have been reported: monotropic and enantiotropic (Giron, 2001). The irreversible phase transition in polymorphs is known as monotropic. This transition occurs from metastable to stable form of a crystal either by heat or stressing the system using

mechanical forces including compaction and milling. In monotropic phase transitions the polymorph with the high melting point is always the stable form (Figure 1.8 (b)). Enantiotropic phase transition is the reversible phase transition between a pair of polymorphs which occurs at a transition temperature (T_t) and the polymorphs are known as enantiotrophs to each other. During a heating process, if a temperature is below the transition temperature, the system would be monotropic but above T_t, the more stable polymorph is obtained. Figure 1.8 (a) shows that below T_t polymorph A is stable while at temperature above T_t polymorph B becomes thermodynamically more stable because of low free energy compared to polymorph A.

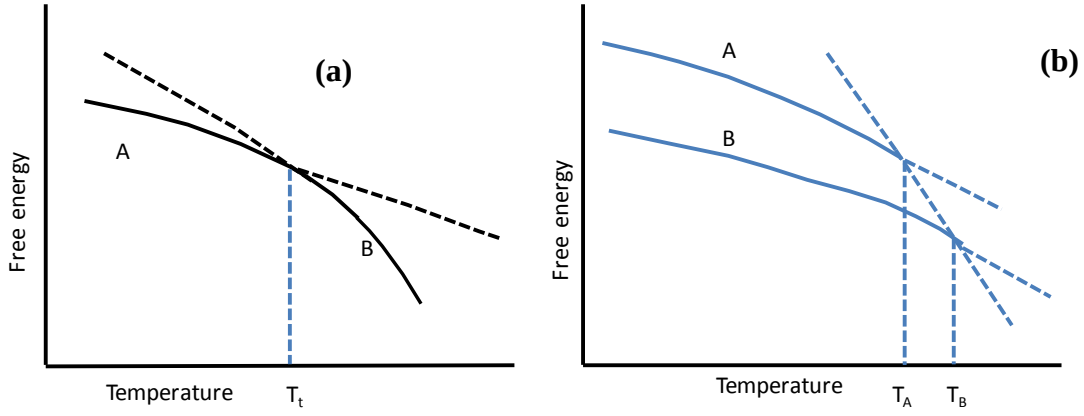

Figure 1.8 Schematic representation of (a) enantiotropic (b) monotropic and phase transitions. In enantiotropic phase transition the polymorph A is stable below transition temperature (T_t) whereas above T_t the polymorph B becomes more stable compared to A. In monotropic phase transition the polymorph B is more stable because of high melting point (T_B) compared to A which has low melting point (T_A).

1.3.1 Nanocrystals and their Method of Preparation

Nanocrystals have been defined as crystalline particles with at least one dimension less than or equal to 100 nm (Fahlman, 2007). However, there is

still no general agreement as to the definition of “nano” (Van Eerdenbrugh et al., 2008) in the pharmaceutical literature. According to a number of authors nanocrystals are crystalline particles that have a size below 1 micron and consist of drug component with minimum amount of surface active agents required for its stabilisation (Gao et al., 2008). Owing to particle size being below one micron and the resulting high surface area to volume ratio, nanocrystals have the potential to improve dissolution rates of hydrophobic drugs with consequent increase in bioavailability (Patravale and Kulkarni, 2004).

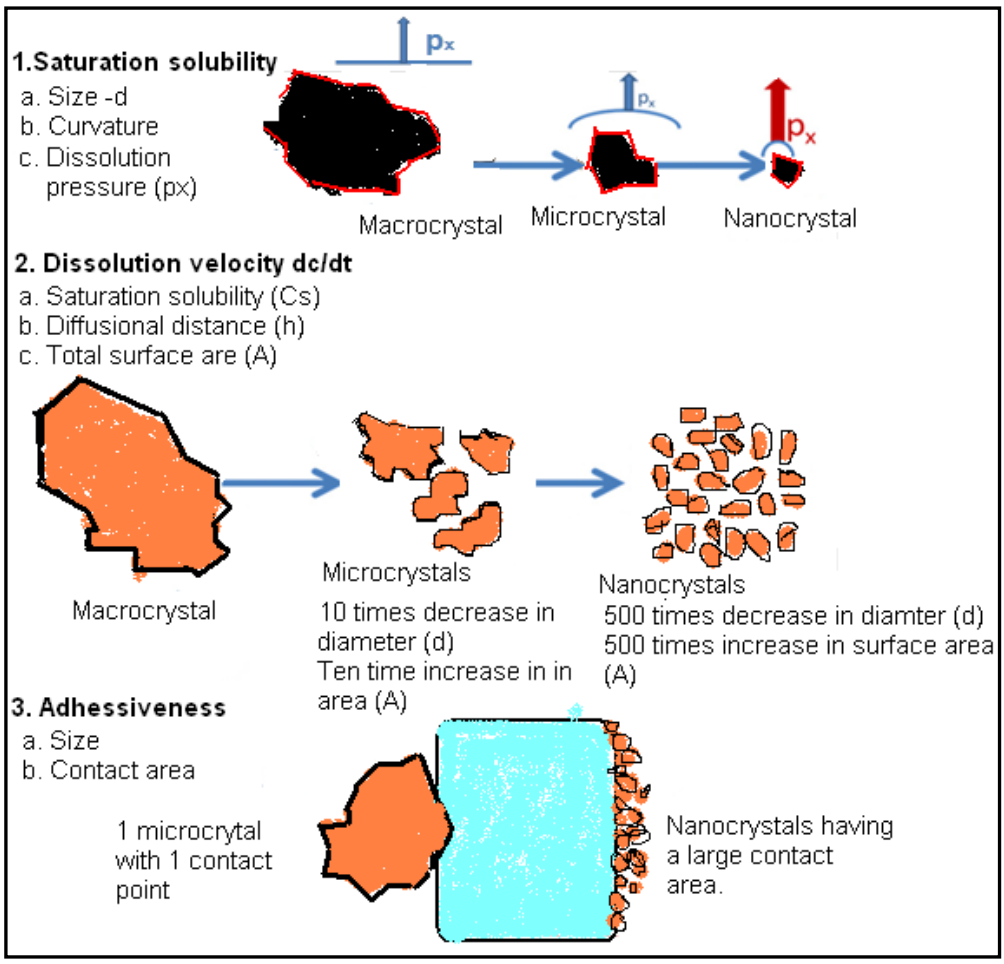

Figure 1.9 Distinctive characteristics of nanocrystals after (Muller et al., 2011)

Nanocrystals can remove poor solubility issues of BCS class II drug molecules due to their distinctive features which include increased saturation solubility, higher dissolution velocity, and fast adhesiveness to cell membrane (Müller et al., 2011) (Figure 1.9).

Nanocrystals can be prepared using a variety of methods which can generally be classified into the following two categories.

(a) Top down approaches (Rabinow, 2004)

(b) Bottom-up approaches (Patravale and Kulkarni, 2004)

Top down methods rely upon size reduction by which large particles of drugs are broken down by attrition into smaller particles. In contrast, bottom-up processes involve building the nanocrystals up from the molecular state generally by crystallisation. Figure 1.10 represents the general principle employed for production of the nanocrystals by the two approaches.

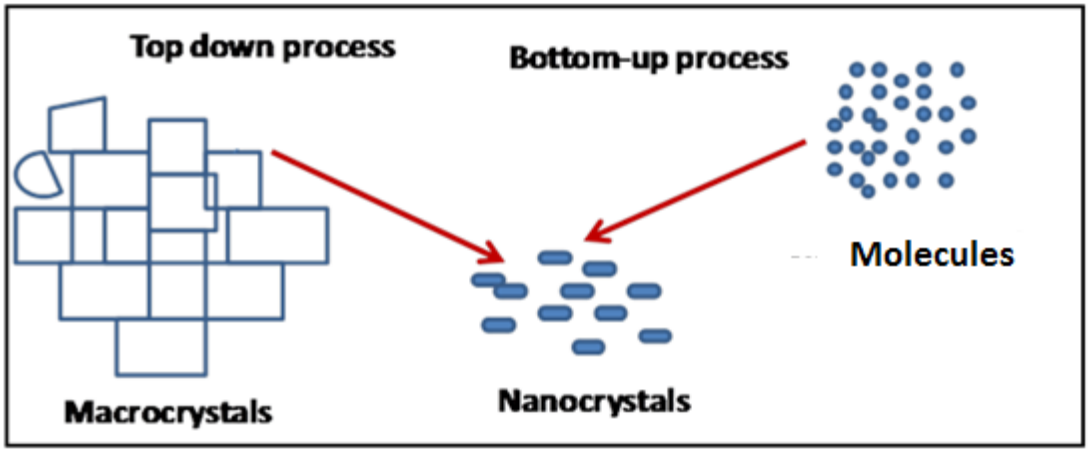

Figure 1.10 Two commonly used approaches for production of nanocrystals

1.3.1.1 Top down Approaches

Size reduction methods which utilises top down principles include media milling (Nanocrystal R), high pressure homogenization (HPH) in water

(Dissocubes, Skype Pharma) and combined precipitation and HPH (Nanoedge, Baxer). In the media milling method, the major forces responsible for breaking of the particles are provided by the milling media, which can be cross linked polystyrene resin, stainless steel, alumina, zirconium stabilized with yttrium, glass or zirconium oxide ((Muller, 2001, Liversidge et al., 1992). Typically the size of the starting materials is less than the 100 µm whilst the final size of the resultant particle is less than 400nm (Liversidge and Cundy, 1995, Liversidge et al., 1992, Merisko-Liversidge et al., 2003). The HPH approach produces nanosuspensions by exploitation of high shear forces, cavitation and continuous collision of the particles as the drug suspension is pushed through a narrow gap of 25µm. The number of homogenization cycles and associated homogenization pressure are the key parameters that have influence on particle size. A third important approach is precipitation combined with HPH (Nanoedge), where the nanosuspension produced by a precipitation process is stirred using high stirring forces producing a resultant nanosuspension with long term stability. All top-down approaches have the capacity to produce low and high concentration (1-400mg/ml) nanosuspensions with particle size less than 400nm. Drugs which are simultaneously poorly soluble in organic and aqueous media however have limitations with these methods. Other issues include contamination of the final product with milling media and high cost equipment (Patravale and Kulkarni, 2004).

1.3.1.2 Bottom-up Approaches

The bottom-up approach involves precipitation from solution where the hydrophobic drug is dissolved in organic solvent which is then mixed with a

stabiliser solution that is typically aqueous. The aqueous stabiliser solution acts as an anti-solvent and on mixing and causes supersaturation leading to consequent precipitation of the nanocrystals. A number of different methods utilise the basic principle of bottom-up approach, a notable one being precipitation by compressed antisolvent (PCA) which utilises supercritical CO_2 as an antisolvent in which drug and polymer solution is injected into the chamber which contains CO_2 in compressed form to yield nanocrystals (Bodmeier and McGinity, 1998).

Another variation is rapid expansion from supercritical to aqueous solution (RESAS) (Rabinow, 2004, de Waard et al., 2010).Poorly soluble drugs in the presence of stabiliser solutions are nucleated and consequently stabilised in nanosuspension form.

Spray freezing into liquid process (SFL) was developed by the University of Texas at Austin in 2001, in which a drug/excipient is directly atomized into compressed liquid, typically CO_2, helium, ethane, argon or hydrofluroethane. Use of this approach produces frozen nanoparticles which can be isolated as a solid by lyophilisation (Williams et al., 2002).

Evaporative precipitation into aqueous solution (EPAS) utilises organic solvents having low boiling points in which the drug is first dissolved before being pumped through a heated tube which heats the solution above the normal boiling point of the solvent. This heated solution is sprayed through a narrow atomized nozzle into a heated aqueous stabiliser solution which results in precipitation of a nanosuspension (Williams et al., 2002). Physical instability has been a major issue with nanosuspensions prepared using bottom approach. Nanosuspensions with broader size distribution result in

differential dissolution rate of API. Smaller particles are thermodynamically unstable relative to larger particles which results in dissolution of the small particles in favour of deposition over the surface of the large particles. This phenomenon is referred to as Ostwald's ripening and results in physical instability of nanosuspensions. Lindfors (2004) developed a novel bottom-up process to control Ostwald ripening process. Miglyol (a medium chain triglyceride) was selected as a crystal growth inhibitor and dissolved in the solvent containing the drug, which when mixed with the anti-solvent resulted in a stable nanosuspension (Lindfors, 2004).

Microchannel reactors (MCR) have also been investigated for production of stable nanocrystals, where solutions containing hydrophobic drug and aqueous stabiliser solutions are passed through the microchannel feeds from their respective storage containers. Mixing of the two solutions at the contact points of the two channels results in precipitation and consequent production of the nanoparticles (Buzea et al., 2007). Nanosuspension with narrow size distribution can be produced by controlled parameters of the MCR set up (Zhao et al., 2007). The methodology however does not readily scale up and the reactors are prone to blockages.

Perhaps the simplest and cost-efficient bottom-up method is controlled re-precipitation. The challenge here is to obtain stable nanocrystals for a range of drugs, and also to be able to deal with drugs that have a low solubility in both aqueous and organic media.

1.4 Characteristics and Performance of Nanocrystals

1.4.1 Stabilisation of Nanocrystals

When particle size is reduced new surfaces are formed leading to increased surface area and consequent increases in free energy. The rate of agglomeration is directly proportional to the free energy of the particles. Equation 1.8 represents this relationship

$$\Delta G = \gamma_{s/l}.\Delta A \qquad \textbf{Equation 1.8}$$

Where $\gamma_{s/l}$ the interfacial tension which determines the stability of the particles but can be reduced by inclusion of a suitable surface active agents and ΔA represents the change in surface area associated with reduction in particle size (Rabinow, 2004). It has been reported previously that lack of Ostwald ripening is a favourable condition for long term stabilisation of nanosuspensions (Peter and Muller 1996). Ostwald ripening is one of the challenging issues associated with the crystal growth in nanosuspensions prepared by both top down and bottom up methods. The broader size distribution of nanosuspensions is one of the well-known reasons which cause crystal growth by Ostwald ripening (Patravale et al., 2004). Owing to high saturation solubility the small particles are diffused towards the surroundings of larger particles. The relationship between the saturation solubility and particle size has been described by Ostwald Freundlich's equation (Equation 1.10) which shows that smaller particles have high saturation solubility compared to the larger particles. Additionally the smaller particles have high surface to volume ratio and free energy which tend to diffuse towards the large particles. The solution around the large particles

becomes supersaturated because of the high concentration of the small particles in the surroundings with subsequent integration into the large particles and crystal growth. In addition due to depletion of the area surrounding the small particles the solution is no longer saturated resulting in dissolution of the drug and complete elimination of the small particle zone. Inhibition of Ostwald ripening in nanosuspensions is still an issue which needs to be addressed. Selection of appropriate polymers and surfactants can play an imperative role to address this issue. Moreover, surfactants and polymers can stabilise nanosuspensions by electrostatic and steric mechanisms of stabilisation. Non-ionic surfactants or polymers form a layer on the surface of nanoparticles and prevents their agglomeration by blocking motion towards one another. When the two particles surrounded by an adsorbed no ionic surfactants or polymers approach each other there would be increase in polymeric or non-ionic surfactant concentration between the particles which will increase the total energy with a subsequent repulsion of the particles (Van Eerdenbrugh et al., 2008). Electrostatic stabilisation by charged surfactants provides a barrier to agglomeration which is achieved by repulsive interactions between the electrical double layers around the approaching particles in nanosuspension. The concept of the energy barrier and its prevention of interactions between particles has been described by the DLVO theory (Derjaguin, 1941) (Figure 1.11). The interactions of the solid particles in liquid dispersion are described by this theory in two ways. Either attraction or repulsion forces among the components of the dispersion can occur. Forces of attraction between particles include, van der Waals forces alongside repulsion forces resulting from the electrical double layers. In

addition there is another type of force that can also exist which comes from the shell of solvent molecules around the drug particles which could either be attractive or repulsive.

In electrostatic stabilization the stabilizer will affect the repulsive electrostatic energy (vel). It has been shown clearly in the classical DLVO diagram that a perfect barrier does not allow the particles to agglomerate by achieving the required Lifshitz-van der Waals energy (Vlw). Thus repulsive force is produced due to this barrier.

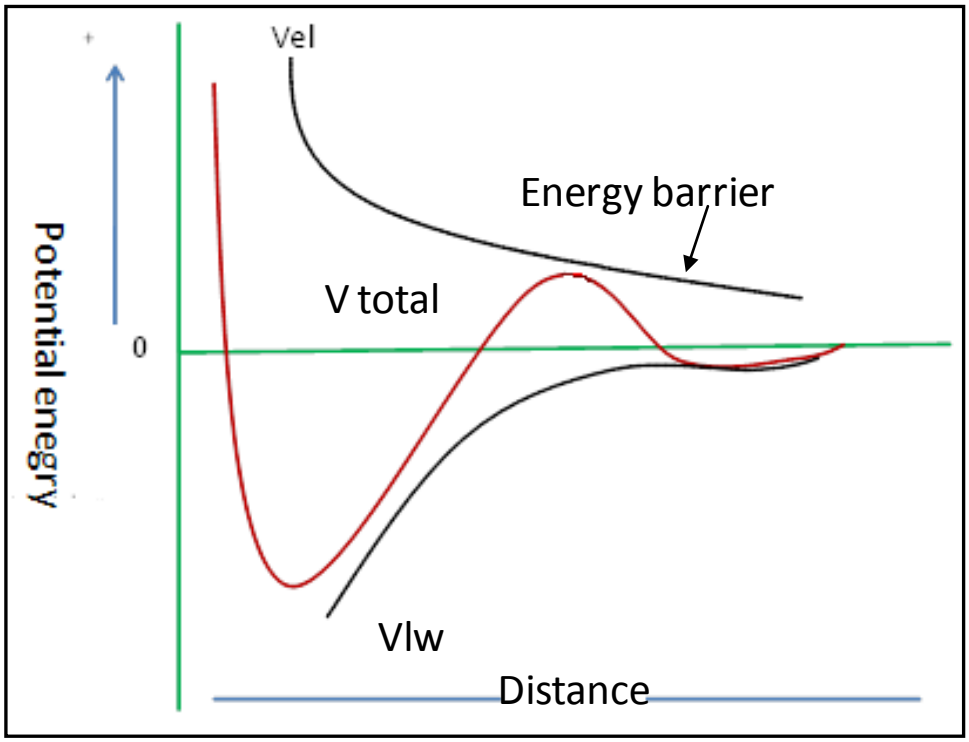

Figure 1.11 Variation in potential energy against the inter particles distance. Vlw = Lifshitz van der Waals energy and Vel shows electrostatic energy (Classical DLVO theory).

1.4.2 Absorption and Bioavailability

The rate of dissolution of solid substance can be described by the Noyes–Whitney dissolution model (Noyes and Whitney, 1897).

$$\frac{dc}{dt} = A.D\left(\frac{C_s - C_x}{h}\right)$$ **Equation 1.9**

Here dc/dt shows the dissolution rate, A is the drug surface area to be dissolved, D represents the diffusion coefficient, Cs is the saturation solubility , Cx and h show the bulk concentration of drug and thickness of the diffusion pathway respectively. Unquestionably, the above model indicates that the greater the surface area of drug particles, the faster the dissolution of the drug with subsequent quick release of drug resulting in faster absorption through intestinal membrane. Owing to the smaller particles size, nanocrystals having immense surface area which can lead to higher dissolution rates and result in faster absorption and consequently higher bioavailability for therapeutic agents. Although the benefits of nanocrystals are primarily accrued from vastly increased surface area, increases in saturation solubility are also believed to be possible, especially in the sub 100 nm size range, with consequent increases in dissolution rate as described by the Freundlich Ostwald equation (Müller and Peters, 1998) as shown in Equation 1.10

$$S = S_\infty \exp(2\gamma M/r\rho RT)$$ **Equation 1.10**

where S is the saturation solubility of the nanoparticle, S_∞ is the saturation solubility of the large crystals, γ is the interfacial tension of the crystal-medium interface, M is the molecular weight of the compound, r is radius of the particle, ρ is the density, R is the gas constant and T is the temperature. At particle sizes of ≤100 nm the stated equation predicts increases in solubility of approximately 10-15 %. Increases in solubility in excess of 50% have however been reported as the particle size is reduced from 2.5 µm to

300 nm (Müller and Peters, 1998). Additional relationships between surface curvature, vapour pressure and particle size are also described by the Kelvin equation (Böhm and Müller, 1999). According to this relationship, smaller particles with increased surface curvature have been shown to demonstrate markedly higher vapour pressure compared to coarser micron sized particles. The transfer of molecules from liquid to gas has been reported to be identical to transformation of molecules from solid phase to liquid medium. The dissolution pressure therefore becomes equivalent to vapour pressure which is likely to be increased for smaller sub-micron particles (Junghanns and Müller, 2008).

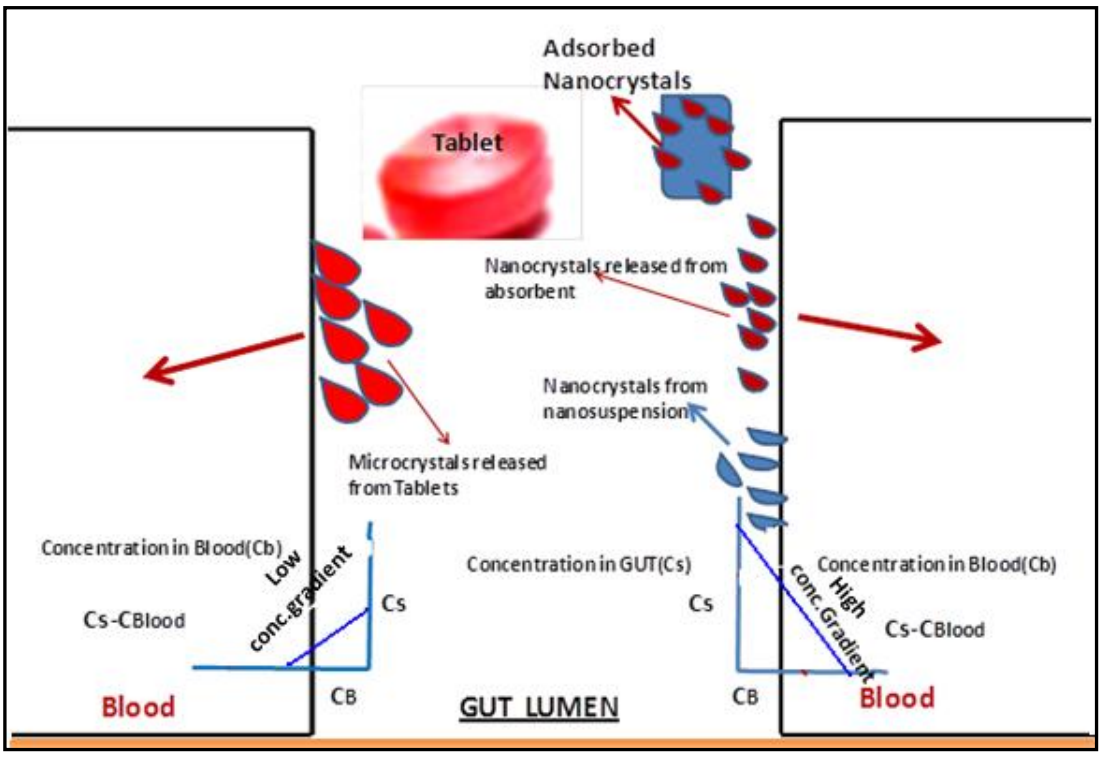

Figure 1.12 Comparative absorption mechanism of micro and nanocrystals from gut lumen. Adopted from (Mauludin et al., 2008).

The use of nanocrystals in particular for increasing surface area, dissolution rate and bioavailability is fast becoming a platform solution (Muller, 1999) (Figure 1.12).

1.5 Molecular Modelling and Simulation

Molecular modelling and simulation is the application of computational techniques to model the behaviour of molecules and molecular systems using atomic theory and inter-molecular forces.

The paramount feature of molecular simulations is to provide insight into the molecular level description of a system. Additionally molecular simulation can yield dynamical information e.g. diffusion coefficient and thermodynamics quantities such as free energies.

The methodology provides insights into how molecules react or interact and hence in a way provides atomic resolution in the behaviour of collections of molecules comprising complex systems. The technique is receiving increasing attention in computational biology, computational chemistry and material sciences complementing the traditional experimental approaches. In combination with experiments, the simulations help to rationalise experimental results and also aid the design of better experiments.

There are different levels to describe the intermolecular forces in molecular simulations. For example when electronic structures become important then quantum mechanics which is computationally more expensive approach is likely to be employed. On the other hand, in molecular simulations using molecular mechanics approach, no bond formation and breaking occurs and integrity of the molecules are retained. Therefore it is worthwhile to employ molecular mechanics approximation which is the less expensive computational approach while enabling the simulation of 100000 atoms using standard computing laboratory facilities.

1.5.1 Quantum Mechanics

Quantum mechanics models focus on electrons and their distributions towards describing molecular structures and the derived properties of these systems including energies. Quantum mechanics models are considered paramount for investigating chemical reactions in which covalent bonds are broken and formed. The basic quantum mechanics model for a molecular system is based on the time dependent Schrödinger's equation which takes the following form (see Equation 1.11).

$$H\Psi = \mathrm{E}\Psi \qquad \textbf{Equation 1.11}$$

where H is the Hamiltonian of the system, Ψ is the wave function, which is considered to represent the coordinates of the electrons and nucleus and E is the energy of the system. The Hamiltonian represents the sum of the kinetic and potential energies arising from the interaction of nuclei n (A+B) and electrons and takes the form

$$H = K_n + K_e + U_{ne} + U_{ee} + U_{nn} \qquad \textbf{Equation 1.12}$$

Where K_n and Ke are the kinetic energies of the nuclei and electrons respectively. Whilst U_{ne}, U_{ee} and U_{nn} are the nucleus – electron, electron – electron and nucleus –nucleus potential energy terms respectively.

Schrödinger's wave equation is a many-body equation and can only be solved exactly for hydrogen and for helium. For more complex atoms which have more than one electron and molecular systems it is necessary to use approximations. For example Born–Oppenheimer approximation suggested that the equilibration of electrons is not dependent on the movement of nuclei. Nuclei can be considered as static objects being heavier and which move very slowly compared to the electrons (Goodman, 1998). Nevertheless these

methods are computationally intensive which restricts this approach to systems that involve bond making and breaking and where the electronic structure is important.

1.5.2 Molecular Mechanics

Molecular mechanics utilises the principle of classical mechanics to model the geometry and dynamics of the molecules. In molecular mechanics, atoms are considered as spheres whose effective radii are determined either by theoretical or experimental approaches. Whereas bonds are treated as springs which can be stretched, bended and twisted. The stiffness attributes of the bonds rely on the bonded elements and types of bonds which include single, double and covalent bonds. In addition the non bonded interactions including van der Waals and electrostatic interactions are also considered. Molecular mechanics models give the static energy or the total potential energy which is obtained by adding up all the potential terms describing the bonded and non-bonded interactions. The potential function takes the following form

$$U_{total} = \sum U_{stretching} + \sum U_{torsion} + \sum U_{bending} + \sum U_{vdw} + \sum U_{electrostatics}$$

(Equation 1.13)

This set of bonded and non-bonded interaction energy terms together with associated parameters for the different atom types is called a force field (Figure 1.13). The important interaction potentials are described as follow.

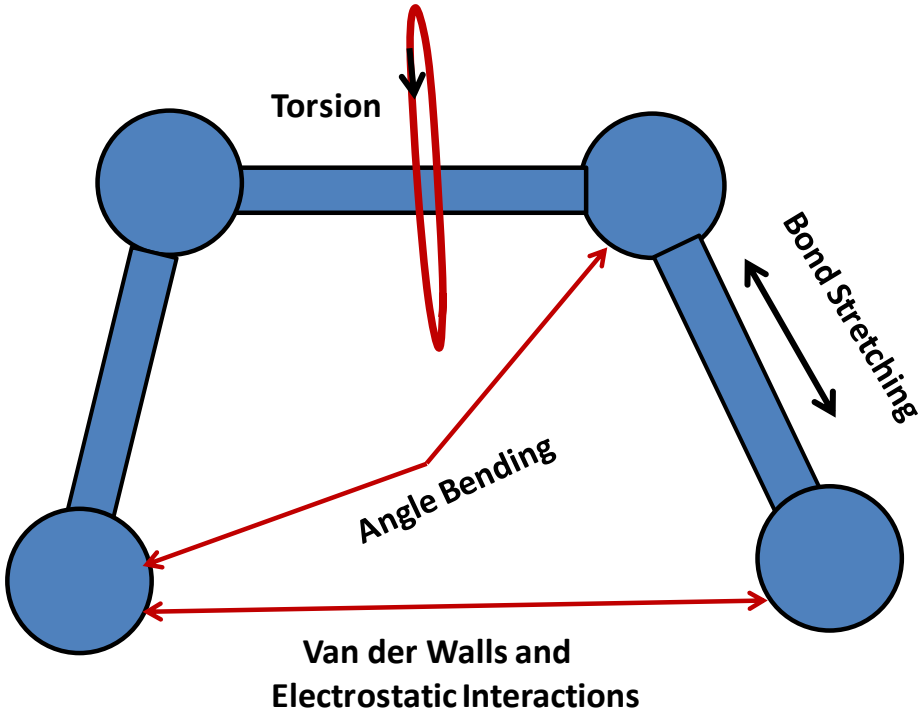

Figure 1.13 Common potential terms representing a typical force field

(a) Bond Stretching

The bond stretching energy, $U_{stretching}$, is that required to stretch the bond between two given atoms from the equilibrium bond length l_o (see Figure 1.14). It is represented by

$$U_{stretching} = \frac{1}{2}K(l - l_0)^2 \qquad \textbf{Equation 1.14}$$

Where K shows the force constant for the bond, and l_o is the equilibrium bond length. For calculation of Ustretching two parameters (lo and K) must be known (Jensen, 2007).

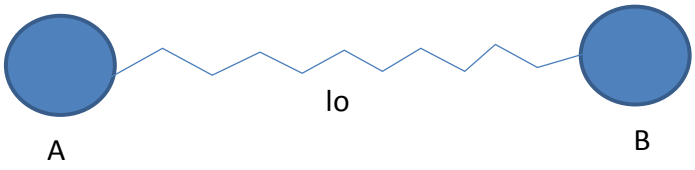

Figure 1.14 Representation of bond stretching

(b) Angle Bending

$U_{bending}$ is the energy associated with bending of the angle between three atoms ABC (see Figure 1.15) and takes the following form:

$$U_{bending} = \frac{1}{2} K\theta(\theta - \theta_0)^2 \qquad \textbf{Equation 1.15}$$

Where θ is angle between atoms I, j and k. At least two parameters KΦ and Φ_0 are required to determine $U_{bending}$, which can be obtained by IR spectroscopy and x-ray diffraction respectively.

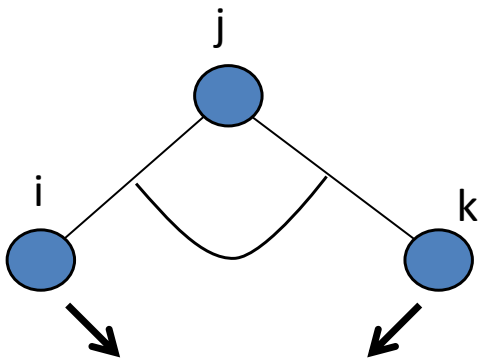

Figure 1.15 Representation of valence angle bending

(c) Bond Torsion

Utorsion is the energy associated with the rotation of a single bond in a chain of four atoms (I, j, k, l) connected each other. Rotation about bonds gives rise to the different conformations that a molecule can adopt. For example ethane has two conformations namely staggered and eclipsed. The stable conformer of ethane is the staggered form with lower energy in which the hydrogen atoms do not exist in the same plane on carbon atom, owing to repulsion between the electrons orbitals of the hydrogen atoms (see Figure 1.16).

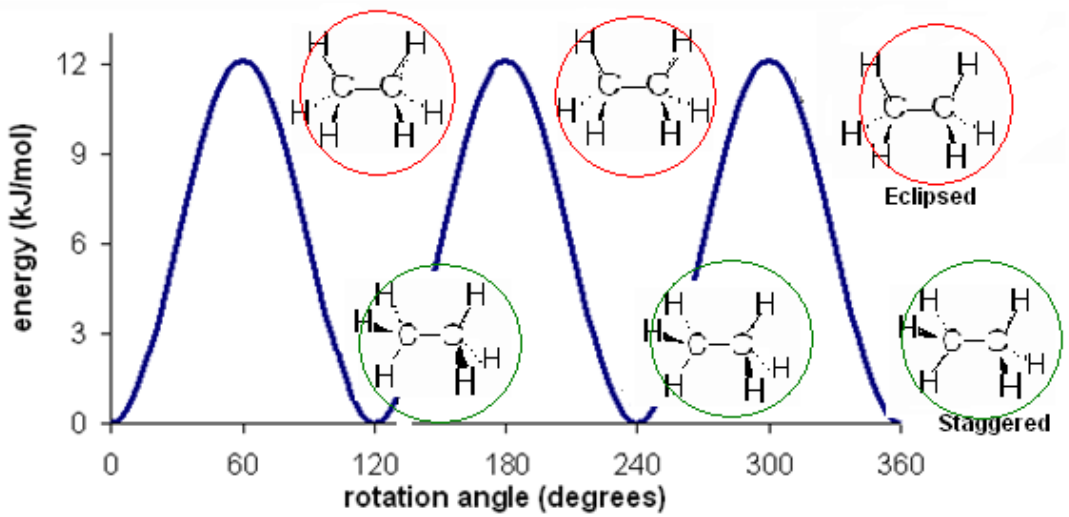

Figure 1.16 Conformation in ethane molecule

The value of torsion energy is usually low compared to the bending and stretching energy (Jensen, 2007). Utorsion is represented as follow (Equation 1.16).

$$U_{tor} = \mathrm{A}\big(1 + \cos\left(m\emptyset - \delta\right)\big) \qquad \textbf{Equation 1.16}$$

Where A is the barrier for rotating around the bond, m is the periodicity parameter and σ shows reference angle. For instance m = 3 in sp^3-sp^3 bond and σ =0, and m = 2 and σ = 180 in sp2-sp2 bond (Ullmann, 2007). ∅ shows torsional angle between I, j, k and l.

(e) Van der Waals Energy

Van der Waals interactions represent the sum of attractive and repulsive forces between non bonded atoms. Atomic nuclei are surrounded by a cloud of electrons and the respective size of the atom is measured by van der Waal's radius. When two atoms are at equilibrium distance which is equal to the sum of their van der Waals radii, a substantial energy will be required to bring them more closer (Figure 1.17 a). This is because of the repulsive forces resulting from interaction of the electronic clouds. Whereas when two

atoms are at optimum distance from each other, energy will also be required to pull them apart owing to induced dipole interactions (Figure 1.17 c).

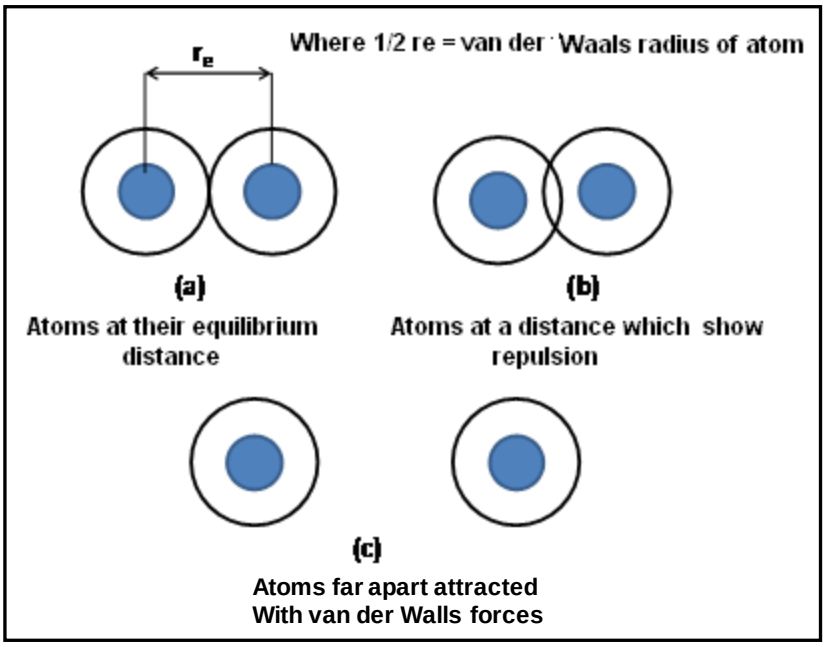

Figure1.17 Van der Waals interactions

Various potentials are employed to establish the van der Waals potential energy relationship between atoms as a function of separation distance. The Lennard-Jones potential (Smit, 1992, Verlet, 1967) is however the most efficient and computationally acceptable term which takes the following form

$$V_{lj} = 4\varepsilon\left[(\sigma/r)^{12} - (\sigma/r)^{6}\right] \qquad \textbf{Equation 1.17}$$

Herein $1/r^{12}$ represents the repulsive term which is likely to be dominated at a short distance. Whilst $1/r^{6}$ shows the attractive part which dominates more at longer distances, σ is the collision diameter at a distance where the energy is zero and ε is the magnitude of the maximum attraction energy (Jensen, 2007)(see Figure 1.18).

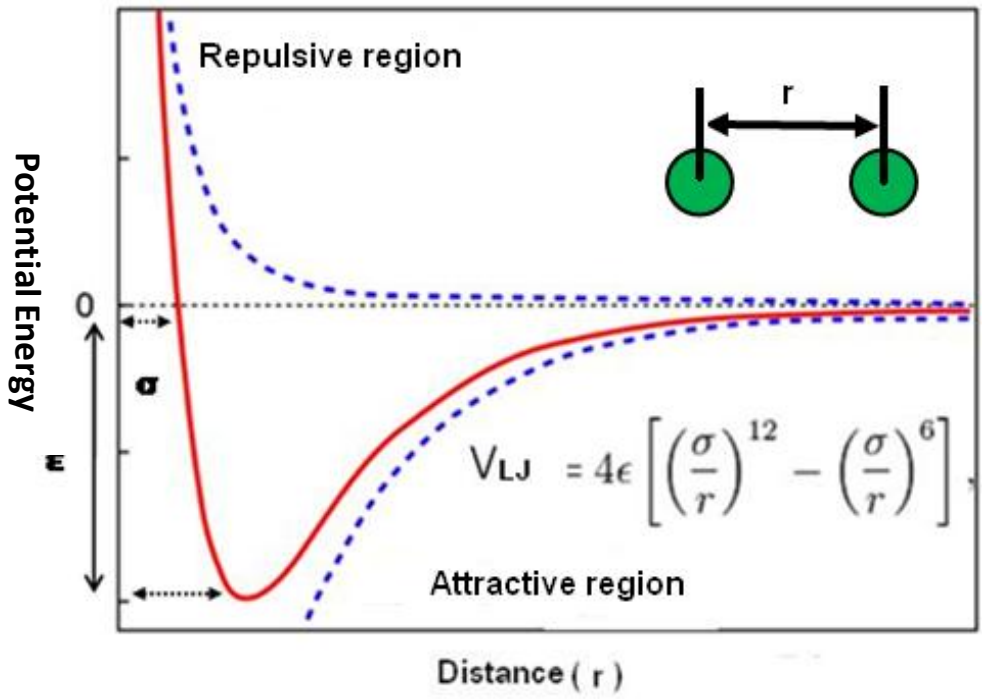

Figure 1.18 The Lennard-Jones potential.

(d) Electrostatic Potential

Atoms within molecules exist with partial charges due to different electronegativity values that result in electrostatic interactions between molecules. These forces of interactions include charge –charge interactions, charge – dipole interactions and dipole–dipole interactions. For example, in the carbonyl functional group there is a partial negative charge on the oxygen and a partial positive charge on the carbon atom. The positive head group of one molecule is attracted by negative group of the other molecule. Electrostatic potential is based on Columbic equation which takes the form:

$$U_{el} = \frac{Q_i\, Q_j}{4\pi\varepsilon_\circ r_{ij}} \qquad \textbf{Equation 1.18}$$

Where Q_iQ_j are the charges on atoms i and j respectively, ε_0 is the dielectric constant and r_{ij} is the separation distance between.

1.5.3 Molecular Simulation Methods

There are two important methods of molecular simulations: Monte Carlo and molecular dynamics simulation.

1.5.3.1 Monte Carlo Method

At the end of Second World War von Neuman, Ulam and Metropolis developed the Monte Carlo method to investigate the diffusion of neutrons in fissionable materials (Meteopolis and Ulam, 1949). This method was named after the well known casino “Monte Carlo casino” in the capital city of Monaco. This method utilises random numbers and probability to solve a range problems. This method has widespread application which includes evaluation of definite integrals in mathematics to calculations of risk in business. In molecular simulations, this method is used to determine the equilibrium structure and properties of molecular systems by moving individual atoms or molecule randomly and calculating the energy of the new configuration to assess the feasibility of the configuration. The choice of accepting or rejecting a move is based on criteria, which for molecular simulations is typically that of Metropolis(Metropolis et al., 1953). Thermodynamic properties of the system are calculated by taking the average of the physical properties of all molecular configurations generated over the entire period of simulation once the system has equilibrated.

1.5.3.2 Molecular Dynamics (MD) Simulation

During the 1970s molecular dynamic simulations received widespread attention owing to the emergence of powerful computers. Molecular dynamics simulations employ Newton’s equations of motion to generate a

trajectory of the molecular motion of interacting molecules, the interactions being described by a forcefield. At the heart of the method is Newton's second law:

$$\boldsymbol{F} = m\boldsymbol{a} \qquad \textbf{Equation 1.19}$$

F is the force acting on the atom, whereas m and a show mass and acceleration of the atoms respectively.

The most widely used integration algorithm to solve the equations of motion is Verlet algorithm which takes the following form

$$r_i(t + \Delta t) = 2r_i(t) - r_i(t - \Delta t) + \Delta t^2 \frac{\boldsymbol{F_i}(t)}{\boldsymbol{m_i}} \qquad \textbf{Equation 1.20}$$

This algorithm enables the calculation of the new positions of atoms r_i (t + Δt) at time t + Δt using the positions r_i (t) and acceleration a_i (t) at the present time t and the positions r_i (t –Δt) from previous time (t - Δt).

The initial atomic positions usually come from either by X-ray or neutron diffraction or may be generated based on intuition. In principle, if the system has no strong barriers the system should converge from any starting configuration to the equilibrium structure in the simulation.

1.5.3.3 Statistical Mechanics

The MD simulations explore the molecular level behaviour whilst our interest is primarily on the macroscopic properties of the system which include average structure and dynamics, and also thermodynamic quantities such enthalpy and free energy. The link between the microscopic level information such as atomic position and velocities and the macroscopic properties is statistical mechanics (Leach 2001). The macroscopic properties are actually the averages of microscopic properties which are obtained from the

instantaneous state of the system. In statistical mechanics, an ensemble is an assembly of all the possible configurations that a system can exist in. A configuration here is defined here as a microstate for which the atomic positions and momenta of all the atoms in the system have a given set of values. If the momentum or coordinates of one of the particles is changed, we have a new configuration. To link the microstates to thermodynamics a number of statistical mechanical ensembles have been defined, which enable the comparison of calculated thermodynamic quantities to be with real world experimental values. The important ensembles are given below:

(a) NVE; This ensemble is also called microcanonical ensemble where the number of atoms (N), volume (V), and energy (E) are fixed.

(b) NPT; Isobaric –isochoric ensemble (in this ensemble the number of atoms (N), pressure (P) and temperature (T) are fixed. This corresponds to experiments at constant temperature and pressure.

(c) NVT ; Canonical ensemble (a system where the number of atoms (N), volume (V) and temperature (T) are constant.

(d) NST; This ensemble is characterised as a system where (a number of atoms N, stress σ and temperature T are kept constant)

1.5.3.4 Simulation Cell and Periodic Boundary Conditions

In MD simulations the atoms to be simulated are contained in a three dimensional container which is termed a simulation cell. Such a simulation cell does not have solid interacting walls and hence has surfaces. Therefore the collection of molecules contained in the cell will be exposed to vacuum. For a typical simulation, the volume element comprising the molecules will be

small and surface effects will dominate. In view of this the molecular system being simulated cannot be seen as bulk. To remove surface effects, the simulation system has periodic boundary conditions wherein the cell is effectively replicated all round the original simulation cell. Figure 1.19 shows a simulation cell with a dark background surrounded by eight identical cells which are formed by replication of the central simulation cell. Each of these cells contains periodic images of the atoms present in the original simulation cell. If some of the atoms leave the central simulation cell they re enters to the central simulation cell from the replicate cell at the opposite side. For example in Figure 1.19 the simulation cell shown with red lines does not have atoms 1 and 2 but atoms 1' and 1' which are images of the 1 and 2 re enters from the left side. Nonetheless PBCs can cause complication where, for example, an atom interacts twice either its own image or the same atom. An interaction cut off radius r_{cut} is considered to be important to overcome this problem. The interaction cut off should not be more than half of the dimension of the simulation cell. Cut off radius plays an important role in MD simulation to minimise the necessary calculations with subsequent accurate model (Leach, 2001).

During MD simulations the particles move by a time stepping procedure which is based on a characteristic time step. The simulation time step should neither be too small nor large, because a small time step will require a large number of steps to sample a trajectory of a system for a fixed time period. Whilst using too large time step can cause high energy overlaps between atoms with consequent instability of the system (Leach, 2001). Constraints can be employed to fix the bond lengths and angles of flexible molecules to

allow the users to run a simulation for a large time step. The bond stretching frequencies and bond angle bending frequencies are of the order of $30ps^{-1}$ and $10ps^{-1}$respectively. Therefore to eliminate the high frequency components of the molecules, the bond lengths are often constrained (Van Gunsteren and Karplus, 1982) . As a result of this, the time step for integrating equations of motion can be increased with consequent improved efficiency of the MD simulation.

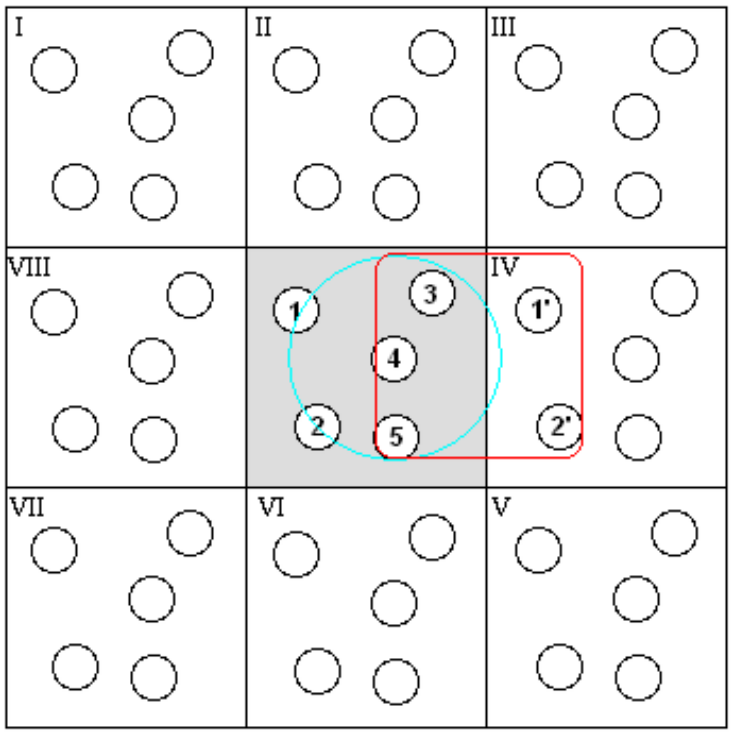

Figure 1.19 Simulation cell showing periodic boundary conditions in two dimensions. The central shaded box is surrounded by its periodic images. In the central box there are five molecules and the sky blue circle shows cut off for interaction. If some molecules for example 1 and 2 leave the central box then the counterparts (1' and 2') renter from the surrounding box.

1.6 Molecular Simulation of Crystal Growth and Nucleation

It is extremely difficult to investigate the crystal nucleation and growth, particularly the earliest stages of crystallisation, at the molecular level using experimental approaches. Molecular dynamics simulations can therefore be

employed to investigate the mechanics of crystallisation processes (Anwar and Boateng, 1998). According to classical homogeneous nucleation theory, the formation clusters of solute molecules occur before nucleation (Bennema, 1974). It has been inferred from experiments that order in solute molecules occurs prior to nucleation and crystal growth (Sohnel and Garside, 1988, Larson and Garside, 1986). There have been different arguments towards the structure of prenucleation clusters. Weisbuch (1994). Ya and Velikov have concluded that the arrangement of molecules within the prenucleation clusters were similar to that associated with the newly formed crystals. However other researchers do believe that composition and structure of the prenucleation clusters are rather different than the eventual crystalline phase of the compound (Oxtoby, 1998). To date, there is little proper understanding to investigate the origin of secondary nucleation (Myerson, 2002a). In addition, the effect of impurities and additives on crystallisation is still the focus of experimental studies. It is possible that the nucleation process could be promoted, inhibited or retarded by appropriate additives (Weissbuch et al., 2003). Nucleation in solution is followed by crystal growth which involves different processes in bulk solution, adsorption layer near to the crystal surface and crystal surface itself. For example diffusion of solute molecules to the adsorbed layer around the crystal surface and subsequently incorporation of the adsorbed molecules into the crystal lattice (Weissbuch et al., 2003). Hypotheses which include surface roughening and solvent adsorption on crystal surface have been reported to influence the molecular level interactions and the effects of solvent on crystal growth (Bourne et al., 1978). However explanation of these mechanisms still remains challenging

using experimental approaches. MD simulations have therefore been employed to investigate the interaction of solvents at crystal surfaces (Hussain and Anwar, 1999), processes in adsorption layer near to the crystal surface (Huitema et al., 1999) and crystal growth and dissolution (Piana and Gale, 2005, Cheong and Boon, 2010)

1.7 Simulation Approaches to Nanocrystal Stability and Phase Transformation

Stability of nanocrystals has become a major hurdle in exploiting their special properties. In this regards molecular simulations could help to improve the methodology for nanoparticle production. As the crystal size decreases its surface area and interfacial free energy increase compared to its bulk free energy which can result in aggregation and crystal growth in suspension. Typically a range of experiments are employed to rationalise surfactants and polymers for stabilisation of nanocrystals in a required phase. Molecular simulation could be used to ascertain the key factors and develop strategies for stabilisation.

Phase stability is another issue associated with nanocrystals. When a particle size is reduced, the surface free energy becomes more significant and the difference in surface energies between different polymorphic forms could determine which phase is the stable one on the nanoscale range. Thus a particular phase could be stable in the bulk and yet be unstable in the nanoscale range. The effect of size particularly at the scale down to nanocrystals on phase stability has been investigated for a number of compounds including TiO2, ZrO2 and Al2O3 (Ranade et al., 2002, McHale et al., 1997, Garvie, 1978). The key issue with the observed nanocrystal phase

is however to investigate whether this is just a highly metastable phase or it is thermodynamically the real stable phase. Molecular simulation approaches could be used to calculate both the surface and bulk free energies to address this issue (Anwar and Zahn, 2011).

1.8 Aims and Objectives

Crystalline nanosuspensions have been identified as a promising technology to address poor solubility issues, although several challenges including stabilisation and control of particle size distribution for nanosuspensions and scale up issues still need to be addressed. Much of earlier studies used high energy nanoparticle preparation methods and these have particular issues. The intention of this study was to revisit the simplest approach of re-precipitation and to identify the critical parameters including effect of stabilisers types and concentration as well as process conditions. We utilise a combined approach of both experiments and molecular modelling and simulation not only to determine the optimum parameters but also to gain mechanistic insight. The experimental studies utilised the three rather distinct, relatively insoluble drugs, the hypoglycaemic glibenclamide, the anti-inflammatory ibuprofen, and the anti-malarial artemisinin. These drug molecules were chosen as they all could potentially benefit in terms of their bioavailability from being formulated as nanocrystals. Recovery of nanocrystals in the solid form from nanosuspensions is also a technical challenge. The goal is is to recover the nanocrystals in the dry form which when incorporated in a solid dosage form can yield the near original nanocrystal characteristics e.g. dissolution rate. We have developed a

method that utilises large single crystals as carriers for adsorbing nanocrystals from nanosuspension.

Crystallisation of the drug molecules occurs by nucleation which is the key step to control the particle size distribution and size of the crystal. As this process takes place at atomistic level which is difficult to be visualised using experimental approaches (Schüth et al., 2001). Computer simulation approaches including Monte Carlo and molecular dynamics simulation have been used to investigate this process. However these methods are limited only to crystallisation processes which take place from melt. Also large cpu usage and long simulation time is required which limit these methods. In view of this the coarse grained molecular dynamics simulation method was employed to explore the earliest stages of the anti-solvent precipitation.

The phase stability of nanocrystals was investigated using molecular simulation for the model compound glycine (Chapter 5). Phase stability of nanocrystals is a challenge to investigate since nanocrystals can persist in metastable states and it becomes difficult to identify whether the stabilized phase is thermodynamically stable or metastable because of large barriers (Zahn & Anwar, Chem. Eur. J. 2011, 17, 11186 – 11192). The stability of the glycine crystals was investigated for both bulk and nanocrystals as function of both temperature and pressure.

Chapter 2

Nanocrystal Preparation: Low-Energy Precipitation Method Revisited

2.1 Introduction

Nanocrystals and their composites can exhibit markedly different properties with respect to bulk phases and hence offer new opportunities (Moriarty, 2001, Parak et al., 2003, Horn and Rieger, 2001, Paul and Robeson, 2008, Choi and Awaji, 2005). For pharmaceuticals, nanocrystals promise to resolve the issue of poor bioavailability of poorly soluble drugs (Rabinow, 2004, Müller and Keck, 2012, Müller et al., 2011b, Müller et al., 2011a, Gao et al., Jinno et al., 2006, Merisko-Liversidge et al., 1996). The immense surface area of the particles, increased saturation solubility, and the decreased diffusional pathway adjacent to the nanocrystal surface all converge to enhance the bioavailability (Müller et al., 2011a, Buckton and Beezer, 1992, Wu and Nancollas, 1998, Moeschwitzer and Mueller, 2006, C.M. Keck, 2010). The difficulty in exploiting this technology is the technical challenge of generating and stabilising nano crystalline products. Nanocrystals can be prepared by a variety of methods, which in general terms can be categorized

as comminution (top down) or controlled precipitation (bottom up) (Müller et al., 2011a). Although the technology is maturing, there are still important issues and limitations. Top down processes which include milling (Merisko-Liversidge et al., 2003, Peltonen and Hirvonen, 2010, Plakkot et al., 2011) and high pressure homogenization (Majuru and Oyewumi, 2009, Zhang et al., 2007) usually require long processing times, high energy input, and tend to yield a broad particle size distribution. There is also a concern with regards to contamination of the products from the milling media (Keck and Müller, 2006) . With respect to the precipitation methods, there are many variants including simple precipitation (Chan and Kwok, 2011, Matteucci et al., 2006, Hu et al., 2010), spray freezing into a liquid(Williams et al., 2002, de Waard et al., 2008) precipitation from a supercritical fluid using an anti-solvent (Tom and Debenedetti, 1991, Cansell et al., 2003, Byrappa et al., 2008), and microfluidics (Panagiotou et al., 2009, Ali et al., 2011, Panagiotou et al., 2007). Precipitation has also been employed in combination with homogenization (Kipp et al., 2003). The major limitations with precipitation are considered to be uncontrolled particle growth which has resulted in its adoption for only a few selected molecules (Gao et al., 2008, Müller et al., 2001).

Top-down technology for nanocrystal preparation has undergone rapid innovation with recently emerging methods such as Baxter's NANOEDGE technology being termed as 2nd generation methods (Müller and Keck, 2008). Furthermore these methods have been actively adopted by the pharmaceutical industry with an increasing number of commercial products supplemented by those in development pipelines (Rabinow, 2004). In

contrast, the precipitation approach has had relatively little interest with only a handful of publications (Chan and Kwok, 2011) and to our knowledge, no commercial exploitation, which raises some questions. Do precipitation methods suffer from major technical challenges? Are such methods unable to reproducibly yield crystals in the low nanometre range? Do the resulting nanocrystals show physical instability? The simple precipitation method is patented under the trade name Hydrosol, the patent being owned by Sandoz/Novartis (List and Sucker, 1995) which might act as a barrier to further commercial interest. As for the lack of exploitation, could it be that the patent holders do not have appropriate applications? Or have they encountered significant technical challenges?

Here we revisit the precipitation method in its simplest form, re-precipitation using an anti-solvent without any high-energy input (no high speed shear mixing or sonication, just a stirrer). Probably the major perceived limitation of precipitation approaches is that they may work for some specific molecules but are not general, being unable to accommodate a wide range of molecules. The implication is that the few published studies present only the successes. We report a systematic study where we have prepared stable crystalline nanocrystals with uniform size distributions by precipitation of three rather distinct (see molecular structures in Figure 2.2) relatively insoluble drugs including the hypoglycaemic glibenclamide, the anti-inflammatory ibuprofen, and the anti-malarial artemisinin.

These drug molecules were chosen as there is potential to enhance the rate and/or extent of drug absorption through presentation in the form of nanocrystals. No other molecules were considered and hence there are no

unreported ‘failures’. For each of the drug molecules, systematic experiments have been carried out to identify the key formulation and process variables that influence the particle size and the physical stability of the resulting nanosuspensions. What becomes clear is that the challenge is physico-chemical rather than mechanical, involving the identification of molecule-specific crystal growth inhibitors and/or stabilizers, an issue which appears to be at the heart of preparing stable nanocrystals irrespective of how they are generated (Van Eerdenbrugh et al., 2008, Verma et al., 2010, Wu et al., 2011, Lindfors, 2004). To identify what determines the choice of stabilizer(s) for a particular compound it is necessary to understand their mechanism of action. Towards this particular objective we have attempted to rationalise the molecular interactions at the dominant crystal surfaces with the inhibitors/stabilizers and carried out molecular modelling studies using Material studio software.

2.2 Materials and Methods

2.2.1 Materials

Glibenclamide (Batch No: PPC/08/GLB/057) was purchased from Anzen Exports Kolkata India. Ibuprofen (Batch No: 7050-1077) was purchased from Anzen Exports Kolkata India Hypromellose USP (hydroxypropylmethylcellulose) (Batch No: 7068037, 8028213, grades: 605 and 615 and viscosity: 6cps and 15cps) were obtained from Shin-etsu-Japan Chemical Ltd. PVP K-30 (Batch No: 08297047GO) was provided for free by BASF Germany. PEG-400 (Catalogue No: P/3676/08 and Batch No:

0742478) was purchased from Fisher Scientific UK limited. Acetonitrile (Catalogue No: A/0626/17 and Batch No: 0809411) was purchased from Fischer Scientific. Ammonium di hydrogen phosphate monobasic, (Catalogue No: 1382384 and batch number: 09717), progesterone (Catalogue No: 1262521 and Batch No: 81702), calcium phosphate dibasic (Catalogue No: C7263-500G and Batch No: 047K0035), monobasic potassium phosphate >99% (Catalogue No: P5655 and Batch No: 097K0067) and calcium phosphate dibasic (Catalogue No: C7263-500g and Batch No: 047K0035) were purchased from Sigma Aldrich. NaOH pellets (Catalogue No: B882848 127 and Batch No: 301675N) were purchased from BDH Laboratory England. Sodium deoxycholate (NaDC) (Batch No: D6750), pluronic F127 (Batch No: 038K0113) and pluronic F68 (Batch No: 018K0029) were purchased from Sigma Aldrich. Copper grid (200 mesh) coated with Formvar/Carbon (Code No: S162) purchased from Agar Scientific. Artemisinin (Batch No: 100916, supplier: Chengdu Wagott Pharmaceutical Co, Ltd) was gifted by Institute of Material Medica China.

2.2.2 Methods

2.2.2.1 Preparation of Glibenclamide, Iburprofen and Artemisinin Nanosuspensions

The methodology is based on standard precipitation using an anti-solvent (Figure 2.1). The drug is dissolved in a solvent and then injected at a defined rate into the anti-solvent (being water for the three drug substances investigated) containing growth inhibitors/stabilizers. For each drug, a series of precipitations were carried out at a millilitre scale (batch size: 3ml) to

identify the most appropriate stabilizers and process conditions (temperature, agitation rate and infusion rate) to yield stable nanocrystals. For the 3ml batch size, the amount of anti-solvent stabilizer solution was 2.7ml while the solvent solution was 0.3ml. The respective solvent solutions comprised ibuprofen at a concentration of 30 mg/ml in ethanol (0.3ml),

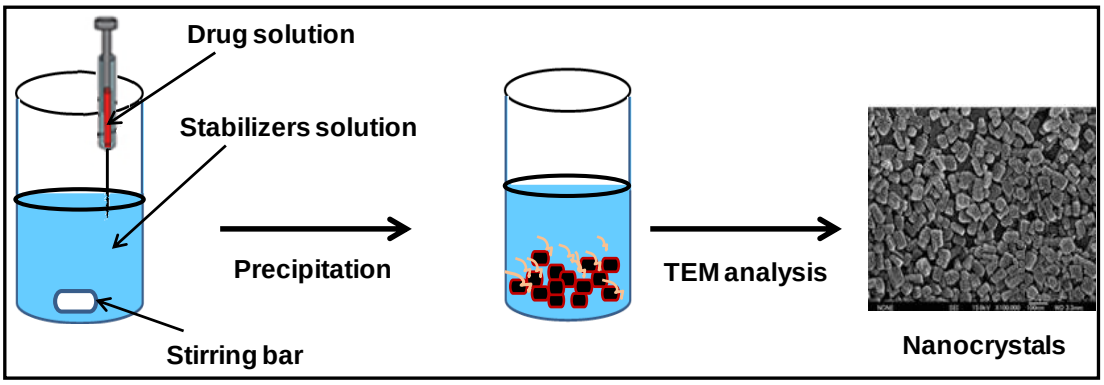

Figure 2.1 Schematic representation of a typical antisolvent method

glibenclamide at 5 mg/ml in polyethylene glycol 400 (PEG400), and artemisinin at 15 mg/ml in ethanol. Stabilizers investigated included hydroxypropylmethylcellulose (HPMC), polyvinylpyrrolidone (PVP K30), sodium deoxycholate (NaDC), Pluronic F68, Pluronic F127, Tween 80, sodium lauryl sulphate (SLS), soya lecithin and miglyol (triglyceride). Structures of some of these are given in Figure 2.2.

Once the stabilizers were identified for each drug, the effect of the three crystallization process conditions, temperature, agitation rate, and infusion rate, was investigated using a factorial design at two levels for each of the three drugs. The temperature of the crystallization vials was controlled at either 25°C or 40°C, the agitation rate at 600 rpm or 1200 rpm, and the infusion rate of the anti-solvent solution was set at 60 or 100 ml/minute. A set

of eight experiments shown in Table 4.1 was employed for nanosuspensions of the three drugs.

To assess the scalability of the process, batch sizes of 10, 100 and 400 ml were manufactured for each of the drugs using the optimum formulation and process.

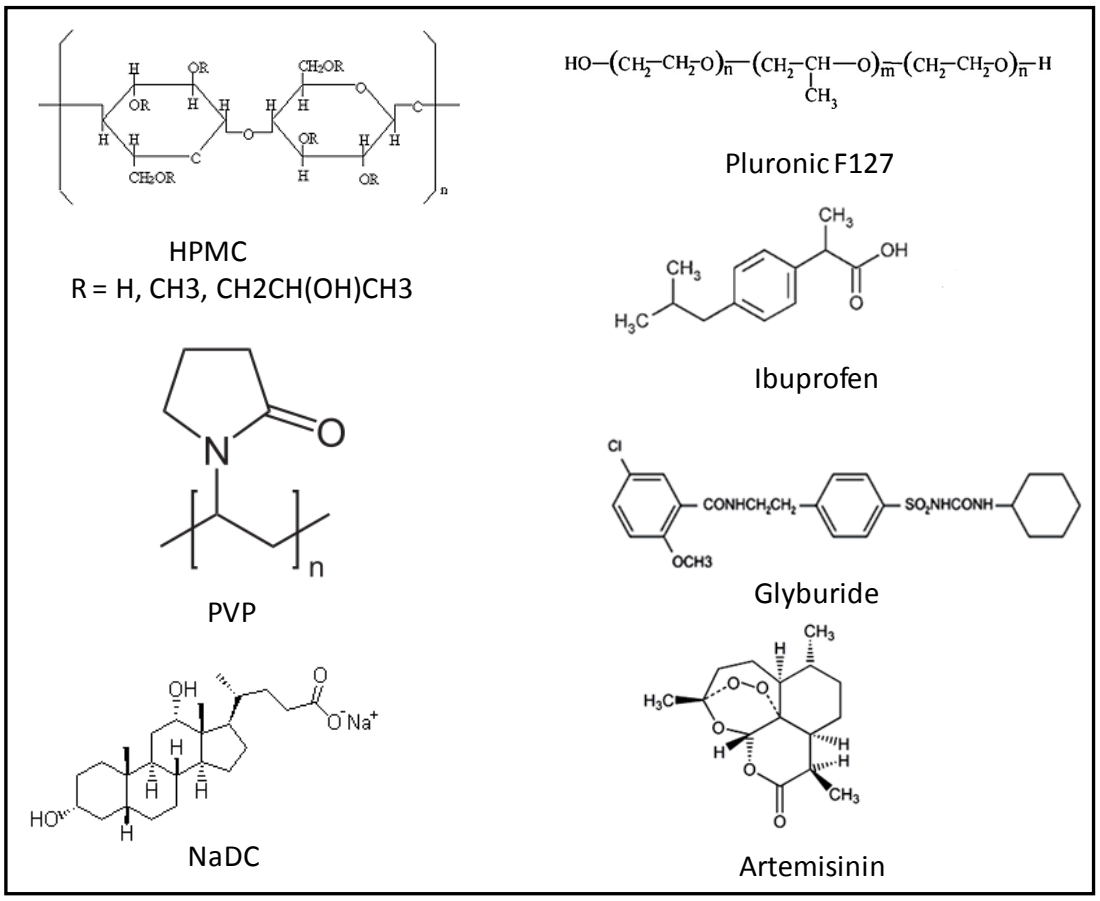

Figure 2.2 Molecular structures of APIs, and some of the surfactants and polymers used in this study.

Table 2.1. Full factorial design for the preparation of ibuprofen, glibenclamide and artemisinin nanosuspensions under controlled process variables. Temperature: (+ = high = 40 0C and - = low= 25 0C), Stirring rate: (+ = high =1200rpm) and - = low = 600rpm). Infusion rate: (+ = high = 100ml/minute and - = low = 50ml/minute)

Batch No	Mixing Temperature (°C)	Infusion Rate(ml/minute)	Stirring Rate(ml/minute)
1	+	+	+
2	-	-	-
3	+	-	+
4	+	-	-
5	-	+	+
6	-	+	-
7	+	+	-
8	-	-	+

2.2.2.2 Particle Size Measurements

The particle size of the nanocrystals was determined using at-line measurements with the Malvern Zetasizer Nano-Zs dynamic light scattering (DLS) instrument (Malvern Instruments, UK). The mean particle size was determined from three measurements. NanosphereTM (Catalogue no; 3060A, mean diameter 59.0nm±2.5) and duke standard TM (Catalogue no; 8050, diameter 500.0nm±0.02) were used to calibrate performance of the Zetasizer.

2.2.2.3 Particle Morphology

Evaluation by scanning electron microscopy (SEM) of raw ibuprofen, glibenclamide and artemisinin drug substances was carried out using a Quanta 400 SEM (FEI Company, Cambridge, UK) to produce photomicrographs at a range of magnifications. Sample preparation involved fixing of raw ibuprofen, glibenclamide, and artemisinin to a metal stub with the aid of double sided adhesive tape. The scanning electron microscopy

(SEM) instrument was calibrated with a gold grid supplied with the instrument. Sample preparation for transmission electron microscopy (TEM) involved deposition of a single drop of the nanosuspension onto a 200 mesh copper grid coated with Formvar/Carbon (code no S162) followed by drying at ambient temperature. The sample was then negatively stained using 2% magnesium uranyl acetate solution because of its low conductivity. Transmission electron microscopy (TEM) was then carried out by loading the sample on transmission electron microscope at 120KV.The TEM used was (JEM-1200EX, Japan Electron Optics Laboratory Corporation Japan).

2.2.2.4Determination of melting point and heat of fusion by DSC.

Differential scanning calorimetery (DSC) of the unprocessed and processed glibenclamide, ibuprofen and artemisinin was carried out using the DSC module of the TA instruments Q2000 Series Thermal Analysis system (TA Instrument West (UK). Indium (99%, melting point 156.6) was used to calibrate the DSC and performance was confirmed using a zinc standard with a melting point of 419.50 °C. The unprocessed and processed samples of glibenclamide and artemisinin were then scanned under a stream of nitrogen gas at a flow rate of 50ml/minute from 25 – 200 °C. Whilst processed and unprocessed ibuprofen samples were scanned from 0°C to 110 °C, using heating rate 10 °C /min. All samples were analysed in triplicate.

2.2.2.5 Powder x-ray Diffraction (PXRD)

The crystallinity of the nanocrystals was assessed by powder X-ray diffraction (PXRD) (and DSC, see above) using dried powders recovered from the nanosuspensions by centrifugation at 14500 rpm for 60 minutes and

drying under ambient conditions. PXRD studies were carried out using a Bruker D-8 powder diffractometer (Bruker Kahlsruhl, Germany). For the nanocrystal samples we employed a silicon-well sample holder, whilst for the original raw drug material a plastic sample holder was used. Calibration of the PXRD was carried out using a corundum standard. The samples were scanned in triplicate over the range 5-50° 2θ at a rate of 1º 2θ/min using a copper Kα radiation source at a wavelength of 1.542 Å and with 1 mm slits.

2.2.2.6 Stability Studies

The stability of nanosuspensions was monitored for one month at the three different temperatures, 4°C, 25°C, and 40°C, to establish the extent of particle growth through agglomeration and Ostwald ripening. Particle size measurements of the stored nanosuspensions were conducted at regular time intervals over the one month period (0, 5, 10, 15,20,25,30 days) using DLS. The drug content was also analyzed at regular intervals using a Waters 2695 HPLC system connected to a UV detector. The Ultra II TM C18 5µm 250×4.6mm column was used at a temperature of 30°C. The solvent system used as the mobile phase for glibenclamide assay consisted of monobasic ammonium phosphate (0.02M) and acetonitrile at a ratio of 45:55 v/v. The mobile phase for ibuprofen consisted of 50:50 v/v acetonitrile and water at PH 2.5 adjusted with orthophosphoric acid. The flow rate of the mobile phase was set at 1.5 ml/min and 1 ml/min for glibenclamide and ibuprofen respectively. The mobile phase used for artemisinin was 60/40 v/v acetonitrile and water at a flow rate of 1 ml/minute. The wavelength of the UV detector was set at 254 nm, 214 nm and 216 nm for glibenclamide, ibuprofen, and artemisinin, respectively.

2.2.2.7 Dissolution Rate Testing

The dissolution rate of the glibenclamide nanocrystals was compared with a glibenclamide microsuspension (mean particle size ~5µm) prepared by crushing and sonication of a marketed 5mg glyburide tablet (Glibenclamide (UK name) 5mg tablets, batch no. 9A06HL, manufacturer Teva UK Ltd) in a liquid medium composed of 1% HPMC and 1%PVPK-30. Nanosuspension dissolution was also compared to that of the intact marketed 5mg glyburide (glibenclamide) tablet. Dissolution rate of the ibuprofen nanocrystals was compared with micronized ibuprofen powder of mean particle size ~9µm, and a 200mg ibuprofen marketed tablet (Ibuprofen 200mg tablets, Batch no. LL11845, manufacturer Wockhard Ltd UK). The dissolution rate of artemisinin nanocrystals was compared with micronized artemisinin powder of mean particle size ~2µm. The dissolution rates were monitored using the USP apparatus 2 (paddle method) at 75 rpm. The dissolution medium for glibenclamide was phosphate buffer pH= 7.5 whilst for ibuprofen it was phosphate buffer at pH 7.2. The dissolution rate of artemisinin nanocrystals was determined in distilled water at 200 rpm using the method reported in reference (Kakran et al., 2010).

For all determinations the temperature was set to 37°C ± 0.3°C. 5mL aliquots were collected using a syringe filter (0.02 µm) at 0, 2, 6, 10, 15, 30, 45 and 60 minutes after addition of the formulations to the dissolution vessels. We noted that the filter allowed nanocrystals below 20 nm to pass resulting in some overestimate of drug dissolution. The size of syringe filter has been employed previously by others for dissolution studies of nanosuspensions (Sylvestre et al., 2011, Shekunov et al., 2006, Pardeike et al., 2011,

Jünemann and Dressman, 2012). However, the expectation is that particles < 20 nm size crystals are likely to dissolve almost immediately in the dissolution test. After each sampling time the dissolution media was replenished with 5ml of fresh dissolution medium. The aliquots were analyzed for the drug using a reverse phase high performance liquid chromatography (RP-HPLC) method, as detailed above.

2.2.2.8 Effect of Supersaturation on Particle Size

The effect of supersaturation on nanocrystal size was investigated by carrying out a series of preparations using the optimum formulation and process at different temperatures (5, 15, 25, 35 and 45°C) for which the supersaturation was estimated from determined solubilities of the drugs in the final vehicles. Use of temperature to vary the supersaturation rather than varying the concentration of the drug in the solute has the advantage of sampling a wider range of supersaturations, since the upper limit of solute concentration is fixed. Also, increasing the drug concentration would require associated changes in concentration of the stabilizers.

The equilibrium solubility of glibenclamide, ibuprofen, and artemisinin in each of the final suspension vehicles was determined by stirring an excess of amount of the drug in a vial containing 10ml of the respective vehicle at the temperatures 15°C, 25°C, 35°C and 45°C (temperature control $\pm$ 2°C) and an agitation rate of 200 rpm for 48 hours. All the samples were filtered through 0.22µm filter and analyzed using HPLC.

2.2.2.9 Identification of the Molecular Interactions at the Dominant Crystal Surfaces

The crystal morphology of the three drugs was predicted using the molecular modelling software Materials Studio 4.1 based on the attachment energy model (Materials Studio software package). We employed the CVFF force field with force-field assigned charges (Maple et al., 1994). This force field has been found to be effective for a large number of drug materials, being able to reproduce the crystal structures to a better than 5% deviation in their lattice parameters (Shariare et al., 2012). The goal here was not to accurately predict the crystal morphology but rather to identify the major crystal surfaces that are likely to dominate the crystal morphology and then to explore the molecular interactions characterising these surfaces. The dominant crystal surfaces of the three drugs were examined visually with a view to rationalising the molecular interaction of the surface with crystal growth inhibitors/stabilizers.

2.3 Results and Discussions

2.3.1 Preparation of Ibuprofen, Glibenclamide and Artemisinin Nanosuspensions

For all three drug molecules we were able to prepare stable nanocrystals using the simple anti-solvent precipitation technique, wherein the drug was dissolved in an appropriate solvent and then injected using a syringe into a stirred vial containing aqueous solution of growth inhibitors/stabilizers (the anti-solvent). The distinctiveness of the molecules revealed itself in the choice of the growth inhibitors/stabilizers and the ultimate nanocrystal size distribution obtained. For ibuprofen the effective growth inhibitors/stabilizers

were hydroxypropylmethylcellulose (HPMC 15cps) and Pluronic F127 (1% w/v concentration) (Table 2.2). The nanocrystals obtained had a particle size of 92 ± 2.5 nm and a polydispersity index of 0.15±0.01 (Figure 2.3 (b)). Glibenclamide nanocrystals required a combination of HPMC (15cps) and PVPK-30 (1%w/v) (Table 2.3) with the HPMC (15cps) + Pluronic F127 combination being ineffective. The particle size and PDI values obtained for glibenclamide nanocrystals were 298nm ± 3.5 and 0.2 ± 0.02 respectively (Figure 2.3(a)). Artemisinin was more challenging and the surfactants and polymers employed for ibuprofen and glibenclamide were not found to be effective. The eventual optimum choice was sodium deoxycholate (NaDC) (0.2%w/v), Pluronic F127, and PVPK-30 (0.5%w/v) (Figure 2.4), which yielded nanocrystals of size 400.0 ± 3.5 nm, which are larger than the size range obtained for ibuprofen and glibenclamide (Figure 2.3 (c)).

To gain a better understanding of the re-precipitation process, we attempted to identify the critical process parameters using a full factorial design involving the variables stirring rate, temperature, and infusion rate, each at two levels (Table 2.5). Evaluation of the process parameters and interactions indicated that low temperature (25°C), high stirring rate (1200 rpm), and high infusion rate (100 ml/min) were necessary to achieve minimal particle size. Similar results have been reported previously (Lindfors, 2004). Each of these factors can increase the local supersaturation, which we believe is the main consequence in each case. For instance, high stirring and infusion rate enhance micro-mixing between the two phases, maintaining high local supersaturation (Matteucci et al., 2006). Lower temperature reduces the drug solubility, again enhancing supersaturation. The increased local

supersaturation is considered to increase the number of nuclei formed hence minimising the amount of solute available for subsequent crystal growth (Zhang et al., 2009).

Table 2.2. Effect of different stabilisers on particle size of Ibuprofen nanocrystals.

Stabilisers	Particle Size (nm) ± SD						
	Day 0	**Day 5**	**Day 10**	**Day 15**	**Day 20**	**Day 25**	**Day 30**
1% PLURONIC F-68	292 ±3.5	340 ±4.5	375 ±2.5	400 ±3.0	460 ±5.0	485 ±2.0	550 ±5.0
1% PVP + 1% HMPC(6cps)	475 ±4.5	502 ±3.2	542 ±4.0	578 ±2.5	600 ±3.5	625 ±2.0	654 ±2.5
0.5% HPMC (15cps)+ 0.5% PVP+ 0.2%SLS	180 ±5.0	200 ±4.0	245 ±4.5	300 ±5.0	333 ±2.5	340 ±2.0	385 ±2.5
1% HPMC (15)+ 1% PVP+ 0.5%SLS	160 ±3.5	185 ±4.2	190 ±4.0	195 ±3.5	225 ±3.0	265 ±2.5	285 ±2.0
1% Pluronic F-68 +0.5%PVP +0.5%SLS	396 ±2.5	400 ±3.5	415 ±4.0	425 ±4.5	440 ±4.0	500 ±3.0	525 ±3.5
1% HPMC (15cps) +1%Pluronic F-127	92 ±3.0	95 ±2.5	100 ±2.0	102 ±3.0	105 ±3.5	108 ±2.0	110 ±2.5
1% PVP	325 ±3.5	350 ±4.5	375 ±5.0	400 ±3.5	500 ±2.0	525 ±2.5	585 ±2.5
1% HPMC(15cps)	200 ±5.5	225 ±4.5	245 ±4.0	285 ±3.5	300 ±3.0	310 ±3.0	325 ±2.0
1% Pluronic F-127	320 ±4.5	330 ±4.0	340 ±4.0	365 ±3.5	385 ±3.0	415 ±2.5	425 ±2.5
0.5%PVP+0.5%HPMC(15cps)	550 ±5.2	565 ±5.5	585 ±5.0	590 ±4.5	610 ±4.0	620 ±3.0	630 ±3.0
1.0%PVP+0.5%HPMC (15cps)	630 ±6.0	645 ±5.2	660 ±4.0	685 ±4.5	702 ±3.5	710 ±3.0	725 ±3.5

We explored the possibility of scaling up from the 3ml quantities employed for the precipitation studies and prepared batches of 10, 100, and 400 ml quantities. The nanocrystal sizes obtained from these batches were similar to those achieved in small scale experiments. Furthermore, stability and dissolution rates were also essentially unchanged. We do not see any significant challenges in scaling up beyond 400ml but the process will require a chemical engineering approach to maintain maximum mixing of fluids at the saturated solution/anti-solvent interface and efficient heat transfer involving the possible use of multiple nozzles.

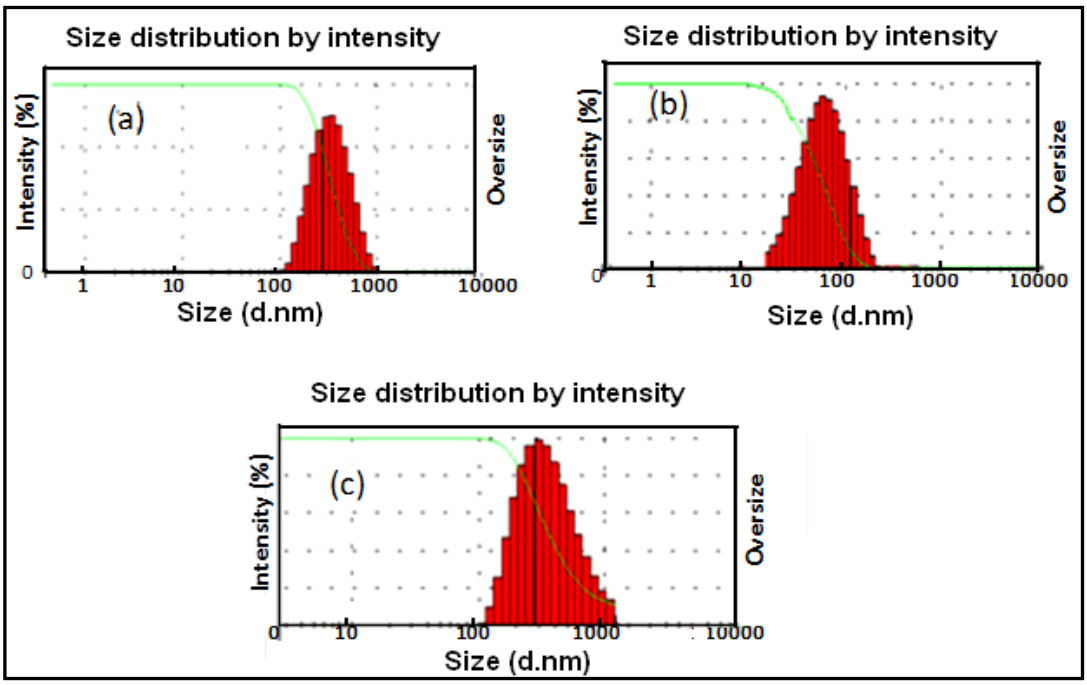

Figure 2.3 Particle size distribution of (a) glibenclamide; (b) ibuprofen and (c) artemisinin

Table 2.3. Effect of different stabilisers on particle size of Glibenclamide nanocrystals

Stabilisers	Particle Size (nm) ± SD						
	Day 0	Day 5	Day 10	Day 15	Day 20	Day 25	Day 30
1% HPMC (15cps)	400 ±2.5	490 ±4.5	546 ±3.5	615 ±3.0	700 ±4.0	950 ±2.0	1000 ±3.0
1% HPMC (6cps)	500 ±4.5	600 ±5.2	685 ±4.0	780 ±3.5	915 ±3.5	1045 ±4.0	1200 ±2.0
0.5%PVPK-30 +0.5% HPMC (6cps)	375 ±5.0	400 ±5.5	475 ±3.0	502 ±2.5	545 ±2.5	675 ±3.0	845 ±2.0
0.5% HPMC (6cps)+ 0.5% PVPK-30+ 0.2%SLS	340 ±3.5	360 ±4.2	385 ±4.0	450 ±3.5	500 ±3.0	525 ±2.5	580 ±2.0
1% HPMC (6cps)+ 1% PVPK-30+ 0.5%SLS	320 ±2.5	330 ±3.5	350 ±4.0	425 ±4.5	440 ±4.0	500 ±3.0	1605 ±3.0
1% PVPK-30	520 ±3.0	575 ±2.5	665 ±2.0	789 ±3.0	1000 ±3.5	1500 ±2.0	110 ±2.5
0.5%PVPK-30+0.5%HPMC(15cps)	315 ±3.5	335 ±4.5	345 ±5.0	360 ±3.5	385 ±2.0	400 ±2.5	405 ±3.5
1.0%PVPK-30+0.5%HPMC(15cps)	300 ±5.5	310 ±4.5	326 ±4.0	340 ±3.5	360 ±3.0	370 ±3.0	378 ±3.0
1.0%PVPK-30+1.0%HPMC(6cps)	305 ±5.5	325 ±4.0	350 ±4.0	365 ±4.5	372 ±3.0	385 ±3.5	390 ±2.5
1% HPMC (15cps) +1%PVPK-30+ .3%Miglyol	290 ±5.2	300 ±5.2	320 ±4.2	365 ±4.5	375 ±4.0	390 ±2.5	400 ±3.0
0.5% HPMC (15cps) + 0.5% PVPK-30 +0.3% Miglyol	300 ±6.5	320 ±4.0	340 ±3.5	360 ±5.0	370 ±4.0	385 ±3.0	415 ±2.5
1%HPMC (6cps)+ 1%PVPK-30+0.3% Miglyol	305 ±4.0	330 ±3.5	350 ±5.0	365 ±4.0	375 ±3.0	390 ±2.0	400 ±3.0
1%HPMC (15cps)+ 1%PVPK-30	298 ±3.5	330 ±4.0	326 ±3.0	331 ±4.2	333 ±2.5	336 ±3.0	338 ±3.5

Table 2.4. Effect of different stabilisers on particle size of artemisinin nanocrystals

Stabilisers	Particle Size (nm) ± SD						
	Day 0	**Day 5**	**Day 10**	**Day 15**	**Day 20**	**Day 25**	**Day 30**
0.2%Pluronic F127+0.2%PVPK-30+0.1%NaDC	570 ±2.0	602 ±4.5	645 ±3.5	685 ±4.0	715 ±5.0	785 ±2.5	815 ±3.0
0.5%Pluronic F127+0.5%PVPK-30+0.2%NaDC	400 ±3.5	412 ±3.2	420 ±4.0	434 ±4.5	442 ±3.5	450 ±3.0	455 ±2.0
0.5%HPMC+0.5%PVPK-30+0.1%NaDC	1000 ±5.0	1140 ±5.5	1300 ±3.0	1420 ±4.0	1700 ±2.5	1825 ±3.0	1980 ±2.0
0.5%Pluronic F127+0.5%PVPK-30+0.1%NaDC	463 ±3.2	488 ±4.2	503 ±4.0	515 ±3.5	522 ±4.0	530 ±2.5	538 ±2.0
0.2%Pluronic F127+0.5%PVPK-30+0.2%NaDC	508 ±2.5	530 ±3.5	544 ±5.0	574 ±4.5	590 ±4.0	607 ±5.0	614 ±3.0
0.2%Pluronic F127+0.2%PVPK-30+0.2%NaDC	558 ±3.0	597 ±2.5	626 ±4.0	685 ±3.0	705 ±3.5	750 32.0	785 ±2.5
1%HPMC+1%PluronicF127	1500 ±5.5	1800 ±4.5	2000 ±5.0	2225 ±3.5	2450 ±3.0	2800 ±2.5	3000 ±3.5
0.5%Pluronic F127+0.2%PVPK-30+ 0.2%NaDC	515 ±6.0	550 ±4.5	600 ±4.0	625 ±5.5	675 ±3.0	700 ±3.0	715 ±3.0
0.2%Pluronic F127+0.5%PVPK-30+0.1%NaDC	543 ±5.5	566 ±4.0	591 ±4.0	610 ±4.5	629 ±3.0	637 ±3.5	647 ±2.5
1%HPMC+1%PVPK-30+0.2%NaDC	800 ±4.2	900 ±5.2	1200 ±4.2	1360 ±4.5	1500 ±4.0	1800 ±2.5	1905 ±3.0
0.5%Pluronic F127+0.2%PVPK-30+0.1%NaDC	604 ±6.5	625 ±4.0	650 ±3.5	685 ±5.0	710 ±4.0	725 ±3.0	755 ±2.5
1%Tween80+1%HPMC	1800 ±3.0	1950 ±3.5	2100 ±5.0	2200 ±4.0	2375 ±3.0	2400 ±2.0	2465 ±3.0

Table 2.5. Effect of the process parameters on particle size of Ibuprofen, Glibenclamide and Artemisinin nanocrystals.

Average effect of process parameters	Level Used	Average Particle Size (nm)		
		Ibuprofen	Glibenclamide	Artemisinin
A A	+ -	165±5.5 94±3.5	365±4.5 298±5.5	503±5.0 405±3.5
B B	+ -	95±6.0 145±3.5	302±4.5 360±6.0	395±4.0 462±5.0
C C	+ -	93±4.0 204±3.0	305±2.5 412±4.5	410±5.0 520±2.5
AB AB	- + + -	96±6.0 215±6.5	300±4.0 405±5.5	400±3.5 528±6.2
BC BC	++ - -	100±3.0 250±2.5	310±2.5 465±4.0	398±6.5 565±4.5
AC AC	- + + -	98±3.0 275±4.5	300±6.0 460±4.5	408±5.5 580±3.5
ABC ABC	- + + + - -	98±2.0 300±3.2	295±2.5 496±3.0	400±5.4 602±4.0

2.3.2 Morphology Studies

All particles of raw glibenclamide sample were found to have a regular morphology when analysed at 400X magnification level. The average particle size was found 70 micron. Figure 2.4 (a) shows scanning electron micrographs of raw glibenclamide sample. TEM images of glibenclamide nanoparticles (Figure 2.4 (b)) were taken at 50K and the average particle size of the particle was found to be 0.2µm. Ibuprofen crystals were mostly in separate state from each other and some adjacent to one another and other clustered on each other (Figure 2.4 (c)) (Aly Nada, 2005). The images were more prominent at higher magnification (200X). Particle size measurements (118µm x 25.81µm) of bulk ibuprofen were taken at 200X magnification.

Image of bulk ibuprofen (Figure 2.4 (c)) shows the varying sizes of crystal present in the bulk ibuprofen sample.

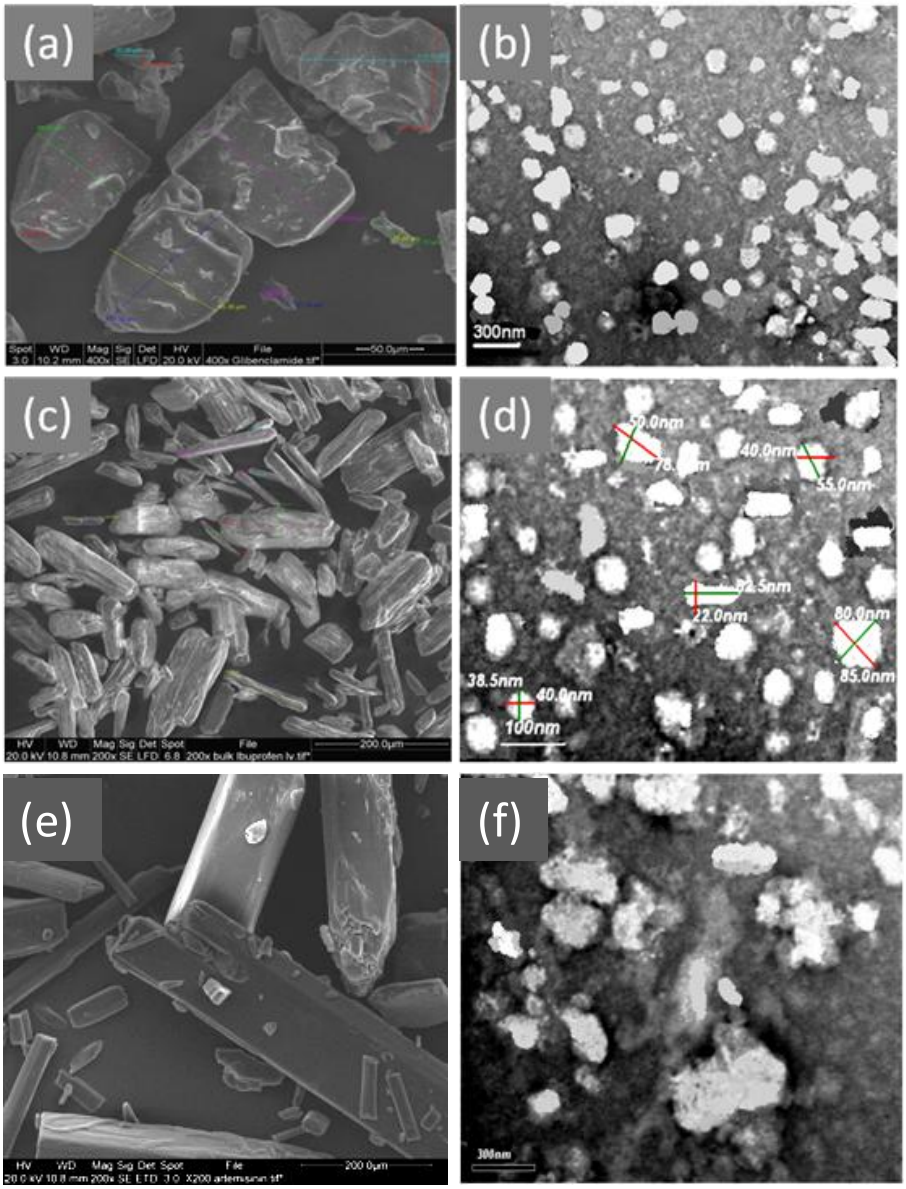

Figure 2.4 SEM and TEM images of unprocessed (a), processed (b) glibenclamide, unprocessed (c), processed (d) ibuprofen and unprocessed (e), processed (f) artemisinin particles.

TEM images of ibuprofen were taken at 200K and showed that the particles were crystalline in nature with average particle size of 90nm (Figure 2.4(d)). Artemisinin samples analysed at 200X magnification level were found to have triclinic crystals (Figure 2.4 (e)). The average particle size was found to be

300micron. TEM images of artemisinin were taken at 80K and the average particle size was below 400nm (Figure 2.4 (f)). Representative transmission electron microscope (TEM) images of the samples are shown Figure 2.4, which confirms particle size being in the nanometre range and being consistent with the dynamic light scattering determination.

2.3.3 DSC and PXRD Studies

For all three drugs, the nanocrystals obtained were found to be crystalline when characterized using a combination of differential scanning calorimetery (DSC) and powder X-ray diffraction (PXRD). With the DSC, a single sharp melting endotherm was observed for all samples including nanocrystalline and original powdered materials (Figures 2.5, 2.6 and 2.7). There was a slight reduction in the melting onset temperature (T_{onset}) and melting peak maximum for the nanocrystal samples relative to the unprocessed samples. The heat of fusion was also decreased for the nanocrystal samples (Table 2.6). This behaviour has been observed previously being attributed to traces of the polymer(s) adsorbed on the surface of nanocrystals (Valleri et al., 2004, Bunjes et al., 2000). With respect to powder X-ray diffraction, the nanocrystal samples gave peaks in essentially identical positions to those of the original powders thus confirming the identity and crystallinity (Figure 2.8). The peaks were slightly broadened as expected due to particle-size broadening effects, which become important for small particle sizes. The marked variation in the peak intensity of the unprocessed samples is considered to be due to preferred orientation effects.

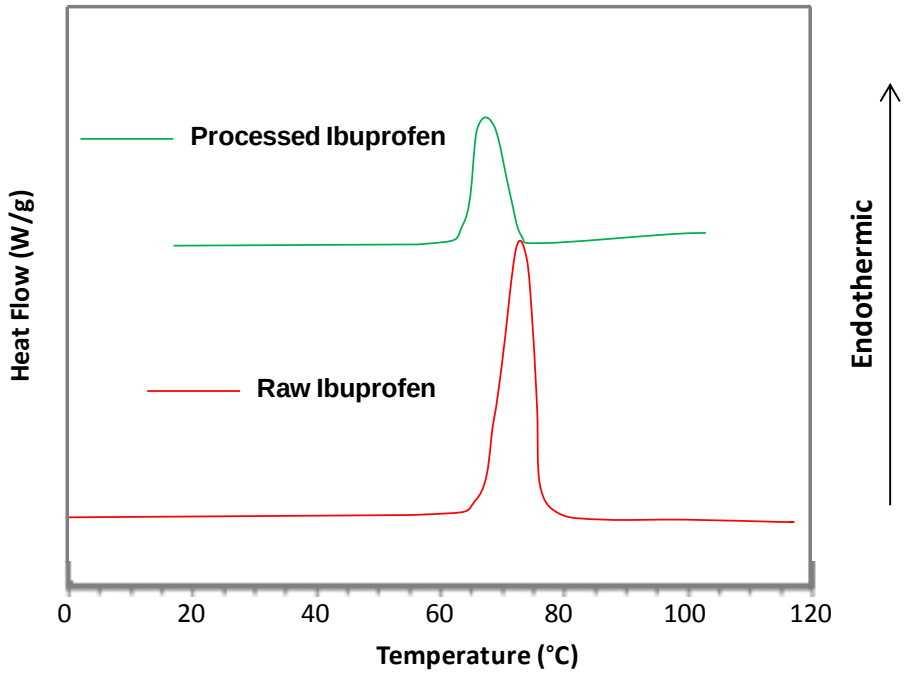

Figure 2.5 Representative DSC profiles of processed and unprocessed ibuprofen particles

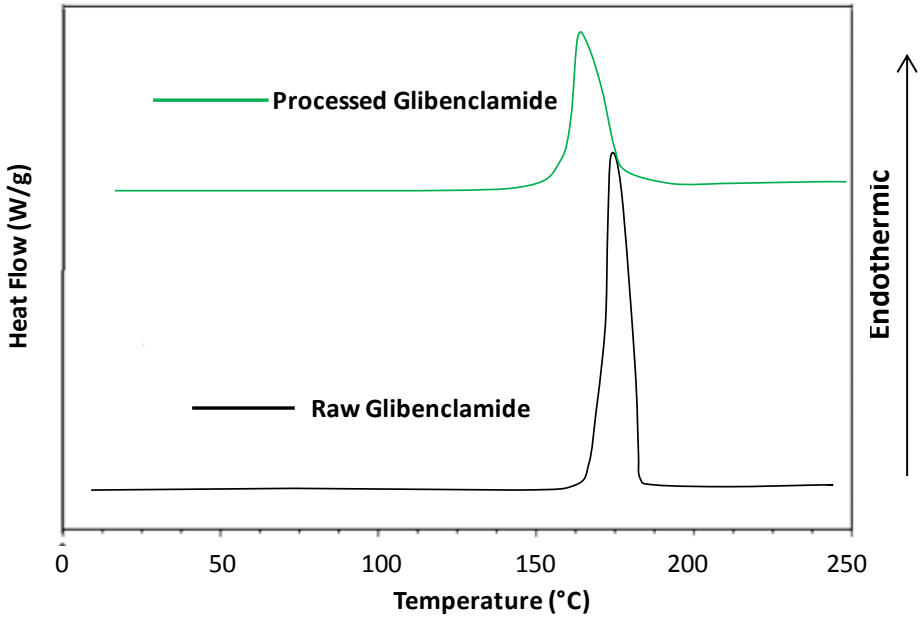

Figure 2.6 Representative DSC profiles of processed and unprocessed glibenclamide particles

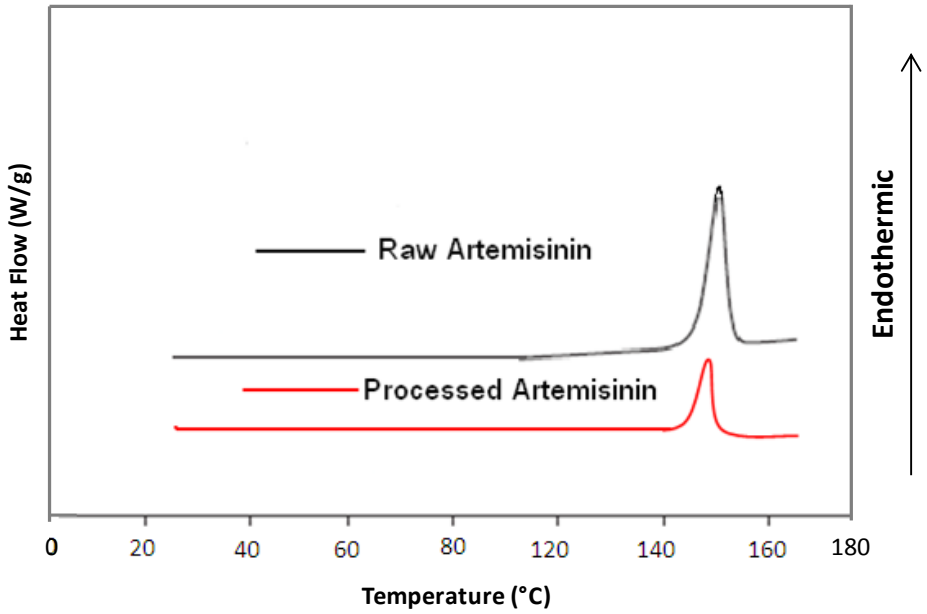

Figure 2.7 Representative DSC profiles of processed and unprocessed artemsinin particles

Table 2.6 DSC profile of unprocessed a processed samples of ibuprofen, glibenclamide and artemisinin

Drug	Melting point (°C)	Heat of fusion (j/g)
Raw ibuprofen	74.09 ±1.5	151.80 ±1.2
Ibuprofen nanocrystal	70.00 ±1.0	123.50 ±2.0
Raw glibenclamide	174.75 ±2.0	100.00 ±1.0
Glibenclamide nanocrystal	172.00 ±1.2	89.00 ±1.4
Raw artemisinin	154.20±1.3	80.00 ±1.5
Artemisinin nanocrystal	150.00±1.6	64.00 ±2.2

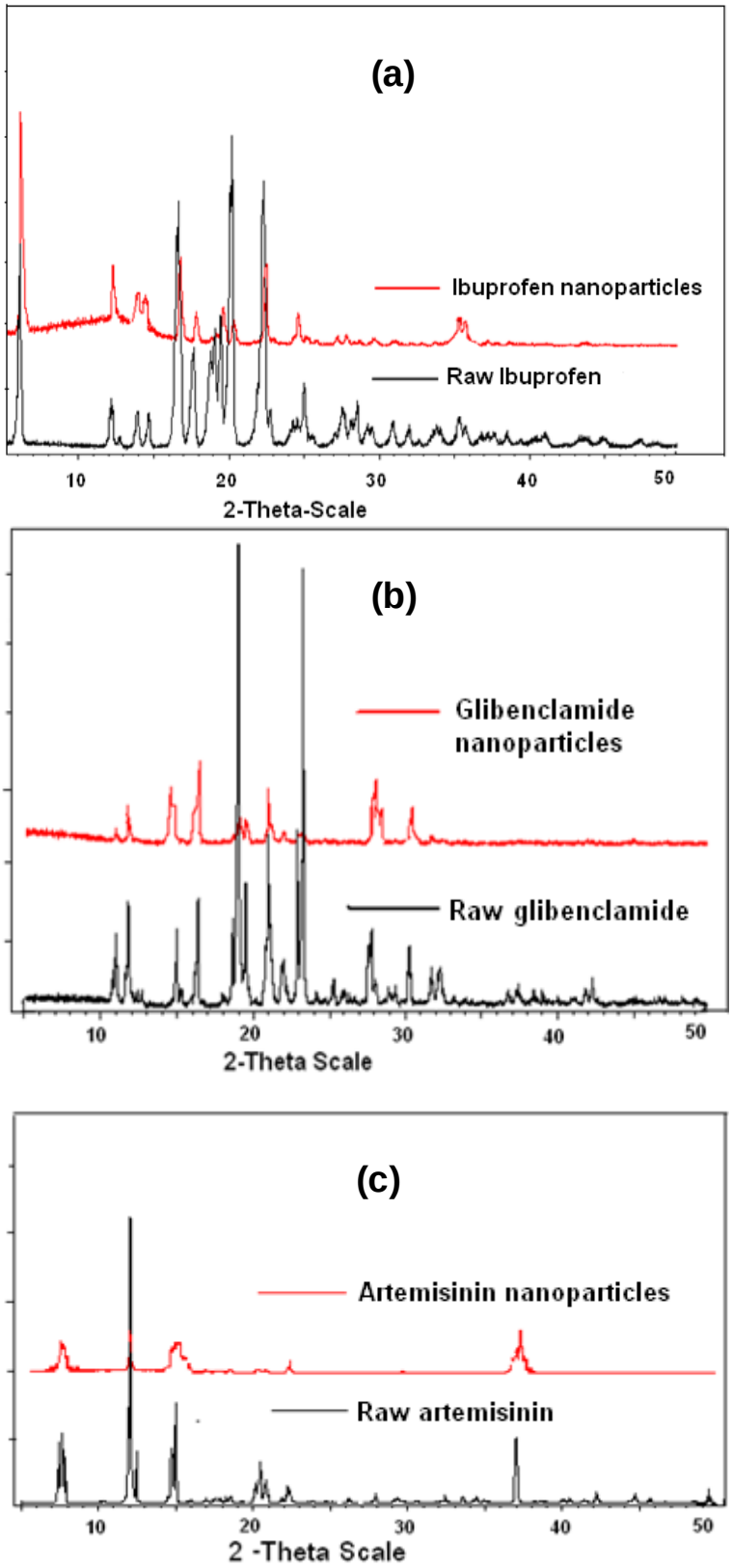

Figure 2.8 Powder X-ray diffraction patterns of the nanocrystals and the original powdered drug for (a) ibuprofen, (b) glibenclamide, and (c) artemisinin. X-ray radiation source was copper Kα, λ=1.542 Å.

2.3.4 Stability Studies

The effect of different combinations of stabilizers on the particle size of nanocrystals of ibuprofen as a function of storage at 25°C is given Table 2.2. The effectiveness of the stabilizers as single components can be ranked as HPMC (15cp; 1% w/w) > Pluronic F127 (1% w/w) > Pluronic F68 ≈ PVP (1% w/w). Of the various combinations tested the combination of 1% HPMC(15cp) + 1% Pluronic F127 is the most effective by far, yielding a very low particle size and high particle size stability on storage. The effect of stabilizers on the particle size for glibenclamide is shown in Figure 2.3. Single stabilizer components (1% HPMC (6cps), 1% HPMC (15cps) and 1% PVP), as with ibuprofen, yielded nanocrystals of a relatively low particle size but were not effective in maintaining and stabilizing the particle size on storage. Interestingly, a number of combinations of stabilisers are equally effective, including mixtures of HPMC+PVP and HPMC+PVPK-30. Inclusion of sodium lauryl sulphate or miglyol appears to have little effect. All these combinations yield stable nanosuspensions with a particle size of around 350-400 nm. The best combination is HPMC (15cps; 1% w/w) + PVPK-30 (1% w/w) which yields stable nanocrystals of size ~300 nm. The effect of stabilizers on the nanocrystal size and stability for artemisinin is shown in Figure 2.4. The data here are markedly different from those observed for ibuprofen or glibenclamide; the smallest attainable nanocrystal size just exceeding 400nm (which is much larger than the optimum particles sizes obtained for ibuprofen and glibenclamide).Particle size stability was in general terms poor with micron-sized crystals appearing in some of the nanosuspensions on storage. In this case, the polymer HPMC even in combination with other stabilizers

was essentially infective. A combination of PVP (0.5% w/w) + Pluronic F127 (0.5% w/w) + sodium deoxycholate (0.2%w/w) gave the lowest particle size and best stability.

The stability of the optimum formulations of the nanosuspensions was further assessed at 4, 25 & 40 ° C for up to 1 month. Ibuprofen, glibenclamide and artemisinin nanosuspensions were stable at 4 and 25 ° C for up to a month but showed an increase in particle size at 40°C over the one month storage period. Particle growth observed at higher temperature is probably related to Ostwald ripening (Deng et al., 2010). Furthermore for HPMC based formulations, 40°C is close to the gel point of the polymer which might also affect its role as a stabilizer (Bajwa et al., 2009, Ford, 1999). The nanosuspensions were found to be physically and chemically stable at over the storage period of 1 month. HPLC analysis showed that > 99.9% of the expected levels of glibenclamide, ibuprofen and artemisinin were recovered from the nanosuspensions, indicating that no significant loss or degradation of the drugs occurred during nanocrystal preparation or on storage.

2.3.5 Dissolution Studies

The dissolution rate of the suspended nanocrystals of glibenclamide, ibuprofen and artemisinin was compared to the micronized samples of the drug substances and marketed products and shown in(Figures 2.9, 2.10 and 2.11). In all cases the dissolution rate of the nanocrystals was significantly faster than the micronized powder and the marketed products. This is encouraging even though we are aware that enhanced dissolution rates may not always translate into enhanced bioavailability.

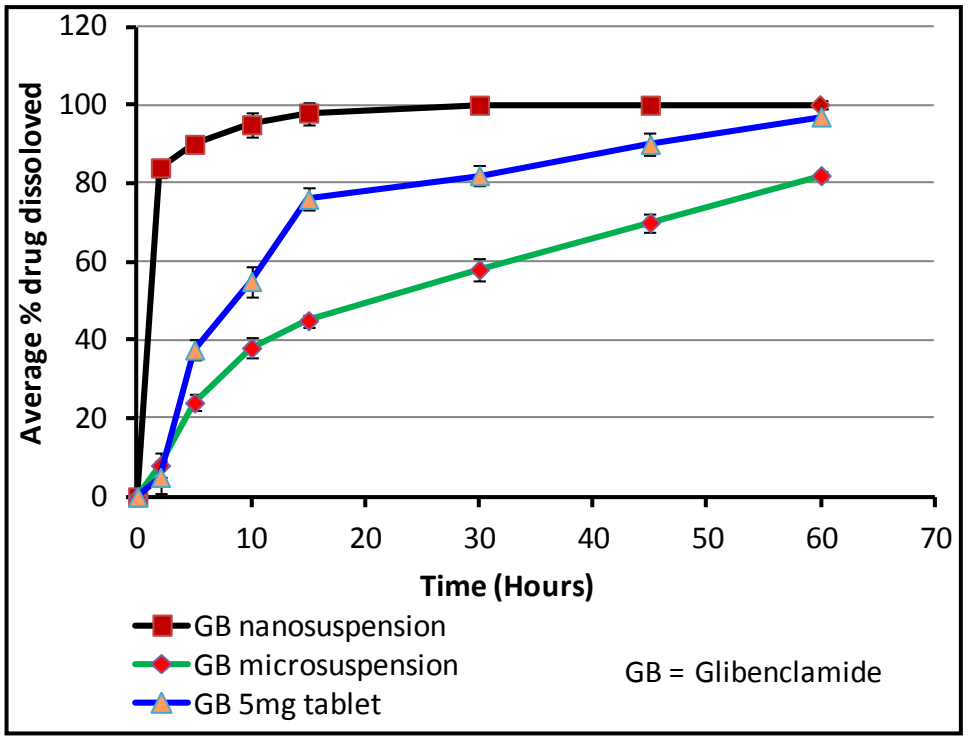

Figure 2.9 Comparison of dissolution profiles of glibenclamide nanosuspension with microsuspension formulations and marketed tablets

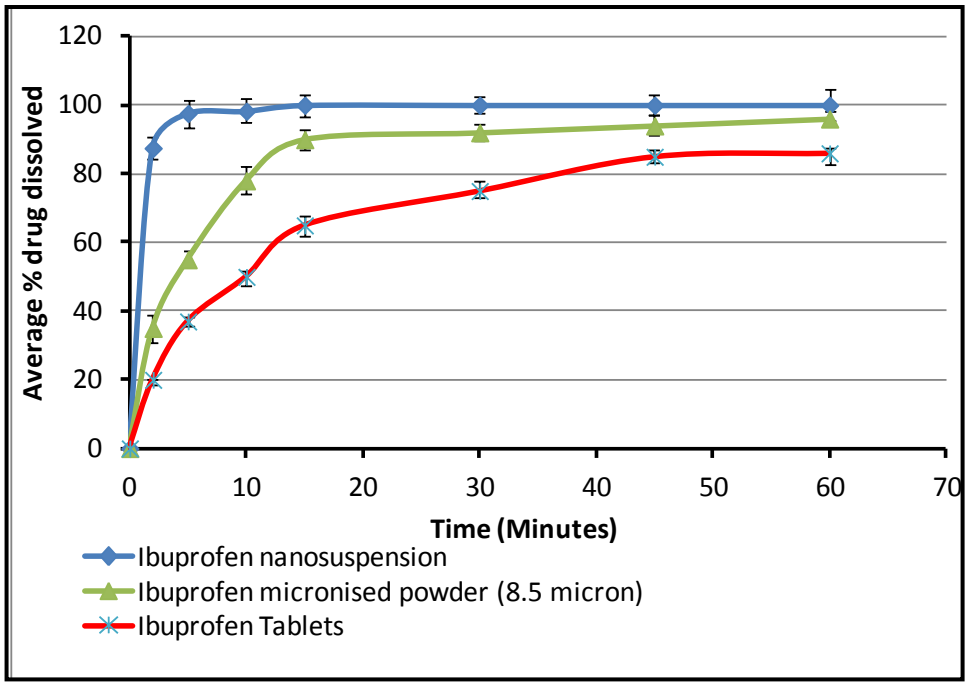

Figure 2.10 Comparison of dissolution profiles of ibuprofen nanosuspension with microsuspension formulations and marketed tablets

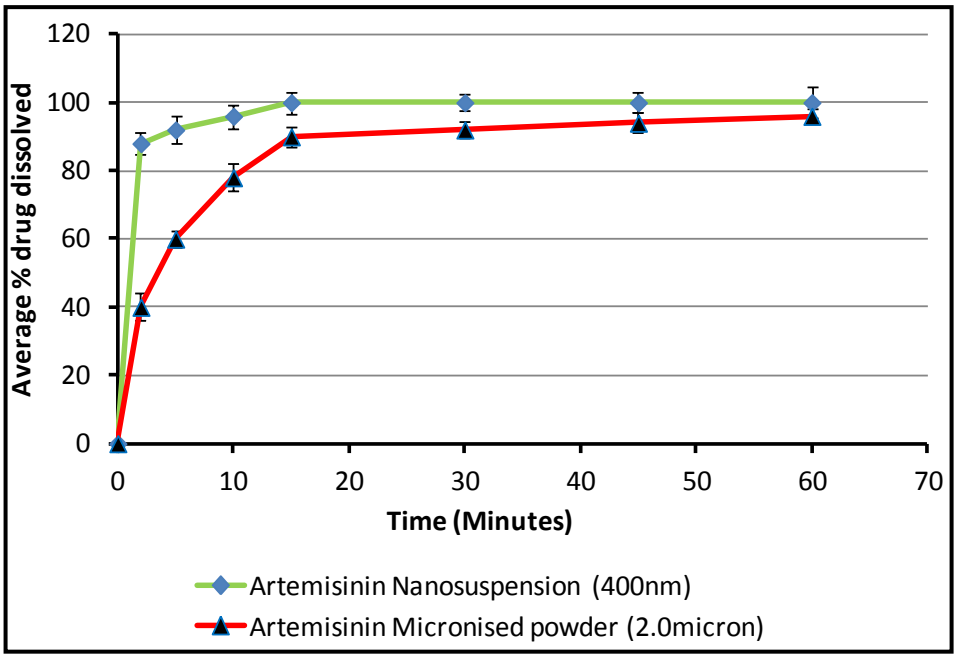

Figure 2.11. Comparison of the dissolution profiles of the artemisinin nanosuspension with microsuspension formulations.

2.3.6 Effect of Supersaturation

The two fundamental questions in using the precipitation method for preparing nanocrystals are (a) what determines the (initial) nanocrystal size and (b) how can we stabilize the subsequent crystal growth and particle aggregation? Possible determinants of the initial particle size include supersaturation, the nature of the stabilizers/inhibitors in the anti-solvent media and their molecular organization, and factors intrinsic to the molecule and how they govern the kinetics of nucleation. We have a general understanding of the effects of supersaturation. Higher supersaturation reduces the critical nucleus size, increasing the probability (and hence rate) of nucleation. This gives rise to the formation of an increased number of crystallites of a relatively small size, since much of the solute is consumed by the large number of emerging crystallites limiting the amount of solute

available for subsequent crystal growth. Is supersaturation the dominant determinant of nanocrystal size in these systems? Particle size as a function of supersaturation is plotted in Figure 2.12 for each of the three drug materials. (The raw solubility and supersaturation data are given in Table 2.7). If supersaturation is the dominant factor, one should expect all the data points to lie on a straight line with a negative gradient, characterizing the inverse relationship that higher supersaturations give rise to low particle size. Data for an individual drug molecule does indeed show such a relationship but there is no overall overlap of these data between the three molecules. Instead these data show systematic shifts in the particle size for a given supersaturation depending on the molecule. The lack of overlap of the data between the molecules suggests that supersaturation whilst being an important factor is not the dominant factor.

For a given supersaturation the particle size of artemisinin nanocrystals is larger than that for glibenclamide, which in turn is larger than that for ibuprofen. The implication is that the rate of nucleation of artemisinin is relatively lower (as is the rate of nucleation of glibenclamide relative to ibuprofen), which might be due to an intrinsic factor of the molecule or the nucleation rate is retarded by the anti-solvent media containing the crystal growth inhibitors/stabilizers. The intrinsic factors determining nucleation include the rate of molecular diffusion of the molecule, which will dictate the kinetics of the initial phase separation to form clusters of the solute, and the ease or otherwise with which the molecules adopt the molecular orientation and lattice positions characterising the emerging crystal in spontaneous fluctuations. Given that rapid nucleation is expected to result in nanocrystals

of smaller dimensions, these considerations suggest that effective stabilizers for bottom-up nanocrystal preparation methods should at best have the ability to promote the rate of nucleation and at worst not retard it. Indeed, many of the effective stabilizers employed here and by others have surface activity whilst small molecule surfactants are also employed in nanocrystal precipitation, suggesting that these molecules may be playing a role in reducing the interfacial free energy for nucleation and hence enhancing the nucleation rate.

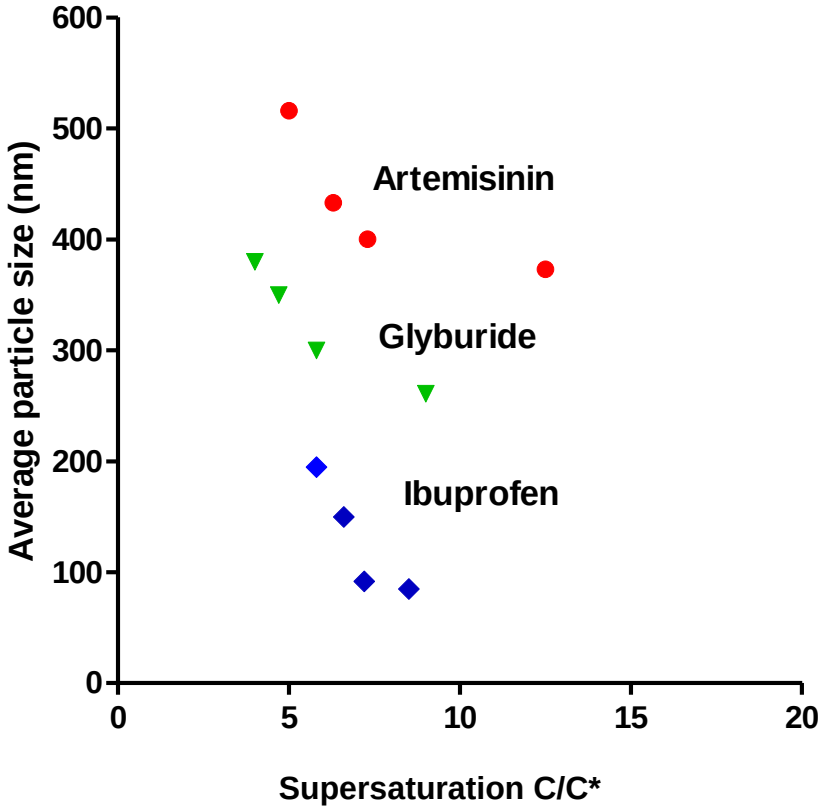

Figure 2.12. Nanocrystal particle size as a function of supersaturation for ibuprofen, glibenclamide and artemisinin

Table 2.7 Solubility of ibuprofen, glibenclamide, and artemisinin in 10% anti-solvent phase as function of temperature, along with estimated supersaturation and the resulting nanocrystal particle size.

Drugs	Temperature / °C	Solubility / µg/ml	Supersaturation / C/C*	Average particle size / nm
Ibuprofen	15	350.0±4.0	8.5±1.0	85.0±4.5
	25	415.0±2.5	7.2±1.2	92.0±2.5
	35	450.0±3.0	6.6±2.0	165.0±5.0
	45	510.0±1.5	5.8±1.5	195.0±4.0
Glibenclamide	15	55.0±2.0	9.0±2.2	261.0±5.2
	25	85.0±2.5	5.8±2.7	298.0±3.0
	35	105.0±3.0	4.7±1.5	350.0±2.5
	45	125.0±2.2	4.0±1.0	380.0±4.0
Artemisinin	15	125.0±1.5	12.5 ±2.8	373.0±5.5
	25	205.0±2.0	7.3 ±3.2	400.0±3.5
	35	235.0±2.5	6.3 ±3.0	433.0±4.2
	45	300.0±2.1	5.0±2.0	516.0±3.5

2.3.7 Modelling Studies

Given that each of the three drugs requires a different combination of crystal growth inhibitors/stabilizers to achieve the minimum crystal size and longer term stability to crystal growth, these results suggest that there is probably no generic set of inhibitors/stabilizers that yield stable, low particle-size nanocrystals. The specific nature of the molecule and/or exposed crystal surfaces appear to be critical in determining what stabilizers are likely to be effective. We therefore attempted to rationalise the choice of effective stabilizers for each of the drug substances by examining the intermolecular interactions on the dominant crystal faces for each drug and stabilizer molecules found to be effective. The crystal morphology for each drug was predicted using the attachment energy model which allowed us to identify the major faces. The predicted morphologies are intrinsic i.e. depend only on the internal intermolecular forces and do not consider how the solvent or stabilizers may modulate the morphology. The predicted major faces and the

associated percentage areas of the facets for each of the drug crystals are given in Table 2.8, while the morphologies and the structures of the dominant crystal faces are shown in Figures 2.13, 2.14, and 2.15.

For ibuprofen the predicted morphology is a flat platelet with the faces (100) dominating the morphology (69%) (Figure 2.13). The next significant faces are the (011) and (002) with percentage facet areas of 14 and 11 % respectively. The dominant face (100) is terminated entirely by alkyl groups, as is one of the minor faces, (002) (11%). For ibuprofen, both PVP and Pluronic F68 individually were essentially ineffective, while HPMC and Pluronic F127 individually were marginally better, and the combination of HPMC+Pluronic F127 being markedly superior. The glibenclamide morphology is more 3-dimensional (Figure 2.18). The dominant faces in this case are (011) with 36%, (10-1) with 23%, and (110) with 17% of the total surface area. These faces are all largely polar in nature. The essential stabilizers appear to be HPMC + PVPK-30. The morphology for artemisinin is a flat prism with the dominant faces being (002) with 40%, (100) with 31%, and (011) with 9% of the surface area (Figure 2.15). All three faces largely expose alkyl groups, with the surfaces (002) and (100) also revealing some polar groups inter-dispersed in a dominantly non-polar surface. In this case the effective stabilizers are a combination of Pluronic F127, PVP-K and sodium deoxycholate.

Apriori, one could argue that an effective stabilizer system should include an appropriate surfactant to lower the interfacial energy to nucleation, thus enhancing the nucleation rate, and other components that minimise crystal growth to favour nucleation and stabilize the crystallite surface to aggregation.

Considering the crystal surfaces and the molecular structures of the most effective stabilisers, there appears to be no apparent pattern as to the choice of stabilizers for a particular drug. A potential lead is that for ibuprofen and artemisinin, both of which have non-polar crystal surfaces, Pluronic F127 appears to be more effective than Pluronic F68 in yielding stable, low particle-size nanocrystals. The Pluronics are tri-block polymers comprising a *hydrophobic* propylene oxide (PO) polymer block in the middle of two *hydrophilic* ethylene oxide (EO) polymer blocks. The respective structures of Pluronic F68 and Pluronic F127 are $(EO)_{80}$–$(PO)_{27}$–$(EO)_{80}$ and $(EO)_{101}$–$(PO)_{56}$–$(EO)_{101}$, suggesting the larger molecular weight and more hydrophobic polymer is more appropriate for crystals with non-polar surfaces. The difficulty in linking molecular level interactions between stabilizer molecules and crystal surfaces is not surprising given that these systems are highly complex, comprising multiple components and the dynamic nature of the precipitation process itself.

Table 2.8 Dominant crystal surfaces predicted from crystal morphology prediction calculations for ibuprofen, glibenclamide, and artemisinin.

Drug	Face	% Facet Area
Ibuprofen	100	65
	011	14
	002	11
Glibenclamide	011	36
	10-1	23
	110	17
Artemisinin	020	41
	110	34
	011	18

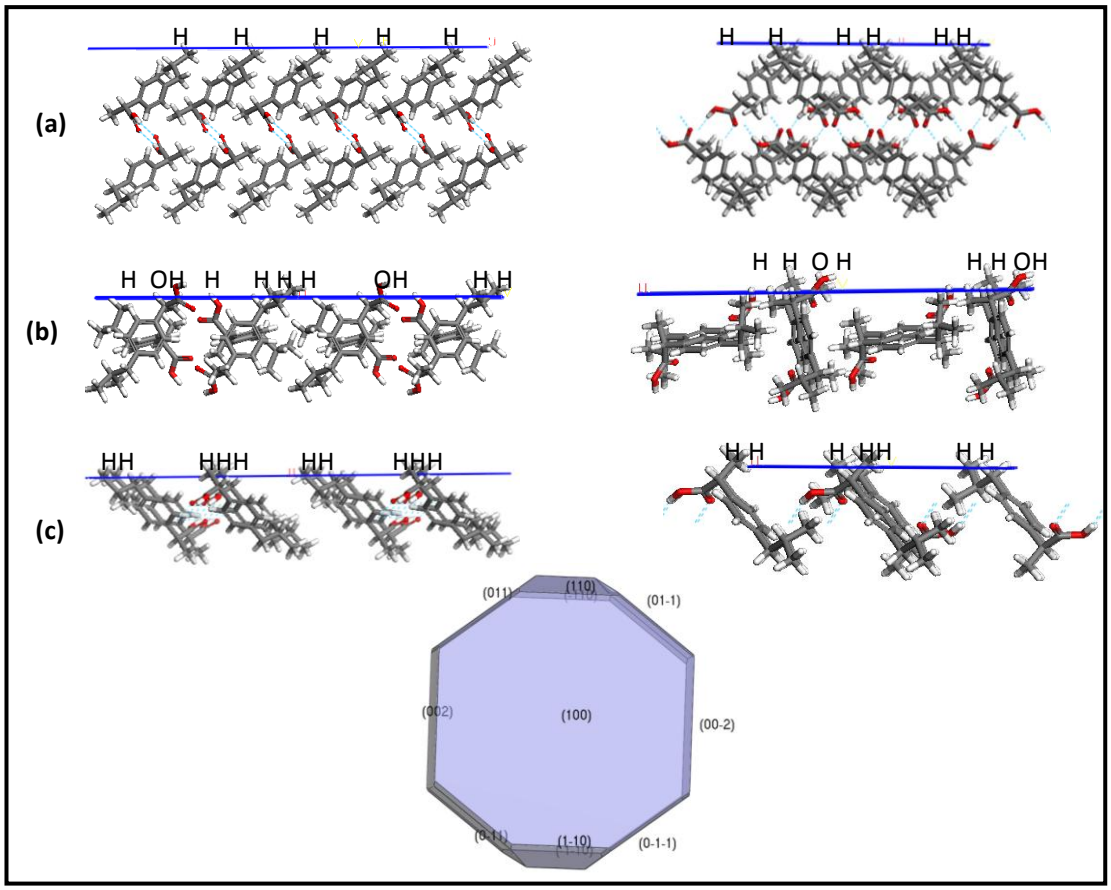

Figure 2.13 Predicted crystal morphology for ibuprofen along with the dominant crystal surfaces. (a) (100) face with 65% of the surface area; (b) (011) face with 14% of the surface area; (c) (002) face with 11% of the surface area.

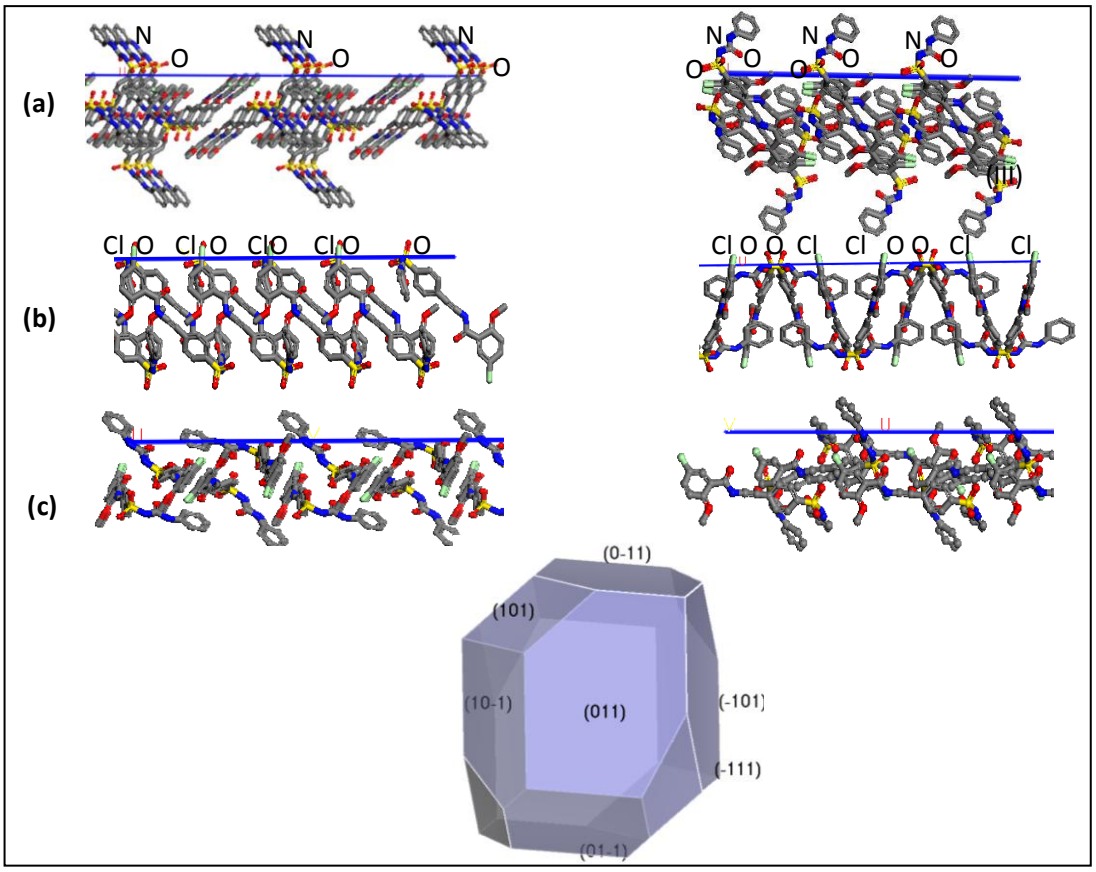

Figure 2.14 Predicted crystal morphology for glibenclamide along with the dominant crystal surfaces. (a) (011) face with 36% of the surface area; (b) (10-1) face with 23% of the surface area; (c) (110) face with 17% of the surface area.

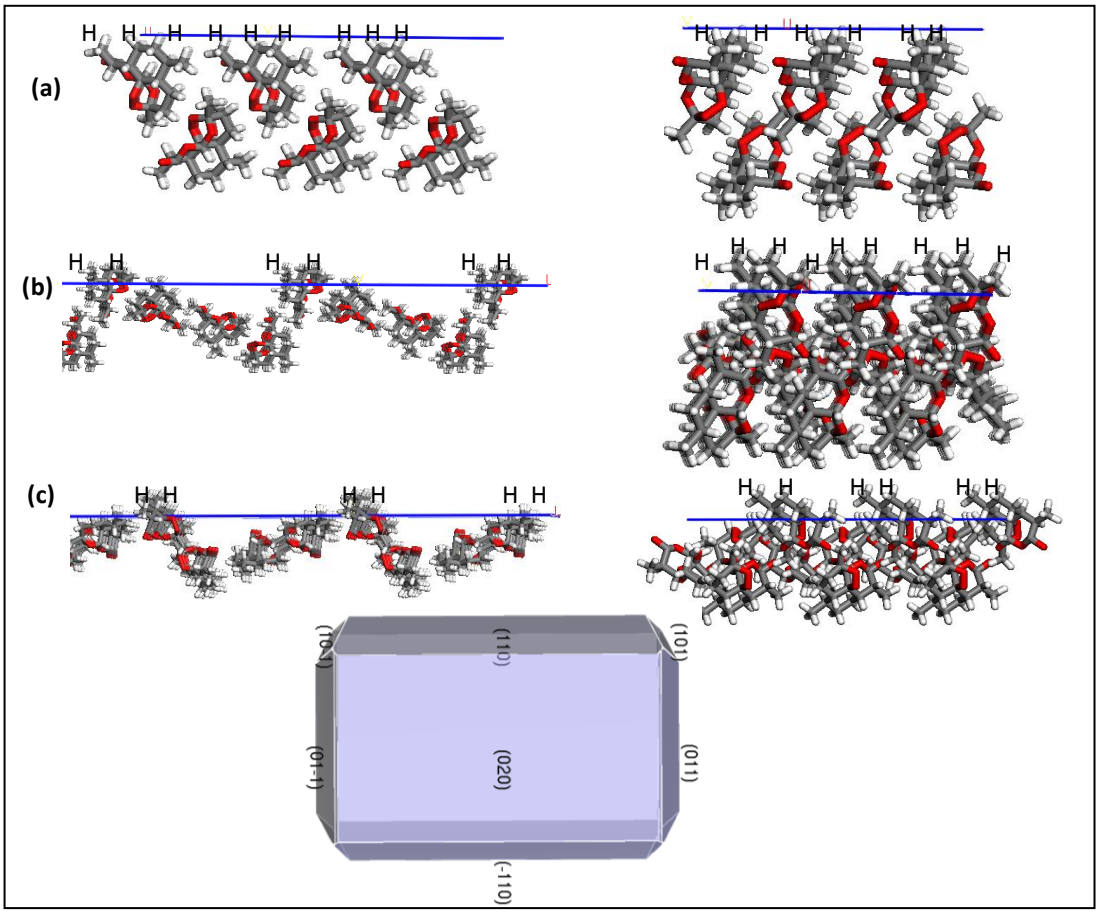

Figure 2.15 Predicted crystal morphology for artemisinin along with the dominant crystal surfaces. (a) (020) face with 41% of the surface area; (b) (110) face with 34% of the surface area; (c) (011) face with 18% of the surface area.

In summary this study demonstrated that a low energy precipitation method generally works for fabrication of nanocrystals of different molecules with marked increase in dissolution rate compared to the micronized and marketed products. Stable nanocrystals with uniform particle size were prepared for the three model compounds, glibenclamide, ibuprofen, and artemisinin, which are all practically insoluble in water and have diverse molecular structures and crystal packing. The choice of crystal growth inhibitors/stabilizers was found to be critical and specific for each drug. The effect of the process variables, temperature, stirring rate, and the solute

solution infusion rate into the anti-solvent, was rationalized in terms of how these factors influence the local supersaturation attained at the earliest stages of precipitation. The dissolution of the nanocrystals in aqueous media under physiological conditions was shown in all cases to occur almost instantaneously, being markedly more rapid than that observed for micronized suspensions of the model drugs and their marketed tablet formulations. Rationalization of the choice of optimum stabilizers in terms of molecular interaction with the exposed crystal surfaces proved to be difficult.

Chapter 3

Nanocrystal Recovery Using Carrier Particles

3.1 Introduction

The ‘poorly solubles’ problem is a significant issue for many marketed drugs and potential drug candidates. Indeed up to 40% of molecules in the development pipelines and approximately 60% of the molecules derived from high throughput screens exhibit markedly low aqueous solubility (Merisko-Liversidge and Liversidge, 2008, Stegemann et al., 2007) The issue with poorly soluble drugs is that the low aqueous solubility can result in poor and erratic bioavailability. Low aqueous solubility can result from a low inclination of the molecule to be solvated by water and/or from a notable resistance of the crystal structure to dissolve owing to a high lattice energy (Kipp, 2004). For these molecules, consistent and enhanced bioavailability can be achieved if the dissolution rate can be sufficiently enhanced, or if the active substance is solubilised. Approaches that can enhance dissolution include engineering stable amorphous or metastable solid forms of the drug, micronisation,(Charoenchaitrakool et al., 2000) solid dispersions (Serajuddin, 1999), and the more recent addition, nanocrystals (Gao et al., 2012, Müller

and Keck, 2012, Muller and Akkar, 2004, Keck and Müller, 2006, Wang et al., 2012, Müller et al., 2011, Masuda, 2011).

Nanocrystals offer an immense surface area, an increased saturation solubility, and a decrease in the diffusional pathway adjacent to the nanocrystal surface, which all converge to substantially increase the rate of dissolution (Müller et al., 2011, Buckton and Beezer, 1992, Wu and Nancollas, 1998, Moeschwitzer and Mueller, 2006, C.M. Keck, 2010, Ponchel et al., 1997). The use of nanocrystals and nanosuspensions is fast becoming a platform technology, in particular in addressing the problem of poorly soluble (Muller, 1999, Müller and Keck, 2012). Although the technology is maturing, there are still important issues and limitations. A particular issue is the need and difficulty in recovering/isolating the nanocrystals in the dry state for incorporation, for instance, in solid dosage forms. Nanocrystals of drugs are generally produced in suspension and the solid must then isolated by removing the solvent. Current methods for isolating nanocrystals in the dry state include spray drying (Hu et al., 2010, Patravale and Kulkarni, 2004, Chaubal and Popescu, 2008, Liu et al., 2010, Mou et al., 2011, Basa et al., 2008), freeze drying(de Waard et al., 2009, Choi et al., 2004, Beirowski et al., 2011, Abdelwahed et al., 2006) and spray granulation(Bose et al., 2012, Keck and Müller, 2006, Abdelwahed et al., 2006, Kocbek et al., 2006). Spray drying can introduce instability owing to the heat and high energy involved the process (Freitas and Müller, 1998). Freeze drying is an expensive, time consuming process which can adversely affect the resulting particle size distribution (Abdelwahed et al., 2006). Additionally isolated nanocrystals

using nanosuspension as granulating fluid has exhibited decrease in dissolution rate (Basa et al., 2008).

We report here a simple approach for recovering nanocrystals from a suspension using inert carrier particles. Whilst the concept of using carrier particles is not new (consider its widespread application in dry-powder inhaler formulations (Hooton et al., 2008, Hickey, 2005, HW Frijlink, 2004, Ian Ashurst, 2000, Prime et al., 1997, de Boer et al., 2012) and in ordered mixing(C. W. Yip & J. A. Hersey, 1976, Hersey, 1975, Yeung and Hersey, 1979), to our knowledge this is the first open literature application of this approach for isolating nanocrystals from suspension. The isolated nanocrystal-carrier particles in powder form present the possibility of developing solid dosage forms such as tablets and capsules for oral administration with a marked potential for enhancement in dissolution rate. A key gain is the complete elimination of the problems of aggregation and Ostwald's ripening that plague nanocrystals in a liquid environment. The nanocrystal-carrier particles are shown to consistently reproduce the high dissolution rate of the original nanocrystal suspension. The methodology is robust and from the industry's perspective relatively low cost. Given that adsorption of the nanocrystals onto the carrier particle must depend on the particle size, crystallinity, and surface characteristics of the respective particles, we evaluated the adsorption efficiency for nanocrystals of two model drug compounds, ibuprofen and glibenclamide (Figure 3.1), produced by comminution, and in the case of glibenclamide also by simple precipitation. We have also attempted to rationalize the variation in adsorption efficiency

observed for the two compounds in terms of the molecular interactions at the crystal surfaces.

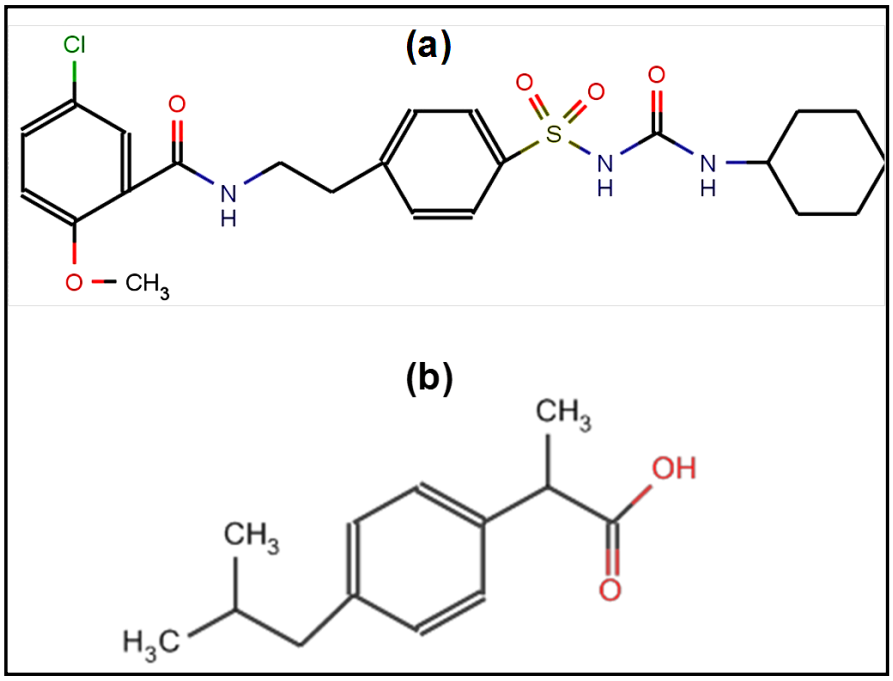

Figure 3.1 Molecular structure of (a) glibenclamide and (b) ibuprofen (These structures have been created using (Marvin sketch)

3.2 Materials and Methods

3.2.1 Materials

The chosen model drugs glibenclamide (Batch No. PPC/08/GLB/057) and ibuprofen (Batch No. 7050-1077) were purchased from Anzen Exports, Kolkata, India and Albemarle Corporation, USA, respectively. Hydroxypropylmethylcellulose (HPMC) of viscosity grades 6 cps (Batch No: 8028213) and 15cps (Batch No. 7068037) were kindly provided by Shin-Etsu, Japan. Polyvinylpyrrolidone K-30 (PVP) (Batch No. 08297047GO) was purchased from BASF, Germany. Sodium lauryl sulphate (SLS), (Batch No. 08421LE), sodium hydroxide (NaOH) (Batch No. S47417-479) and

monobasic potassium phosphate (MPP) (Batch No. SZE90330) were purchased from Sigma Aldrich, UK. Polyethylene glycol 400 (PEG-400) (Batch No. 0917861) and acetonitrile (Batch No. 0809411) were purchased from Fisher Scientific, UK. Dibasic calcium phosphate (DCP) (Batch No. A0280641) was purchased from Acros Organics, Belgium.

3.2.2 Methods

3.2.2.1 Preparation of Glibenclamide and Ibuprofen Nanocrystals by Controlled Comminution

Nanocrystals of glibenclamide and ibuprofen were prepared using the DENA DM100 size reduction system (Sulaiman, 2007). The DENA DM100 system comprises a fast rotating conical rotor constructed from a soft polymer, which sits inside a conical polymeric sleeve. Grinding media (0.2 mm yttrium reinforced zirconium beads) are housed inside indentations within the rotor which form a narrow gap between the outer sleeve and rotor. The high shear and turbulence generated within this narrow gap provide the potential for rupture and shearing of particles leading to ultrafine product in the sub-micron size range. The suspension produced during processing is continually recycled through a stainless steel screen which retains the grinding media and prevents contamination of product. The drug material was presented for size reduction in the form of a stabilized aqueous suspension, with the dispersion media (150 ml) being composed of sodium lauryl sulphate (0.1% w/w), PVP-K30 (0.5 %w/w) and 6 cP grade HPMC (0.5 %w/w). The drug substance was mixed with the stabiliser solution give a 250 ml suspension containing 2.6 %w/w of the drug material. The resultant suspension was then

placed into the feedstock hopper of the size reduction system. The suspension was processed for 60 minutes by recycling through the size reduction chamber. In-process samples were taken at intervals of 5, 10, 15, 30, 45 and 60 minutes with the particle size being measured by dynamic light scattering (DLS) using the Zetasizer Nano instrument (Malvern Instruments Ltd, UK).

3.2.2.2 Preparation of Glibenclamide Nanosuspension Using Controlled Crystallization Method

The nanoparticles of glibenclamide were fabricated by infusing 2.7ml of the stabilizer solution comprising of HPMC (15cps) (1% w/v) and PVP K-30 (0.5 %w/w) at an infusion rate of 100ml/minute into 0.3 ml of drug solution (5mg/ml) dissolved in polyethylene glycol 400 (PEG-400). The solution was stirred in a 10ml vial using a magnetic stirrer at 1200rpm with the sample temperature maintained at 25°C. Five replicate batches were prepared to ascertain the variability in the process. The process was also replicated at scales of 10ml, 100ml and 400ml using identical process conditions.

3.2.2.3 Particle Size Measurements

Particle size of the nanocrystals and associated polydispersity index (PI) determinations were conducted in triplicate by dynamic light scattering (Zetasizer® NanoS, Malvern Instruments, UK), which measures the hydrodynamic diameter including the solvation layer around each particle (Aboofazeli et al., 2000).

3.2.2.4 PXRD Studies

The crystallinity of the nanocrystals was assessed by powder X-ray diffraction (PXRD) (and DSC, see above) using dried powders recovered from the nanosuspensions by centrifugation at 14500 rpm for 60 minutes and drying under ambient conditions. PXRD studies were carried out using a Bruker D-8 powder diffractometer (Bruker Kahlsruhl, Germany). For the nanocrystal samples we employed a silicon-well sample holder, whilst for the original raw drug material a plastic sample holder was used. Calibration of the PXRD was carried out using a corundum standard. The samples were scanned in triplicate over the range 5-50° 2θ at a rate of 1º 2θ/min using a copper Kα radiation source at a wavelength of 1.542 Å and with 1 mm slits.

3.2.2.5 Chemical Stability of the Nanocrystal Suspensions

The glibenclamide and ibuprofen content in the respective nanosuspensions was determined using an HPLC system consisting of a Waters 2695 Model connected to a UV detector. For glibenclamide the UV detector wavelength was set at 254nm. The mobile phase solvent system comprised monobasic ammonium phosphate (0.02M) and acetonitrile at a ratio of (45/55 v/v). The flow rate of the mobile phase was set at 1.5ml/minute. An Ultra II TM C18 5µm 250×4.6mm column was used which was maintained at a temperature of 30°C. For ibuprofen content the wavelength of the UV detector was set at 214nm and a Vydac® 202TP C18 5µm, 4.6 × 250mm, column was employed, being maintained at a temperature of 30°C. The mobile phase consisted of a binary 50:50 v/v mixture of water and acetonitrile. The pH of mobile phase was 2.8 and the flow rate of the mobile phase was set at 1ml/minute. All the samples were analysed in triplicate.

3.2.2.6 Nanocrystal Particle Size Stability

The particle size stability of glibenclamide and ibuprofen nanosuspensions was monitored regularly using DLS over a period of 1 month, with the nanosuspensions being stored at three different temperatures (4°C, 25°C and 40°C). These studies enabled an assessment of level of agglomeration and Ostwald ripening of the nanocrystals.

3.2.2.7 Nanocrystal Adsorption on Carrier Particles

The carrier particle material was dibasic calcium phosphate. The particle size analysis of dibasic calcium phosphate was carried out, using a laser diffraction particle size analyser (Sympatec HELOS and RODOS, Sympatec Instruments, UK). The adsorption efficiency of the carrier particles was investigated at range of carrier particle concentrations: 30 mg/ml, 60 mg/ml, 90 mg/ml, 120 mg/ml, 150 mg/ml and 180 mg/ml. The dibasic calcium phosphate was added to 10 ml of the nanosuspension samples and stirred for 5 minutes by a magnetic stirrer at about 400 rpm at 25ºC, followed by filtration using a 0.4 micron filter paper. The filtered samples were dried at room temperature and subjected to analysis of active agent content by HPLC. To enable an objective comparison of adsorption efficiency, the glibenclamide nanosuspensions prepared by comminution were diluted to an equivalent concentration of the nanosuspensions prepared by controlled crystallization, giving a final concentration of 1.43mg/ml drug for both process variants.

3.2.2.8 Determination of Ibuprofen and Glibenclamide Contents Adsorbed to Dibasic Calcium Phosphate.

HPLC analysis of the ibuprofen content in the nanocrystal-carrier powders was undertaken by weighing known quantities of the dried adsorbates then diluting with the mobile phase (55/45% v/v acetonitrile and water) to a volume of 100ml to give a nominal concentration of 20 µg/ml assuming that complete adsorption of drug had occurred. The resultant solution was sonicated and then centrifuged for half an hour at 14700rpm to cause the separation of bounded nanocrystals. The supernatant layer was then analysed in triplicate by HPLC. The injection volume for the HPLC during this analysis was maintained at 25 µl. These steps were repeated for glibenclamide content in the adsorbates. However, dilution of the analytical samples was undertaken using the mobile phase 55/45%v/v ammonium phosphate (0.02M) and acetonitrile and an injection volume of 50 µl.

3.2.2.9 Scanning Electron Microscopy (SEM)

SEM images of the raw dibasic calcium phosphate carrier material, along with that of the nanocrystals of glibenclamide and ibuprofen adsorbed on the carrier particles were taken using a Quanta 400 SEM (FEI Company, Cambridge, UK). The SEM studies were carried out to investigate the adsorption of nanocrystals onto the surface of DCP. The samples were prepared by fixing the powder samples on to a metal stub using a double sided adhesive tape followed by gold coating. The instrument was calibrated using a gold grid obtained from the supplier.

3.2.2.10 Dissolution testing

Dissolution studies were performed on nanosuspensions of glibenclamide and ibuprofen, the respective adsorbates on the carrier particles, and existing commercial preparations. Each test employed a dose equivalent to 5 mg of glibenclamide and 200 mg of ibuprofen. The USP dissolution apparatus II (USP, 2008) was employed with 900 ml of the dissolution medium (buffer at pH 7.2) at 37ºC and a paddle speed of 50rpm. Aliquots of 5 ml of the dissolution media were sampled using a syringe filter (0.2 µm) at 0, 2, 6, 10, 15, 30, 45 and 60 minutes, the sample volume being replaced with an equivalent volume of fresh media. All the samples were analysed in triplicate using the HPLC method given above to quantify drug concentration. The % of the nominal dose of each drug released for each of the formulations at specific time intervals was then calculated.

3.3 Results and Discussions

3.3.1 Characterisation of Glibenclamide and Ibuprofen Nanosuspensions

3.3.1.1 Particle Size Measurements Ibuprofen and Glibenclamide Nanosuspensions

The systems being studied, nanosuspensions and nanocrystals adsorbed on carrier particles are clearly heterogeneous in nature. Therefore, one would expect variability in results which can make it hard to generalize findings. In view of this it is essential to characterize the systems thoroughly, to control known factors, and cover the effect of some of broader variables. We have followed this philosophy here and have considered two distinct molecules for

the study and also utilized the two main (and disparate) approaches for preparing nanocrystals, namely top-down comminution and the bottom-up precipitation method. Dibasic calcium phosphate was chosen as the carrier particle material as it has a low aqueous solubility and has previously been reported as good inert carrier for adsorption of microparticles (Seth, 1988).The results clearly reveal that the carrier particle approach to recovering nanocrystals from suspension is effective and robust. It is possible to recover/isolate up to 98% of the nanocrystals in the suspension, and the fast dissolution rate characterizing the nanosuspensions is reproduced by the nanocrystals adsorbed onto the carrier particles.

We were able to prepare stable nanocrystals using both controlled comminution and precipitation. The effectiveness of the comminution approach using the DENA DM100 size reduction system has detailed earlier (Plakkot et al., 2011, Sulaiman, 2007). Here we briefly illustrate this by reference to Figure 3.2 which displays the particle size of the materials as function of processing time. It is apparent that a processing time of about 45 minutes is sufficient to induce the maximum attainable reduction in particle size, after which the gain is minimal. After 60 minutes the respective particle size for glibenclamide and ibuprofen is 342 ± 3 (Figure 3.3) and 440 ± 5 nm (Figure 3.4). Average polydispersity index (PDI) values for both drug materials were <0.5 indicating narrow size distribution for nanosuspension(Deng et al., 2010)

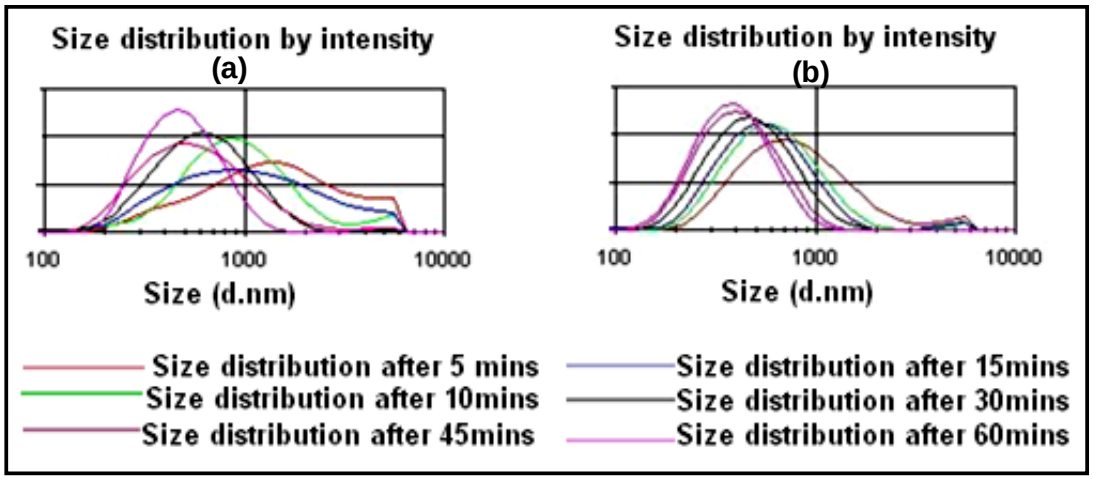

Figure 3.2 Particle size distributions of glibenclamide (a) and ibuprofen (b) as a function of processing time in the DENA DM100 size reduction system

Nanocrystals of glibenclamide prepared by controlled precipitation had an average particle size of approximately 300 ± 3 nm with low polydispersity 0.2 ± 0.02 (Figure 3.5), which is slightly lower than that attained by comminution, 342. Similar particle size profiles were obtained when the process was scaled-up from 10 ml to 100 ml and 400 ml (Figure 3.6).

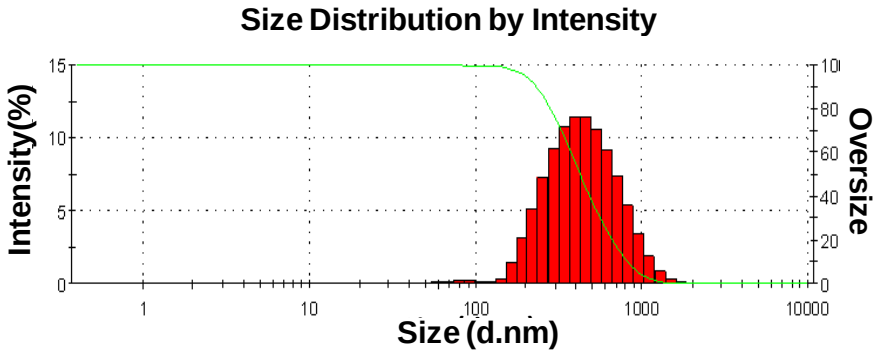

Figure 3.3 Particle size distribution of milled glibenclamide

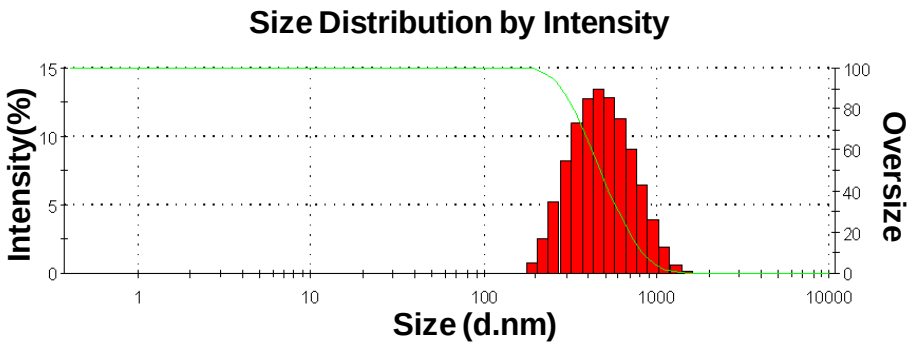

Figure 3.4 Particle size distribution of milled ibuprofen

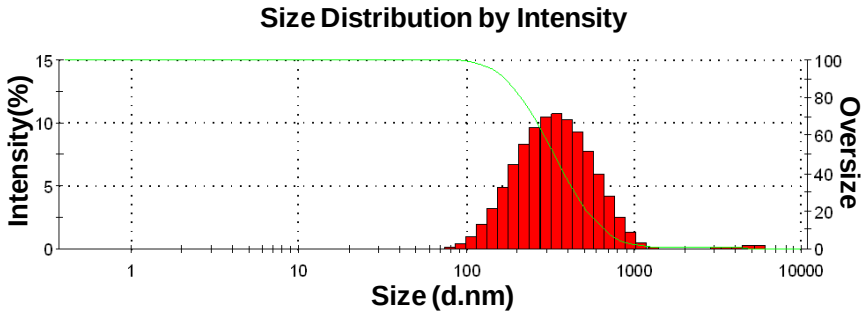

Figure 3.5 Particle size distribution for crystallised glibenclamide

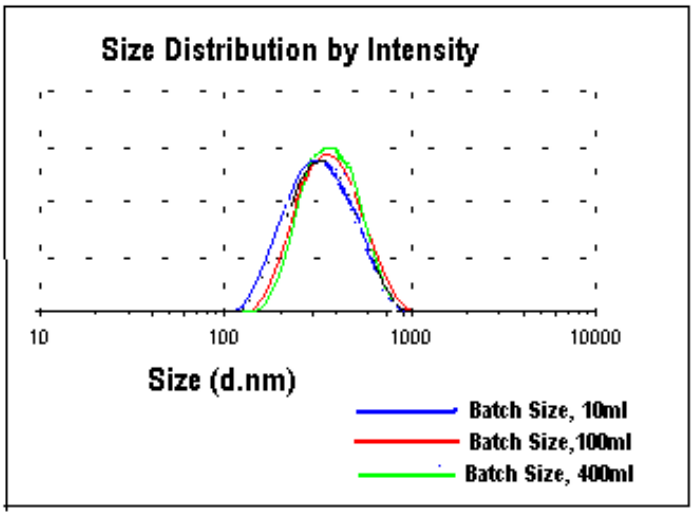

Figure 3.6 Particle size distribution for crystallised glibenclamide nanosuspensions at three different scales (10ml, 100ml and 400ml)

3.3.1.2 PXRD Studies

With respect to powder X-ray diffraction, the nanocrystal samples gave peaks in essentially identical positions to those of the original powders thus confirming the identity and crystallinity (Figure 3.7). The smaller particles can cause broadening and disappearance of some peaks due to small angle reflection by the particles that shifts the peak intensity to lower level (Bunjes et al., 2000).

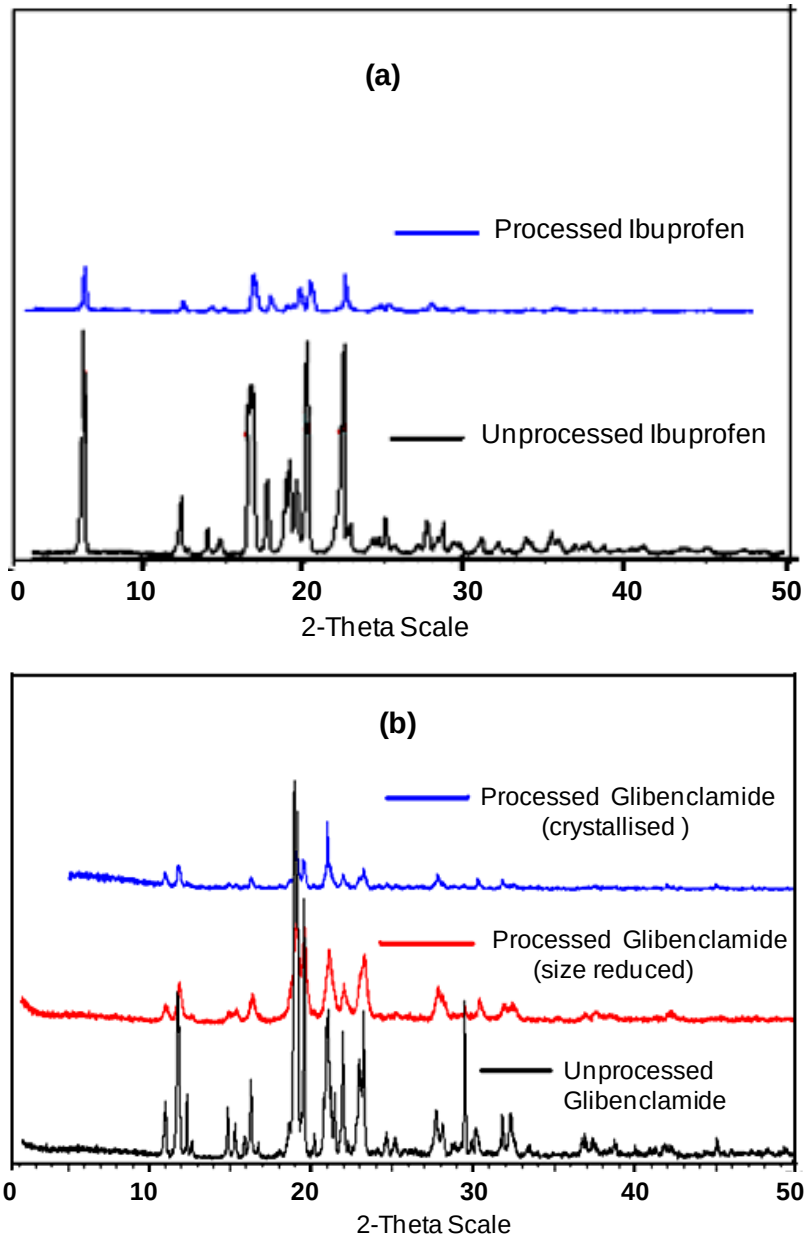

Figure 3.7 PXRD patterns of unprocessed and processed (a) ibuprofen and (b) glibenclamide

The marked variation in the peak intensity of the unprocessed samples is considered to be due to preferred orientation effects.

3.3.1.3 Physical and Chemical Stability Studies.

Physical stability of the nanocrystals is an important issue and nanocrystals in suspensions are prone to aggregation and Ostwald's ripening which can increase particle and also lead to sedimentation and caking. For both drug materials the particle size was found to be relatively stable for up to 30 days, with slight growth over the first 10 – 15 days (Figures 3.8 and 3.9).

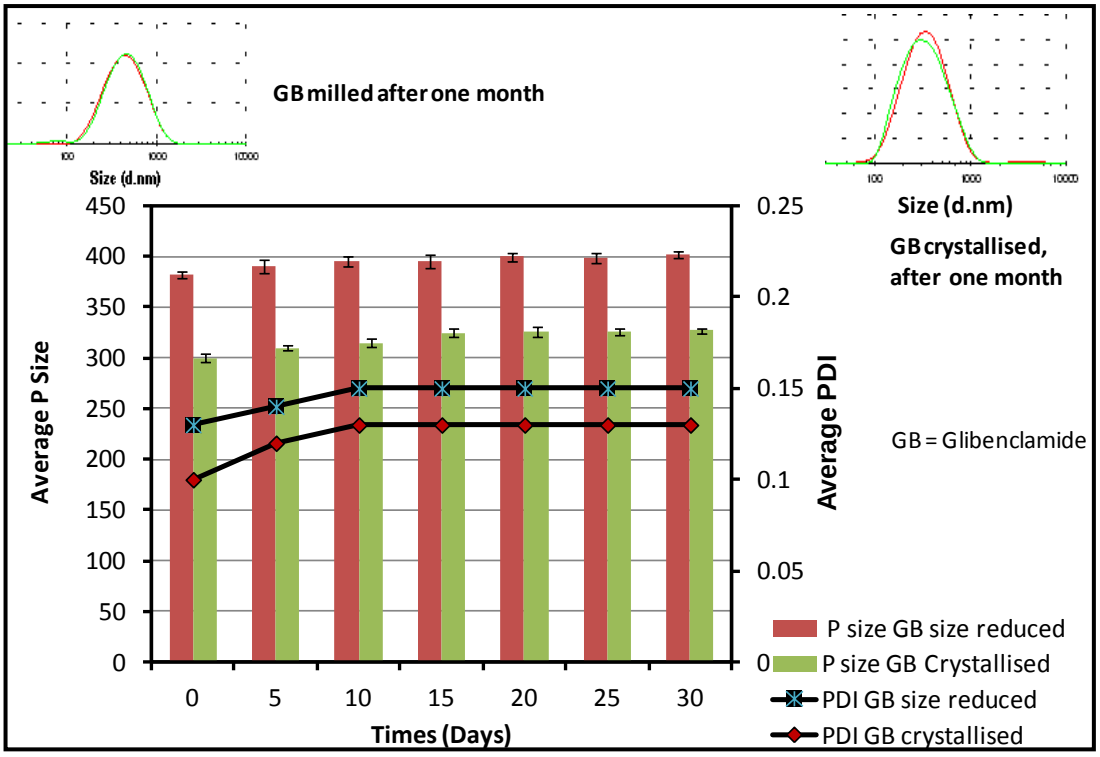

Figure 3.8 Particle size of nanocrystals of glibenclamide as a function of storage time at 25 °C

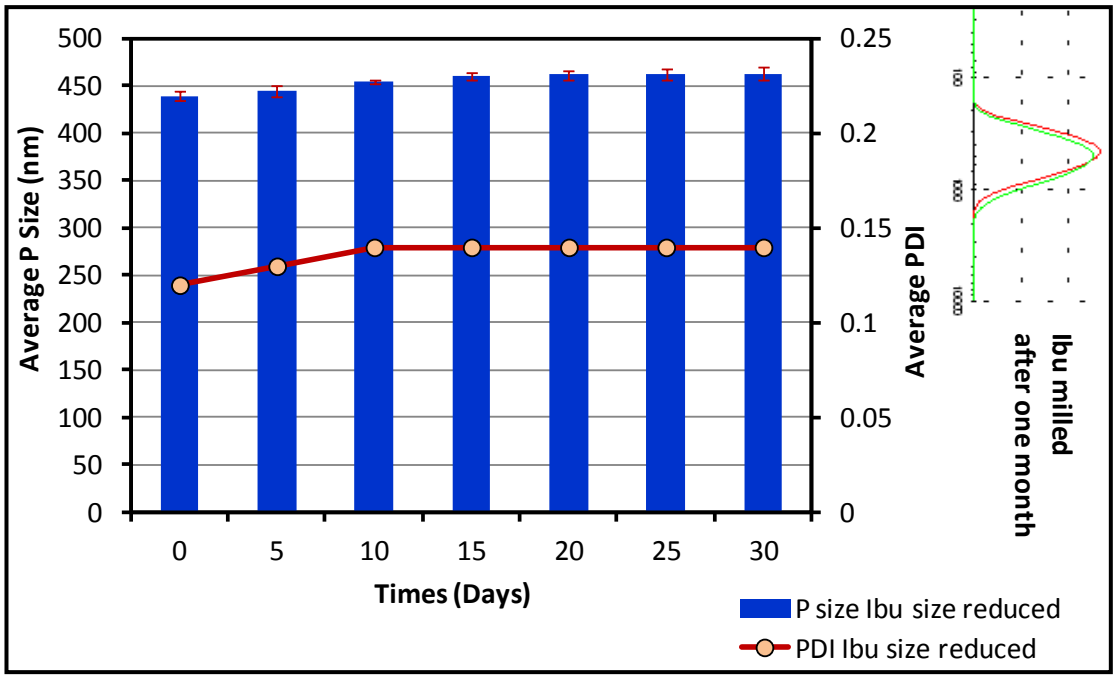

Figure 3.9 Particle size of nanocrystals of ibuprofen, as a function of storage time at 25 °C.

HPLC assay results shown in Table 3.1 demonstrated that >90 % of the nominal drug content was recovered from nanosuspensions of both drugs, whilst for glibenclamide the degree of recovery was greater for the crystallized suspensions than for the formulations produced by size reduction. The slight reduction in drug content observed for the size reduced nanosuspensions for both drugs is probably related to retention of solids on grinding media and on the stainless steel screen which is designed to retain coarse particles and the grinding media within the size reduction chamber.

Table 3.1 Quantification of glibenclamide and ibuprofen nanosuspensions

Samples	Drug concentration (mg/ml) in nanosuspension	Percent nominal
Glibenclamide nanosuspesion (size reduced)	23.5.0± 1.5	90.30± 0.25
Glibenclamide nanosuspesion (crystallized)	0.49 ± 0.2	98.00± 0.5
Ibuprofen nanosusepsnion (size reduced)	23.0±2.0	91.00±2.0

3.3.1.4 Adsorption Studies

Table 3.2 shows HPLC results which demonstrates that greater levels of glibenclamide adsorption were observed at the highest concentrations of DCP ((X90= 44.85 µm), regardless of the method of fabrication (crystallization and comminution). At concentration 180mg/ml the maximum adsorption was found, where >95% of the drug nanocrystals were obtained from the filtrate (Figure 3.10). In this regard, it is probable that greater adsorption was derived from marked increase in the surface area of DCP available for adsorption at high concentration. DCP has previously been reported as good inert carrier for adsorption of microparticles (Seth, 1988). Milled nanocrystals however exhibited a slightly greater affinity for adsorption than the crystallised counterparts. A number of previous articles describing the impact of comminution have suggested that size reduction is often responsible for mechanical activation in which the crystalline surfaces

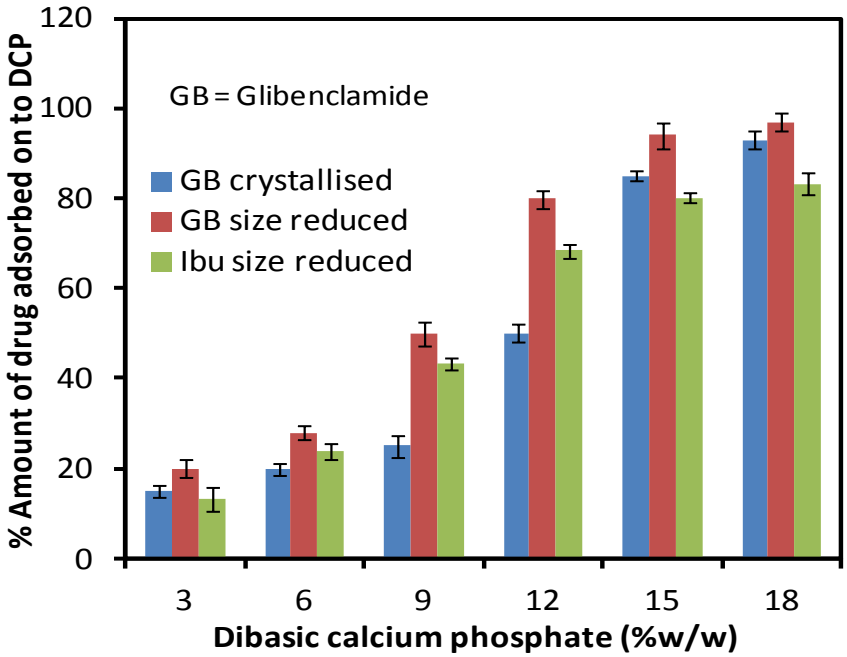

Figure 3.10 The degree of isolation of glibenclamide and ibuprofen nanocrystals onto DCP achieved from both milled and crystallisation as a function of DCP concentration.

become disordered with concomitant increases in surface free energy (Hüttenrauch et al., 1985, Roberts et al., 1994, Verma et al., 2009, Delogu, 2005). It is this increase in surface energy caused by exposure to high energy during processing which is probably responsible for increased adhesion to the inert carrier (Annapragada and Adjei, 1996, Tangsathitkulchai, 2003, Hüttenrauch et al., 1985). At higher concentrations, this enhanced interaction for adsorption was however negligible (where only a 5% difference existed) with ample surface being available for particle adsorption at the highest concentrations of DCP and subsequent saturation of the carrier surface. The stirring and agitation allowed the nanocrystals to be mixed and adsorbed onto the DCP surface.

The DCP adsorbates recovered after mixing with size reduced samples of ibuprofen and glibenclamide also demonstrated the relationship between the

concentration of the inert carrier, and the degree of recovery of drug nanocrystals (Tables 3.2 and 3.3). Nonetheless the results shown in Table 3.2 also demonstrated that the relative affinity of glibenclamide for adsorption onto the surface of DCP particles was markedly greater than for ibuprofen, with only 90% being recovered for ibuprofen particles compared for the levels of 97% observed for size reduced glibenclamide samples. It is probable that this finding relates in part to differences in the molecular nature of the surfaces of nanoparticles constructed from the two drug compounds. Glibenclamide is a molecule which comprises two main functional groups, one being a carboxylic acid and the other an aromatic ring (Figure 3.1). The comparative adsorption tendencies of the drug to DCP have been shown in Figure 3.10. The structure of glibenclamide contains eight hydrogen acceptors and three hydrogen donors and contains moieties rich in both nitrogen and oxygen(Byrn et al., 1986) which provides potential for strong intermolecular interactions with the DCP substrate rich in phosphate groups and water of crystallization.

What might be the essential factors for maximizing the adsorption efficiency and at the same time keeping the self-aggregation of the nanocrystals at a minimum? This problem is similar to that encountered in the design of formulations for dry-powder inhalers, where micron-sized drug particles are adsorbed onto a large carrier particle to deal with the cohesiveness and resulting poor flow of the micronized drug material (Lohrmann et al., 2007, Bunker et al., 2005, Adi et al., 2007, T. Srichana, 1998, De Boer et al., 2005). The two problems, however, are not identical. There are a number of distinctions. For the nanocrystal problem (i) the adsorption occurs in a liquid

medium, which has the potential to modulate the nanocrystal-carrier interaction; (ii) excessively strong adsorption of the nanocrystals onto the carrier particle is not an issue, since the detachment of the nanocrystals is not of interest; (iii) the nanocrystals in suspension are generally stabilized against aggregation and their surfaces will have significant amounts of adsorbed polymer and surfactants.

For the drug-carrier problem in the dry-powder inhaler context, some of the important factors include hygroscopicity, surface roughness, particle size and shape, and surface energy of the respective particles, and drug-carrier adhesion (Saleem et al., 2008, Hooton et al., 2008, Traini et al., 2005, Islam et al., 2005, Srichana et al., 2000, T. Srichana, 1998, Dickhoff et al., 2006, Larhrib et al., 2003, Flament et al., 2004, Zeng et al., 2000, Podczeck, 1999, Price et al., 2002, Adi et al., 2008). Clearly, in the nanocrystal context, hygroscopy is not a factor since we are dealing with solid-solid interactions in a liquid medium. On the other hand, crystal particle size and shape and crystal surface characteristics are pertinent, the latter in particular influencing drug-carrier interaction. A particularly useful concept is the cohesive-adhesive balance (CAB)(Begat et al., 2004, Begat et al., 2005, Hooton et al., 2006, Jones et al., 2008) which characterizes the cohesion of the drug with itself relative to the adhesion of the drug particles to the carrier particles. A CAB ratio < 1 characterizes a situation where the drug's interaction with the carrier particle (adhesion) is stronger than that between the drug particles themselves (cohesion). To maximize the nanocrystal-carrier adsorption efficiency a high adhesive interaction between the nanocrystal and the carrier particle is essential. To keep the self-aggregation of the adsorbed

nanocrystals to a minimum so as to maintain the original surface for rapid dissolution, the requirement is low cohesion between the nanocrystals. Therefore, we need to aspire for a CAB ratio << 1 in developing an appropriate formulation of the nanocrystal suspension and/or in selecting an appropriate carrier particle. Low cohesion between nanocrystals is an essential requirement anyhow in developing stable nanosuspensions. The focus therefore shifts to maximizing the interaction between the nanocrystals and the carrier particles. An additional consideration is how the liquid medium in the nanosuspensions modulates the nanocrystal-particle interaction?. This cannot be predicted for a given system even in general terms, given the heterogeneous nature of nanosuspensions containing surfactant and/or polymer stabilizers. However, in principle a change in the nature of the liquid medium coupled with an appropriate choice of a carrier particle could facilitate adsorption of the nanocrystals onto the carrier due to hydrophobic-type forces. For instance, if the nanocrystal material and the carrier particle were relatively hydrophobic, then in an aqueous medium the hydrophobic forces would actively promote the adsorption process (Israelachvili and Pashley, 1984, Ducker et al., 1994, Liang et al., 2007). Indeed these considerations suggest that a one-step process using the precipitation method in the presence of carrier particles could be an effective approach.

We noted above that the adsorption efficiency for the two drugs prepared by comminution showed a small but a systematic difference, the recovery of glibenclamide nanocrystals being slightly higher at all concentrations of the carrier particles. Whilst the nanocrystal-carrier particle interaction is likely to be complex due to the presence of adsorbed stabilizers and the fact that it

occurs in a aqueous medium, we explored the possibility of rationalizing the differences in the adsorption efficiency on the basis of molecular interactions on the crystal surfaces of the two drug materials. Crystal morphology calculations were undertaken for the drug materials to identify the functional groups exposed at the dominant surfaces of crystals (Chapter 2 (Section 2.2.2.9)). For ibuprofen the habit is dominated by the (100) face (65%) which is essentially non-polar (Figure 2.17). For glibenclamide the calculations revealed two major faces (10-1) (23%) and (011) (36%) both of which are polar in nature exposing SO, NH and CO groups (Figure 2.18). Focusing on the carrier, the major habit face for dibasic calcium phosphate is known to be face (010) is dominated by repeating units of the polar functional groups that include OH and PO_4 (Dickens et al., 1972, MacLennan and Beevers, 1955, Louati et al., 2005, Sivakumar et al., 1998, Abbona et al., 1993).

The dominant faces for the two major morphologies calculated for glibenclamide were characterized by polar functional groups with potential to form hydrogen bonds, which supports the strong adsorption to DCP observed in experimental studies. This type of interaction of DCP with ionic surfactants has also been reported previously (Wei et al., 2007). It can therefore be summarized that ibuprofen with its predominance of non polar functional groups is likely to exhibit lower adsorption than glibenclamide which demonstrates greater potential for hydrogen bonding.

Table 3.2 Quantification of glibenclamide content on the surface of DCP. (*Assumes complete retention of drug on DCP surface)

DCP concentration (mg/ml)	Quantity of powder tested (mg)	Dilution phase (ml)	*Hypothetical drug concentration in diluted sample (µg/ml)	Controlled crystallisation		Comminution	
				Drug contents isolated (µg/ml)	% of the drug isolated± Standard deviation	Drug contents isolated (µg/ml)	% of the drug isolated± Standard deviation
30	124.5	100	20	3.00	15.00±1.00	4.00	20.00±1.5
60	246.9	100	20	4.10	20.5±2.25	5.60	28.00±2.0
90	369.35	100	20	5.40	27.00±3.00	10.00	50.00±2.5
120	491.8	100	20	10.00	50.00±1.50	16.00	80.00±1.2
150	614.25	100	20	17.00	85.00±1.00	18.80	94.00±1.0
180	736.7	100	20	18.40	92.00±1.25	19.50	97.5.00±0.50

Table 3.3 Quantification of DCP powder recovered after mixing with glibenclamide and ibuprofen nanosuspensions size reduced (*Assumes complete retention of drug on DCP surface)

DCP concentration (mg/ml)	Quantity of powder tested (mg)	Dilution phase (ml)	*Hypothetical drug concentration in diluted sample (µg/ml)	Comminution (ibuprofen)		Comminution (glibenclamide)	
				Drug contents isolated (µg/ml)	% of the drug isolated± Standard deviation	Drug contents isolated (µg/ml)	% of the drug isolated± Standard deviation
30	124.5	100	20	3.00	15.00±1.00	4.00	20.00±1.5
60	246.9	100	20	4.00	20.00±2.25	5.60	28.00±2.0
90	369.35	100	20	5.00	25.00±3.00	10.00	50.00±2.5
120	491.8	100	20	10.00	50.00±1.50	16.00	80.00±1.2
150	614.25	100	20	16.40	82.00±1.00	18.80	94.00±1.0
180	736.7	100	20	18.00	90.00±1.25	19.50	97.5.00±0.50

.

3.3.1.5 SEM Studies

In addition to HPLC analysis, SEM micrographs of the pure DCP powders and DCP recovered from ibuprofen and glibenclamide nanosuspensions were generated (Figure 3.11)

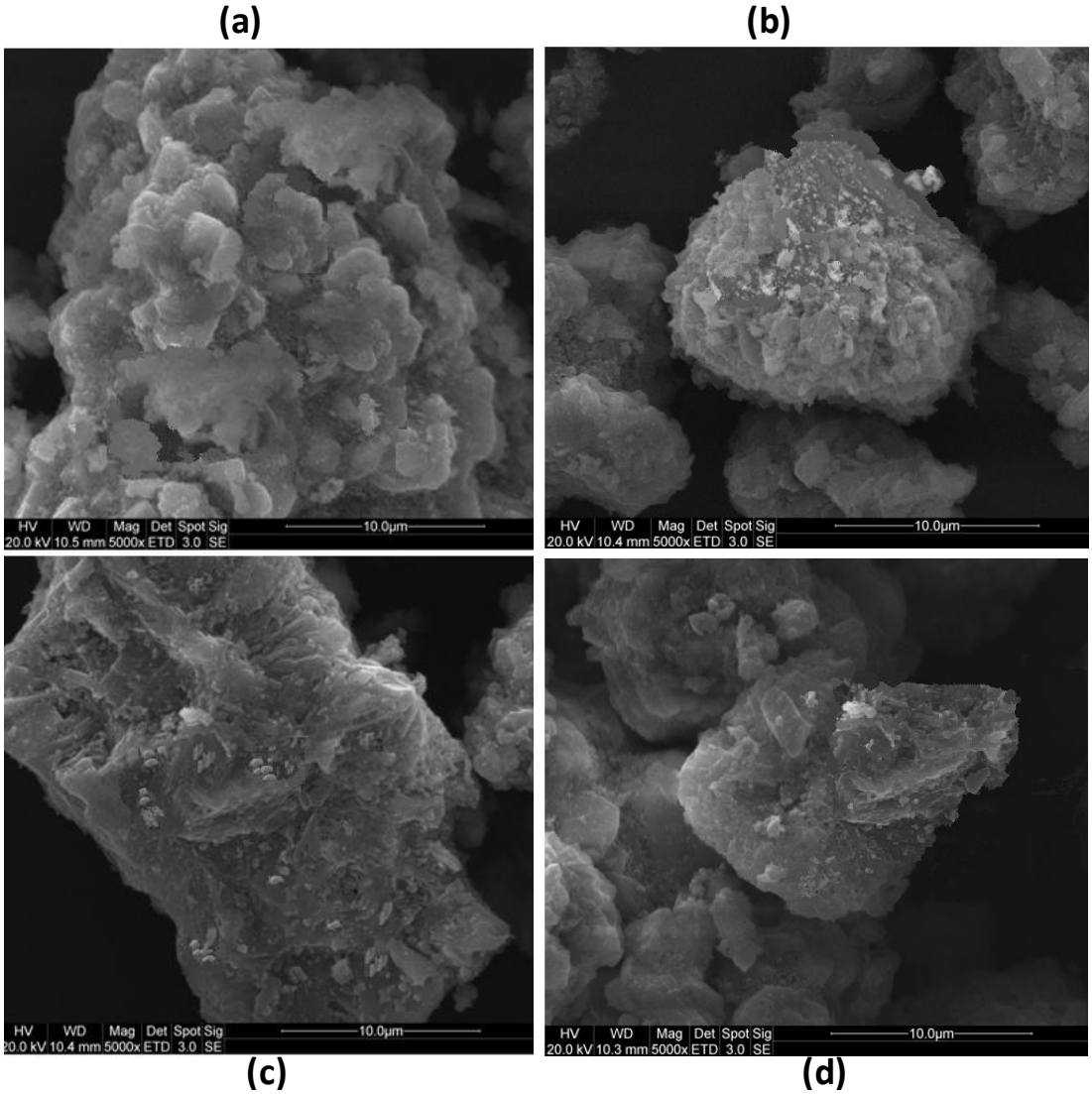

Figure 3.11 SEM micrographs of untreated DCP powder and DCP recovered from nanosuspensions; (a) = Untreated DCP powder; (b) = DCP recovered from Ibuprofen nanosuspension (milled); (c) = DCP recovered from Glibenclamide nanosuspension (milled) and (d) = DCP recovered from glibenclamide nanosuspension (crystallized).

SEM micrographs of the DCP powder recovered from the nanosuspensions mixed with a concentration of 180mg/ml showed that nanocrystals were

adsorbed extensively on to the surface, which can be observed as small white deposits. However no deposits were observed on the surface of the pure DCP powders (Figure 3.11 (a)). Similarly SEM micrographs of DCP powder recovered from crystallized glibenclamide showed fewer nanocrystals deposits than the formulation produced using size reduced drug. (Figure 3.11 (d))

3.3.1.6 Dissolution Studies

The dissolution rates of the glibenclamide and ibuprofen nanosuspensions and the respective nanocrystals adsorbed on the carrier particles are compared in Figure 3.12, along with suspensions of the micronized drugs and marketed tablets. These data revealed the expected rapid dissolution for the nanosuspensions for both drug materials, with about 90% dissolving within the first 5 minutes or so. Remarkably the dissolution of the nanocrystals adsorbed on the carrier particles is also rapid, being only 5-10% lower in value at the 5-10 minute sampling points after which the difference becomes insignificant. As expected, the dissolution rates of the suspensions of the micronized drugs and the respective tablet formulations are markedly lower.

The results described in Figure 3.12 show that dissolution rate of glibenclamide (size reduced and crystallized) and ibuprofen nanosuspensions (size reduced) was a faster than observed for the microsuspension and marketed tablets. More than 90% of the glibenclamide nanosuspension dissolved in 5 minutes which has also been reported previously (Van Eerdenbrugh et al., 2008). Approximately 100% of the drug from nanosuspensions had already dissolved between 28-55 minutes. There

was observed slight reduction in dissolution rate for the adsorbed nanocrystal compared to the nanosuspensions of glibenclamide. However these formulations showed marked increase in dissolution rate compared to the respective glibenclamide microsuspension, marketed tablets and raw powder. In addition for ibuprofen nanosuspensions there was observed enhanced dissolution rate compared to the commercial products. The drug nanosuspensions and the adsorbed ibuprofen on DCP showed > 80% dissolution rate within 2 and 10 minutes respectively which is faster compared to the spray and freeze dried nanosuspensions (Van Eerdenbrugh et al., 2008). Remarkably the dissolution of the nanocrystals adsorbed on the carrier particles is also rapid, being only 5-10% lower in value at the 5-10 minute sampling points after which the difference becomes insignificant.

The lack of significant lowering of the dissolution rate for the adsorbed nanocrystals on the carrier particles (relative to the nanosuspensions) suggests that the adsorbed nanocrystals largely remain isolated from each with very little loss in surface area due to self-aggregation. Clearly this is an essential requirement for the proposed approach of isolating/recovering nanocrystals by means of carrier particles from a suspension.

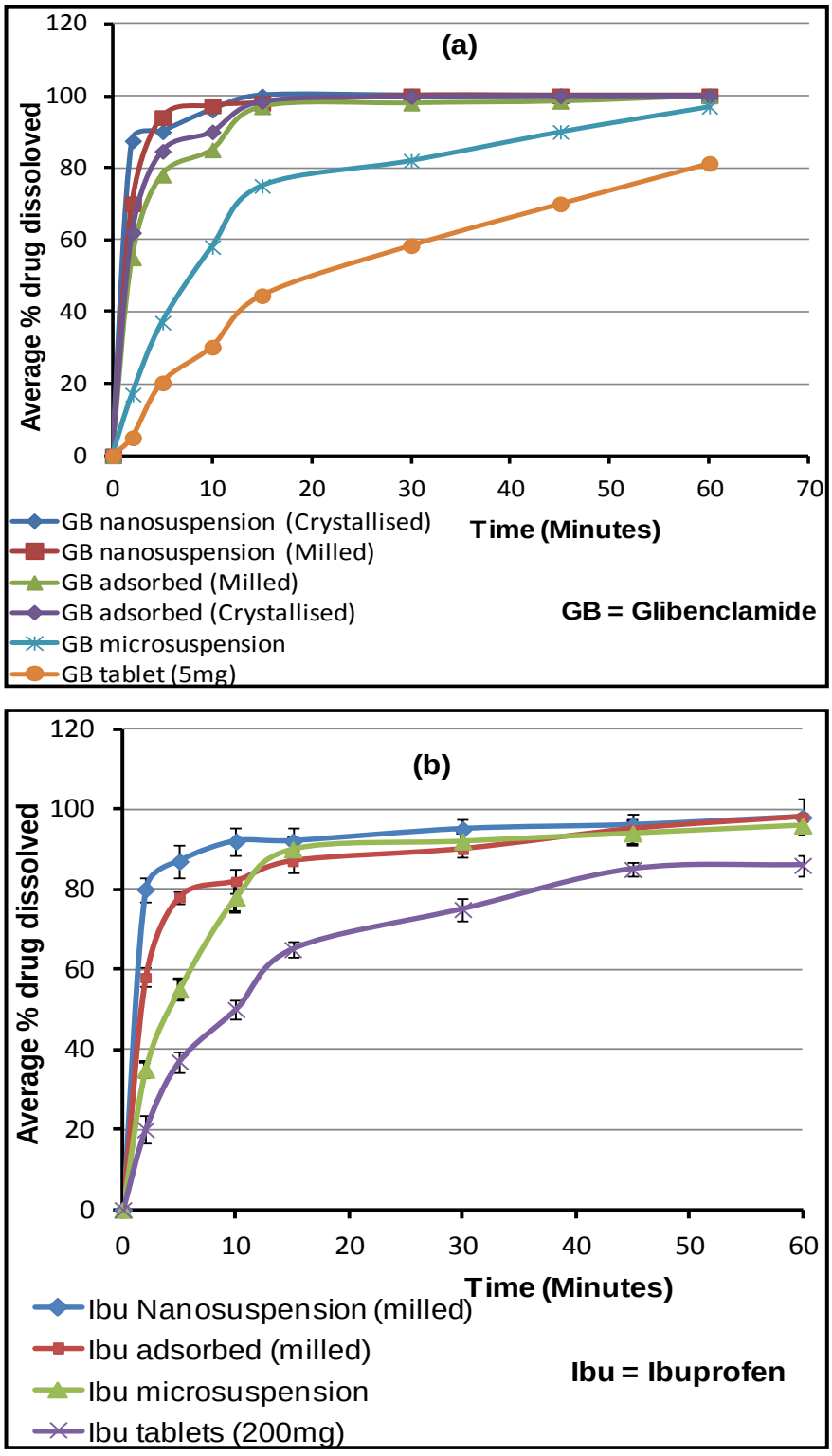

Figure 3.12 Dissolution profiles of nanosuspensions, adsorbed nanocrystals on carried particles, suspensions of the micronized drug and marketed tablets of (a) glibenclamide, (b) ibuprofen.

In summary this study demonstrated that nanocrystals without significant decrease in surface area can be isolated from nanosuspensions using water insoluble large carrier particles. We isolated nanocrystals of the two drugs (ibuprofen and glibenclamide) prepared by both comminution and crystallization. However it became evident that both carrier/drug surface morphology and the methods producing nanocrystals can affect the drug carrier interaction with subsequent isolation of the nanocrystals from nanosuspension. The drug surfaces with polar functional groups which form hydrogen bonding with carrier particles can lead to comparatively greater adsorption onto DCP. It was also observed that nanocrystals produced by crystallization have less affinity for the inert support material (DCP) compared to the size reduced nanocrystals. The greater tendency of size reduced nanocrystals to be adsorbed onto DCP surfaces can be because of the high surface free energy caused by mechanical activation. Our objective towards isolation of nanocrystals on DCP which have enhanced dissolution rate was also achieved because the isolated nanocrystals demonstrated marked dissolution rate compared to micronized and marketed tablets.

Chapter 4

Coarse Grained Simulation of the Earliest Stages of Anti-Solvent Precipitation

4.1 Introduction

Nanocrystals are fast becoming a platform solution to address the issue of poor solubility associated with hydrophobic drugs, offering immense surface area which enhances the dissolution rate. An important set of methods for preparing nanocrystals are the bottom up approaches detailed in Section 1.3.1, which include PCA, RESAS, SFL and EPAS. At the heart of bottom-up precipitation methods is crystal nucleation and growth, aspect of which we still do not entirely understand (Ruckenstein and Djikaev, 2005). The crystallisation process is central to a range of processes taking place in nature, pharmaceutical, food and chemical industries. In manufacturing, crystallization is employed both for purification and particle formation (Erdemir et al., 2009). A number of products including dyes, explosive and materials used in photography are formed by crystallization processes. In addition, approximately more than 90% of active pharmaceutical ingredients (APIs) and excipients are in crystalline form and controlled crystallization is essential to engineering pharmaceutical particles (Morris et al., 2001, Valder and Merrifield, 1996). The key step in crystallisation is nucleation as this determines the characteristics of the final solid formed. It is an important

step in generation of nanocrystals using anti solvent precipitation methodology.

In the anti-solvent method for preparing nanocrystals, the organic solution containing the drug is mixed into an antisolvent containing surfactants and polymers. The nucleation rate during mixing of the two phases depends on the level of supersaturation (LaMer and Dinegar, 1950). Nucleation is followed by growth of the particles by condensation which involves diffusion of molecules to the surface to be incorporated into the solid phase and coagulation (Weber and Thies, 2002).

The particle size of nanocrystals depends on supersaturation and rate of nucleation, the higher the nucleation rate the smaller the particle size. During crystallisation, if the material can form a number of polymorphic forms, initially the metastable structure is formed with subsequent transformation to stable phase (Kashchiev, 2000). It is therefore imperative to understand the nucleation process and all other factors which influence this process, because proper understanding of this process can control the final product being crystallised (Schüth, 2001). We also need to understand the role of stabilisers in determining the resulting nanocrystal particle size. Whilst we have a good general understanding of how stabilisers can prevent particle growth and aggregation during top-down processes such as comminution and during storage, the role of stabiliser in determining the final particle size using precipitation methods remains an open question.

To get a mechanistic understanding of the earliest stages of crystallisation we need to have an atomistic level resolution, which cannot yet be accessed using experimental techniques (Schüth et al., 2001). In view of this computer

simulation studies including Monte Carlo and molecular dynamic have been carried out to gain molecular level insights into the crystallization process (Esselink et al., 1994, Mandell et al., 1976, Swope and Andersen, 1990). Computer simulations however are still limited in terms of the time and length scales that can be accessed. Thus, if a process is relatively slow and has a random nature (as does the nucleation process) then it may be outside the scope of molecular simulation (Anwar and Zahn, 2011). In view of this we need to employ simpler models and one approach is to use a coarse grained approach (Marrink et al., 2004, Marrink et al., 2007).

Coarse grained models use fewer particles to represent the molecules and hence are considerably more efficient in accessing longer timescales at the cost of chemical specificity. MARTINI force field is used to obtain an optimised and quality coarse grained model. This force filed initially introduced for lipids but now it has been employed for a range of other complex molecules including, amino acids, sterol, surfactants, proteins and polymers (Marrink et al., 2004, Marrink et al., 2007, Monticelli et al., 2008, Bedrov et al., 2006). MARTINI force field is based on a mapping system, which usually group together four heavy atoms as a single bead (4-1 mapping). However for ring structures 3-1 or 2-1 mapping system is also employed. Particles which are considered as interaction sites in this force field include polar, nonpolar, apolar and charged which can be subdivided into other types on the basis of hydrogen bonding capabilities. The subtypes include donor (d), acceptor (a) both (da) and none (0). In addition, the particles are also labelled on the basis of polarity which is from (1-5). Similar potential parameters are employed to describe the bonded and nonbonded

interactions between the particles in coarse grained modelling as used in atomistic modelling. The interaction strength is however different for different types of particles. For example, the LJ parameter (ε) ranges from (5.6 - 2.0kJ/mol). The highest value (5.0kJ/mol) represents the interaction between the strong polar particles. Whereas the lower value (2.0kJ/mol) shows the interaction between polar and apolar particles. On the other hand, the LJ parameter σ = 0.47nm is considered effective for all the normal particle except the ring structures.

In present study we have investigated the early stages of antisolvent precipitation using coarse grained molecular simulation. In the current context the use of a coarse grained approach rather than atomistic models of specific chemicals is not an issue as the objective is to gain generic insight into what happens at a molecular level during anti-solvent precipitation. Thus, the interest is in what happens in general terms when poorly soluble molecules are precipitated, rather than what may happen for a particular system comprising, say, glibenclamide in ethanol using water containing PVP.

4.2 Methodology

4.2.1 Molecular Simulation of the Earliest Stages of Crystallization

The starting system comprised two juxtaposed solution phases, an aqueous phase containing PVP in water, and an ethanol phase containing the drug in solution (Figure 4.1 (a)). This mimics the initial interaction at the interface as the drug solution is dispersed in the aqueous solution containing stabilizers during nanocrystal preparation.

The drug (solute), water, and ethanol molecules were represented by single particles (labelled S, W, and E respectively) interacting with a Lennard-Jones (LJ) potential. The PVP molecule comprised 14 monomer units and consisted of a backbone of linked LJ particles (labelled BB) with attached particles of slighter larger dimension representing the side chain sugar groups (labelled SC). The coarse grained model of PVP is shown in Figure 4.1 alongside the atomistic model for comparison. The coarse grained particles in the PVP backbone and side chains were connected to each other by harmonic bonds using the potential function $U(r)=0.5k(r-r_o)^2$. The bond parameters were taken from the Martini forcefield (Marrink et al., 2007). The equilibrium bond distance between backbone (BB) particles was set to r_o=2.35Å and the force constant to k = 12.5 kJ $mol^{-1}Å^{-2}$. The equilibrium bond distance and force constant parameters for BB–SC bonds were 4.3Å and k = 12.5 kJ mol^{-1} $Å^{-2}$ respectively. The 3-body angle interactions for the particles in the backbone were represented by $U(\theta) =0.5k (\cos\theta-\cos\theta_o)^2$ with k=25.0 kJ mol^{-1} and an equilibrium angle of 180.0°, while for the side chains connected to the backbone we employed $U(\theta)=0.5k(\theta-\theta_o)^2$ with k = 25.0 kJ mol^{-1} $degree^{-2}$ and an equilibrium angle of 90°. The cosine form is appropriate when the equilibrium angle 180.0° for which the harmonic is unstable. The interaction parameters of the various coarse grained particles are given in Table 4.1. The diameter (the LJ σ parameter) of the LJ particles is generally fixed at 0.47 nm, hence making our parameters in this respect consistent with the established Martini force field (Marrink et al., 2007). The LJ ε have been parameterised to approximately correlate with the melting point of the substance or the chemical moieties being represented by the coarse grained

particle using the phase diagram of the LJ system (Agrawal and Kofke, 1995, Anwar and Boateng, 1998). Thus the models of the drug, water, and ethanol have the melting points 423 (150 °C), 273 (0°C), and 159 (-114 °C) K respectively. The backbone particles of the PVP molecule were characterised by interaction parameters that gave a melting point of approximately 90K (-183 °C) for the monomer units (-CH_2-CH_2- equivalent) whilst pyrollidone particle representation had a stronger interaction reflecting a melting point of about 298K (25 °C) for this moiety. The masses of coarse grained (CG) particles of water, ethanol and solute particles were 72 amu. For the PVP model, the CG backbone particles (BB) mass was taken to be 32.0 amu representing a 2-to-1 coarse grained to atomistic mapping while the side chain particles (SC) had a mass of 72.0 amu.

The MD simulations were carried out using DL-POLY2 (Smith et al., 2006) in the constant temperature constant pressure (NPT) ensemble. The temperature and pressure employed were 298K and 1bar respectively using the Hoover algorithm with the thermostat and barostat relaxation times set to 1.0 ps and 10.0 ps respectively. The time step was 20 fs. The van der Waals interactions were truncated at 1.2 nm. The models were uncharged and consequently there were no charge-charge interactions. The system contained a total of 70000 molecules comprising 17500 drug molecules, 17500 ethanol molecules, 34977 water molecules, and 23 PVP molecules. The simulation covered a period of 180 ns.

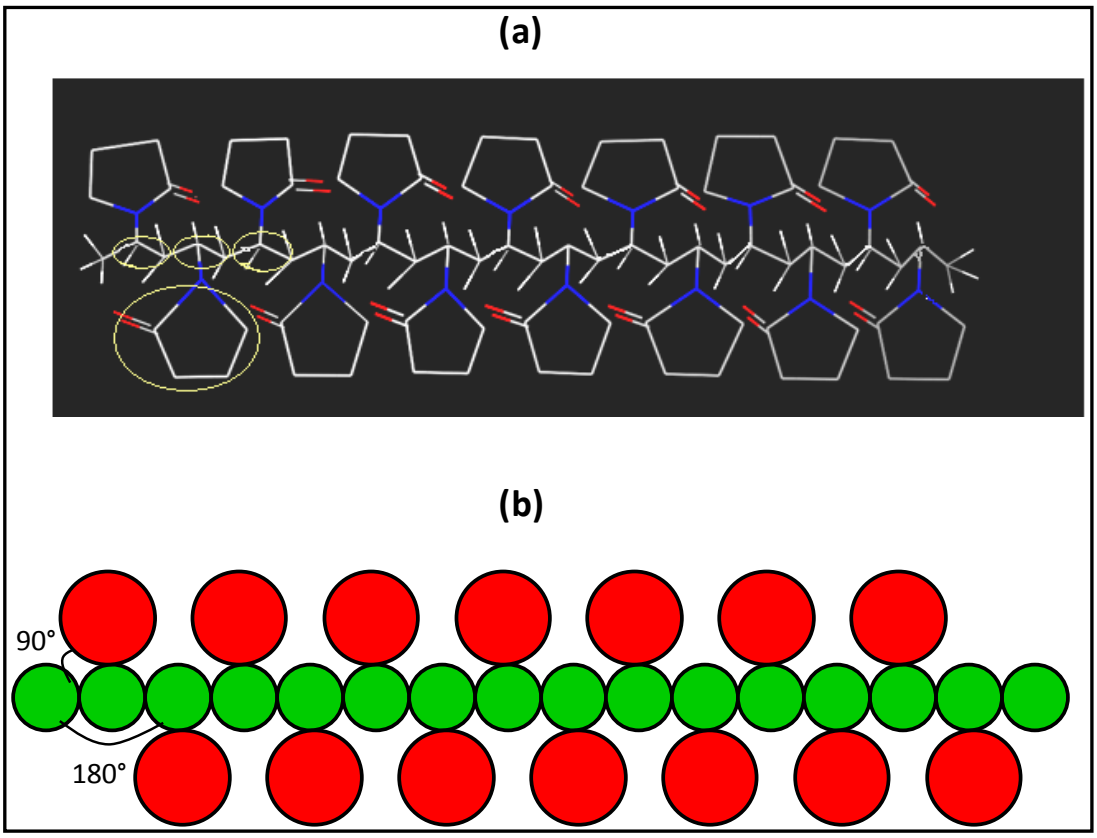

Figure 4.1 (a) Molecular structure of PVP, (b) coarse grained model of PVP, the green particles are referred to as BB (backbone) whilst the red particles are referred to as SC (side chain).

Table 4.1 Lennard-Jones parameters for the coarse grained particles representing solute (S), ethanol (E), water (W) and the polymer PVP (BB-backbone particle; SC = side chain particle).

Particle-Particle Interaction	ε / kJmol^{-1}	σ / Å
BB–BB	1.0	4.7
BB–SC	1.9	4.7
BB–S	2.24	4.7
BB–W	1.81	4.7
BB–E	1.81	4.7
SC–SC	3.6	4.7
SC–S	4.5	4.7
SC–W	3.43	4.7
SC–E	3.43	4.7
S–S	5.0	4.7
S–W	2.0	4.7
S–E	3.50	4.7
W–W	3.28	4.7
W–E	3.28	4.7
E–E	3.28	4.7

4.3 Results and Discussion

4.4 Molecular simulation of the Earliest Stages of Crystallization

Snapshots of the molecular dynamics simulation of the earliest stages of precipitation are shown in Figures 4.2, 4.3 and 4.4. The starting system consists of two solutions, drug in ethanol and an aqueous solution containing the PVP molecules (Figure 4.2 (a)), juxtaposed to each other as might be when the volume element of the drug solution is brought into intimate contact with the anti-solvent media by mixing. Immediately the two solutions begin to mix as the water and the ethanol molecules diffuse across the original solvent boundaries (Figure 4.2 (b)). One might expect the water to diffuse into the solvent solution thereby reducing the interaction of the resulting mixed solution with the

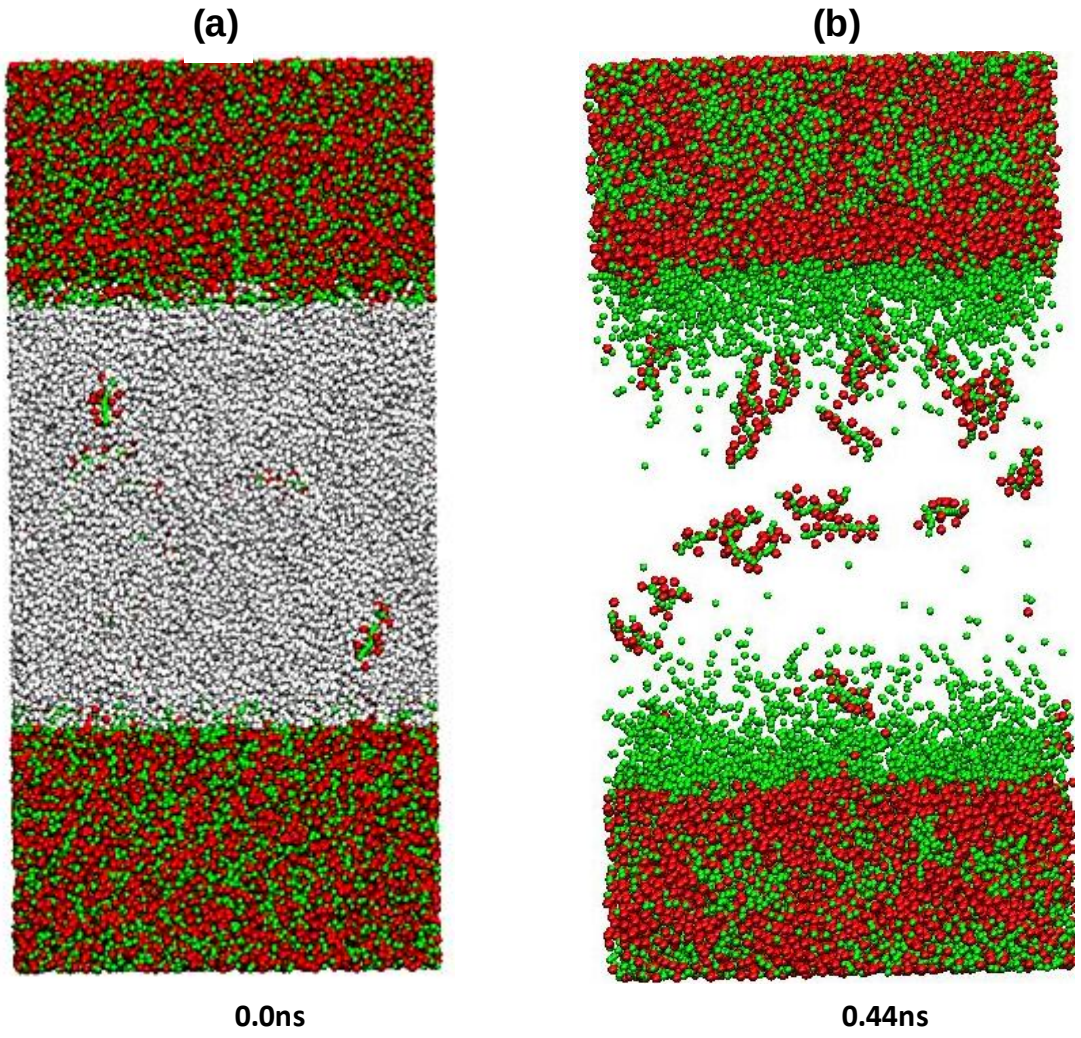

Figure 4.2 Snapshots of the (a) molecular dynamics simulation trajectory for the juxtaposed volume elements of the solute solution and the anti-solvent; (b) snapshot reflecting the initial stages of dispersion of the solute solution into an anti-solvent. The solute is represented by red particles, water by grey particles, and solvent by green particles.

solute molecules and causing them to aggregate and crystallise. The simulations however reveal a slightly different picture. As the two solutions begin to mix, in the main it is not the water molecules that diffuse into the solvent solution to reduce the solute–solvent interaction; rather the ethanol molecules diffuse out from the solute particles into the aqueous environment enabling the solute molecules to aggregate and eventually crystallise (Figure 4.3 (a)). These events are intuitive: the affinity of water for the solute

molecules is low and hence water would not be expected to enter in any significant way into a solute-rich region.

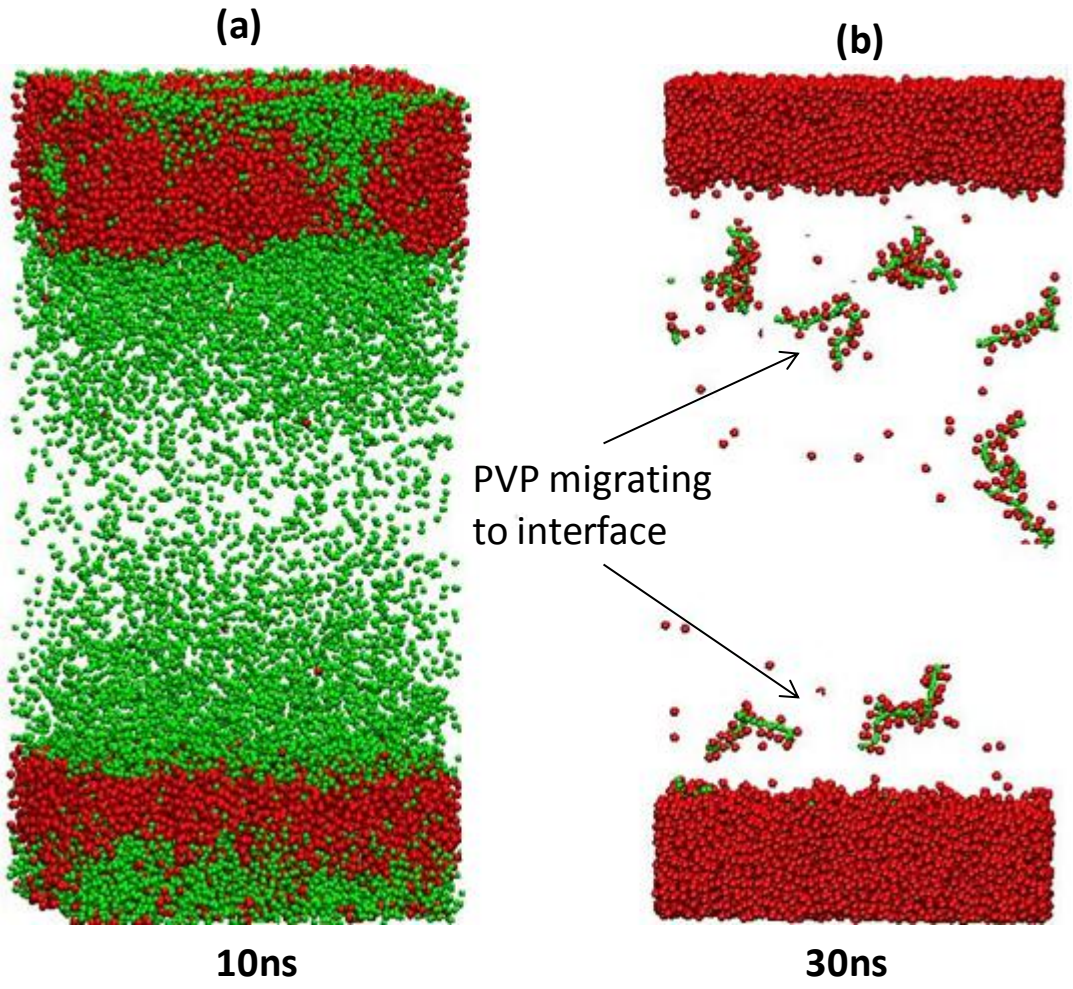

Figure 4.3 Snapshot (a) shows more than 50% of ethanol particles (Green) mixed with water whereas snap shot (b) shows migrating of PVP molecules towards the interfaces. Water particles have been removed to show the diffusion of solute particles.

As for the crystallization process itself, we observe a two-stage process, aggregation of solute particles in a liquid-like mass and then nucleation, which is now an accepted mechanism for nucleation at high supersaturations (Anwar and Boateng, 1998, Bonnett et al., 2003, Zhang and Liu, 2009, Vekilov, 2004). As the solute molecules consolidate and crystallise we observe the migration of the PVP molecules to the crystal surfaces. Being

large molecules the diffusion of the polymer molecules is relatively slow (Figure 4.3 (b) and Figure 4).

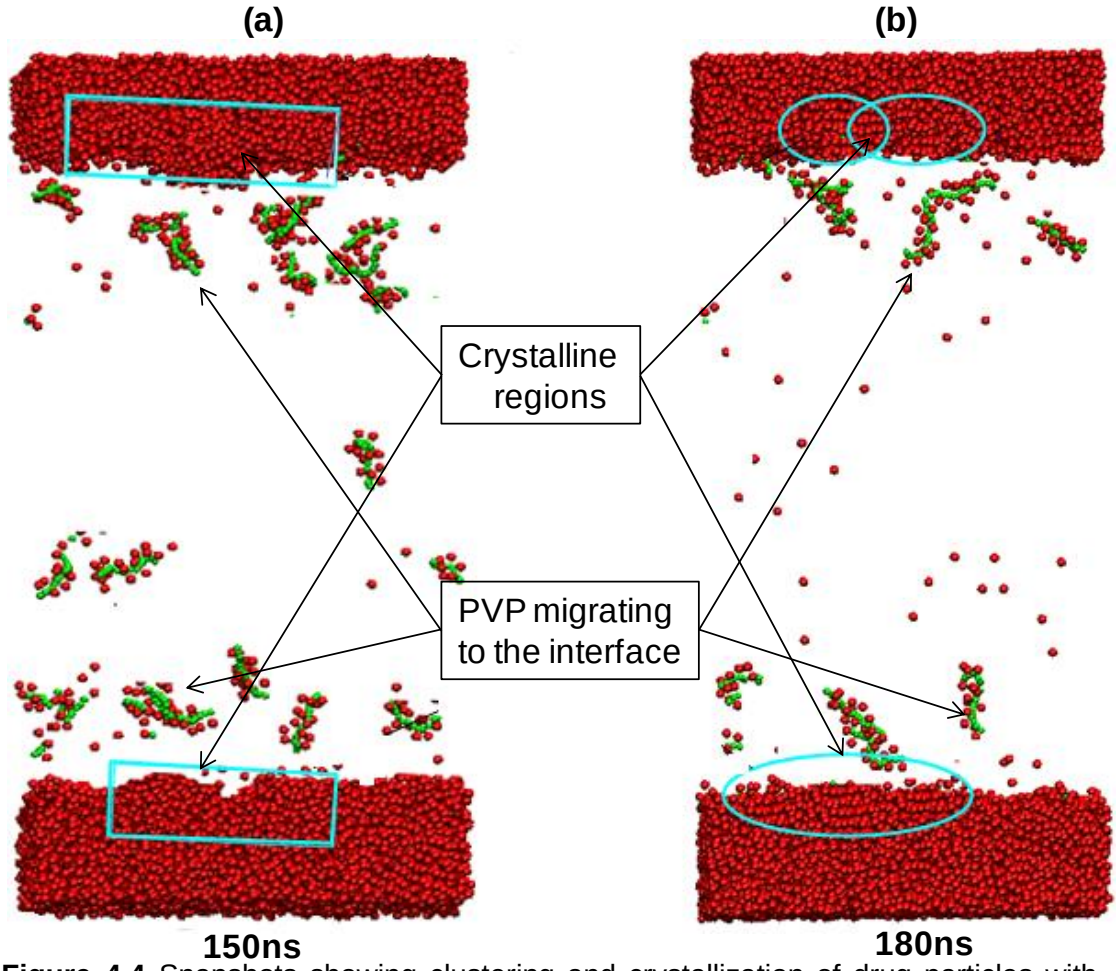

Figure 4.4 Snapshots showing clustering and crystallization of drug particles with PVP particles approaching to the interfaces. Solvent and water particles have been removed to clearly show the crystallization of drug particles.

This suggests that polymers in general, regardless of whether they have surface activity or not, are unlikely to play a significant role in promoting nucleation. The phase separation of the solute molecules from the solvent is a relatively fast process and polymer molecules which diffuse only slowly are unlikely to be involved at the rapidly-emerging solute–solvent interfaces. Furthermore, given that nucleation is likely to involve the two step mechanism, the important interface that limits nucleation will be between the liquid-like solute structure and the emerging nuclei. The polymer molecules

are likely to be within the aqueous volume element and hence would not be expected to be involved within liquid-like solute mass.

One might consider (or infer from the above discussion) that the size of the nanocrystals must be dictated by the volume element of the solvent solution that finds itself isolated within the aqueous solution; the size of this volume element being dependent on the extent and nature of the mixing, which is an issue of bulk mass transfer. Such a consideration, however, cannot explain the observed dependence of nanocrystal size (for any given drug substance) on the attained supersaturation (Horn and Rieger, 2001). To explain this effect, the volume element of the solvent solution must phase separate into a number of smaller clusters, each then nucleating to yield a separate nanocrystal. Simply having many nucleation events within a large solute mass will not yield separate individual crystals but rather a single polycrystalline particle. What might be the drive such a phase separation? At high supersaturations the driving force to nucleation becomes so high such that the barrier to nucleation is minimal and the system exhibits spinodal decomposition (Hilliard, 1970, Favvas and Mitropoulos, 2008), a phase separation process which is limited by diffusion and results in regular density fluctuations. In the current context, spinodal decomposition would mean separate solute clusters within the volume element. The size of these clusters will depend on both the extent of supersaturation and the diffusion coefficient of the solute. These considerations explain not only the dependence of nanocrystal size on attained supersaturation and the issue of a factor (diffusion coefficient) intrinsic to the molecule. Equally importantly, spinodal decomposition also explains why we are able to obtain nanocrystals

using only a magnetic stirrer rather than high-energy mixing techniques; spinodal decomposition causes the volume elements of solute in solvent attained by simple stirring to phase separate into smaller independent clusters.

In summary this study provided physical insight into the formation of nanocrystals during anti-solvent crystallization. It explored the diffusion mechanism of solute, solvent and anti-solvent (water) molecules which lead to phase separation of the two solutions during mixing process. It became evident that the solute molecules here say glibenclamide are crystallized in organic solvent region during mixing of the solvent and antisolvent phases. This is because of the hydrophobic nature of the drug molecules which cannot accommodate the water molecules to be infused and the solvent molecules are diffused towards the water phase. In consequent to that the drug molecules begin to aggregate followed by nucleation and crystallization.

Chapter 5

Phase Stability of Bulk and Nanocrystals of Glycine Using Molecular Simulation

5.1 Introduction

Polymorphism and unpredicted polymorphic phase transformations can present major difficulties and challenges in pharmaceutical development. Different polymorphic forms can exhibit markedly different mechanical and physicochemical properties that include crystal morphology, solubility, dissolution rate, tabletting behaviour, melting point, thermal conductivity and chemical stability (Brittain, 1999, Bernstein, 2002). In pharmaceutical development the selected polymorphic form of an API can often transform from one form to another under the employed tabletting pressure, or on storage depending on humidity and temperature causing problems in development (Carstensen, 1977, Morris et al., 2001, Lee et al., 2008). The control of polymorphism is therefore paramount to producing high quality pharmaceutical products (Singhal and Curatolo, 2004, Vippagunta et al., 2001).

Polymorphism is also an issue for nanocrystals. Like bulk crystals, nanocrystals too can exist in different polymorphic forms. However, the phase stability relationships that characterise bulk crystals need not characterise nanocrystals. Experimental evidence indicates that as particle

size is reduced the phase diagram may change and could lead to a phase which was unstable in the bulk crystal becoming thermodynamically more stable for nanocrystals (Ranade et al., 2002, McHale et al., 1997, Garvie, 1978). Figure 5.1 (a) show the effect of particle size on phase stability of different polymorphs of TiO2 and schematic representation of the effect of size on phase stability as a function of temperature respectively (Figures 5.1(b)).

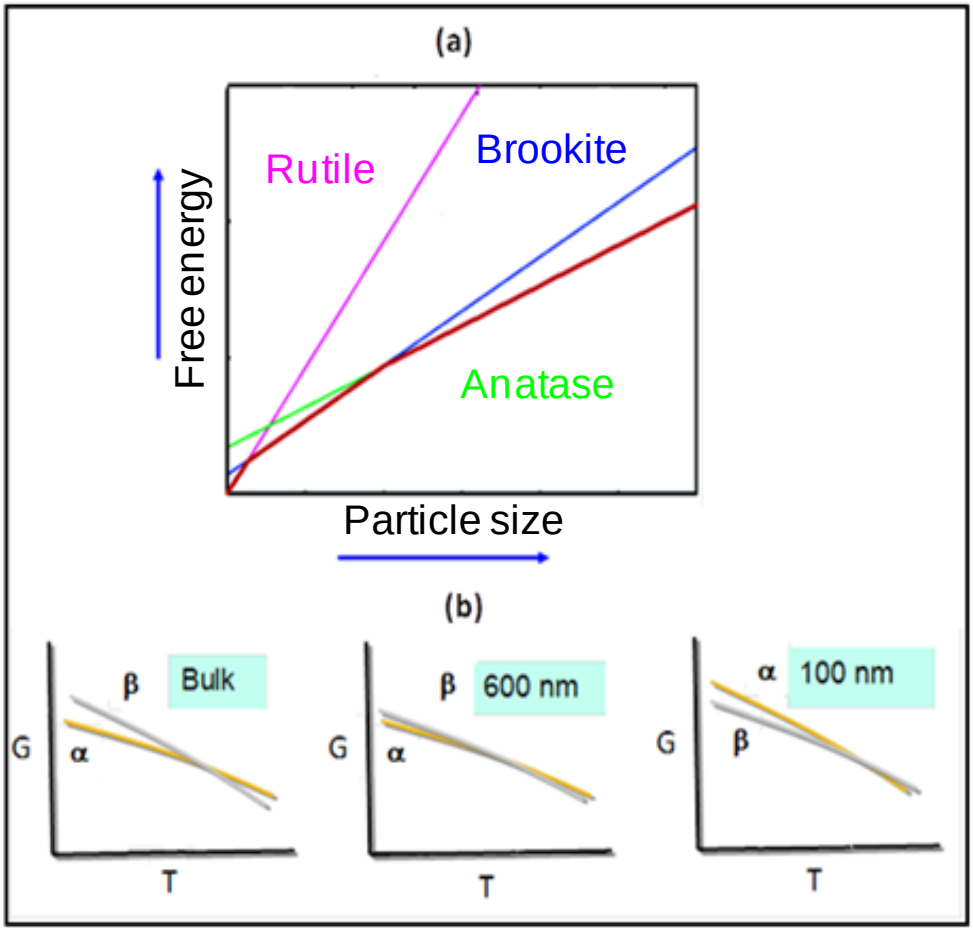

Figure 5.1 (a) Effect of particle size on stability of various phases of TiO2 as a function of particle size (Ranade et al., 2002) and (b) schematic representation of the effect of temperature (T) on phase stability of different phases of a crystal as a function of particle size.

According to the Ostwald step rule, during nucleation the newly created first phase is a metastable phase which transforms subsequently to a stable

phase (Ostwald, 1897). This mechanism was qualified by Stranski and Totomanow (Stranski and Totomanow, 1933) , that the first phase formed is that for which the nucleation barrier is the lowest. The interplay of the bulk and interfacial free energy of the new phase are considered the key determinant for understanding the phase transformation steps until the thermodynamically stable phase is produced (D. Zahn, J. Anwar, Size-Dependent Phase Stability of a Molecular Nanocrystal: a Proxy for Investigating the Early Stages of Crystallization, Chem. Eur. J. 2011, 17, 11186 – 11192). These two quantities alter as a function of particle size of a crystal. Therefore the stability of a particular phase in bulk crystal form could be different from that in the nanocrystal form. Being able to prepare stable nanocrystals of a crystalline phase which otherwise would be unstable in bulk offer new opportunities both technically and commercially e.g. in the form of intellectual property. The present study employs molecular simulation to investigate the phase transformation behaviour between various forms of the model compound glycine in both bulk crystals and nanocrystals as a function of both temperature and pressure. Glycine was chosen as its crystallization behaviour, polymorphic forms and phase transformations are well characterised experimentally.

Glycine (NH2CH2COOH) is one the simplest amino acids and is widely used in a number of pharmaceuticals either by itself or as intermediate agent for synthesis of pharmaceutical compounds which include nucleic acids (Rabesiaka et al., 2010). The molecule exists in its zwitterionic ($H3N^{+}$–CH2–COO^{-}) form both in the solid and in solution. It has three polymorphs α, β and γ at ambient temperature and pressure (Albrecht and Corey, 1939). Recently,

two other polymorphs of glycine (δ-glycine and ε-glycine) have been reported to exist at high pressure (Dawson et al., 2005). All these polymorphs exhibit different physical properties including densities, shapes, space group symmetries, solubility and bioavailability. At ambient temperature and pressure the order of thermodynamic stability between the main polymorphs is as γ > α > β (Sakai et al., 1992). A high temperature and pressure is required for phase transformation between the three polymorphs (Kvick et al., 1980a, Ferrari et al., 2003, Iitaka, 1961, Boldyreva et al., 2003). β- polymorph is the least stable and is rapidly transformed either to α or γ forms in the presence of moisture at room temperature (Kvick et al., 1980a, Ferrari et al., 2003). The β-phase transforms to α-phase at temperature >373K (Iitaka, 1961, Dang et al., 2009, Drebushchak et al., 2002b). The α phase can transform to the more stable γ- phase at around 443K (Park et al., 2003, IITAKA, 1954).

Whilst the γ- phase is thermodynamically stable phase at ambient temperature and pressure, it is possible to crystallise other forms by varying the crystallisation conditions. The important factors affecting the choice of form that crystallises include nature of solvent, concentration of solution, mixing, agitation rate seeding and cooling rate (Myerson, 2002).

All the three ambient temperature and pressure polymorphs of glycine are soluble in water and these can be recrystallised either by cooling or evoparation (Lin and Pepe, 1998). The α-phase with the space group ($P2_{1/n}$) can be obtained by cooling from a supersaturated aqueous solution. The cooling rate of the supersaturated aqueous solution needs to be controlled at a rate of 1K/30 minutes from 353K till room temperature. The β phase with

space group ($P2_1$) was first crystallised from a mixture of water-alcohol solution (Iitaka, 1958). Crystallisation of glycine from a mixture of water ethanol at different ratios resulted in needle-like β-polymorph of glycine crystals (Weissbuch et al., 2005). A decrease in solubility of glycine in a mixture of water-alcohol becomes evident by high content of alcohol with a subsequent increase in solvated glycine monomers followed by precipitation β- polymorph of glycine. The γ-polymorph can be crystallized from supersaturated aqueous solution by evaporation or by acidification of the solution by acetic acid or by making the solution alkaline with ammonium hydroxide (Iitaka, 1958) (He et al., 2006).

The α polymorph of glycine grown from supersaturated aqueous solution with bipyramidal crystal habit is composed of centrosymmetric bilayers of zwitterionic molecules (Figure 5.2) tailored by NH----O hydrogen bond interactions (Weissbuch et al., 2005).

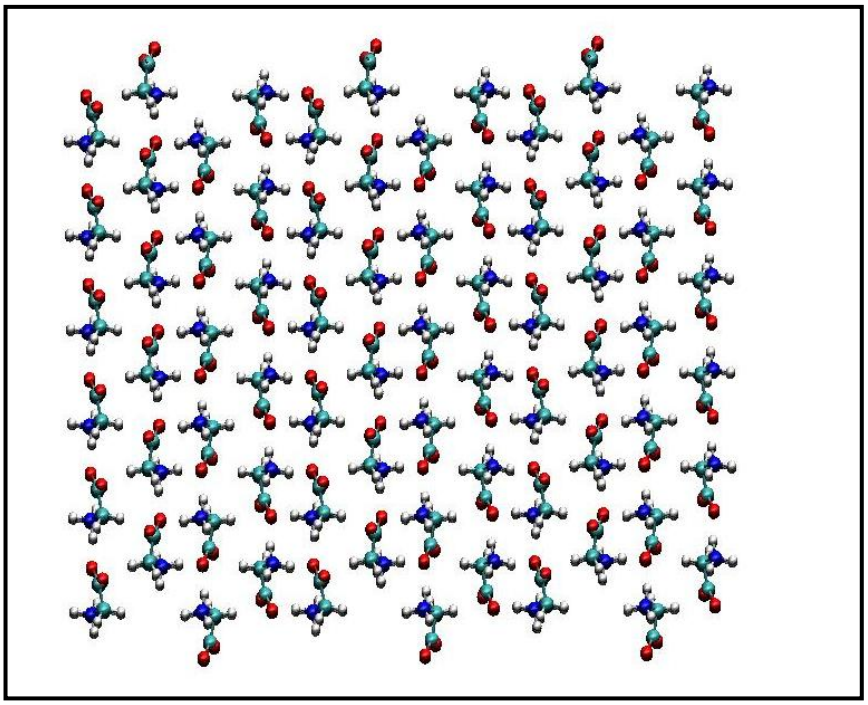

Figure 5.2 Molecular packing arrangement in the α form of glycine (The hydrogen, oxygen and nitrogen atoms are shown in gray, red and sky blue respectively).

The β glycine form comprises a single layered hydrogen bonded monomers units (Figure 5.3) (Iitaka, 1961) . Structurally γ polymorph is quite different to α and β. In the γ polymorph the molecules are linked to each other via hydrogen bonding involving nitrogen and carboxylic oxygen (N···· O), resulting in helical chains which are linked together by lateral hydrogen bonds (N···· O) with a consequent three dimensional lattice (Boldyreva et al., 2003, Iitaka, 1958) (Figure 5.4).

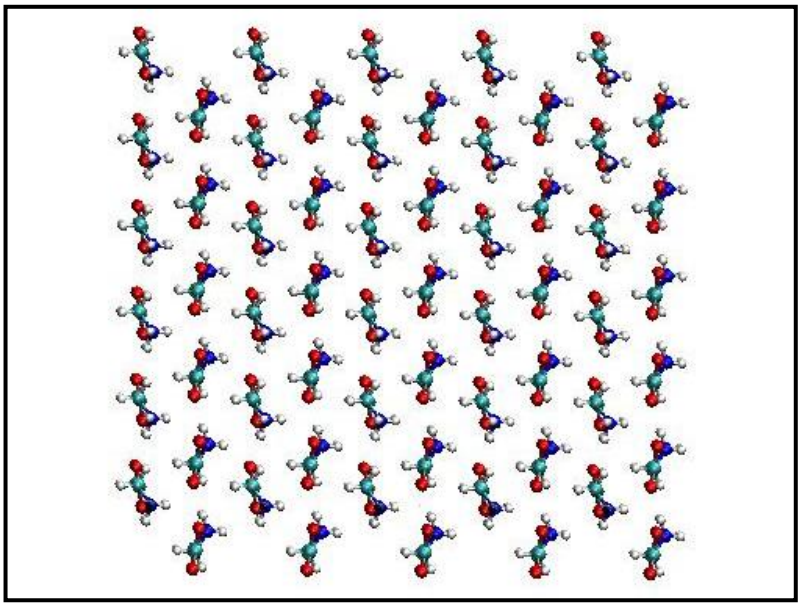

Figure 5.3 Molecular packing arrangement the β form of glycine

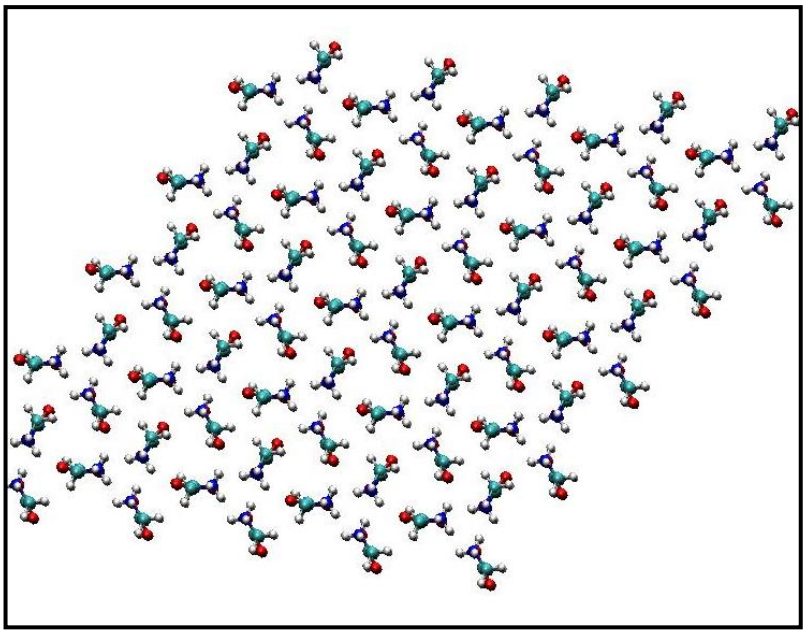

Figure 5.4 Molecular packing arrangements in the γ form of glycine

In contrast to α and β polymorphs the oxygen and nitrogen atoms are in the same direction. In the crystal lattice of γ-glycine every third molecule have the same conformation (Figure 5.4). At ambient temperature the torsion angles of zwitterions tailoring structure of the three polymorphs (α, β and γ) are different from each other which are (161.8°) (Jonsson and Kvick, 1972), (157.41°) (Drebushchak et al., 2002a) and (167.1°) (Kvick et al., 1980b).

A wide range of studies have been conducted to investigate the existence of new polymorphs at high pressure (Dawson et al., 2005, Boldyreva, 2003, Boldyreva, 2007a, Moggach et al., 2008, Boldyreva, 2007b, Perlovich et al., 2001). Two newly investigated high pressure polymorphs (δ-glycine and ε-glycine) have been reported from compressing β and α-polymorphs using high pressure respectively. Among the three polymorphs (α, β and γ), α-polymorph has been reported the most stable high pressure polymorph. Whereas transformation of β and γ occurs respectively to δ and ε-polymorphs at 1.9GPa and 4.3GPa respectively (Dawson et al., 2005).

The present study reveals that α and γ glycine remains stable over the entire range of temperature (300K, 350K, 400K, 450K and 500K) and pressure (10kbar, 20kbar, 30kbar and 50kbar) respectively. In contrast the β phase transforms to the δ phase at a pressure >10kbar and temperature >400K respectively, confirming experimental results. The nanocrystals of the three polymorphs of glycine did not show any phase transformation as function temperature and remained stable.

5.2 Methodology

The molecular dynamics simulations of the three crystalline polymorphs (α, β and γ) of glycine (Figure 5.5) were carried out in the constant stress NST ensemble with Parrinello–Rahman boundary conditions using the program DLPOLY (Smith et al., 2006) for up to 80ns using a time step of 2 fs. Simulations of nanocrystals of glycine molecules as a function of temperature were carried out in vacuum in the NVT ensemble. The simulation box contained 432 molecules (6×3×6 unit cells) for the α polymorph, 360 molecules (6×5×6 unit cells) for β polymorph, and 450 (5x5x6 unit cells) for the γ polymorph of glycine.

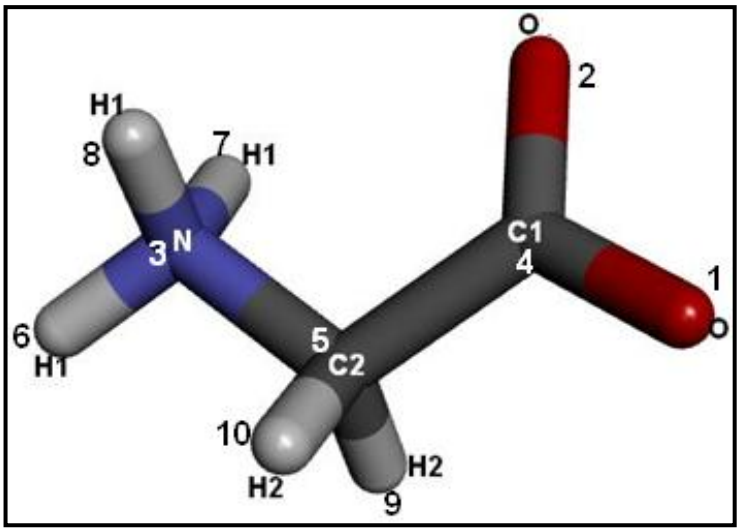

Figure 5.5 Glycine molecule showing the atoms labelled according to atom types in the forcefield file.

The force field used to describe glycine molecules comprised intramolecular terms (bonds, angles, and dihedrals), a Lennard-Jones term for the nonbonded interactions, and a Columbic interaction term. The force field parameters along with the atomic partial charges were from the AMBER forcefield (Sorin and Pande, 2005).

Table 5.1 Partial atomic charges employed by glycine

Atom Number	Atom Type	Charge/e
1	O	-0.7855
2	O	-0.7855
3	N	0.1592
4	C1	0.7231
5	C2	-0.0461
6	H1	0.1984
7	H1	0.1984
8	H1	0.1984
9	H2	0.1984
10	H2	0.1984

The atom numbers along with the charges are show in Table 5.1. All bonds were constrained using the SHAKE algorithm (Table 5.2).

Table 5.2 Bond constraints employed for glycine

Bond type	Bond Constraint (Å)
1-4	1.2500
2-4	1.2500
3-5	1.4710
3-6	1.0100
3-7	1.0100
3-8	1.0100
4-5	1.5220
5-9	1.0900
5-10	1.0900

The angle interactions for the atoms in the molecule were represented by a harmonic potential, $U(\theta) = 0.5k(\theta-\theta_o)^2$ (Table 5.3). The dihedral angles in the structure were represented by a cosine form of potential, $U(\varphi) = A[1 + \cos(m\varphi - \delta)]$ (Table 5.4).

Table 5.3 Force field angle parameters employed for glycine

Angles	k (kJ mol^{-1} $degree^{-2}$)	Value of angles (degree)
5-3-6	50.00	109.50
5-3-7	50.00	109.50
5-3-8	50.00	109.50
6-3-7	35.00	109.50
6-3-8	35.00	109.50
7-3-8	35.00	109.50
1-4-2	80.00	126.00
1-4-5	70.00	117.00
2-4-5	70.00	117.00
3-5-4	80.00	111.00
3-5-9	50.00	109.00
3-5-10	50.00	109.00
4-5-9	50.00	109.00
4-5-10	50.00	109.00
9-5-10	35.00	109.00

Table 5.4 Dihedral angle force field parameters employed for glycine

Dihedrals	A (kcal/mol)	δ (degree)	m (multiplicity)
9-5-4-1	0.00000	0.00	2.0
9-5-4-2	0.00000	0.00	2.0
3-5-4-1	0.00000	0.00	2.0
3-5-4-2	0.00000	0.00	2.0
10-5-4-1	0.00000	0.00	2.0
10-5-4-2	0.00000	0.00	2.0
8-3-5-9	1.40000	0.00	3.0
8-3-5-4	1.40000	0.00	3.0
8-3-5-10	1.40000	0.00	3.0
7-3-5-9	1.40000	0.00	3.0
7-3-5-4	1.40000	0.00	3.0
8-3-5-10	1.40000	0.00	3.0
7-3-5-9	1.40000	0.00	3.0
7-3-5-4	1.40000	0.00	3.0
7-3-5-10	1.40000	0.00	3.0
6-3-5-9	1.40000	0.00	3.0
6-3-5-4	1.40000	0.00	3.0
6-3-5-10	1.40000	0.00	3.0

The van der Waals interaction parameters of the different atoms are shown in Table 5.5. For the electrostatic interactions we employed smooth particle-mesh Ewald with a precision of 1×10^{-5}. The van der Waals and real space interaction cut offs for glycine bulk crystals was 1.2 nm. For the nanocrystals, the van der Waals and electrostatic interactions were both 4.0 nm (i.e. no truncation, covering all interactions), Ewald summation being inappropriate since we no longer have a periodic system.

To investigate the effect of temperature on phase transformation between different polymorphs of the glycine polymorphs, simulations of three polymorphs of glycine in bulk and nanocrystals was carried at a range of temperature that included 300K, 350K, 400K, 450K and 500K using ambient pressure (0.001 kbar).

Table 5.5 Lennard-Jones force field parameters employed for glycine

Atom-Atom Interaction	ε / kJmol^{-1}	σ / Å
O - O	0.210	2.959
N - N	0.170	3.340
C1-C1	0.086	3.400
C2-C2	0.109	3.400
H1- H1	0.016	1.069
H2- H2	0.016	2.471
N - O	0.189	3.150
C1- O	0.134	3.179
C1- N	0.120	3.370
C2- O	0.151	3.179
C2 -N	0.136	3.370
C2- C1	0.097	3.400
H1- O	0.057	2.015
H1- N	0.051	2.205
H1- C1	0.037	2.234
H1- C2	0.041	2.234
H2- O	0.057	2.716
H2- N	0.051	2.906
H2- C1	0.036	2.935
H2-C2	0.041	2.935
H2-H1	0.016	1.770

In addition to assessing the phase transformation of the three polymorphs of glycine (bulk) as a function of pressure, simulations were also carried out a range of pressure (10kbar, 20kbar, 30kbar and 50kbar) and ambient temperature.

5.3 Results and Discussions

5.3.1 Test of force field parameters for glycine polymorphs

The forcefield parameters for glycine were tested to ascertain whether they reproduce the crystal structures of three of the polymorphs of glycine, α, β and γ. The lattice parameters were averaged after short simulations (200ps)

of each of the three polymorphs at 50K and 298K in the constant stress NST ensemble. Should the simulated crystal structure diverge considerably from the starting experimental structures, then the force field would be considered to be inadequate. A sufficient force field should reproduce the lattice parameters (and the crystal packing) to better than 5% deviation from the experimental values for each of the lattice parameters. The simulations at the lower temperature of 50 K were carried out in case there is a phase transformation at ambient conditions. The MD simulations were also carried out for a short duration (200 ps) to enable the structures to relax to yield an equilibrated minimum energy structure but not to enable any phase transformation to take place. For all simulations the crystal structures underwent minor structural changes over a short period of time and then remained converged. The averaged lattice parameters from the MD simulations for the three phases at 50K and 298K are given in Table 5.6 along with the experimental values. The percentage deviation is less than 4% for all lattice parameters.

This result verifies that the force field is good enough to reproduce the crystal structures and hence can be employed with confidence.

Table 5.6 Comparison of averaged lattice parameters from crystal simulations at 50K and 298K with experiment values at ambient temperature.

Glycine polymorph	Unit cell vector	Experimental (Å)	MD at 50K (Å)	MD at 298K(Å)	%Deviation	
					50K	298K
α-glyince	a	30.63	29.75	30.64	2.87	-0.03
	b	35.97	37.13	37.25	-3.22	-3.55
	c	32.78	32.75	32.75	0.09	0.09
β-glycine	a	30.47	30.64	30.64	-0.55	-0.55
	b	30.96	31.86	31.86	2.90	2.90
	c	32.32	31.65	31.65	2.07	2.07
γ-glycine	a	35.19	34.04	34.51	3.26	1.93
	b	35.19	34.04	34.51	3.26	1.93
	c	32.89	32.95	33.03	-0.18	-0.42

5.3.2 Characterisation of the Crystal Structure Using Radial Distribution Functions

It is very difficult to identify the structure visually using molecular dynamics trajectories because the molecules are continuously vibrating. The radial pair distribution function (RDF) can be very useful in describing distance correlations between a pair of atoms (Leach, 1999). RDF calculations give the probability density that a selected atom will be found at a specified distance, and is calculated as an average over all selected atoms and over all configurations of the MD simulation trajectory, after the system has equilibrated.

Glycine molecule is composed of ten atoms which include 2 x O, 5 x H, 1 x N and 2 x C which can result in a range of intermolecular pair interactions to describe the specific packing of atoms around each other in each polymorph.

We calculated all these interactions using the computer code dl_rdf (developed and distributed by J. Anwar, University of Bradford) with a view to identifying particular RDFs (for a given pair of atoms) to enable us to discriminate between the three polymorphs for glycine.

RDFs calculations of different atomic pair interactions were carried out at 300K for α, β and γ glycine. RDFs which categorically discriminate the three polymorphs from each other are (O2-O2, O2-H1, C1-H2, H2-H2, and H1-H2) (Figures 5.6). Given an unknown structure, one would carry the above 5 RDFs to interpret the structure, focussing on intensity and distance at which the peaks occur.

For example, RDFs peaks of (H2-H2) were observed at a distance 2.5Å for γ and α glycine respectively. For β glycine the first medium peak showing (H2-H2) interaction was observed at distance 4Å followed by a relatively sharp peak at distance 5.3Å. A sharp C1-H2 (4-9) peak became evident for γ glycine at a distance 2.3Å followed by a tiny and medium peak for β and α glycine respectively. The peaks showing pair interaction C1-H2 (4-10) in α, β and γ phases appeared at 2.5Å, 4Å and 3.5Å respectively. The intensity of the peak representing β phase is found more intense compared to the other two phases. The H1-H2 pair interaction peaks were observed at distance 3Å, 4Å, and 5Å for β, α and γ glycine respectively. A sharp peak representing O2-O2 pair interaction in γ glycine appeared on 3Å followed by medium and tiny peaks of α and β respectively. The peaks representing O2-H1 interaction appeared at a distance 2Å for α and γ glycine. There was not observed any peak for β glycine at this distance. However two peaks at a distance 3Å and 4Å were observed for β glycine.

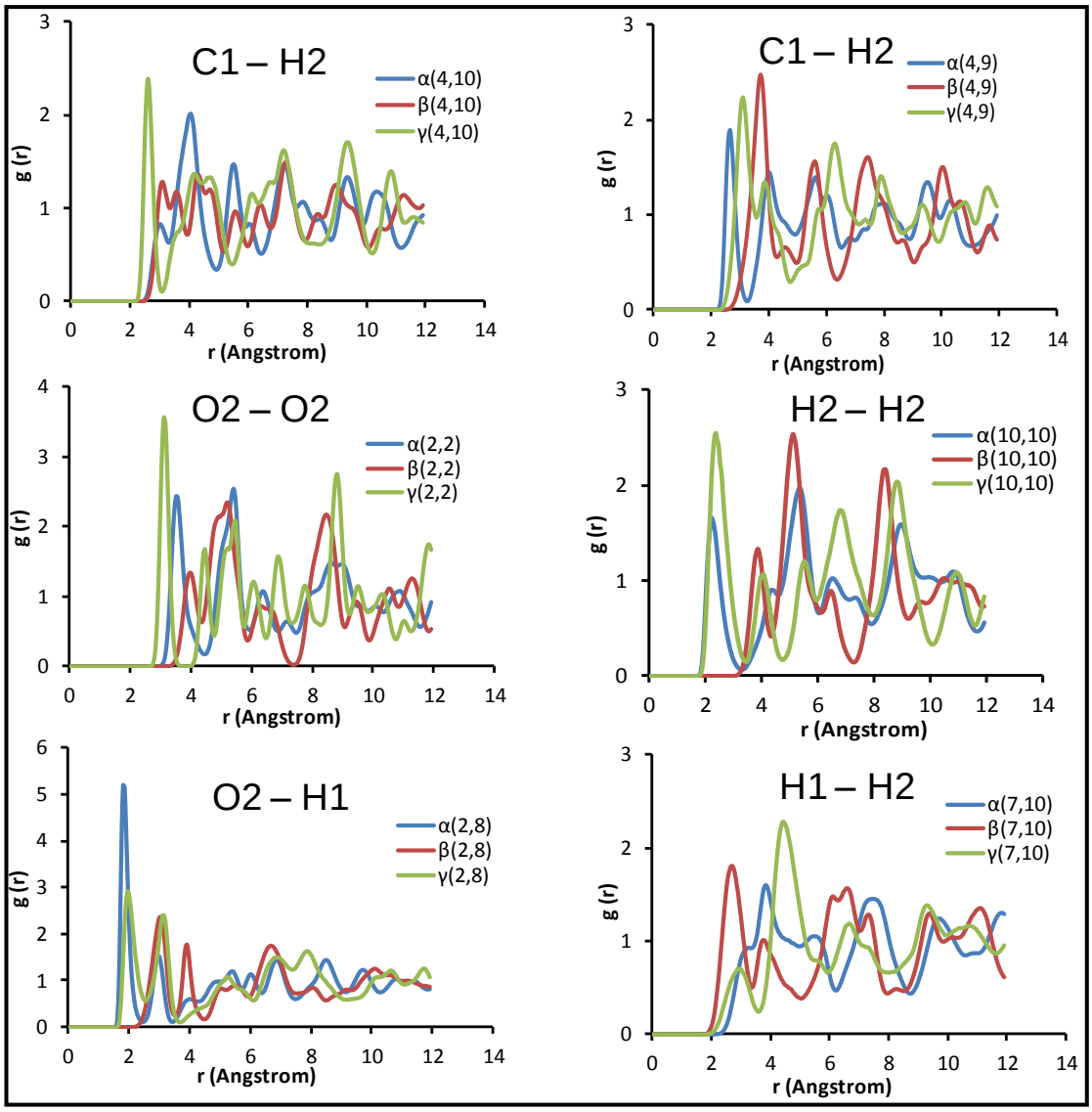

Figure 5.6 RDFs of the selected pair interactions in α, β and γ glycine at 300K.

5.3.3 Simulation of Bulk Crystals of Glycine Forms α, β and γ as a Function of Temperature

The trajectories of simulations of the α, β and γ glycine for the entire range of temperatures (300K, 350K, 400K, 450K and 500K) were visualised. The α and γ glycine remained stable and no phase transformation was observed. The packing arrangement of the molecules in both of these phases was similar at 300K and 500K (Figure 5.7 and Figure 5.8).

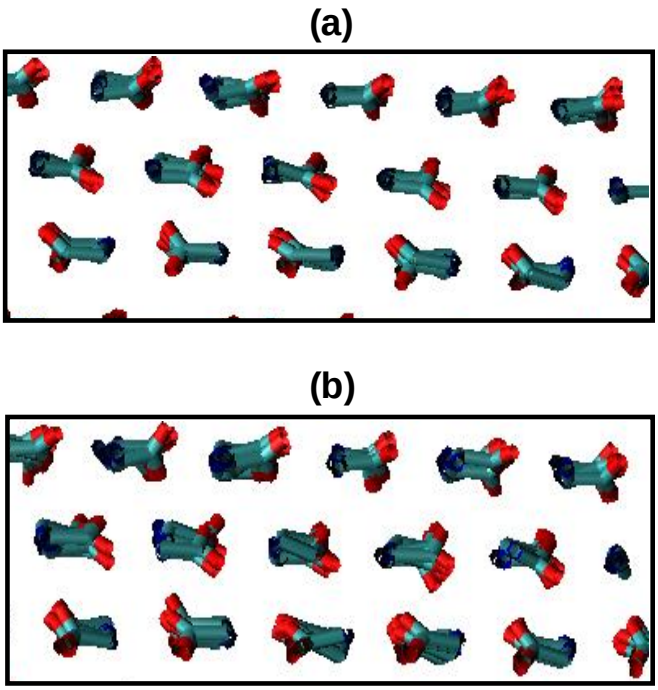

Figure 5.7 Configurations of few molecules of α glycine at (a) 300K and (b) 500K

The β glycine however showed a phase transformation above 400K. Figure 5.9 shows the configurations of β glycine at 300K, 450K and 500K. The packing arrangement of nitrogen and oxygen in β glycine at 450K and 500K is different from the configuration at 300K. At 300K the oxygen (red) and nitrogen (blue) in each line of the crystal lattice point in the same direction. However at 450K and 500K one observes that each third molecule in each line of the crystal lattice is similar with the same alignment of nitrogen and oxygen atoms

(a)

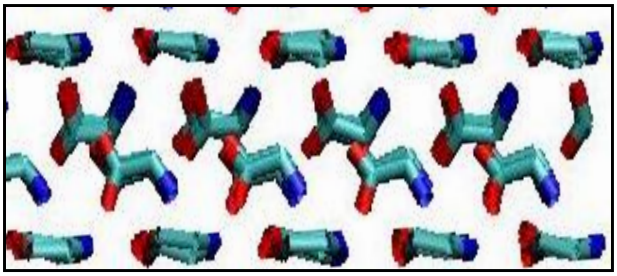

(b)

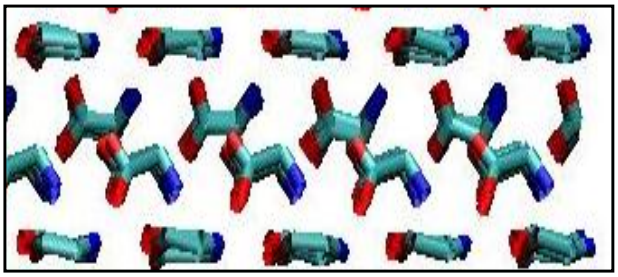

Figure 5.8 Configurations of few molecules in γ glycine at (a) 300K and 500K

This alteration does not exist in the initial configuration of the β glycine. This new phase obtained at 450K and 500K was compared to the configurations of γ and α glycine. However no similarity was found in the packing arrangement of the atoms among all these phases. Consequently we investigated whether the new form could be form δ which has been reported as a result of high pressure. The crystal structure data for form δ was downloaded from the Cambridge Structural Database (CSD, UK) (Allen, 2002). The lattice parameters for the δ form are; a = 11.156Å, b = 5.8644Å and 5.3417Å and the angles are α = 90, β = 125.83 and γ = 90.0 and the structure packs in the space group is $P2_{1/a.}$ The molecules were packed to yield a periodic crystal structure using the software Mercury (version 2.3) (CCDC, Cambridge, UK). The new structure obtained from the β form at 450K and 500K was compared to the δ form and indeed confirmed to be more similar the δ form (Figure 5.10). In each layer of the crystal packing of the newly transformed phase obtained from β glycine the molecules have the

same alignment as δ form. The oxygen and nitrogen atoms are packed in the same patterns in both polymorphs which confirm the transformation of the β polymorph to the δ phase. However the rows in δ phase appear to be shifted relative to each other which do not occur in the transformations. This deviation suggests that transformation occurs but not to the exact δ phase.

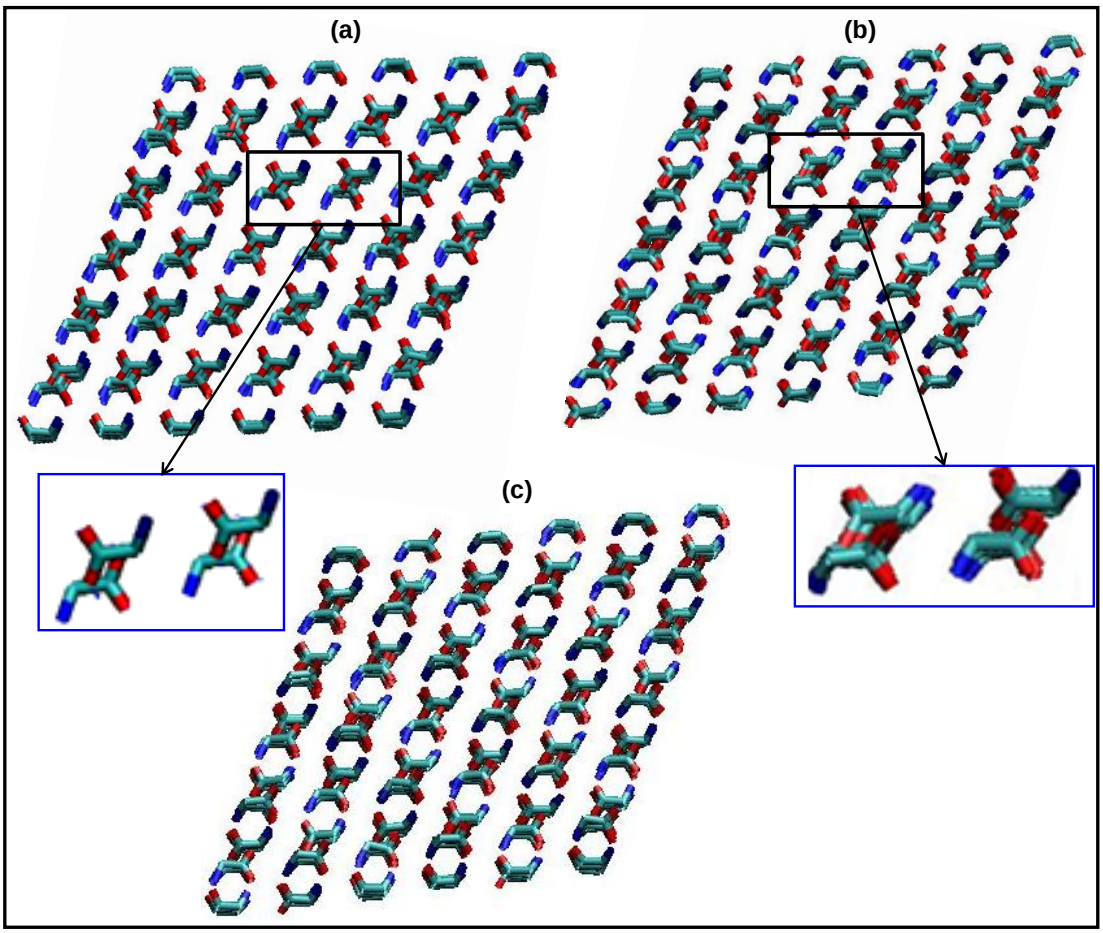

Figure 5.9 Configurations of β glycine at (a) 300K; (b) 450K and (c) 500K. Oxygen and nitrogen atoms are shown in red and blue respectively. The hydrogen atoms have been removed for clarity.

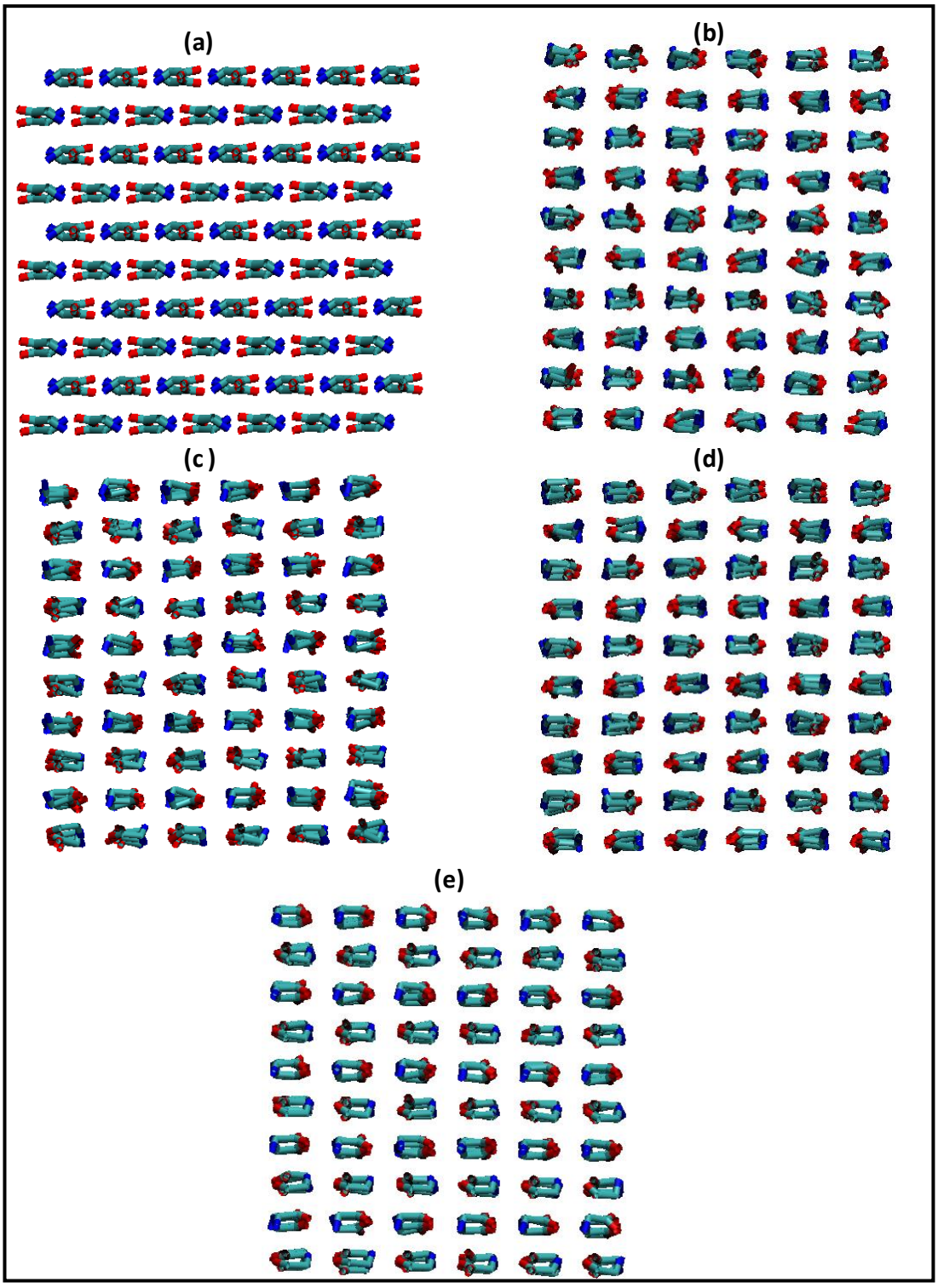

Figure 5.10 Configurations of (a) δ glycine; (b) β glycine at 450K; (c) β glycine at 500K; (d) β glycine at 20kbar and (e) β glycine at 50kbar. (The red sticks show oxygen and blue nitrogen atoms. The hydrogen atoms have been removed to clearly visualise the structure.

5.3.4 RDFs of Selected Atomic Pairs in α, β and γ Glycine.

RDFs of the selected atomic pairs including (O2-O2, C1-H2, O2-H1 and H2-H2) for α and γ glycine calculated at 300K were compared with the the RDFs calculated at (350K, 400K, 450K and 500K) which suggested no phase transformation occurred at higher temperature. Figures 5.11 and 5.13 show pair interaction peaks of α and γ glycine at 300K and 500K. There is little or no change in the location of the selected RDFs at 500K for both of the polymorphs (α and γ). The peaks intensity of the RDFs of the selected atomic pairs for both of these polymorphs was however bit reduced at higher temperature this is because of the expansion of the unit cells which cause the atoms to be located at rather large distance from each other. These results also verify the visual observation of the trajectories of α and γ at the entire range of temperature where we did not see any phase transformation (Figures 5.7 and 5.8).

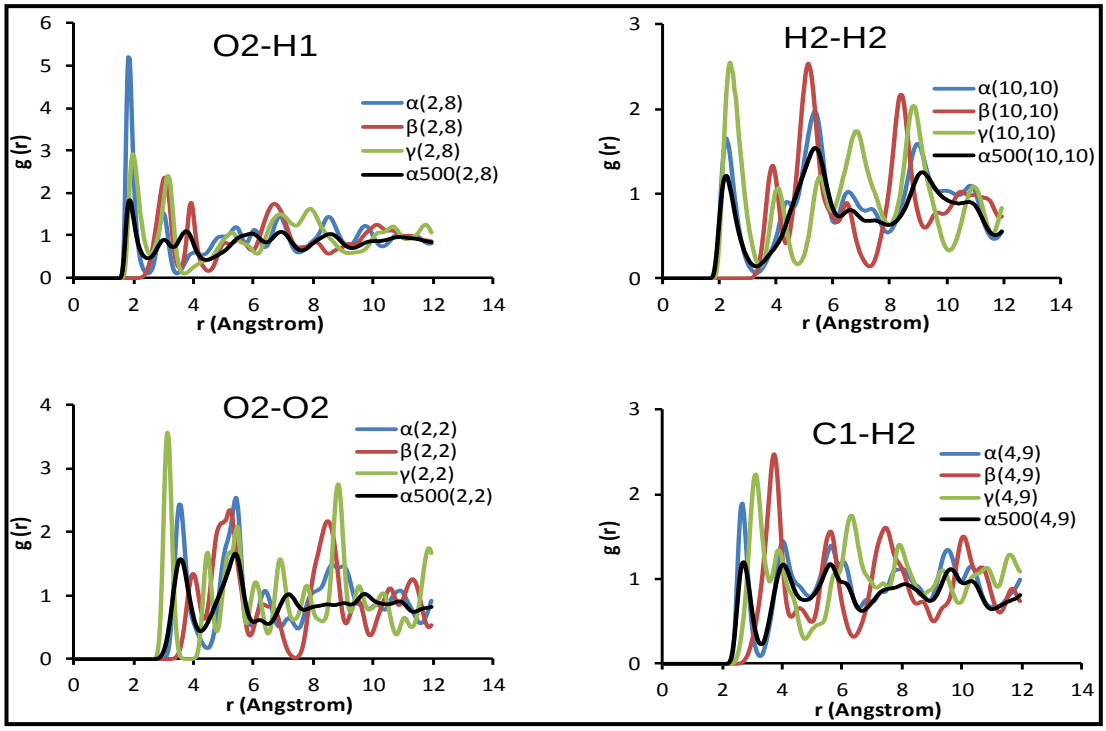

Figure 5.11 RDFs calculation of α, β and γ glycine at 300K and its comparison with the RDFs of α glycine calculated at 500K.

For β glycine the RDFs of the selected atomic pair interaction which include (O2-O2, O2-H1, C1-H2, H2-H2 and H1-H2) at 350K, 400K 450K and 500K (Figure 5.12) showed that a phase transformation occurred above 400K. The peaks representing the above mentioned pair interactions were found different at different distance at 450K and 500K compared to the counterparts at 300K. For example, the RDFs for the O2-H1 pair interaction revealed peaks at 2Å at 450K and 500K, which did not occur at 300K. Furthermore, the sharp peaks of O2-H1 interaction at 3.0Å, 4Å and 6.5Å at 300 K do not exist at 450K and 500K. Similarly the H2-H2 interaction peaks at 4Å, 4.5Å and 8.5Å are not observed at the higher temperatures. Additionally for the H2-H2 interaction a new relatively sharp peak is observed at 2.5Å at 450K and 500K. RDFs of other pair interactions also reveal a similar behaviour. This structural analysis of the β-phase confirms that the β-glycine is transformed to an altogether a new phase other than α and γ at temperature >400K, which visually could be confirmed (see earlier discussion) as the δ-phase.

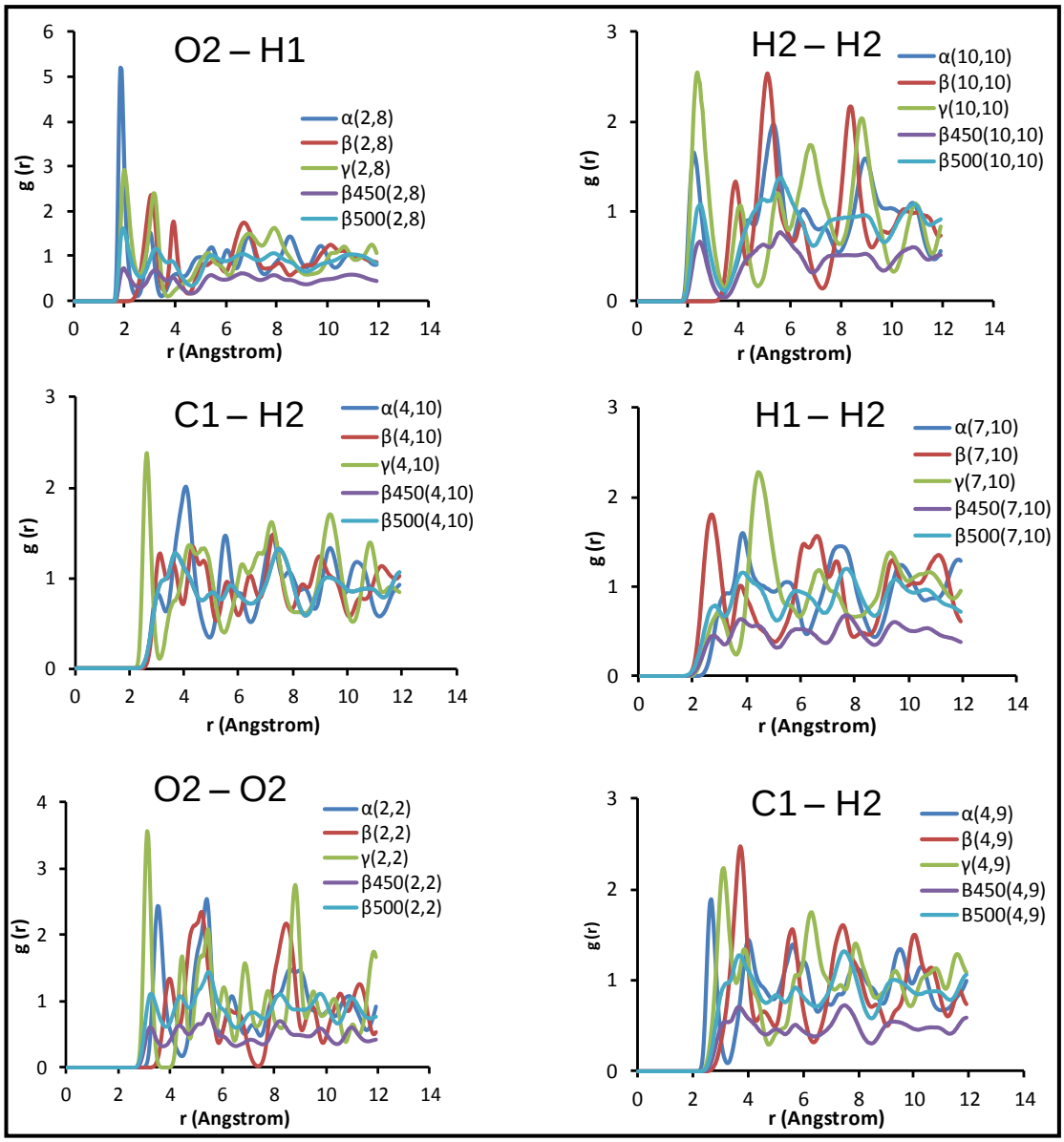

Figure 5.12 RDFs of α, β and γ glycine at 300K and their comparison with the RDFs of the specified pair interactions of β glycine at 500K.

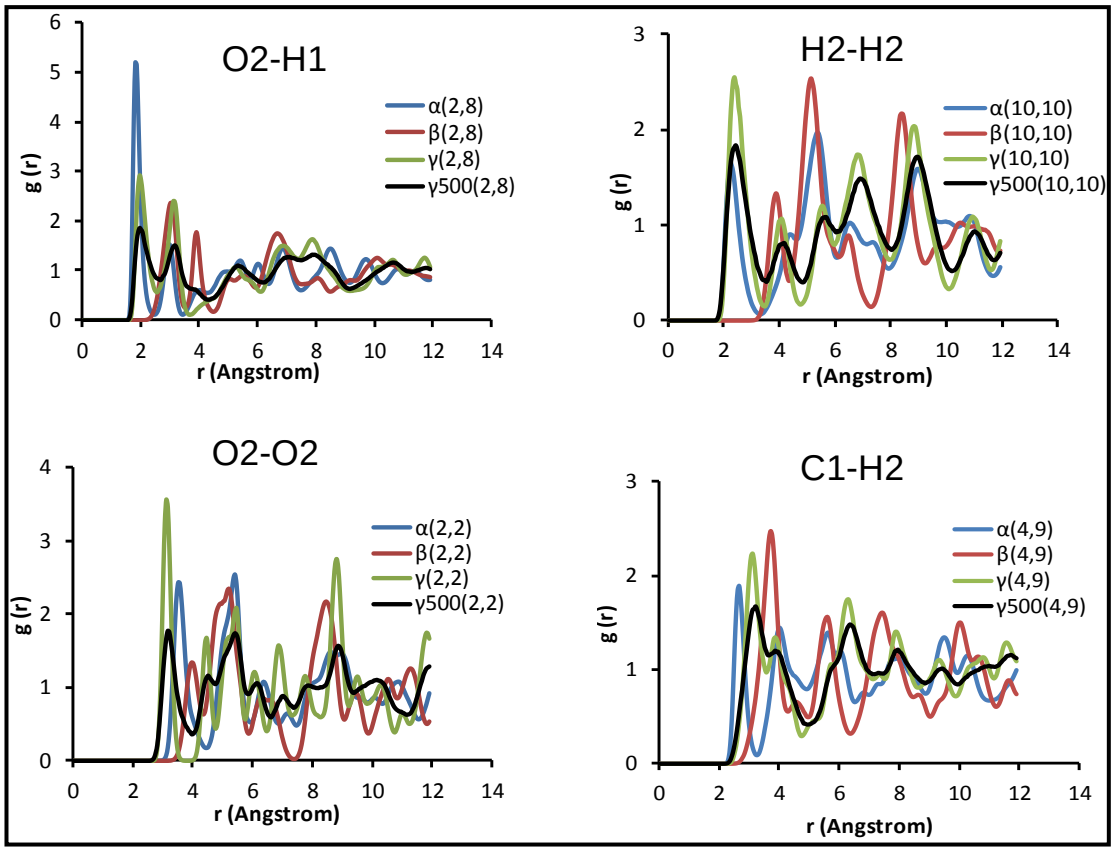

Figure 5.13 RDFs of specified atomic pairs interaction of α, β and γ glycine at 300K and their comparison with the same RDFs of γ glycine at 500K

5.3.5 Potential Energy for α, β and γ Glycine

Potential energy calculations for the three polymorphs of glycine were carried out at 300K, 350K, 400K, 450K and 500K respectively. The system potential energy relies on the packing of molecules or atoms within that structure. The three polymorphs of glycine have different potential energies because of the different arrangement of molecules within each polymorph. The potential energy of the system of a given phase decreases as the system temperature goes up. Assuming entropy change to be minimal, the potential energy should show a step change on phase transformation to a new phase. Figure 5.14 shows that the potential energy for α, β and γ polymorphs was increased with the increase in temperature. The potential energies for α and

γ glycine were remained relatively constant during the entire time period of simulation (80ns). On the other hand, for β glycine both at 450K and 500K there was observed immediate decrease in the potential energy of a system. After 20ns and 50ns there was observed significant fluctuations at 450K and the system energy goes down which remained till end of the simulation. However at 500K the fluctuations in potential energy of the system became evident at 10ns and 30ns which remained decreased till end of the simulation (Figure 5.11(b)). In addition the potential energy/molecule calculations revealed that α phase is the most stable phase which has low potential energy compared to γ and β (Figure 5.15). The potential energies of α and γ constantly increased at high temperature. For the β glycine there was observed bit decline in the energy at 450K and 500 which we also observed in the system energy. To investigate the fluctuation in potential energy of the system the trajectories of β glycine were visualised and It became evident that at 450K and 500K the alignment of the nitrogen and oxygen atoms in molecules of β glycine tend to change in some rows immediately followed by a complete rotation of nitrogen and oxygen atoms above 20ns to be transformed to delta form and the configuration of the β glycine remained same till end of the simulation (80ns) (Figures 5.16 and 5.17).

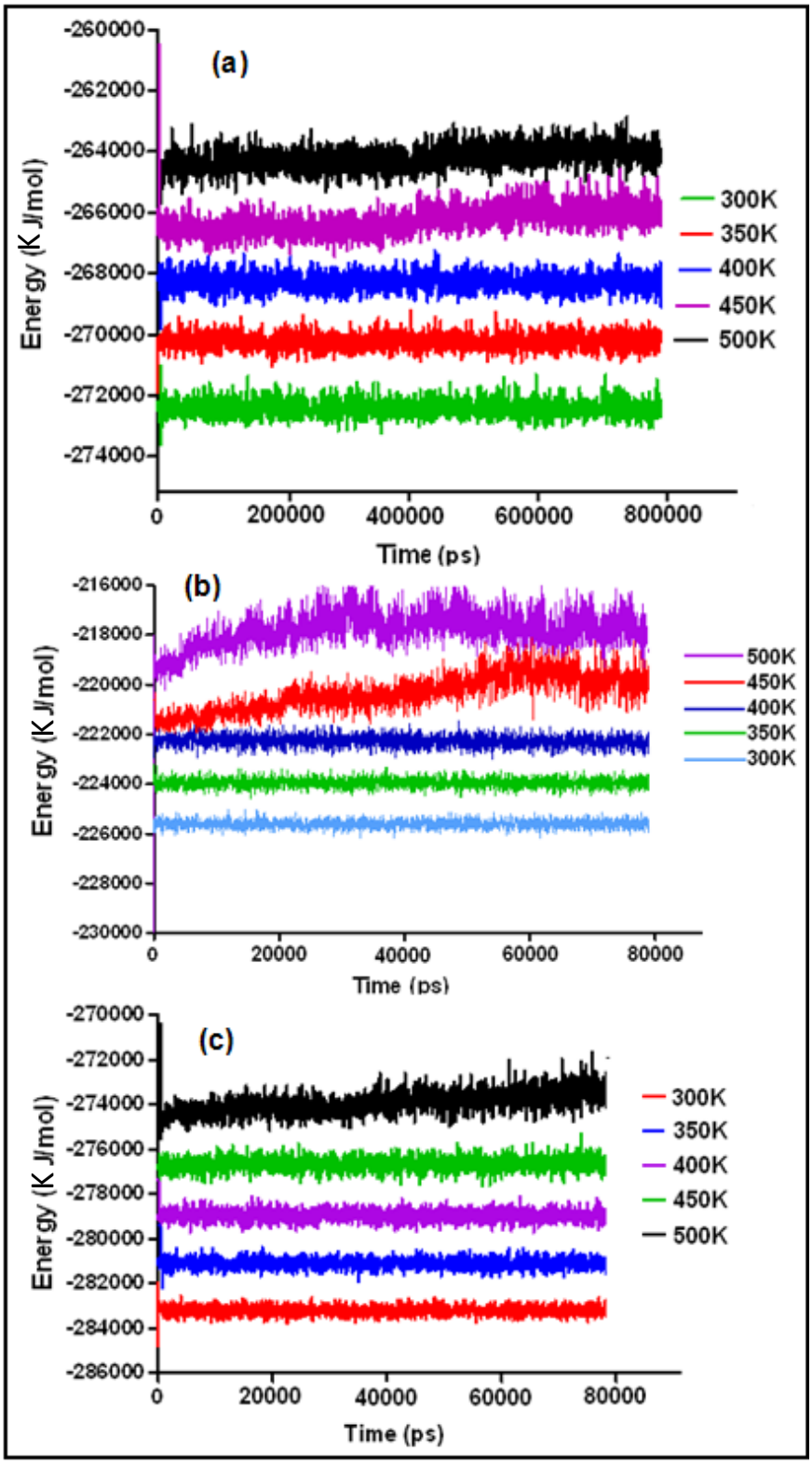

Figure 5.14 Potential energies as a function of time at different temperatures for (a) α; (b) β and (c) γ glycine

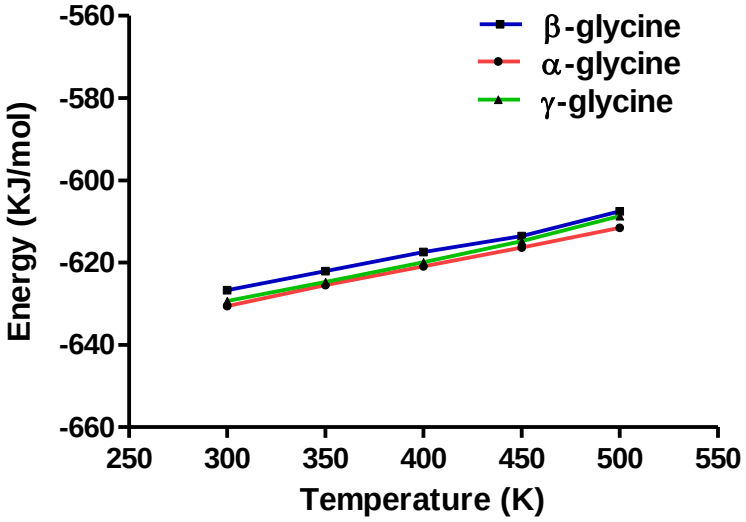

Figure 5.15 Potential energy/molecule of the bulk phases of three polymorphs of glycine as a function of temperature

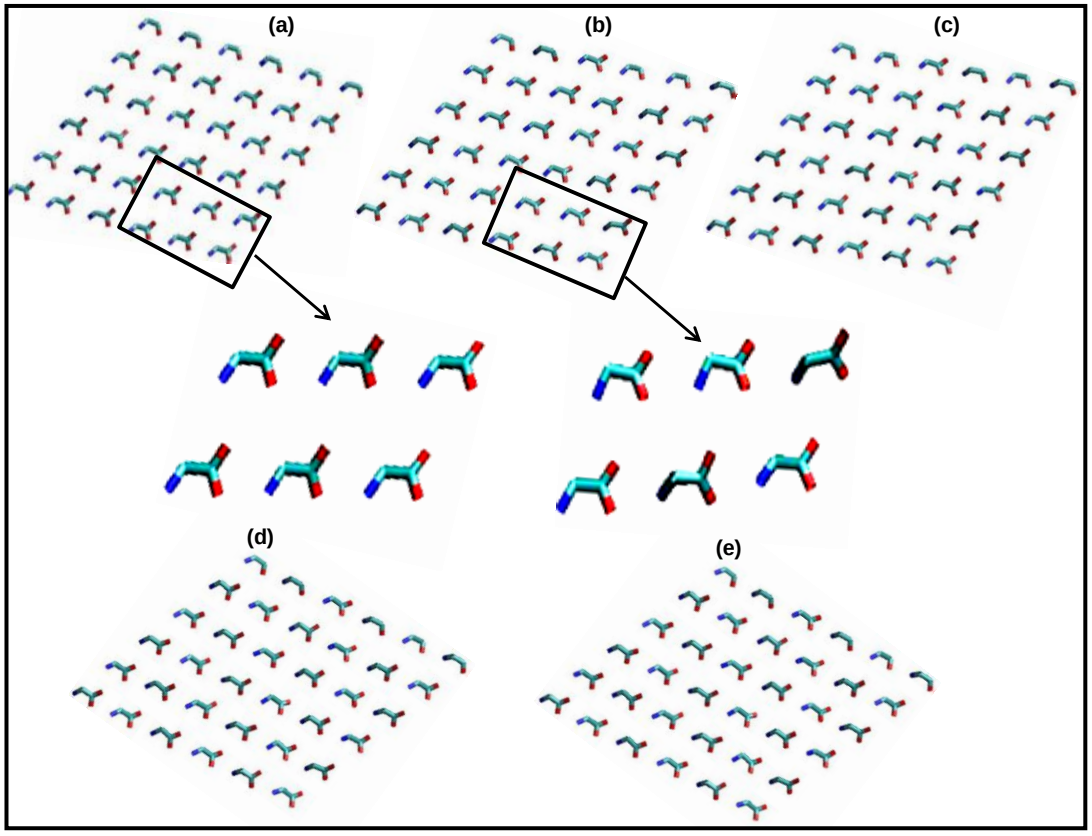

Figure 5.16 Snap shots of β-glycine at (a) 0.0ns; (b) 0.40ns; (c) 20.0ns; (d) 55.0ns and (e) 80.0ns which show step wise phase transformation. The close view shows the alignment of the atoms that begins to change immediately and spreaded towards other lines in the lattice. The structures shown in “d” and “e” are similar (From simulation at 450K).

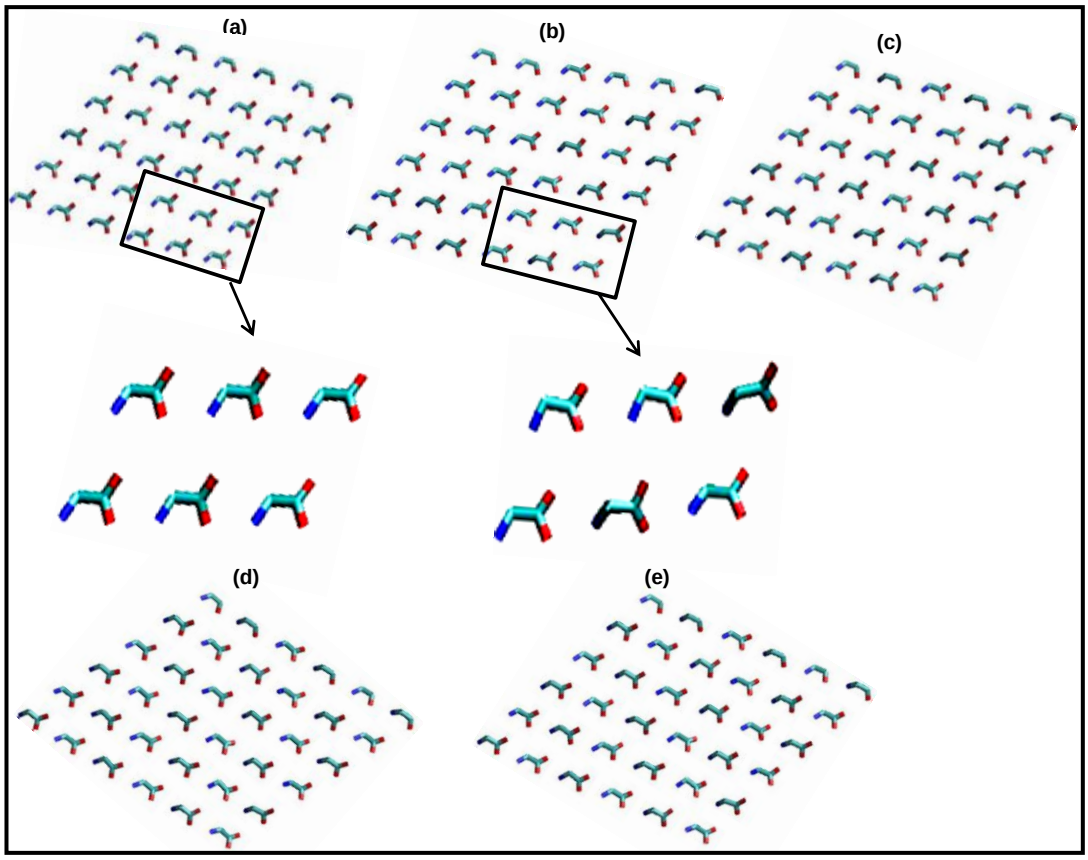

Figure 5.17 Snap shots of β-glycine at (a) 0.0ns; (b) 0.17ns; (c) 10.0ns; (d) 30.0ns and (e) 80.0ns which show step wise phase transformation. The close view shows the alignment of the atoms that begins to change immediately and spreaded towards other lines in the in the lattice. The structures shown in “d” and “e” are similar (From simulation at 500K).

5.3.6 Lattice Parameters of α, β and γ Glycine.

The variation in lattice parameters i.e. cell dimensions and angles and cell volume was examined as a function of temperature for the three polymorphs, α, β and γ. The data is shown in Tables 5.7 and plotted in Figures 5.8

There was not observed any significant increase in the cell axis of unit cell of α glycine at the specified range of temperature. Additionally, the cell angles for α glycine also remained unchanged at higher temperature. There was observed an increase in the unit cell volume of α glycine at temperature > 300K which is because of thermal motion of molecules (Table 5.7).

Table 5.7 Comparison of experimental and calculated lattice parameters of α glycine at different temperature which were averaged over the molecular dynamics simulation trajectory.

Temperature (K)	Unit cell vector (Å), angles (α, β, γ (degree)) and volume $(Å)^3$						
	a	b	c	α	β	γ	Volume $(Å)^3$
300K	5.02	12.41	5.47	90.0	118.00	90.0	310.00
350K	5.04	12.45	5.46	90.0	118.00	90.0	312.00
400K	5.05	12.47	5.47	90.0	118.00	90.0	313.00
450K	5.06	12.50	5.48	90.0	118.00	90.0	315.00
500K	5.09	12.53	5.49	90.0	118.00	90.0	317.00
Experimental	5.10	11.97	5.46	90.0	111.74	90.0	310.13

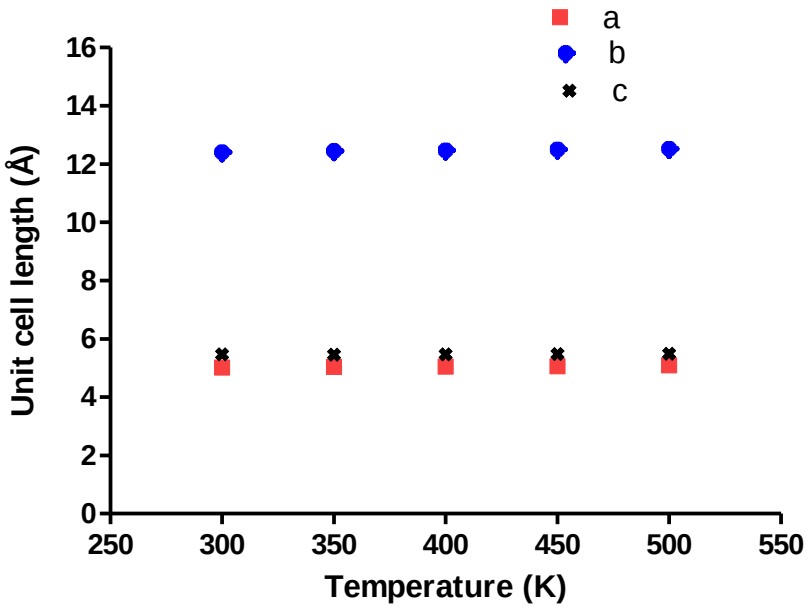

Figure 5.18 Unit cell parameters of α glycine as a function of temperature

For β glycine the cell axis (b and c) were increased at 400K, 450K and 500K (Table 5.8 and Figure 5.19). There was also observed an increase in β angle of unit cell of β glycine. The unit cell volume of β glycine increased at 350K and 400K but this phase did not remain stable at temperature >400K and the unit cell volume decreased with consequent new more stabilised phase (δ form) (Table 5.8).

Table 5.8 Comparison of experimental and calculated lattice parameters of β glycine at different temperature which were averaged over the molecular dynamics simulation trajectory.

Temperature (K)	Unit cell vector (Å), angles (α, β, γ (degree)) and volume $(Å)^3$						
	a	b	c	α	β	γ	Volume $(Å)^3$
300K	5.11	6.52	5.28	90.0	115.00	90.0	159.00
350K	5.11	6.52	5.29	90.0	115.00	90.0	160.00
400K	5.11	6.67	5.35	90.0	115.00	90.0	164.00
450K	5.11	6.64	5.46	90.0	116.00	90.0	157.00
500K	5.12	6.68	5.46	90.0	116.00	90.0	158.00
Experimental	5.07	6.19	5.38	90.0	113.35	90.0	155.54

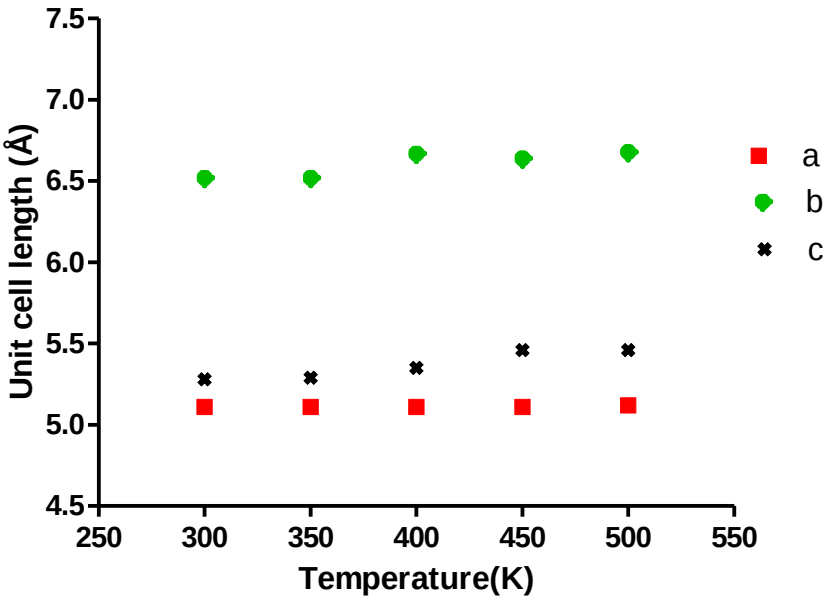

Figure 5.19 Unit cell parameters of β glycine as a function of temperature

On the other hand there was not observed any expansion in the cell axis (a, b and c) for γ glycine at higher temperature (Table5.9 and Figure 5.20). Whilst the cell angles remained unchanged (Table 5.12). Also there was observed expansion in unit cell volume of γ glycine at increased temperature (Table 5.11). The cell parameters calculation for the three polymorphs at the specified range of temperature suggests that α and γ polymorphs remained

stable and did not transform to any other polymorph at higher temperature. However the β glcycine is transformed to a new polymorph when the temperature is increased >400K which has also been confirmed by RDFs and visual observation.

Table 5.9 Comparison of experimental and calculated lattice parameters of γ glycine at different temperature which were averaged over the molecular dynamics simulation trajectory.

Temperature (K)	Unit cell vector (Å), angles (α, β, γ (degree)) and volume $(Å)^3$						
	a	b	c	α	β	γ	Volume $(Å)^3$
300K	6.90	6.90	5.50	90.0	90.0	120.0	227.00
350K	6.91	6.92	5.50	90.0	90.0	120.0	229.00
400K	6.94	6.94	5.50	90.0	90.0	120.0	230.00
450K	6.97	6.97	5.50	90.0	90.0	120.0	232.00
500K	6.98	6.98	5.50	90.0	90.0	120.0	234.00
Experimental	7.03	7.03	5.48	90.0	90.0	120.0	235.12

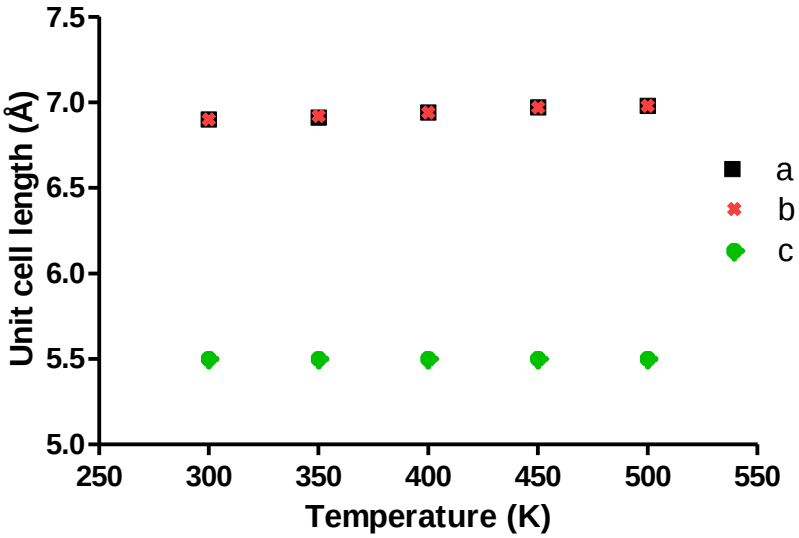

Figure 5.20 Cell parameters of γ glycine as a function of temperature

5.3.7 Simulation of Nanocrystals of α, β and γ Glycine as a Function of Temperature

Selected snapshots of the nanocrystals for each of the forms are given in Figure 5.21. It was observed from visualisation of trajectories of the nanocrystal form of α, β and γ glycine that all the three phases retained their polymorphic forms over the entire range of temperature studied (300K-500K). However it was found that the crystals tend to lose their shapes and the edges of the crystals are deformed and become curved. As the temperature was increased the edges of the crystals became more curved and at 500K the crystals adopt the shape of a sphere. The reason for deformation the edges of a crystal at high temperature is because the system attempts to reduce the surface free energy to adopt the shape with lowest surface to volume ratio i.e. a sphere which is considered thermodynamically more stable because of the low surface free energy. The β phase of glycine was found more spherical with round edges compared to the α and γ phases.

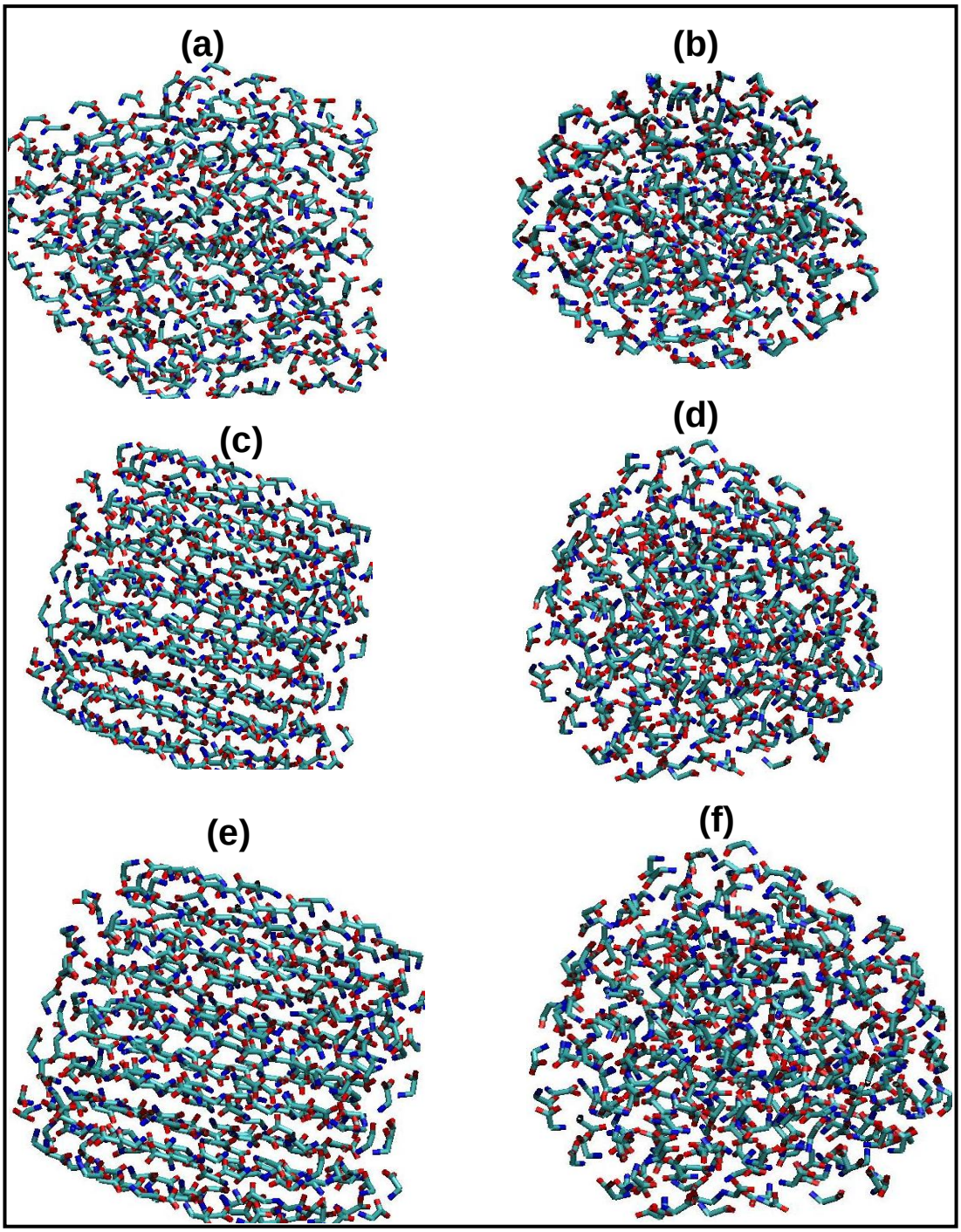

Figure 5.21 Configurations of glycine (a) α glycine at 300K; (b) α glycine at 500K; (c) β glycine at 300K ; (d) β glycine at 500K; (e) γ glycine at 300K ; (f) γ glycine at 500K

5.3.8 RDFs and Potential Energy Calculations for Nanocrystals of α, β and γ Glycine.

RDFs calculations of the selected atomic pairs including (H2-H2, O2-N, O2-H1 and O1-O1) of nanocrystals of three of the polymorphs of glycine (α, β and γ) showed that all the three phases were stable at the entire range of temperature (300K, 350K, 400K, 450K and 500K). These RDFs of the three polymorphs of glycine calculated at 300K, 350K, 400K, 450K and 500K were compared to look at the phase transition. No change in these RDFs was however observed for all the three polymorphs. RDFs of the pair interactions at 300K and 500K are shown in (Figures 5.22, 5.23 and 5.24) and there was not observed any change in the distance of the peaks at higher temperature. These results suggest that all the three polymorphs in nanocrystals phase remained stable at higher temperature. Similarly, the potential energies at 300K, 350K, 400K, 450K and 500K as a function of time increased with the temperature but remained equilibrated during the entire simulation time (80ns) which suggest no phase transformation occurred at the selected range of temperature (Figure 5.12). Figure 5.26 shows the potential energy/molecule of nanocrystal form of three of the polymorphs. It was observed that the β phase which we found the least stable in bulk form and transformed to δ phase becomes stable in nanocrystal form. This is possibly because of the surface free energy which may favour this particular phase. However there was not observed any step change in the energy showing phase transformation. There has been reported that the surface free energy become important when the particle size is reduced and the phase which is

unstable in bulk could be stable in nanocrystal phase (Zahn and Anwar, 2011).

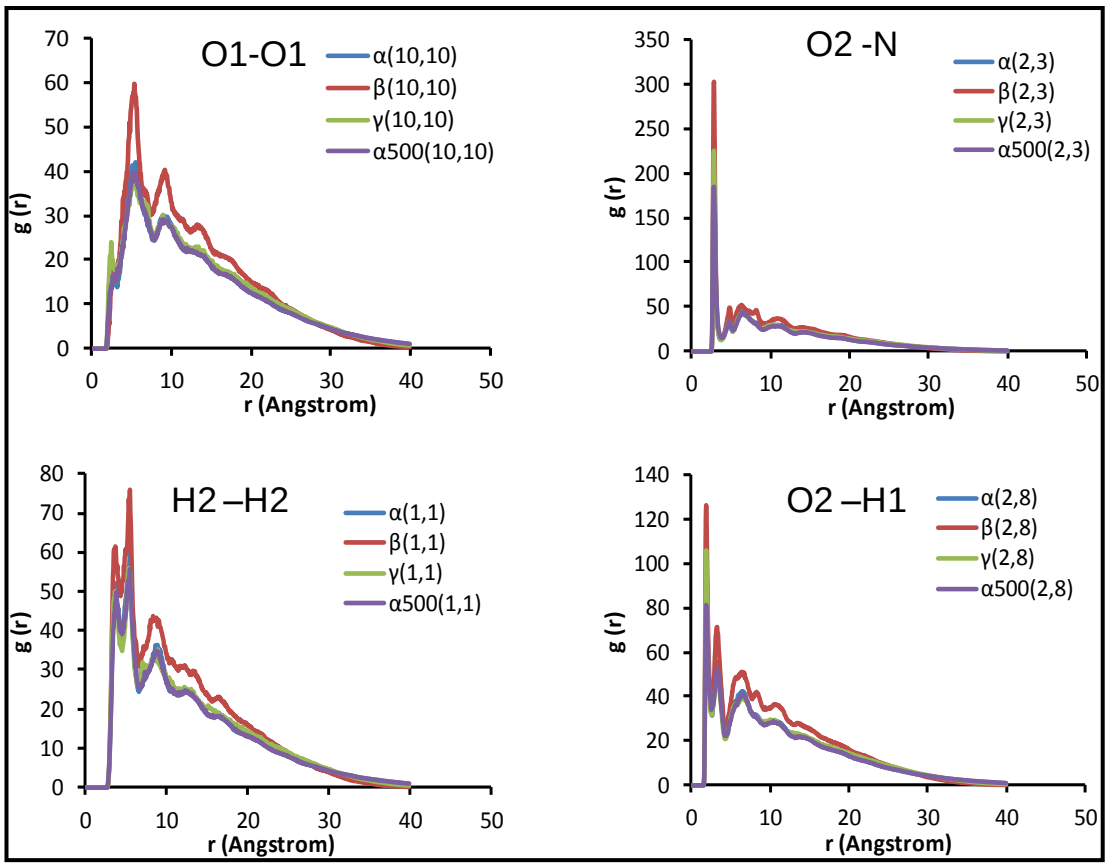

Figure 5.22 RDFs of selected pair interaction of α, β and γ glycine (300K) and their comparison with the RDFs for α glycine calculated at 500K

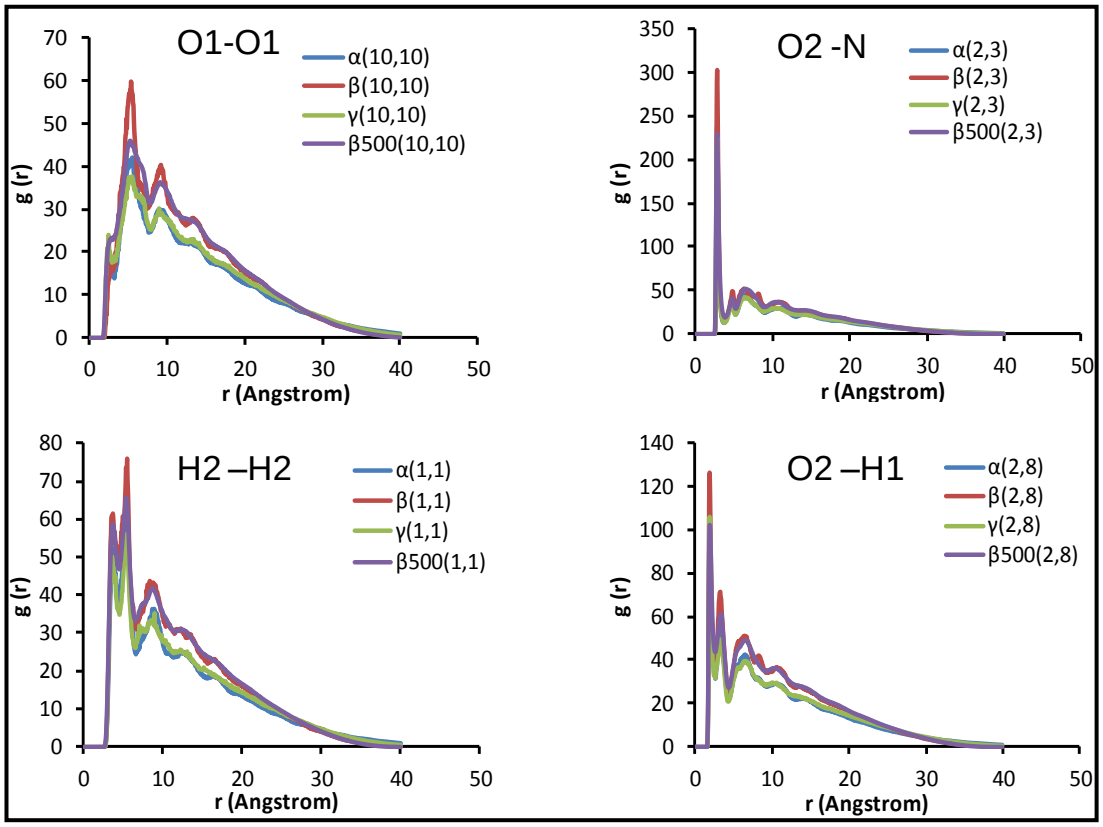

Figure 5.23 RDFs calculation of α, β and γ glycine (300K) and their comparison with the RDFs for β glycine calculated at 500K.

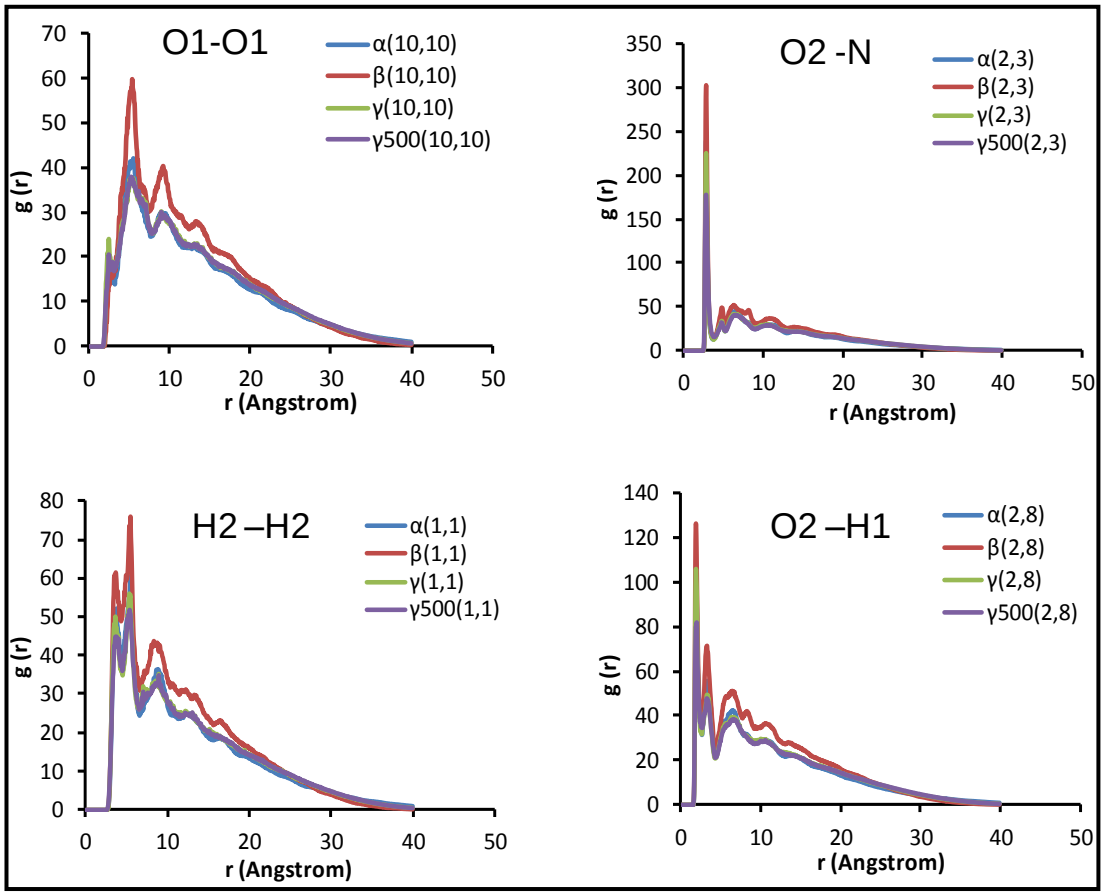

Figure 5.24 RDFs calculation of α, β and γ glycine (300K) and their comparison with the RDFs for γ glycine calculated at 500K.

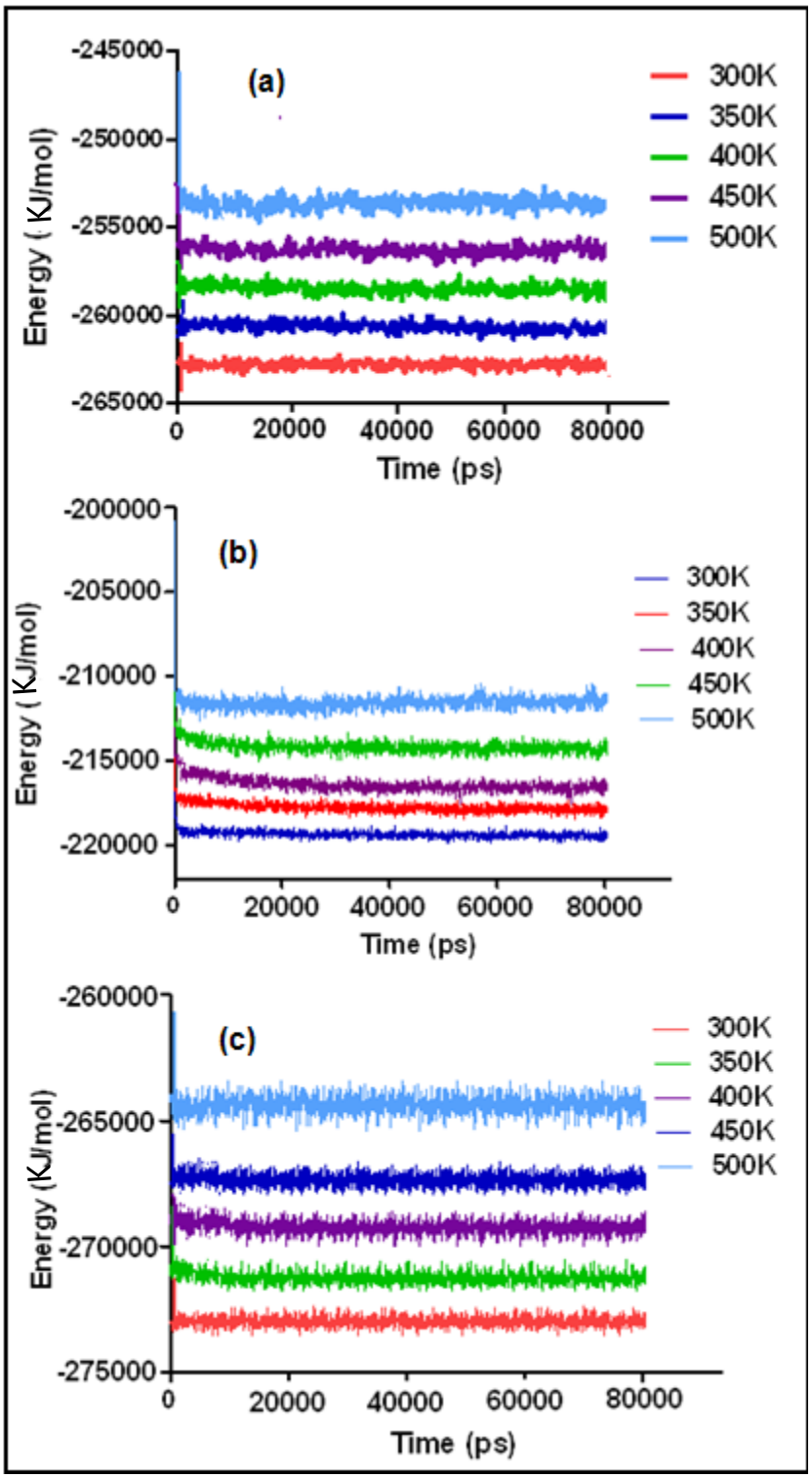

Figure 5.25 Potential energy of (a) α glycine; (b) β glycine; and (d) γ glycine as a function of time at different temperature

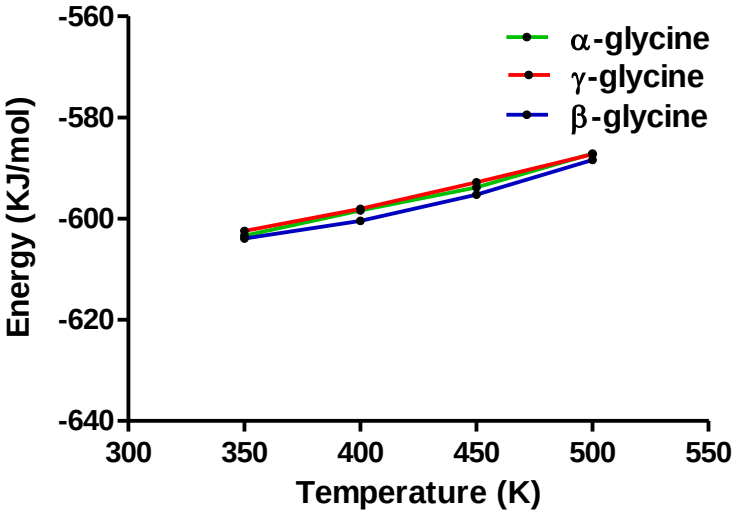

Figure 5.26 Potential energy/molecule of nanocrystal forms of three polymorphs of glycine as a function of temperature.

5.3.9 Simulation of Bulk Phases of Glycine (α, β and γ) as a Function of Pressure.

The trajectories of α, β and γ glycine at elevated pressures were visualised for the entire range of pressure (10kbar, 20kbar, 30kbar and 50kbar). The α and γ phases showed little or no change in the packing arrangement of molecules at high pressures investigated. The crystal lattice of α glycine was little distorted at 50 kbar (Figure 5.27), whilst γ glycine showed no distortion (Figure 5.28). In contrast, the β phase showed a phase transformation at 20kbar. Figure 5.29 shows snapshots from the trajectories of β phase at 10 kbar and 20 kbar. These clearly show the different alignment of nitrogen and oxygen. Every third molecule in each line from left to right in the configuration of β phase obtained at 20kbar has the same alignment/conformation, whereas no such arrangement was observed in the configuration obtained at 10Kbar. Closer examination of the new phase revealed that the structure is that of the δ form. This result is consistent with experimental data in that the

β-δ has transformation also been reported at 19kbar (Dawson et al., 2005). There was not observed any difference in the structures obtained at 20kbar and 50kbar (Figure 5.7).

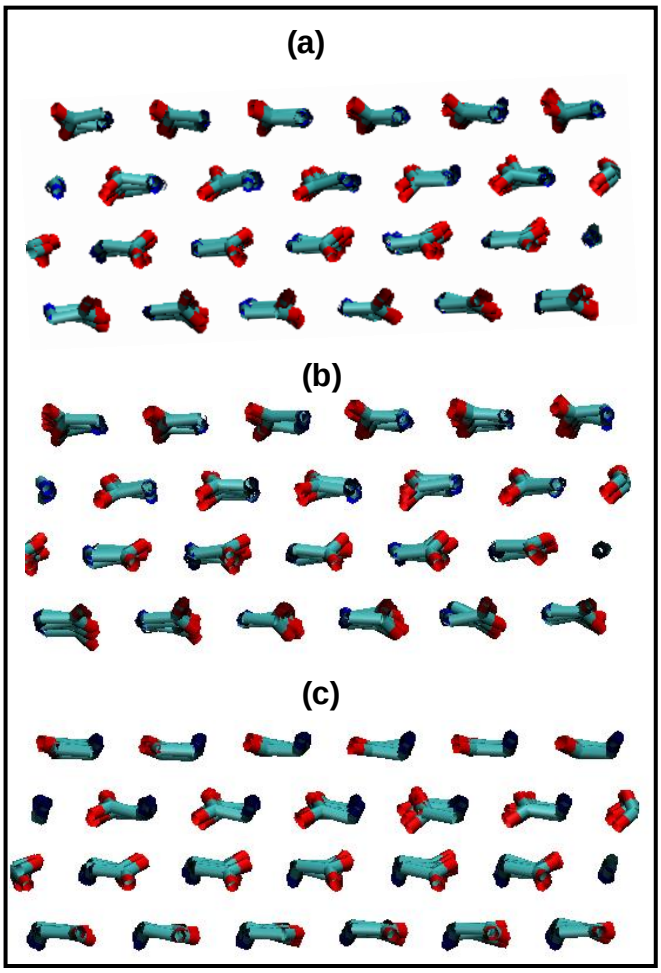

Figure 5.27 Configurations of few molecules in crystal packing of α glycine at (a) 10kbar; (b) 20kbar and (c) 50kbar. (The nitrogen and oxygen atoms are shown in red and dark blue respectively, whereas the hydrogen atoms have been removed to clearly see the phase transformation

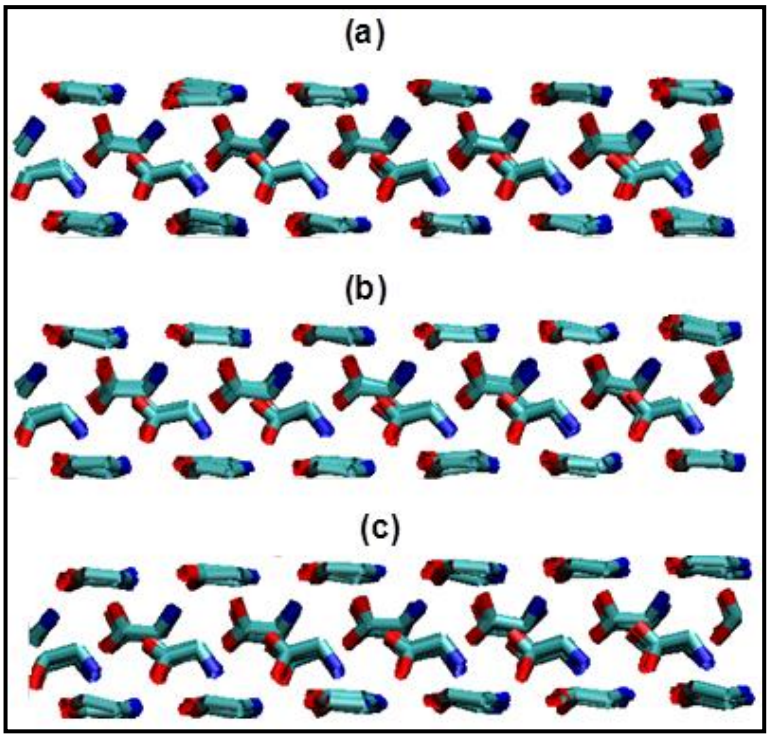

Figure 5.28 Configurations of few molecules in crystal packing of γ glycine at (a) 10kbar; (b) 20kbar and (c) 50kbar

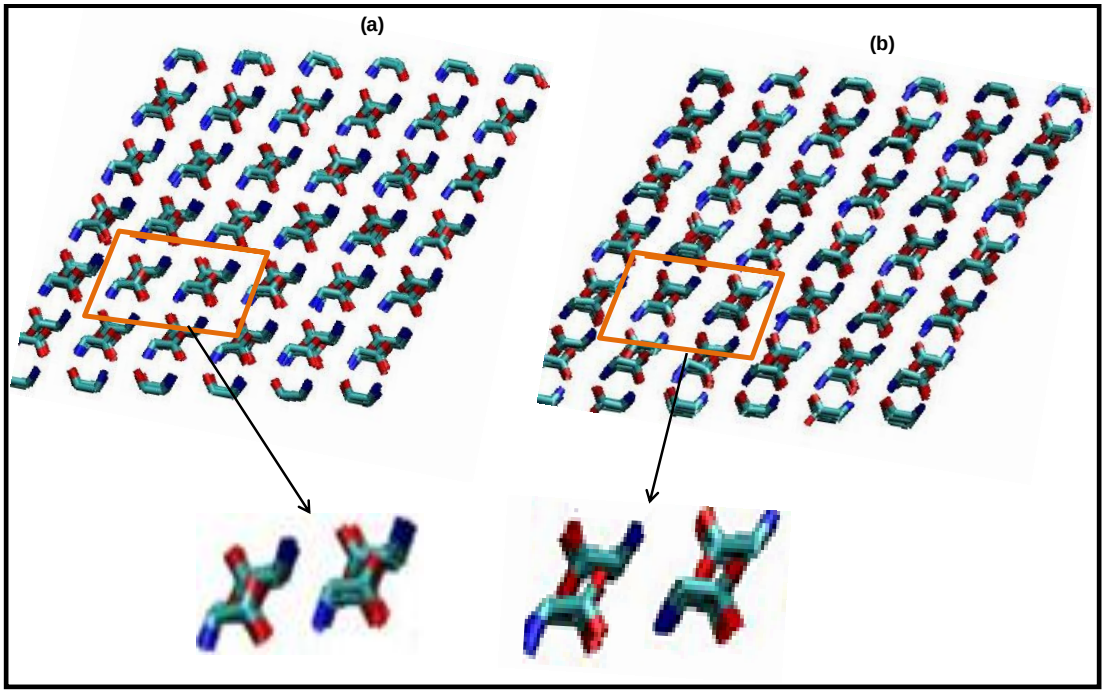

Figure 5.29 Configurations of β glycine at (a) 10kbar and 20kbar. The red and blue sticks show oxygen and nitrogen atoms respectively whereas the hydrogen atoms have been removed to visualise clearly the phase transformation.

5.3.10 RDFs of the Selected Atomic Pairs in α, β and γ Glycine

RDFs of the atomic pairs including (C1-H2, O2-H1, O2-O2, H2-H2 and O1-H1) which discriminate the three polymorphs from each other were determined for equilibrium configurations at 10kbar, 20kbar, 30kbar and 50kbar. These RDFs were compared with the RDFs calculated for three of the polymorphs (α, β and γ) at ambient conditions (300K and .001katm). For α and γ glycine, the RDFs (show in Figures 5.30 and 5.31 respectively) remained unchanged at high pressure, confirming the visual analysis that no phase transformation occurred at the pressures investigated for these phases.

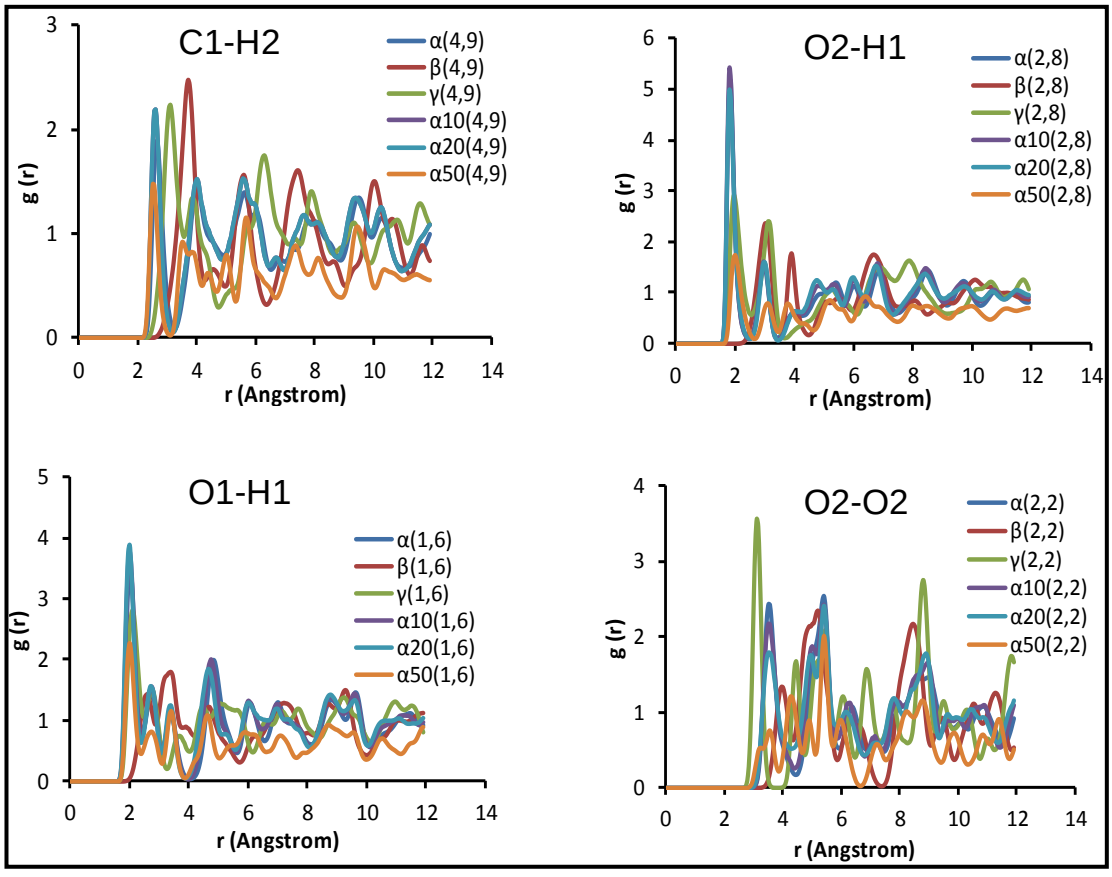

Figure 5.30 RDFs calculation of the specified pair interactions for α, β and γ glycine at ambient conditions and their comparison with the α glycine at high pressure. (10, 20 and 50 show the employed pressure)

All the pair interactions peaks for α and γ glycine appeared on the same distance at high pressure. The peaks intensity for the α glycine at 50kbar was however bit reduced which could be probably caused by the small distortion of the crystal structure (Figure 5.27). It has also been observed experimentally that a very high pressure is required for phase transformation of these two polymorphs (Dawson et al., 2005).

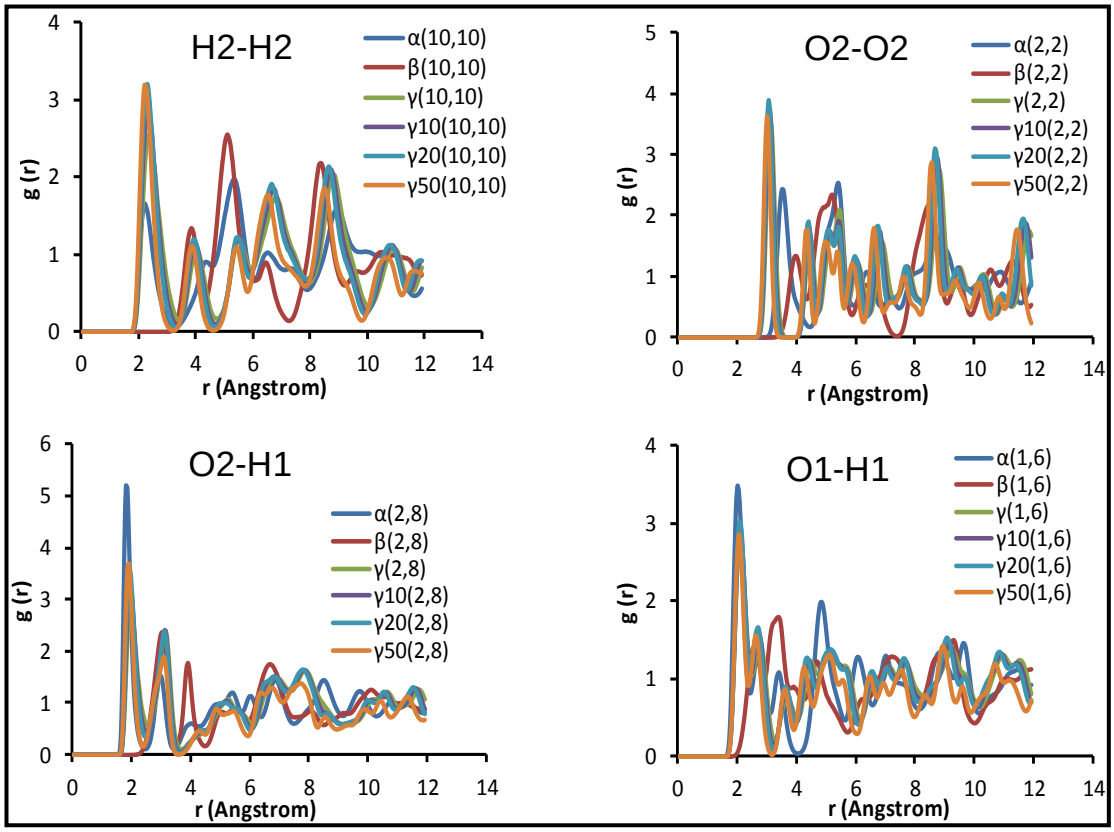

Figure 5.31 RDFs calculation of the specified pair interactions for α, β and γ glycine at ambient conditions and their comparison with the γ glycine at high pressure.(10,20 and 50 show the employed pressure)

For β glycine, however, the RDFs of pair interactions H2-H2, C1-H2, O1-H1 and O2-H1, which clearly discriminate the three polymorphs from each other were found to different at 20 kbar compared with β polymorph at ambient pressure and at 10 kbar (Figure 5.32). This suggests that β polymorph has been transformed to a new polymorph at a pressure (> 10Kbar). For β

glycine, the peaks intensity of the RDFs for specified atomic pairs interaction were increased (Fig 5.33) at 50 kbar, which could be probably caused by the compression of the lattice with subsequent increase of the specified atoms around each other. In addition at high pressure the density of atoms around each other increases because of the less freedom for molecules to vibrate.

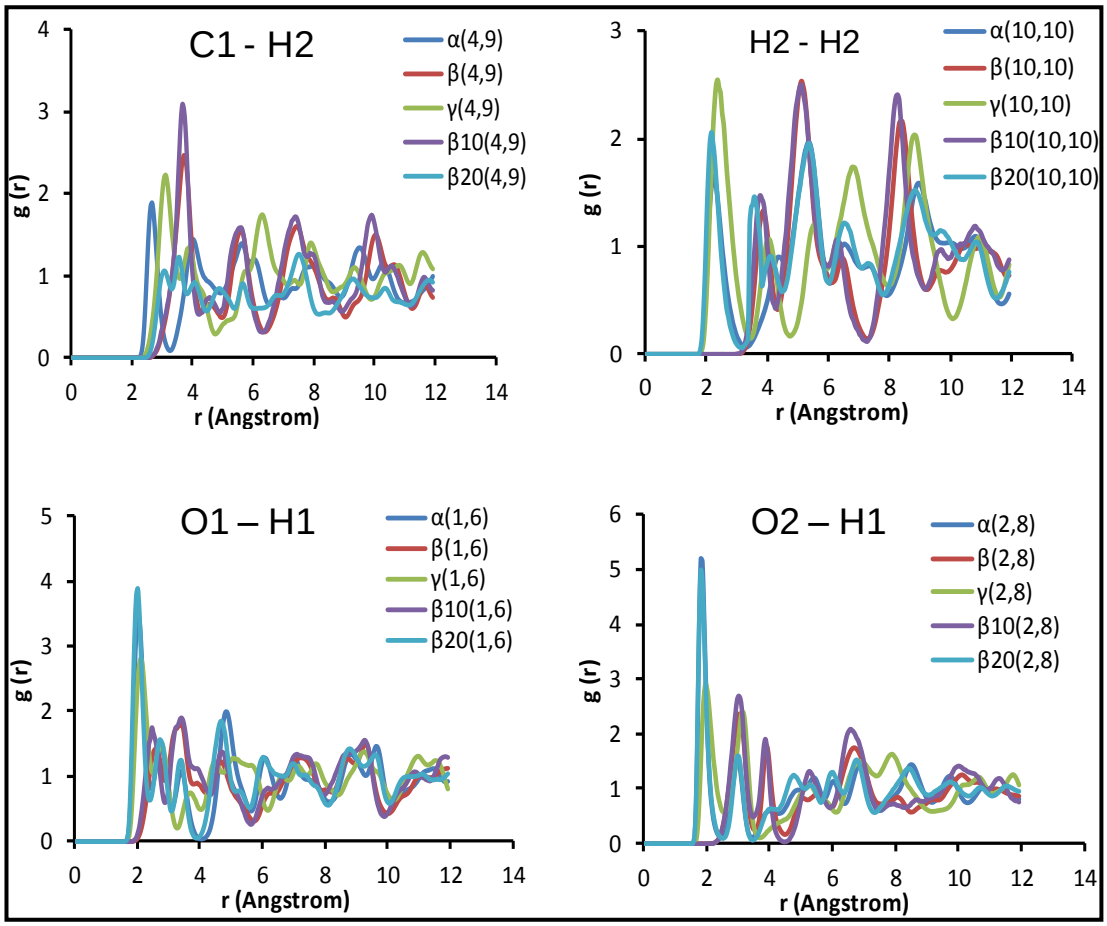

Figure 5.32 RDFs calculation of the specified pair interactions for α, β and γ glycine at ambient conditions and their comparison with the β glycine at high pressure.(10 and 20 are the employed pressure)

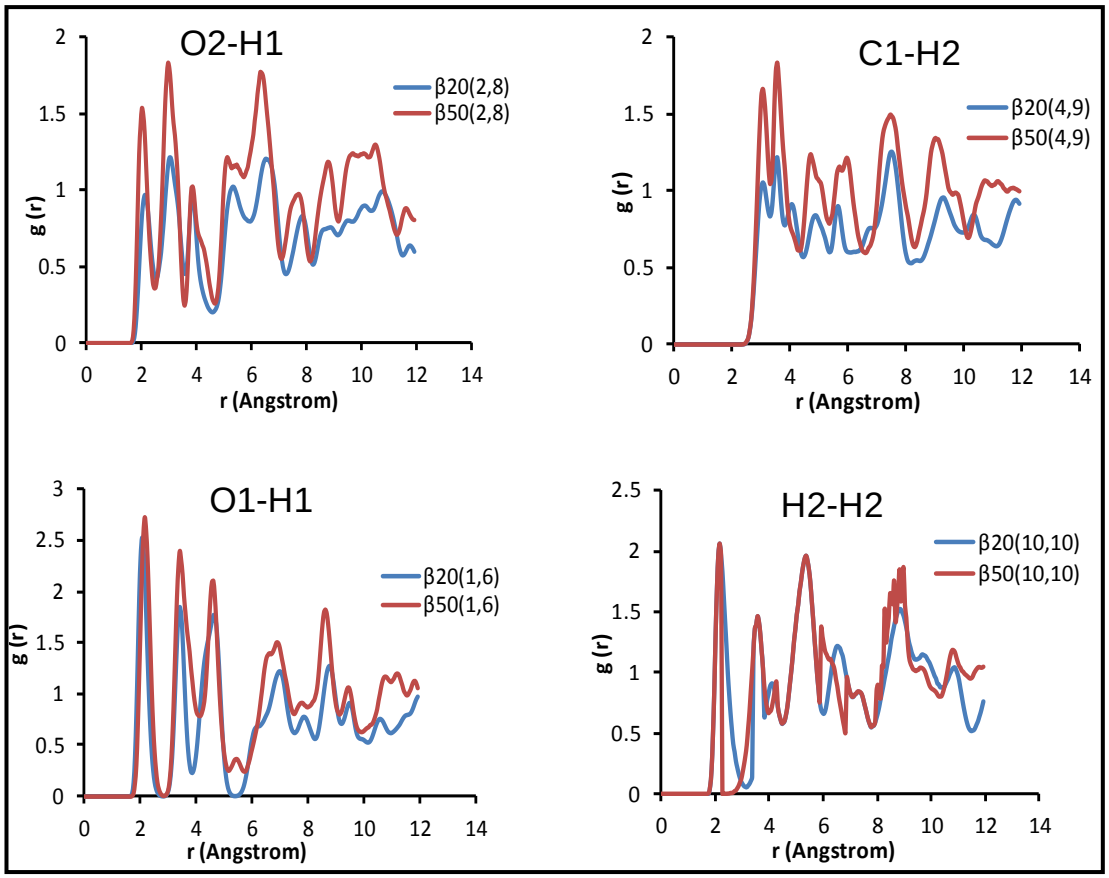

Figure 5.33 Comparison of the RDFs of the specified pair interactions for β glycine calculated at 20kbar and 50kbar

5.3.11 Lattice Parameters

Lattice parameters which include cell axis and angles of α, β and γ glycine were calculated at 10kbar, 20kbar, 30kbar and 50kbar. It was found that “a” and “b” axis of unit cells of α and γ glycine reduced by employing the pressure >10kbar (Table 5.10 and Figure 5.34 (a) and (c)). However no phase transformation was observed in these two polymoprhs as a function of pressure because the atomic pair interactions remained the the same as calculated at 10kbar (Figures 5.30 and 5.31). The structure of α glycine seems bit distorted at high pressure (Figure 5.27) and there was also observed much variations in cell angles at 30kbar and 50kbar (Table 5.10).

The unit cell angles of γ did not change at higher pressure (Table 5.10). For β glycine the axis “a” and “b” were reduced as a results of pressure > 10kbar whereas the “c” axis was increased (Table 5.10 and Figure 5.34 (b)). The β angle of unit cell of β polymorph increased at 20kbar, 30kbar and 50kbar respectively. The other two angles including α and γ remained unchanged at a pressure range (10kbar – 50kbar). These variations in lattice parameters at high pressure for β polymorphs justify the phase transformation in this particular polymorph which has been confirmed both visually and by RDFs calculations of the specified atomic pair interactions.

Table 5.10 Comparison of the lattice parameters of glycine (α, β and γ) at different pressure which were averaged over the molecular dynamics simulation trajectory.

Polymorphs	**Pressure (kbar)**	**Unit cell vector (Å), angles (α, β, γ (degrees)) and volume (Å)^3**						
		a	**b**	**c**	**α**	**β**	**γ**	**volume (Å)^3**
α-Glycine	10	5.01	12.47	5.12	90.0	110.0	90.0	300.00
	20	4.99	12.18	5.02	90.0	110.0	90.0	292.00
	30	4.97	11.65	5.15	92.6	109.0	84.3	282.00
	50	4.92	11.49	5.13	92.7	110.0	83.9	272.00
β-Glycine	10	5.28	6.37	5.20	90.0	110.0	90.0	153.00
	20	4.94	6.12	5.43	90.0	110.0	90.0	147.00
	30	4.93	6.00	5.41	90.0	109.0	84.3	144.00
	50	4.92	5.85	5.34	90.0	110.0	83.9	138.00
γ-Glycine	10	6.80	6.81	5.48	90.0	90.0	120.0	221.00
	20	6.75	6.78	5.45	90.0	90.0	120.0	216.00
	30	6.70	6.70	5.44	90.0	90.0	120.0	212.00
	50	6.62	6.62	5.40	90.0	90.0	120.0	206.00

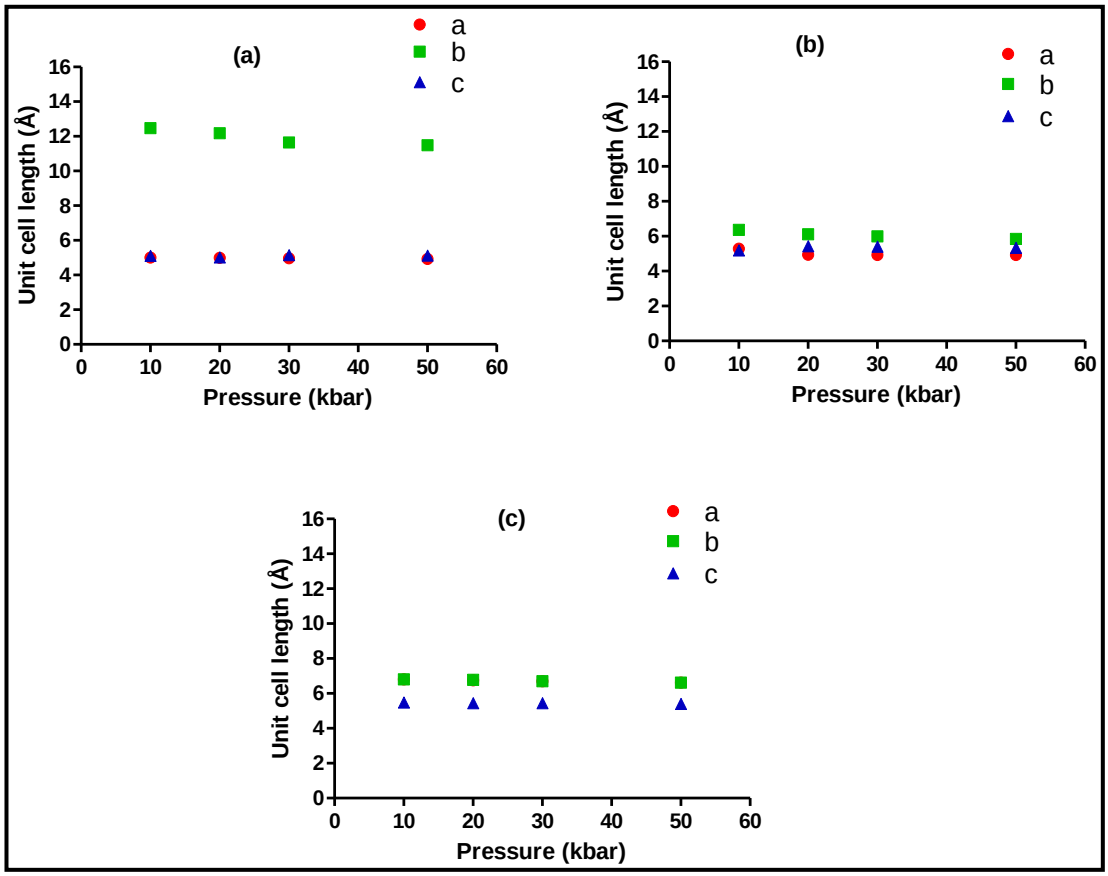

Figure 5.34 Unit cell parameters of (a) α; (b) β and (c) γ glycine as a function of pressure

In conclusion the forcefield parameters for glycine were found to be good enough to reproduce the crystal structures of the various crystalline forms of glycine. The molecular dynamics simulations were able to reproduce the stability of the α and β forms as function of temperature and pressure over the range (300K-500K) and (10kbar-50kbar). Further, the simulations were also were able to reproduce the phase transformation of the β pahse to the δ phase at high temperatures and pressure, being entirely consistent with experiment. The observed delta phase that occurs after the transformation of the beta phase, however, does not have the exact structure of delta phase but shows a slight variation.

The bulk and nanocrystals forms of different polymorphs of a crystal can behave differently at high pressure and temperature. In the case of glycine we observed that stability order for bulk crystals of the three polymorphs is α > γ > β. In contrast for the nanocrystal forms however the stability ranking was changed to β > α > γ. At high temperature and pressure there was observed little expansion and reduction respectively in unit cells of α and γ forms of bulk crystal of glycine. However the arrangement of atoms in the crystal packing remained unchanged. Visual observation, potential energy and RDFs calculation confirmed β – δ phase transformation at high temperature and pressure. This study illustrates the power of molecular dynamics simulations to investigate phase transformation in crystals, even particularly challenging system that contains hydrogen-bonding networks.

Chapter 6

Concluding Remarks and Future Perspective

Greater than 40% of drugs derived through high-throughput screening demonstrate low aqueous solubility. Amongst the range of formulation approaches employed to address this key issue, crystalline nanocrystals and nanosuspensions are rapidly becoming a platform solution, although several challenges including stabilisation and control of particle size distribution for nanosuspensions and scale up issues still need to be addressed. Nanocrystals are rapidly becoming a platform technology due to the immense surface area that they present. Methods for nanocrystal production can be categorized as top down or bottom-up and include milling, high pressure homogenisation, and precipitation. Each of these methods can have specific issues which may include high energy input, long processing times and uncontrolled particle growth. The intention of this study was to revisit the simplest approach of re-precipitation and to identify the critical parameters, including the effect of different stabilisers as well as process conditions. We utilised a combined approach of both experiments and molecular modelling and simulation, not only to determine the optimum parameters but also to gain mechanistic insight.

The uptake of the bottom-up re-precipitation approach to producing nanocrystals appears to be limited. From a technical perspective a perceived limitation of the approach is that the method is not applicable to a wide range of molecules. We have carried a systematic study on three distinct molecules, ibuprofen, glibenclamide and artemsinin, and have shown that stable nanocrystals with uniform size can be prepared in for all three drugs using simple anti-solvent precipitation. The technical challenge appears to be the identification of appropriate stabilizers, which depend on the choice of drug molecule. Also investigated were the effects of the process variables, temperature, stirring rate, and infusion rate. Each of these variables is considered to affect the local supersaturation attained during the anti-solvent precipitation process. Indeed the local supersaturation has been observed to be an important factor in determining the nanocrystal particle size, with higher local supersaturations yielding smaller nanocrystals. We attempted to rationalise the choice of optimum stabilizers in terms of molecular interactions between crystal surfaces and the stabilizer molecules but were unable to make headway. Overall, this comprehensive study demonstrates that conventional crystallisation technology represents an effective approach for preparing nanocrystals in the range 200–400 nm.

Recovery of nanocrystals in the solid form from nanosuspensions is also a technical challenge. The goal is to recover the nanocrystals in the dry form which when incorporated in a solid dosage form can yield the near original nanocrystal characteristics e.g. dissolution rate. We have developed a method described in Chapter 3 that utilises large single crystals of di-calcium phosphate (DCP) as carrier particles for adsorbing nanocrystals from

nanosuspension. This study demonstrated that drug nanocrystals produced by both size reduction and crystallisation can be efficiently isolated on a solid support material (DCP). Both comminuted and crystallised glibenclamide showed an affinity for DCP, whereas nanocrystals produced by comminution showed greater affinity for the carrier, probably owing to greater surface energy induced by mechanical activation. Molecular modelling linked to experimental data indicated that polar functional groups with tendencies to form hydrogen bonds were responsible for adsorption on to the carrier particle surfaces. Adsorbed nanoparticles showed marked improvements in dissolution rate compared to original API, micronised suspensions, and marketed products. Differences in dissolution rate for the adsorbed nanoparticles obtained by two different approaches (milled and crystallized) were negligible. The carrier particles with the adsorbed nanocrystals can potentially be transformed to other solid dosage forms including tablets, capsules and pellets.

Whilst the technology of nanocrystal production is advancing at a rapid pace, we still do not understand the mechanisms that determine the particle size and stability in bottom up processes such a precipitation. There are a range of bottom up methods which have been mentioned in Section 1.3.1 that produce nanocrystal by precipitation of the drug molecules from mixing of the solvent anti solvent. Crystallisation of the drug molecules occurs by nucleation which is the key step to controlling the particle size distribution and size of the crystal. It is therefore imperative to understand this early stage of antisolvent crystallisation. As this process takes place at atomistic level which is difficult to be visualised using experimental approaches

(Schüth et al., 2001). Computer simulation approaches such as Monte Carlo and molecular dynamics simulations have been used to investigate this process but are limited by the random nature of the nucleation process. In view of this the earliest stages of the anti-solvent precipitation process were explored by means of coarse grained molecular dynamics simulation, rather than atomistic simulations which require large cpu resource for an extended period. These coarse grained simulations reveal that the water molecules do not infiltrate the solvent phase containing the drug to any significant extent and therefore do not initiate the aggregation of the solute particles as might be expected. At a molecular level this would mean initial infiltration of water into the solute solution (unlikely given that water has little affinity for the solute particles) and then evacuation of the water as the solute aggregates, which would not be efficient. Instead the simulations reveal that the solvent molecules move towards the water leaving the solute molecules to aggregate which is then followed by nucleation. An important issue is whether the volume element created by the mixing process determines the final size of the nanocrystal. Given that the local supersaturation is an important factor, we argue that spinodal decomposition causes the individual volume elements to phase separate into individual clusters yielding nanocrystals of a size smaller than that of the volume element. This would explain why nanocrystals can arise from simple mixing processes.

We then proceeded to investigate the phase stability of nanocrystals. More than 90% of the APIs in different pharmaceutical dosage forms are in the solid form. This solid might be amorphous or crystalline. The crystalline forms of API can exist in a number of polymorphic forms which have different

physicochemical characteristics resulting in different dissolution rate and bioavailability (Singhal and Curatolo, 2004) . Therefore, it is important to select an appropriate polymorph for a specific dosage form which yields the desired dissolution rate and bioavailability. An important issue is phase stability and the possibility of phase transformation. For example the failure of ritonavir in dissolution tests happened because of a transformation to a new polymorph which has a low solubility (Bauer et al., 2001). Phase stability is an important issue also for nanocrystals, for which the stable phase may be different from that in the bulk phase, hence offering new opportunities, both technical and commercial. In view of this the aim of the study detailed in Chapter 5 was to investigate the phase stability and thermodynamics of both bulk crystals and their nanocrystal counterparts. For this study we investigated crystalline forms of glycine as a model as they are well characterised. The simulations of the crystalline forms were performed as a function of temperature and pressure on bulk and nanocrystals of three phases (α, β and γ) of glycine. This study showed that α and γ phases remained stable at the entire range of temperature (300K, 350K, 400K, 450K and 500K) and pressure (10 lbar, 20 kbar, 30 kbar and 50 kbar). With respect to the β phase, the simulations as a function of evaluated temperature and increased pressure produced a new phase (δ form) which has also been reported experimentally (Dawson et al., 2005). The packing and arrangements of molecules in the new phase obtained from simulation of β glycine as a function of temperature and pressure were found similar to the published δ phase. Additionally, at elevated temperature and pressure the potential energy and RDFs calculations of the specified atomic pairs which

categorically discriminate the three polymorphs from each other confirmed the transformation of β phase to new phase (δ). The simulation of the nanocrystals of the three phases of glycine as a function of temperature showed that all the phases remained stable at the entire range of temperature (300K, 350K, 400K, 450K and 500K). Whereas at this temperature range and increased pressure the β polymorph in bulk phase showed transformation to δ phase above 400K and 10Kbar respectively. This suggested that the crystals behave differently when the particle size is reduced because of the surface free energy. This study reveals that crystal-crystal phase transformations can be predicted for hydrogen-bonded systems. Mechanisms of transformation using molecular simulations could prove to be useful in devising strategies for controlling crystal-crystal phase transformations.

In summary the studies comprising the thesis reveal that stable nanocrystals in ideal pharmaceutical range < 500nm of hydrophobic API molecules can be produced by simple controlled crystallisation method. The selection of suitable stabilisers (polymers and surfactants) and process conditions are critical for producing stable nanocrystals on large scale. This study also presented a novel idea for recovering nanocrystals from nanosuspensions using large crystal of pharmaceutically acceptable career particles. This method is more economical and efficient compared to other methods which have been employed to dry nanosuspensions and include spray drying, freeze drying and spray granulation. The recovery of drug nanocrystal from suspension using inert support materials can be affected both by morphology of drug/carrier and methods producing drug nanocrystals.

The coarse grained simulation studies provided molecular insight into the mechanism of formation of nanocrystals by simple mixing process which determines that the size of the nanocrystal is smaller than the phase separation of the volume elements caused by spinodal decomposition. Molecular simulation studies also showed that phase stability of nanocrystals depends on crystal size and at nanoscale because of the different thermodynamics attributes and the phase becomes stable which was unstable at bulk form. This study can be employed to predict the issue of polymorphism in hydrogen bonded systems.

6.1 Future Perspectives

The key issues associated with nanocrystals produced by bottom up method which still require mechanistic understanding include stability, process scale up, the early stages of nanocrystal formation, and in vivo studies. The simple method of crystallisation that we developed for producing drug nanocrystals would need to be scaled up to test for reproducing drug nanocrystals at large scale. It is still a challenge to understand the early stages of nanocrystal formation in polymeric liquor and how the polymers/surfactants inhibit the crystal growth to rationalising the suitable stabilisers. Further coarse grained simulations could be employed to address this issue. For example the mechanism of crystal growth inhibition by the polymers could be modelled by introducing a large crystal in a solution which contains drug and polymer particles. As there are many studies of preparation of nanocrystals using a variety of methods and how well they perform in in-vitro dissolution tests, there are very few studies investigating the bioavailability of nanocrystals in-

vivo. Clearly in-vivo studies of the prepared nanocrystals and marketed formulations to compare their bioavailability are required.

Solid dosage forms are considered the most attractive, acceptable and widely used among all other dosage forms. Solid dosage forms including tablets and capsules which contain drug nanocrystal can be prepared from the isolated nanocrystals on carrier particles with subsequent solid state characterisation and in-vivo studies. Further to the effect of process and drug surfaces on isolation of nanocrystal from solution, the impact of size of carrier particle needs also to be investigated for recovery of nanocrystals.

Phase stability in nanocrystals is also a key challenge. Molecular simulation can be employed to carry out free energy calculations as a function of particle size to see how the phase diagram changes in going from bulk crystals to nanocrystals. The stability of a phase depends on competition between bulk and free energies. It is therefore important to determine that at what scale the surface free energy becomes significant to give favour to the particular phase. Free energy calculations investigating the size dependent phase stability of inorganic nanocrystals including TiO_2, ZrO_2 and $Al2O_3$ (Ranade et al., 2002) illustrate what is required. .

Chapter 7

References

Abbona, F., Christensson, F., Angela, M. F. & Madsen, H. 1993. Crystal habit and growth conditions of brushite, CaHPO4 2H2O. *Journal of Crystal Growth,* 131, 331-346.

Abdelwahed, W., Degobert, G., Stainmesse, S. & FESSI, H. 2006. Freeze-drying of nanoparticles: Formulation, process and storage considerations. *Advanced Drug Delivery Reviews,* 58, 1688-1713.

Aboofazeli, R., Barlow, D. J. & Lawrence, M. J. 2000. Particle size analysis of concentrated phospholipid microemulsions: II. Photon correlation spectroscopy. *The AAPS Journal,* 2, 1-10.

Adi, H., Larson, I. & Stewart, P. J. 2007. Adhesion and redistribution of salmeterol xinafoate particles in sugar-based mixtures for inhalation. *International Journal of Pharmaceutics,* 337, 229-238.

Adi, H., Traini, D., Chan, H. K. & Young, P. M. 2008. The influence of drug morphology on aerosolisation efficiency of dry powder inhaler formulations. *Journal of pharmaceutical sciences,* 97, 2780-2788.

Agrawal, R. & Kofke, D. A. 1995. Thermodynamic and structural properties of model systems at solid-fluid coexistence. *Molecular physics,* 85, 23-42.

Ali, H. S. M., York, P., Ali, A. & Blagden, N. 2011. Hydrocortisone nanosuspensions for ophthalmic delivery: A comparative study between microfluidic nanoprecipitation and wet milling. *Journal of Controlled Release,* 149, 175-181.

Albrecht, G. & COREY, R. 1939. The crystal structure of glycine. *Journal of the American Chemical Society,* 61, 1087-1103.

Allen, F. H. 2002. The Cambridge Structural Database: a quarter of a million crystal structures and rising. *Acta Crystallographica Section B: Structural Science,* 58, 380-388.

Aly Nada, S. M. A.-S., Bernd W. Mueller 2005. Improving the Physical and Chemical Properties of Ibuprofen. *Pharmaceutical Technology,* 29 (1).

Amidon, G. L., Lennernäs, H., Shah, V. P. & Crison, J. R. 1995. A theoretical basis for a biopharmaceutic drug classification: the correlation of in vitro drug product dissolution and in vivo bioavailability. *Pharmaceutical research,* 12, 413-420.

Anwar, J. & Boateng, P. K. 1998. Computer simulation of crystallization from solution. *Journal of the American Chemical Society,* 120, 9600-9604.

Anwar, J. & Zahn, D. 2011. Uncovering molecular processes in crystal nucleation and growth by using molecular simulation. *Angewandte Chemie International Edition,* 50, 1996-2013.

Annapragada, A. & Adjei, A. 1996. Numerical simulation of milling processes as an aid to process design. *International Journal of Pharmaceutics,* 136, 1-11.

Aungst, B. J. 1993. Novel formulation strategies for improving oral bioavailability of drugs with poor membrane permeation or presystemic metabolism. *Journal of Pharmaceutical Sciences,* 82, 979-986.

Bajwa, G. S., Sammon, C., Timmins, P. & Melia, C. D. 2009. Molecular and mechanical properties of hydroxypropyl methylcellulose solutions during the sol: gel transition. *Polymer,* 50, 4571-4576.

Basa, S., Muniyappan, T., Karatgi, P., Prabhu, R. & Pillai, R. 2008. Production and in vitro characterization of solid dosage form incorporating drug nanoparticles. *Drug development and industrial pharmacy,* 34, 1209-1218.

Bauer, J., Spanton, S., Henry, R., Quick, J., Dziki, W., Porter, W. & Morris, J. 2001. Ritonavir: an extraordinary example of conformational polymorphism. *Pharmaceutical research,* 18, 859-866.

Bedrov, D., Ayyagari, C. & Smith, G. D. 2006. Multiscale modeling of poly (ethylene oxide)-poly (propylene oxide)-poly (ethylene oxide) triblock copolymer micelles in aqueous solution. *Journal of Chemical Theory and Computation,* 2, 598-606.

Beirowski, J., Inghelbrecht, S., Arien, A. & Gieseler, H. 2011. Freeze drying of nanosuspensions, 1: Freezing rate versus formulation design as critical factors to preserve the original particle size distribution. *Journal of pharmaceutical sciences,* 100, 1958-1968.

Begat, P., Morton, D. A. V., Staniforth, J. N. & Price, R. 2004. The cohesive-adhesive balances in dry powder inhaler formulations II: Influence on fine particle delivery characteristics. *Pharmaceutical research,* 21, 1826-1833.

Begat, P., Price, R., Harris, H., Morton, D. & Staniforth, J. 2005. The influence of force control agents on the cohesive-adhesive balance in dry powder inhaler formulations. *Kona,* 23, 109-121.

Bennema, P. 1974. Crystal growth from solution--theory and experiment. *Journal of Crystal Growth,* 24, 76-83.

Bernstein, J. 2002. *Polymorphism in Molecular Crystals*, Oxford UniversityPress, New York.

Blagden, N., De Matas, M., Gavan, P. T. & York, P. 2007. Crystal engineering of active pharmaceutical ingredients to improve solubility and dissolution rates. *Advanced Drug Delivery Reviews,* 59, 617-630.

Bodmeier, R. & Mcginity, J. W. 1998. Solvent selection in the preparation of poly (DL-lactide) microspheres prepared by the solvent evaporation method. *International Journal of Pharmaceutics,* 43, 179-186.

Böhm, B. H. L. & Müller, R. H. 1999. Lab-scale production unit design for nanosuspensions of sparingly soluble cytotoxic drugs. *Pharmaceutical Science & Technology Today,* 2, 336-339.

Boldyreva, E. 2007a. High-pressure polymorphs of molecular solids: when are they formed, and when are they not? Some examples of the role of kinetic control. *Crystal Growth & Design,* 7, 1662-1668.

Boldyreva, E., Drebushchak, V., Drebushchak, T., Paukov, I., Kovalevskaya, Y. A. & SHUTOVA, E. 2003. Polymorphism of glycine, Part I. *Journal of thermal analysis and calorimetry,* 73, 409-418.

Boldyreva, E. V. 2003. High-pressure-induced structural changes in molecular crystals preserving the space group symmetry: anisotropic distortion/isosymmetric polymorphism. *Crystal engineering,* 6, 235-254.

Boldyreva, E. V. 2007b. High-pressure diffraction studies of molecular organic solids. A personal view. *Acta Crystallographica Section A: Foundations of Crystallography,* 64, 218-231.

Bonnett, P., Carpenter, K., Dawson, S. & Davey, R. 2003. Solution crystallisation via a submerged liquid–liquid phase boundary: oiling out. *Chem. Commun.*, 698-699.
Esselink, K., Hilbers, P. & Van Beest, B. 1994. Molecular dynamics study of nucleation and melting of n-alkanes. *The journal of chemical physics,* 101, 9033.

Brittain, H. J. 1999. *Polymorphism in Pharmaceutical Solids*, M. Dekker:New York.

Bose, S., Schenck, D., Ghosh, I., Hollywood, A., Maulit, E. & Ruegger, C. 2012. Application of Spray Granulation for Conversion of a Nanosuspension into a Dry Powder Form. *European Journal of Pharmaceutical Sciences*.

Bourne, J., Davey, R. & Mcculloch, J. 1978. The growth kinetics of hexamethylene tetramine crystals from a water/acetone solution. *Chemical Engineering Science,* 33, 199-204.
Buckton, G. & Beezer, A. E. 1992. The relationship between particle size and solubility. *International Journal of Pharmaceutics,* 82, R7-R10.

Bunjes, H., Koch, M. H. J. & Westesen, K. 2000. Effect of particle size on colloidal solid triglycerides. *Langmuir,* 16, 5234-5241.

Bunker, M., Davies, M. & Roberts, C. 2005. Towards screening of inhalation formulations: measuring interactions with atomic force microscopy. *Expert Opinion on Drug Delivery,* 2, 613-624.

Burton, W., Cabrera, N. & Frank, F. 1951. The growth of crystals and the equilibrium structure of their surfaces. *Philosophical Transactions of the Royal Society of London. Series A, Mathematical and Physical Sciences,* 243, 299-358.

Buzea, C., Pacheco, II & Robbie, K. Year. Nanomaterials and nanoparticles: sources and toxicity. *In*, 2007. AVS.

Byrn, S., Pfeiffer, R., Stephenson, G., Grant, D. & Gleason, W. 1994. Solid-state pharmaceutical chemistry. *Chemistry of materials,* 6, 1148-1158.

Byrappa, K., Ohara, S. & Adschiri, T. 2008. Nanoparticles synthesis using supercritical fluid technology – towards biomedical applications. *Advanced Drug Delivery Reviews,* 60, 299-327.

Cansell, F., Aymonier, C. & Loppinet-Serani, A. 2003. Review on materials science and supercritical fluids. *Current Opinion in Solid State and Materials Science,* 7, 331-340.

Carstensen, J. T. 1977. *Pharmaceutics of Solids and Solid Dosage Forms*, John Wiley & Sons: New York.

Charoenchaitrakool, M., Dehghani, F., Foster, N. R. & Chan, H. K. 2000. Micronization by rapid expansion of supercritical solutions to enhance the dissolution rates of poorly water-soluble pharmaceuticals. *Ind. Eng. Chem. Res,* 39, 4794-4802.

Choi, M., Briancon, S., Andrieu, J., Min, S. & Fessi, H. 2004. Effect of freeze-drying process conditions on the stability of nanoparticles. *Drying technology,* 22, 335-346.

Choi, S. M. & Awaji, H. 2005. Nanocomposites - a new material design concept. *Science and Technology of Advanced Materials,* 6, 2-10.

Chan, H.-K. & Kwok, P. C. L. 2011. Production methods for nanodrug particles using the bottom-up approach. *Advanced Drug Delivery Reviews,* 63, 406-416.

Charoenchaitrakool, M., Dehghani, F., Foster, N. R. & Chan, H. K. 2000. Micronization by rapid expansion of supercritical solutions to enhance the dissolution rates of poorly water-soluble pharmaceuticals. *Ind. Eng. Chem. Res,* 39, 4794-4802.

Chaubal, M. V. & Popescu, C. 2008. Conversion of nanosuspensions into dry powders by spray drying: a case study. *Pharmaceutical research,* 25, 2302-2308.

Cheong, D. W. & Boon, Y. D. 2010. Comparative study of force fields for molecular dynamics simulations of α-glycine crystal growth from solution. *Crystal Growth & Design*.

C.M. Keck, R. H. M. 2010. SmartCrystals – Review of the Second Generation of Drug Nanocrystal, in: V.P. Torchilin, M.M. Amiji, (Eds.), Handbook of Materials for Nanomedicine (Pan Stanford Series on Biomedical Nanotechnology), Pan Stanford Publishing,. 555–580

C. W. Yip & J. A. Hersey 1976. Ordered powder mixing. *Nature,* 262, 202-203.

Dang, L., Yang, H., Black, S. & Wei, H. 2009. The Effect of Temperature and Solvent Composition on Transformation of β-to α-Glycine As Monitored in Situ by FBRM and PVM. *Organic Process Research & Development,* 13, 1301-1306.

Dawson, A., Allan, D., Belmonte, S., Clark, S., David, W., Mcgregor, P., Parsons, S., Pulham, C. & SAWYER, L. 2005. Effect of high pressure on the crystal structures of polymorphs of glycine. *Crystal Growth & Design,* 5, 1415-1427.

De Waard, H., Frijlink, H. W. & Hinrichs, W. L. J. 2010. Bottom-up preparation techniques for nanocrystals of lipophilic drugs. *Pharmaceutical research*, 1-4.

De Waard, H., Hinrichs, W. L. J. & Frijlink, H. W. 2008. A novel bottom–up process to produce drug nanocrystals: Controlled crystallization during freeze-drying. *Journal of Controlled Release,* 128, 179-183.

Deng, J., Huang, L. & Liu, F. 2010. Understanding the structure and stability of paclitaxel nanocrystals. *International Journal of Pharmaceutics,* 390, 242-249.

Derjaguin, B. V., Landau, L 1941. Theory of the stability of strongly charged lyophobic sols and of the adhesion of strongly charged particles in solutions of electrolytes. *Acta Phys. Chim. 14*, 633-634.

Desiraju, G. R. 2001. Crystal engineering: outlook and prospects. *Current Science,* 81, 1038.

De boer, A., Dickhoff, B., Hagedoorn, P., Gjaltema, D., Goede, J., Lambregts, D. & Frijlink, H. 2005. A critical evaluation of the relevant parameters for drug redispersion from adhesive mixtures during inhalation. *International Journal of Pharmaceutics,* 294, 173-184.

De Boer, A. H., Chan, H. K. & Price, R. 2012. A critical view on lactose-based drug formulation and device studies for dry powder inhalation: Which are relevant and what interactions to expect? *Advanced Drug Delivery Reviews,* 64, 257-274.

De Waard, H., Grasmeijer, N., Hinrichs, W., Eissens, A., Pfaffenbach, P. & Frijlink, H. 2009. Preparation of drug nanocrystals by controlled crystallization: application of a 3-way nozzle to prevent premature crystallization for large scale production. *European Journal of Pharmaceutical Sciences,* 38, 224-229.

Delogu, F. 2005. Thermodynamics on the nanoscale. *The Journal of Physical Chemistry B,* 109, 21938-21941.

Deng, J., Huang, L. & Liu, F. 2010. Understanding the structure and stability of paclitaxel nanocrystals. *International Journal of Pharmaceutics,* 390, 242-249.

Dickens, B., Bowen, J. & Brown, W. 1972. A refinement of the crystal structure of CaHPO4 (synthetic monetite). *Acta Crystallographica Section B: Structural Crystallography and Crystal Chemistry,* 28, 797-806.

Dickhoff, B., De Boer, A., Lambregts, D. & Frijlink, H. 2006. The effect of carrier surface treatment on drug particle detachment from crystalline carriers in adhesive mixtures for inhalation. *International Journal of Pharmaceutics,* 327, 17-25.

Dirksen, J. & Ring, T. 1991. Fundamentals of crystallization: kinetic effects on particle size distributions and morphology. *Chemical Engineering Science,* 46**,** 2389-2427.

Drebushchak, T. N., Boldyreva, E. V. & Shutova, E. S. 2002a. β-Glycine. *Acta Crystallographica Section E: Structure Reports Online,* 58, o634-o636.

Drebushchak, V., Boldyreva, E., Drebushchak, T. & Shutova, E. 2002b. Synthesis and calorimetric investigation of unstable< i> β</i>-glycine. *Journal of Crystal Growth,* 241, 266-268.

Ducker, W. A., Xu, Z. & Israelachvili, J. N. 1994. Measurements of hydrophobic and DLVO forces in bubble-surface interactions in aqueous solutions. *Langmuir,* 10, 3279-3289.

Elwell, D. & Scheel, H. J. 1975. C*rystal growth from high-temperature solutions*, Academic Press New York

Erdemir, D., Lee, A. Y. & Myerson, A. S. 2009. Nucleation of crystals from solution: classical and two-step models. *Accounts of chemical research,* 42, 621-629.

Fahlman, B. D. 2007. *Materials chemistry*, Springer.

Favvas, E. & Mitropoulos, A. C. 2008. What is spinodal decomposition. *J. Eng. Sci. Tech. Rev,* 1, 25-27.

Ferrari, E. S., Davey, R. J., Wendy, I., Gillon, A. L. & Towler, C. S. 2003. Crystallization in polymorphic systems: the solution-mediated transformation of β to α glycine. *Crystal Growth & Design,* 3, 53-60.

Flament, M. P., Leterme, P. & Gayot, A. 2004. The influence of carrier roughness on adhesion, content uniformity and the in vitro deposition of terbutaline sulphate from dry powder inhalers. *International Journal of Pharmaceutics,* 275, 201-209.

Floyd, A. G. 1999. Top ten considerations in the development of parenteral emulsions. *Pharmaceutical Science & Technology Today,* 2, 134-143.
Frank, F. 1949. Crystal growth. *Disc. Faraday Soc,* 5, 48.

Freitas, C. & Müller, R. 1998. Spray-drying of solid lipid nanoparticles (SLNTM). *European Journal of Pharmaceutics and Biopharmaceutics,* 46, 145-151.

Ford, J. L. 1999. Thermal analysis of hydroxypropylmethylcellulose and methylcellulose: powders, gels and matrix tablets. *International Journal of Pharmaceutics,* 179, 209-228.

Garside, J. & Davey, R. 2000. From molecules to crystallizers: An Introduction to crystallization. Oxford University Press.

Garvie, R. 1978. Stabilization of the tetragonal structure in zirconia microcrystals. *The Journal of Physical Chemistry,* 82, 218-224.

Gao, L.; Liu, G.; Ma, J.; Wang, X.; Zhou, L.; Li, X. 2012. Drug nanocrystals: In vivo performances. *Journal of Controlled Release* , *160*, (3), 418-430..

GAO, L., Zhang, D. & Chen, M. 2008. Drug nanocrystals for the formulation of poorly soluble drugs and its application as a potential drug delivery system. *Journal of Nanoparticle Research,* 10, 845-862.

Garvie, R. 1978. Stabilization of the tetragonal structure in zirconia microcrystals. *The Journal of Physical Chemistry,* 82, 218-224.

Giron, D. 2001. Investigations of polymorphism and pseudo-polymorphism in pharmaceuticals by combined thermoanalytical techniques. *Journal of thermal analysis and calorimetry,* 64, 37-60.

Goodman, J. M. 1998. *Chemical applications of molecular modelling,* The royal society of chemistry, United Kingdom.

Hartman, P. 1973. *Crystal Growth: an Introduction, edited by P. Hartman*, Amsterdam: North Holland.

Hersey, J. A. 1975. Ordered mixing: a new concept in powder mixing practice. *Powder Technology,* 11, 41-44.

HE, G., Bhamidi, V., Wilson, S. R., Tan, R. B. H., Kenis, P. J. A. & Zukoski, C. F. 2006. Direct growth of γ-glycine from neutral aqueous solutions by slow, evaporation-driven crystallization. *Crystal Growth & Design,* 6, 1746-1749.

Hickey, M. J. T. A. A. J. 2005. Dry Powder Inhaler Formulation. *Respiratory Care,* 50, 1209-1227.

Hilliard, J. E. 1970. Spinodal decomposition in Phase transformations, Metals Park, OH. *American Society for Metals,* , 497-560.

Hooton, J. C., Jones, M. D., Harris, H., Shur, J. & Price, R. 2008. The influence of crystal habit on the prediction of dry powder inhalation formulation performance using the cohesive-adhesive force balance approach. *Drug development and industrial pharmacy,* 34, 974-983.

Hooton, J. C., Jones, M. D. & Price, R. 2006. Predicting the behavior of novel sugar carriers for dry powder inhaler formulations via the use of a cohesive–adhesive force balance approach. *Journal of pharmaceutical sciences,* 95, 1288-1297.

Horn, D. & Rieger, J. 2001. Organic nanoparticles in the aqueous phase—theory, experiment, and use. *Angewandte Chemie International Edition,* 40, 4330-4361.

Huitema, H., Van Hengstum, B. & Van der Eerden, J. 1999. Simulation of crystal growth from Lennard-Jones solutions. *The journal of chemical physics,* 111, 10248.

Hussain, M. & Anwar, J. 1999. The riddle of resorcinol crystal growth revisited: molecular dynamics simulations of -resorcinol crystal-water interface. *Journal of the American Chemical Society,* 121, 8583-8591.

Hu, J., NG, W. K., Dong, Y., Shen, S. & Tan, R. B. H. 2011. Continuous and scalable process for water-redispersible nanoformulation of poorly aqueous soluble APIs by antisolvent precipitation and spray-drying. International Journal of Pharmaceutics, 404, 198-204.

Hu, J., NG, W., Dong, Y., Shen, S. & Tan, R. 2010. Continuous and scalable process for water-redispersible nanoformulation of poorly aqueous soluble APIs by antisolvent precipitation and spray-drying. *International Journal of Pharmaceutics*.

Hüttenrauch, R., Fricke, S. & Zielke, P. 1985. Mechanical activation of pharmaceutical systems. *Pharmaceutical research,* 2, 302-306.

HW Frijlink, A. D. B. 2004. Dry powder inhalers for pulmonary drug delivery *Expert. Opin. Drug Deliv.,* 1, 67-86.

Ian Ashurst, A. M., David Prime and Barry Sumby 2000. Latest advances in the development of dry powder inhalers. *Research focus,* 3, 246-256.

Iitaka, Y. 1954. A new form of glycine. *Proceedings of the Japan Academy,* 30, 109-112.

Iitaka, Y. 1958. The crystal structure of gamma glycine. *Acta Crystallographica,* 11, 225-226.

Iitaka, Y. 1961. The crystal structure of [gamma]-glycine. *Acta Crystallographica,* 14, 1-10.

Islam, N., Stewart, P., Larson, I. & Hartley, P. 2005. Surface roughness contribution to the adhesion force distribution of salmeterol xinafoate on lactose carriers by atomic force microscopy. *Journal of pharmaceutical sciences,* 94, 1500-1511.

Israelachvili, J. & Pashley, R. 1984. Measurement of the hydrophobic interaction between two hydrophobic surfaces in aqueous electrolyte solutions. *Journal of colloid and interface science,* 98, 500-514.

J.A. Dirksen, T. A. R. 1991. Fundamentals of crystallization: kinetic effects on particle size distributions andmorphology. *Chemical Engineering Science,* 46, 2389–2427.
Jensen, F. 2007. *Introduction to computational chemistry*, Wiley.

Jinno, J., Kamada, N., Miyake, M., Yamada, K., Mukai, T., Odomi, M., Toguchi, H., Liversidge, G. G., Higaki, K. & Kimura, T. 2006. Effect of particle size reduction on dissolution and oral absorption of a poorly water-soluble drug, cilostazol, in beagle dogs. *Journal of Controlled Release,* 111, 56-64.

Jones, M. D., Harris, H., Hooton, J. C., Shur, J., King, G. S., Mathoulin, C. A., Nichol, K., Smith, T. L., Dawson, M. L. & Ferrie, A. R. 2008. An investigation into the relationship between carrier-based dry powder inhalation performance and formulation cohesive-adhesive force balances. *European Journal of Pharmaceutics and Biopharmaceutics,* 69, 496-507.

Jonsson, P. G. & Kvick, A. 1972. Precision neutron diffraction structure determination of protein and nucleic acid components. III. The crystal and

molecular structure of the amino acid-glycine. *Acta Crystallographica Section B: Structural Crystallography and Crystal Chemistry,* 28, 1827-1833.

Junghanns, J. & Müller, R. 2008. Nanocrystal technology, drug delivery and clinical applications. *International Journal of Nanomedicine,* 3, 295.

Jünemann, D. & Dressman, J. 2012. Analytical methods for dissolution testing of nanosized drugs. *Journal of Pharmacy and Pharmacology (doi: 10.1111/j.2042-7158.2012.01520.x)*.

Kakran, M., Sahoo, N. G., LI, L. & Judeh, Z. 2010. Dissolution of artemisinin/polymer composite nanoparticles fabricated by evaporative precipitation of nanosuspension. *Journal of Pharmacy and Pharmacology,* 62, 413-421.

Kashchiev, D. 2000. *Nucleation: basic theory with applications*, Butterworth-Heinemann, Oxford.

Kipp, J. E., Wong, J. C. T., Doty, M. J. & Rebbeck, C. L. 2003. Microprecipitation method for preparing submicron suspensions. United States Patent 6,607,784, Baxter International Inc. (Deerfield, IL), USA,.

Kipp, J. 2004. The role of solid nanoparticle technology in the parenteral delivery of poorly water-soluble drugs. *International Journal of Pharmaceutics,* 284, 109-122.
KItamura, M. 2002. Controlling factor of polymorphism in crystallization process. *Journal of Crystal Growth,* 237, 2205-2214.

Kocbek, P., Baumgartner, S. & Kristl, J. 2006. Preparation and evaluation of nanosuspensions for enhancing the dissolution of poorly soluble drugs. *International Journal of Pharmaceutics,* 312, 179-186.

Kvick, A., Canning, W., Koetzle, T. & Williams, G. 1980a. An experimental study of the influence of temperature on a hydrogen-bonded system: the crystal structure of-glycine at 83 K and 298 K by neutron diffraction. *Acta Crystallographica Section B: Structural Crystallography and Crystal Chemistry,* 36, 115-120.

Kvick, A., Canning, W., Koetzle, T. & Williams, G. 1980b. An experimental study of the influence of temperature on a hydrogen-bonded system: the crystal structure of γ-glycine at 83 K and 298 K by neutron diffraction. *Acta Crystallographica Section B: Structural Crystallography and Crystal Chemistry,* 36, 115-120.

Lamer, V. K. & Dinegar, R. H. 1950. Theory, production and mechanism of formation of monodispersed hydrosols. *Journal of the American Chemical Society,* 72, 4847-4854.

Larhrib, H., Martin, G. P., Marriott, C. & Prime, D. 2003. The influence of carrier and drug morphology on drug delivery from dry powder formulations. *International Journal of Pharmaceutics,* 257, 283-296.

Larson, M. & Garside, J. 1986. Solute clustering in supersaturated solutions. *Chemical Engineering Science,* 41, 1285-1289.

Lawrence, M. J. & Rees, G. D. 2000. Microemulsion-based media as novel drug delivery systems. *Advanced Drug Delivery Reviews,* 45, 89-121.

Leach, A. R. 2001. *Molecular modelling: principles and applications*, Addison-Wesley Longman Ltd.

Lee, I. S., Kim, K. T., Lee, A. Y. & Myerson, A. S. 2008. Concomitant crystallization of glycine on patterned substrates: The effect of pH on the polymorphic outcome. *Crystal Growth and Design,* 8, 108-113.

Lehn, J. M. 1988. Supramolecular chemistry—scope and perspectives molecules, supermolecules, and molecular devices (Nobel Lecture). *Angewandte Chemie International Edition in English,* 27, 89-112.

Liang, Y., Hilal, N., Langston, P. & Starov, V. 2007. Interaction forces between colloidal particles in liquid: Theory and experiment. *Advances in colloid and interface science,* 134, 151-166.

Lin, C., Gabas, N.Canselier, JP & Pepe, G. 1998. Prediction of the growth morphology of aminoacid crystals in solution: I. α-Glycine. *Journal of Crystal Growth,* 191, 791-802.

Lindfors, L. 2004. Aqueous dispersion comprising stable nanoparticles of a water-insoluble thiazole derivative and excipients like middle chain triglycerides. WO Patent WO/2004/069,226.

Lipinski, C. A. 2002. Poor Aqueous Solubility-an Industry Wide Problem in ADME screening. *American Pharmaceutical Review,* 5, 82-85.

List, M. & Sucker, H. 1995. Hydrosols of pharmacologically active agents and their pharmaceutical compositions comprising them. US patent : 5389382

Liu, Y., Sun, C., Hao, Y., Jiang, T., Zheng, L. & Wang, S. 2010. Mechanism of dissolution enhancement and bioavailability of poorly water soluble celecoxib by preparing stable amorphous nanoparticles. *Journal of Pharmacy & Pharmaceutical Sciences,* 13, 589-606.

Liversidge, G. G. & Cundy, K. C. 1995. Particle size reduction for improvement of oral bioavailability of hydrophobic drugs: I. Absolute oral bioavailability of nanocrystalline danazol in beagle dogs. *International Journal of Pharmaceutics,* 125, 91-97.

Liversidge, G. G., Cundy, K. C., Bishop, J. F. & Czekai, D. A. 1992. Surface modified drug nanoparticles. US patent: 5145684.

Loftsson, T. & Brewster, M. E. 1996. Pharmaceutical applications of cyclodextrins. 1. Drug solubilization and stabilization. *Journal of pharmaceutical sciences,* 85, 1017-1025.

Lohrmann, M., Kappl, M., Butt, H. J., Urbanetz, N. A. & Lippold, B. C. 2007. Adhesion forces in interactive mixtures for dry powder inhalers-Evaluation of a new measuring method. *European Journal of Pharmaceutics and Biopharmaceutics,* 67, 579-586.

Louati, B., Hlel, F., Guidara, K. & Gargouri, M. 2005. Analysis of the effects of thermal treatments on CaHPO4 by 31P NMR spectroscopy. *Journal of alloys and compounds,* 394, 13-18.

Maclennan, G. & Beevers, C. 1955. The crystal structure of dicalcium phosphate, CaHPO4. *Acta Crystallographica,* 8, 579-583.

Majuru, S. & Oyewumi, M. O. 2009. *Nanotechnology in Drug Development and Life Cycle Management,in: M.M. de Villiers, P. Aramvit, G.S. Kwon (Eds.),(pages 597-619)*.

Mandell, M., Mctague, J. & Rahman, A. 1976. Crystal nucleation in a three-dimensional Lennard-Jones system: A molecular dynamics study. *The journal of chemical physics,* 64, 3699.

Maple, J., Hwang, M. J., Stockfisch, T. P., Dinur, U., Waldman, M., Ewig, C. S. & Hagler, A. T. 1994. Derivation of class II force fields. I. Methodology and quantum force field for the alkyl functional group and alkane molecules. *Journal of Computational Chemistry,* 15, 162-182.

Marashall, P. V. 1987. The role of crystalline modifications in powder compaction. *PhD, University of Bradford.*

Marrink, S. J., De Vries, A. H. & Mark, A. E. 2004. Coarse grained model for semiquantitative lipid simulations. *The Journal of Physical Chemistry B,* 108, 750-760.

Marrink, S. J., Risselada, H. J., Yefimov, S., Tieleman, D. P. & De Vries, A. H. 2007. The MARTINI force field: coarse grained model for biomolecular simulations. *The Journal of Physical Chemistry B,* 111, 7812-7824.

Masuda, Y. 2011. *Nanocrystal,* Croatia, InTech, pages 1-494. ISBN: 978-953-307-199-2

Matteucci, M. E., Hotze, M. A., Johnston, K. P. & Williams III, R. O. 2006. Drug nanoparticles by antisolvent precipitation: Mixing energy versus surfactant stabilization. *Langmuir,* 22, 8951-8959.

Materials Studio software package. Accelrys, Inc. 2006.

Mauludin, R., Müller, R. H. & Keck, C. M. 2008. Development of an oral rutin nanocrystal formulation. *International Journal of Pharmaceutics*.

Mchale, J., Auroux, A., Perrotta, A. & Navrotsky, N. 1997. Surface energies and thermodynamic phase stability in nanocrystalline aluminas. *Science,* 277, 788.

Merisko-Liversidge, E., Liversidge, G. G. & Cooper, E. R. 2003. Nanosizing: a formulation approach for poorly-water-soluble compounds. *European Journal of Pharmaceutical Sciences,* 18, 113-120.

Merisko-liversidge, E. M. & Liversidge, G. G. 2008. Drug nanoparticles: formulating poorly water-soluble compounds. *Toxicologic pathology,* 36, 43.

Merisko-Liversidge, E., Sarpotdar, P., Bruno, J., Hajj, S., Wei, L., Peltier, N., Rake, J., Shaw, J., Pugh, S. & Polin, L. 1996. Formulation and antitumor activity evaluation of nanocrystalline suspensions of poorly soluble anticancer drugs. *Pharmaceutical research,* 13, 272-278.

Meteopolis, N. & Ulam, S. 1949. The monte carlo method. *Journal of the American Statistical Association,* 44, 335-341.

Metropolis, N., Rosenbluth, A. W., Rosenbluth, M. N., Teller, A. H. & Teller, E. 1953. Equation of state calculations by fast computing machines. *The journal of chemical physics,* 21, 1087.

Moeschwitzer, J. & Mueller, R. H. 2006. New method for the effective production of ultrafine drug nanocrystals. *Journal of Nanoscience and Nanotechnology,* 6, 3145-3153.

Moggach, S. A., Parsons, S. & Wood, P. A. 2008. High-pressure polymorphism in amino acids. *Crystallography Reviews,* 14, 143-184.

Moeschwitzer, J. & Mueller, R. H. 2006. New method for the effective production of ultrafine drug nanocrystals. *Journal of Nanoscience and Nanotechnology,* 6, 3145-3153.

Monticelli, L., Kandasamy, S. K., Periole, X., Larson, R. G., Tieleman, D. P. & MARRINK, S. J. 2008. The MARTINI coarse-grained force field: extension to proteins. *Journal of Chemical Theory and Computation,* 4, 819-834.

Morris, K. R., Griesser, U. J., Eckhardt, C. J. & Stowell, J. G. 2001. Theoretical approaches to physical transformations of active pharmaceutical ingredients during manufacturing processes. *Advanced Drug Delivery Reviews,* 48, 91-114.

Moriarty, P. 2001. Nanostructured materials. *Reports on Progress in Physics,* 64, 297-381.

Mou, D., Chen, H., Wan, J., XU, H. & Yang, X. 2011. Potent dried drug nanosuspensions for oral bioavailability enhancement of poorly soluble drugs with pH-dependent solubility. *International Journal of Pharmaceutics*.

Muller, R. H. & Akkar, A. 2004. Drug Nanocrystals of Poorly Soluble Drugs. *Encyclopedia of Nanoscience and Nanotechnology,* 2, 627-638.

Müller, R. H., Gohla, S. & Keck, C. M. 2011. State of the art of nanocrystals – Special features, production, nanotoxicology aspects and intracellular delivery. *European Journal of Pharmaceutics and Biopharmaceutics,* 78, 1-9.

Müller, R. H. & Peters, K. 1998. Nanosuspensions for the formulation of poorly soluble drugs: I. Preparation by a size-reduction technique. *International Journal of Pharmaceutics,* 160, 229-237.

Muller, R. H. B., R.; Kruss, B.; Peters, K. 1999. *Pharmaceutical Nanosuspensions for Medicament administration as Systems with Increased Saturation Solubility and Rate of Solution*. US patent: 5858410

Muller, R. H. J., C.; Kayser, O 2001. Nanosuspension as particulate drug formulations in therapy rationale for development and what we can expect for the future. *Adv. Drug Deliv. Rev*, 47, 3-19 .

Müller, R. & Keck, C. 2012. Twenty years of drug nanocrystals: Where are we, and where do we go? *European Journal of Pharmaceutics and Biopharmaceutics,* 80, 1-3.

Müller, R. H. & Keck, C. M. 2008. Second generation of drug nanocrystals for delivery of poorly soluble drugs: smartCrystal technology. *European Journal of Pharmaceutical Sciences,* 34, S20-S21.

Müller, R. H., Shegokar, R., Gohla, S. & Keck, C. M. 2011b. Nanocrystals: Production, Cellular Drug Delivery, Current and Future Products. *Intracellular Delivery*, 411-432.

Mullin, J. W. 2001. *Crystallization,* Fourth edition, Butterworth-Heinemann.

Myerson, A. S. 2002a. *Handbook of industrial crystallization*, Butterworth-Heinemann, pages 33-100.
Myerson, A. S. 2002b. *Handbook of industrial crystallization,* Butterworth-Heinemann, pages 43-51

Myerson, A. S. 2002. *Handbook of industrial crystallization*, Butterworth-Heinemann, pages 33-100.

Noyes, A. A. & Whitney, W. R. 1897. The rate of solution of solid substances in their own solutions. *J. Am. Chem. Soc,* 19, 930-934.

Ostwald, W. 1897. Studies on formation and transformation of solid materials. *Z. Phys. Chem,* 22, 289-330.

Oxtoby, D. W. 1998. Nucleation of first-order phase transitions. *Accounts of chemical research,* 31, 91-97.

Panagiotou, T., Mesite, S., Fisher, R. & Gruverman, I. Year. Production of stable drug nanospensions using microfluidics reaction technology. *In*, 2007. 246-249.

Panagiotou, T., Mesite, S. V. & Fisher, R. J. 2009. Production of norfloxacin nanosuspensions using microfluidics reaction technology through solvent/antisolvent crystallization. *Industrial & Engineering Chemistry Research,* 48, 1761-1771.

Parak, W. J., Gerion, D., Pellegrino, T., Zanchet, D., Micheel, C., Williams, S. C., Boudreau, R., Gros, M. A. L., Larabell, C. A. & Alivisatos, A. P. 2003. Biological applications of colloidal nanocrystals. *Nanotechnology,* 14, R15-R27.

Pardeike, J., Strohmeier, D. M., Schrödl, N., Voura, C., Gruber, M., Khinast, J. G. & Zimmer, A. 2011. Nanosuspensions as advanced printing ink for accurate dosing of poorly soluble drugs in personalized medicines. *International Journal of Pharmaceutics*, 420, 93-100.

Park, K., Evans, J. M. B. & Myerson, A. S. 2003. Determination of solubility of polymorphs using differential scanning calorimetry. *Crystal Growth & Design,* 3, 991-995.

Patravale, V. B. & KULKARNI, R. M. 2004. Nanosuspensions: a promising drug delivery strategy. *Journal of Pharmacy and Pharmacology,* 56, 827-840.

Paul, D. R. & Robeson, L. M. 2008. Polymer nanotechnology: Nanocomposites. *Polymer,* 49, 3187-3204.

Peltonen, L. & Hirvonen, J. 2010. Pharmaceutical nanocrystals by nanomilling: critical process parameters, particle fracturing and stabilization methods. *Journal of Pharmacy and Pharmacology,* 62, 1569-1579.

Perlovich, G., Hansen, L. K. & Bauer-brandl, A. 2001. The Polymorphism of Glycine. Thermochemical and structural aspects. *Journal of thermal analysis and calorimetry,* 66, 699-715.

P.T. Cardew, R. J. D. 1985. Kinetic of Solvent Mediated Polymoprhic transformations,. *Proocedings of the Royal Society,* 398, 415–428.

Peters, K., Mu¨ ller, R. H. (1996) Nanosuspensions for the oral application of poorly soluble drugs proceedings European Symposium on Formulation of Poorly-available Drugs for Oral Administration. APGI, Paris, pp 330–333

Piana, S. & GALE, J. D. 2005. Understanding the barriers to crystal growth: dynamical simulation of the dissolution and growth of urea from aqueous solution. *Journal of the American Chemical Society,* 127, 1975-1982.

Plakkot, S.; de Matas, M.; York, P.; Saunders, M.; Sulaiman, B. 2011. Comminution of ibuprofen to produce nano-particles for rapid dissolution. *International Journal of Pharmaceutics Volume 415* (1-2), 307-314.

Podczeck, F. 1999. The influence of particle size distribution and surface roughness of carrier particles on the in vitro properties of dry powder inhalations. *Aerosol Science & Technology,* 31, 301-321.

Ponchel, G., Montisci, M. J., Dembri, A., Durrer, C. & Duchêne, D. 1997. Mucoadhesion of colloidal particulate systems in the gastro-intestinal tract. *European Journal of Pharmaceutics and Biopharmaceutics,* 44, 25-31.

Price, R., Young, P., Edge, S. & Staniforth, J. 2002. The influence of relative humidity on particulate interactions in carrier-based dry powder inhaler formulations. *International Journal of Pharmaceutics,* 246, 47-59.

Prime, D., Atkins, P. J., Slater, A. & Sumby, B. 1997. Review of dry powder inhalers. *Advanced Drug Delivery Reviews,* 26, 51-58.

Rabesiaka, M., Sghaier, M., Fraisse, B., Porte, C., Havet, J.-L. & Dichi, E. 2010. Preparation of glycine polymorphs crystallized in water and physicochemical characterizations. *Journal of Crystal Growth,* 312, 1860-1865.

Rabinow, B. E. 2004. Nanosuspensions in drug delivery. *Nature Reviews Drug Discovery,* 3, 785-796.

Ranade, M., Navrotsky, A., Zhang, H., Banfield, J., Elder, S., Zaban, A., Borse, P., Kulkarni, S., Doran, G. & Whitfield, H. 2002. Energetics of nanocrystalline TiO2. *Proceedings of the National Academy of Sciences of the United States of America,* 99, 6476.

R.H.Müller,K.Mäder,K.Krause.VerfahrenzurschonendenHerstellungvonhochf einenMicro-/Nanopartikeln, PCT Application PCT/EP00/06535, Germany, 2000.

Roberts, R., Rowe, R. & York, P. 1994. The relationship between indentation hardness of organic solids and their molecular structure. *Journal of Materials Science,* 29, 2289-2296.

Ruckenstein, E. & Djikaev, Y. 2005. Recent developments in the kinetic theory of nucleation. *Advances in colloid and interface science,* 118, 51-72.

Saleem, I., Smyth, H. & Telko, M. 2008. Prediction of dry powder inhaler formulation performance from surface energetics and blending dynamics. *Drug development and industrial pharmacy,* 34, 1002-1010.

Sakai, H., Hosogai, H., Kawakita, T., Onuma, K. & Tsukamoto, K. 1992. Transformation of [alpha]-glycine to [gamma]-glycine. *Journal of Crystal Growth,* 116, 421-426.

Schüth, F., Bussian, P., Ågren, P., Schunk, S. & Lindén, M. 2001. Techniques for analyzing the early stages of crystallization reactions. *Solid state sciences,* 3, 801-808.
Schwarz, C., Mehnert, W., Lucks, J. S. & Müller, R. H. 1994. Solid lipid nanoparticles (SLN) for controlled drug delivery. I. Production, characterization and sterilization. *Journal of Controlled Release,* 30, 83-96.

Schüth, F. 2001. Nucleation and crystallization of solids from solution. *Current Opinion in Solid State and Materials Science,* 5, 389-395.

Serajuddin, A. T. M. 1999. Solid dispersion of poorly water-soluble drugs: early promises, subsequent problems, and recent breakthroughs. *Journal of pharmaceutical sciences,* 88, 1058-1066.

Seth, P. 1988. Novel pharmaceutical compositions containing hydrophobic practically water-insoluble drugs adsorbed on pharmaceutical excipients as carrier; process for their preparation and the use of said compositions. US Patent: 4721709.

Serajuddin, A. T. M. 1999. Solid dispersion of poorly water-soluble drugs: early promises, subsequent problems, and recent breakthroughs. *Journal of pharmaceutical sciences,* 88, 1058-1066.

Shariare, M. H., Leusen, F. J. J., De Matas, M., York, P. & Anwar, J. 2012. Prediction of the Mechanical Behaviour of Crystalline Solids. *Pharmaceutical research,* 29, 319-331.

Shegokar, R. & Müller, R. H. 2010. Nanocrystals: Industrially feasible multifunctional formulation technology for poorly soluble actives. *International Journal of Pharmaceutics,* 399, 129-139.

Shekunov, B. Y., Chattopadhyay, P., Seitzinger, J. & Huff, R. 2006. Nanoparticles of poorly water-soluble drugs prepared by supercritical fluid extraction of emulsions. *Pharmaceutical research,* 23, 196-204.

Singhal, D. & Curatolo, W. 2004. Drug polymorphism and dosage form design: a practical perspective. *Advanced Drug Delivery Reviews,* 56, 335-347.

Sivakumar, G., Girija, E., Narayana Kalkura, S. & Subramanian, C. 1998. Crystallization and characterization of calcium phosphates: brushite and monetite. *Crystal Research and Technology,* 33, 197-205.

Smit, B. 1992. Phase diagrams of Lennard-Jones fluids. *Journal of chemical physics,* 96, 8639-8640.

Smith, W., Forester, T., Todorov, I. & Leslie, M. 2006. The DL poly 2 user manual. *CCLRC, Daresbury Laboratory, Daresbury, Warrington WA4 4AD, England*.
Sohnel, O. & Garside, J. 1988. Solute clustering and nucleation. *Journal of Crystal Growth,* 89, 202-208.

Sorin, E. J. & Pande, V. S. 2005. Exploring the helix-coil transition via all-atom equilibrium ensemble simulations. *Biophysical Journal,* 88, 2472-2493.

Srichana, T., Brain, A., Marriott, C. & Martin, G. P. 2000. A study of drug-carrier interactions in dry powder inhaler formulations using the Andersen cascade impactor, X-ray microanalysis and time of flight aerosol beam spectrometry (TOFABS). *Chemical and Pharmaceutical Bulletin-tokyo-,* 48, 167-174.

Steed, J. W., Atwood, J. L. & Corporation, E. 2000. *Supramolecular chemistry*, Wiley Online Library.

Stegemann, S., Leveiller, F., Franchi, D., De Jong, H. & Lindén, H. 2007. When poor solubility becomes an issue: from early stage to proof of concept. *European Journal of Pharmaceutical Sciences,* 31, 249-261.

Stranski, I. & Totomanow, D. 1933. Seed formation speed and Ostwald's step rule [J]. *Z Phys Chem,* 163, 399-408.

Subramanian, S. & Zaworotko, M. J. 1995. Manifestations of noncovalent bonding in the solid state. vi: h4 (cyclam) 4+(cyclam= 1, 4, 8, 11-tetraazacyclotetradecane) as a template for crystal engine ering of network hydrogen-bonded solids. *canadian journal of chemistry,* 73, 414-424.

Sulaiman, B. 2007. "The Milling System" Patent no: WO/2007/020407.

Sylvestre, J. P., Tang, M. C., Furtos, A., Leclair, G., Meunier, M. & Leroux, J. C. 2011. Nanonization of megestrol acetate by laser fragmentation in aqueous milieu. *Journal of Controlled Release,* 149, 273-280.

Swope, W. C. & Andersen, H. C. 1990. 10^6-particle molecular-dynamics study of homogeneous nucleation of crystals in a supercooled atomic liquid. *Physical Review B,* 41, 7042.

T. Srichana, A. B., G.P. Martin and C. Marriott 1998. The determination of drug-carrier interactions in dry powder inhaler formulations. *J. Aemul Sci. ,* 29, S757-S758.

Tangsathitkulchai, C. 2003. The effect of slurry rheology on fine grinding in a laboratory ball mill. *International Journal of Mineral Processing,* 69, 29-47.

Traini, D., Rogueda, P., Young, P. & Price, R. 2005. Surface energy and interparticle force correlation in model pMDI formulations. *Pharmaceutical research,* 22, 816-825.
Tom, J. W. & Debenedetti, P. G. 1991. Particle formation with supercritical fluids—a review. *Journal of Aerosol Science,* 22, 555-584.

Ullmann 2007. *Ullmann's modelling and simulation,* Weinheim, Chichester, Willey-VCH, pp. 307-439.

Valder, C. & Merrifield, D. 1996. Pharmaceutical technology. *Smith Kline Beecham R&D News,* 32, 1.

Valleri, M., Mura, P., Maestrelli, F., Cirri, M. & Ballerini, R. 2004. Development and evaluation of glyburide fast dissolving tablets using solid dispersion technique. *Drug development and industrial pharmacy,* 30, 525-534.

Van Eerdenbrugh, B., Van Den Mooter, G. & Augustijns, P. 2008. Top-down production of drug nanocrystals: Nanosuspension stabilization, miniaturization and transformation into solid products. *International Journal of Pharmaceutics,* 364, 64-75.

Van Gunsteren, W. F. & Karplus, M. 1982. Effect of constraints on the dynamics of macromolecules. *Macromolecules,* 15, 1528-1544.

Van Eerdenbrugh, B., Froyen, L., Van Humbeeck, J., Martens, J. A., Augustijns, P. & Van Den Mooter, G. 2008. Drying of crystalline drug nanosuspensions--The importance of surface hydrophobicity on dissolution behavior upon redispersion. *European Journal of Pharmaceutical Sciences,* 35, 127-135.

Vekilov, P. G. 2004. Dense liquid precursor for the nucleation of ordered solid phases from solution. *Crystal Growth & Design,* 4, 671-685.

Verlet, L. 1967. Computer" experiments" on classical fluids. I. Thermodynamical properties of Lennard-Jones molecules. *Physical Review,* 159, 98.

Verma, S., Kumar, S., Gokhale, R. & Burgess, D. J. 2010. Physical stability of nanosuspensions: Investigation of the role of stabilizers on Ostwald ripening. *International Journal of Pharmaceutics,* Volume 406, , 145-152.

Verma, S., Gokhale, R. & Burgess, D. J. 2009. A comparative study of top-down and bottom-up approaches for the preparation of micro/nanosuspensions. *International Journal of Pharmaceutics,* 380, 216-222.

Von HippeL, A. 1962. The Molecular Designing of Materials. Massachusetts inst of tech cambridge lab for insulation research.

Vippagunta, S. R., Brittain, H. G. & Grant, D. J. W. 2001. Crystalline solids. *Advanced Drug Delivery Reviews,* 48, 3-26.

Wang, G. D., Mallet, F. P., Ricard, F. & Heng, J. Y. Y. 2012. Pharmaceutical nanocrystals. *Current Opinion in Chemical Engineering,* 1, 102-107.

Weber, M. & Thies, M. C. 2002. Understanding the RESS process. *Supercritical Fluid Technology in Materials Science and Engineering: Syntheses, Properties, and Applications, pp 387-427*

Weissbuch, I., Torbeev, V. Y., Leiserowitz, L. & Lahav, M. 2005. Solvent effect on crystal polymorphism: Why addition of methanol or ethanol to aqueous solutions induces the precipitation of the least stable β form of glycine. *Angewandte Chemie International Edition,* 44, 3226-3229.

Williams, R. O., Johnston, K. P., Young, T. J., Rogers, T. L., Barron, M. K., YU, Z. & HU, J. 2002. Process for production of nanoparticles and microparticles by spray freezing into liquid. US patent : 6862890.

Weissbuch, I., Lahav, M. & Leiserowitz, L. 2003. Toward stereochemical control, monitoring, and understanding of crystal nucleation. *Crystal Growth & Design,* 3, 125-150.

Wei, K., Lai, C. & Wang, Y. 2007. Formation of monetite nanoparticles and nanofibers in reverse micelles. *Journal of Materials Science,* 42, 5340-5346.

Williams, R. O., Johnston, K. P., Young, T. J., Rogers, T. L., Barron, M. K., Yu, Z. & Hu, J. 2002. Process for production of nanoparticles and microparticles by spray freezing into liquid. US patent : 6862890.

Wu, L., Zhang, J. & Watanabe, W. 2011. Physical and chemical stability of drug nanoparticles. *Advanced Drug Delivery Reviews,* 63, 456-469.

WU, W. J. & Nancollas, G. H. 1998. A new understanding of the relationship between solubility and particle size. *Journal of Solution Chemistry,* 27, 521-531.

Yeung, C. C. & Hersey, J. A. 1979. Ordered powder mixing of coarse and fine particulate systems. *Powder Technology,* 22, 127-131.

Zeng, X. M., Martin, G. P., Marriott, C. & Pritchard, J. 2000. The influence of carrier morphology on drug delivery by dry powder inhalers. *International Journal of Pharmaceutics,* 200, 93-106.

Zahn, D. & Anwar, J. 2011. Size-Dependent Phase Stability of a Molecular Nanocrystal: a Proxy for Investigating the Early Stages of Crystallization. *Chemistry-A European Journal,* 17, 11186-11192.

Zhang, D., Tan, T., Gao, L., Zhao, W. & Wang, P. 2007. Preparation of azithromycin nanosuspensions by high pressure homogenization and its

physicochemical characteristics studies. *Drug development and industrial pharmacy,* 33, 569-575.

Zhang, T. H. & Liu, X. Y. 2009. Nucleation: What Happens at the Initial Stage? *Angewandte Chemie International Edition,* 48, 1308-1312.

Zhang, G. G. Z., Law, D., Schmitt, E. A. & Qiu, Y. 2004. Phase transformation considerations during process development and manufacture of solid oral dosage forms. *Advanced Drug Delivery Reviews,* 56, 371-390.

Zhao, H., Wang, J. X., Wang, Q. A., Chen, J. F. & YUN, J. 2007. Controlled liquid antisolvent precipitation of hydrophobic pharmaceutical nanoparticles in a microchannel reactor. *Industrial & Engineering Chemistry Research,* 46, 8229-8235.

Zhang, Z. B., Shen, Z. G., Wang, J. X., Zhao, H., Chen, J. F. & Yun, J. 2009. Nanonization of Megestrol Acetate by Liquid Precipitation. *Industrial & Engineering Chemistry Research,* 48, 8493-8499.